Field and modelling investigations of permafrost conditions in Labrador, northeast Canada

Robert Way

Thesis submitted to the
Faculty of Graduate and Postdoctoral Studies
in partial fulfillment of the requirements for the
Doctorate of Philosophy in Geography

Department of Geography, Environment and Geomatics
Faculty of Arts
University of Ottawa

ABSTRACT

The Permafrost Map of Canada shows the region of Labrador in northeast Canada as spanning conditions from continuous permafrost in the north to isolated patches in the south. However, few studies have documented this and the most detailed field information comes from research in the 1960s and 1970s, with contemporary permafrost distribution largely unexamined. An extensive investigation of contemporary permafrost conditions throughout Labrador and portions of northeastern Québec was undertaken between 2013 and 2017 to fill this knowledge gap. A multi-scale approach to analyzing permafrost distribution was employed, including collection of detailed field information at selected sites, establishment of climate and ground monitoring apparatus at more than 35 different locations and spatial numerical permafrost modelling of permafrost conditions across the region.

Spatio-temporal infilling was used with thin plate spline interpolation to generate temporally-consistent climate grids for 1948-2016 at a monthly resolution for all of Labrador-Ungava. Evaluation of derived air temperature grids against meteorological observations and remote field monitoring stations showed an overall accuracy of 0.8 ± 0.3 °C on a monthly timescale. The grids were used to generate freezing and thawing degree-days maps to facilitate permafrost modelling.

Field investigations in the coastal barrens of southeastern Labrador (51.5°N to 54°N) used geophysics (DC electrical resistivity tomography), standard field methods and ground temperature monitoring to characterize very isolated patches of permafrost observed to be up to 8 m thick beneath palsas and peat plateaus. Permafrost was inferred to be absent in wetland, forested and forest-tundra areas inland, notwithstanding average air temperatures lower than at the coast. However, field investigations undertaken farther north in the coastal community of Nain, NL (56.3°N) showed permafrost to be present at numerous sites within the community in tundra, forested and disturbed settings. Boreholes and geophysics showed permafrost less than 20 m thick at several locations including beneath existing and proposed building locations. These investigations of permafrost along a latitudinal gradient highlight the contrasting permafrost environments found in coastal regions of Labrador.

Field data from monitoring stations across Labrador (n=83) were used to analyze the interrelationships of key variables in permafrost modelling. Snow depth, not mean annual air temperature, was the strongest single determinant of mean temperatures at the ground surface and at ~1 m depth. Ground temperature variability was most related to land cover class with a critical late-winter snow depth of 70 cm or less inferred to be sufficient to prevent the formation of permafrost at the monitoring sites. Testing of several different land cover datasets for permafrost model parameterization gave errors in ground surface temperature ranging from ±0.9 to ±2.1°C.

A new estimate of the distribution of permafrost at high resolution (250 m x 250 m) was generated for all of Labrador-Ungava using a modified version of the temperature at the top of permafrost model. Predicted ground temperatures for long-term climate normal ranged regionally from -9°C (for high elevations in northern Québec) to +5°C (for southeastern Labrador-Québec). Modelling of permafrost for specific temporal windows (1948-1962; 1982-1996; 2000-2014) suggested that permafrost area increased from the middle of the 20th Century to a potential peak extent (36% of the total land area) in the 1990s. Subsequent warming is predicted to have caused a decrease in permafrost extent of one-quarter (95 000 km^2) even if air temperatures rise no further, providing air and ground temperatures equilibrate.

The field observations in this thesis validated research conducted in the interior of Labrador during 1970s which directly linked permafrost presence or absence to snow thickness. Permafrost was more widespread than would be expected in coastal areas based on the region's mean annual air temperatures which suggests that specific geomorphologic and meteorological settings may allow permafrost to persist in otherwise unsuitable regions. Land cover type, through its influence on snow distribution, was shown to be a key variable whose changes must be considered when examining future permafrost conditions in the region.

ACKNOWLEDGEMENTS

This thesis would not have been possible without the help and guidance provided by my mentors, my family and the many others who supported this project and its goals. Running a major research endeavour in Labrador has been a logistical challenge and it could not have been implemented without the advice and support of the people and communities of Labrador. It cannot be quantified how much I have benefited from the traditional knowledge shared with me by residents of all backgrounds and I would like to thank the Nunatsiavut Government for having supported my work specifically, and the Innu Nation and Nunatukavut Community Council for permitting environmental research on their traditional lands. I would like to thank my supervisor Dr. Antoni Lewkowicz for his unwavering confidence in my abilities and for the opportunity he has provided me by encouraging me to pursue research on permafrost in Labrador. Despite operating research projects throughout Canada, Toni has always found some time for Labrador and for this I am truly appreciative. I would also like to thank all of the support staff in the Department of Geography (now GEG) at the University of Ottawa who helped me navigate the complexities of the university system. A special thank you to Nathalie Maras and Jean Bjornson, both of whom provided logistical support to my project. I would like to thank my committee members, Dr. Michael Sawada, Dr. Denis Lacelle and Dr. Sharon Smith for their advice and guidance at various points during my PhD program and for making time to read this dissertation during the busy summer research season. I would like to thank Dr. Michel Allard for serving as the external examiner for this dissertation and for the useful commentary that improved all of the manuscripts contained within.

This project could have never been possible without the love and support from my wonderful parents Brenda and George Way and my extended family found throughout Labrador and elsewhere. My parents were continually supportive of this research and opened their home(s) to me and my assistants' countless times while we were in the field. This generosity cannot be understated. I would like to give special thanks to my Aunt Patricia Way ('Patty') and Uncle Gary Bird ('Stig') who not only hosted us at their home in Cartwright, Labrador each summer but also contributed to my project through conversations and discussions on permafrost landforms in the area. The visits to Cartwright each summer were always a highlight because of the beautiful landscape and warm conversations. Thank you to my cousin James Way who helped me establish the first monitoring sites back in October of 2012, and more recently who joined me on a mountainous snowmobile trip to download data in the Mealy Mountains in April of 2017.

I would like to thank Dr. Jack Ives for the lovely talks we had on permafrost (and glaciers) in Labrador. It is truly an inspiration to be able to try and build on the earlier work by Dr. Ives and others who first explored permafrost in Labrador. Similarly, I would like to thank Drs. Bruce Roberts, Michel

Allard, Stephan Gruber and Sebastian Westermann for providing insights into discontinuous permafrost during our brief chats. I would like to personally thank Drs. John Jacobs, Darroch Whitaker, Luise Hermanutz, Andre Viau and Konrad Gajewski for so many useful conversations about the climate, ecology and wildlife in northeastern Canada, and for the provision of field and meteorological data from the Mealy Mountains, the Torngat Mountains National Park and the Kamestastin region. I also would like to acknowledge New Millennium Development, Hydro Québec and Nalcor Energy for providing access to meteorological station and field data for Labrador and northeastern Québec.

Analysis of the field data provided collected throughout this dissertation was frequently shaped by guidance from Steven Mosher who invested a huge amount of time encouraging and teaching me the usefulness of programming in R. I am truly indebted to him for this help and for helping me debug complicated coding issues. Thank you to Drs. Andre Viau and Konrad Gajewski for allowing me to use the computer lab space and for letting me feel at home at the 'LPC'. Similarly, I have a great deal of gratitude to Dr. Philip Bonnaventure, Olivier Bellehumeur-Génier and Dr. Matthew Ladd for the many chats on permafrost science or modelling or just life in general. Academic pursuits are much more palatable with friends like you. To my helpful field assistants, Maxime Duguay, Alexander Brooker and Clarke Turpin, I apologize for the wind, rain, flat tires and rough trips in boat/snowmobile but I am so happy that I have had the chance to share these experiences with you all. Finally, for the last three years I have been so fortunate to have my girlfriend Caitlin, who not only has supported me throughout my PhD but has actively embraced this research as a field assistant on four separate occasions. I have been so happy to be able to share my love of Labrador with you and I apologize for asking you to proofread so often.

I would like to acknowledge financial support through the Nunatsiavut Government via the post-secondary student support program throughout my PhD and during my undergraduate degree. Without this support, studying at the University of Ottawa would not have been possible. I would like to thank the W. Garfield Weston Foundation for choosing me to be a recipient for W. Garfield Weston Award for Northern Research on multiple occasions (MSc/PhD/PDF), and for the Northern Resident Scholarship during year 2 of my PhD. This support greatly enhanced my research and overall research experience throughout my graduate studies. Likewise, I would like to thank the Royal Canadian Geographical Society for selecting me for the James Bourque Scholarship and the Natural Sciences and Engineering Research Council of Canada for the support of a Canada Graduate Scholarship throughout my PhD. I would like to acknowledge financial assistance for the project's research costs from the Natural Sciences and Engineering Research Council of Canada, the University of Ottawa and the Northern Scientific Training Program.

"The good life is one inspired by love and guided by knowledge" - Bertrand Russell

TABLE OF CONTENTS

LIST OF TABLES

LIST OF FIGURES

CHAPTER 1: INTRODUCTION

1.1 Introduction

The Earth has warmed by ~0.85°C since 1880 with a near-unanimous scientific consensus that human activity is the main driver of recent warming (Cook et al. 2013). In the Northern Hemisphere extratropical region, warming has occurred in two distinct phases with an early 20th century warm period associated with externally forced natural variability and anthropogenic forcing (Suo et al. 2013; Cawley et al. 2015) and a recent period that is nearly 100% caused by anthropogenic forcings due to greenhouse gas emissions. A distinct fingerprint of anthropogenic global warming is the process of Arctic amplification which enhances the response of high latitude earth systems to climatic changes (Serreze and Barry 2011). These systems are particularly vulnerable to environmental change due to feedback mechanisms such as the snow-ice albedo positive feedback (Serreze and Barry 2011). Correspondingly, since 1979 the Arctic has warmed at a rate of 0.6°C/decade, approximately 3.5 times the global rate (Comiso and Hall 2014; Cowtan and Way 2014) (Figure 1-1). Due to rapid Arctic warming initiated over the past several decades, elements of the terrestrial and marine cryosphere have shown dramatic changes (Derksen et al. 2012). For example, glaciers and ice caps have begun receding (Paul et al. 2004; Anderson et al. 2008; Way 2015; Serreze et al. 2017), sea ice has dramatically reduced in area and volume (Comiso and Hall 2014), ice sheets have rapidly lost ice (Helm et al. 2014) and permafrost has degraded in parts of the discontinuous zone (James et al. 2013) while ground temperatures have increased in the continuous zone (Romanovsky et al. 2010; Smith et al. 2010).

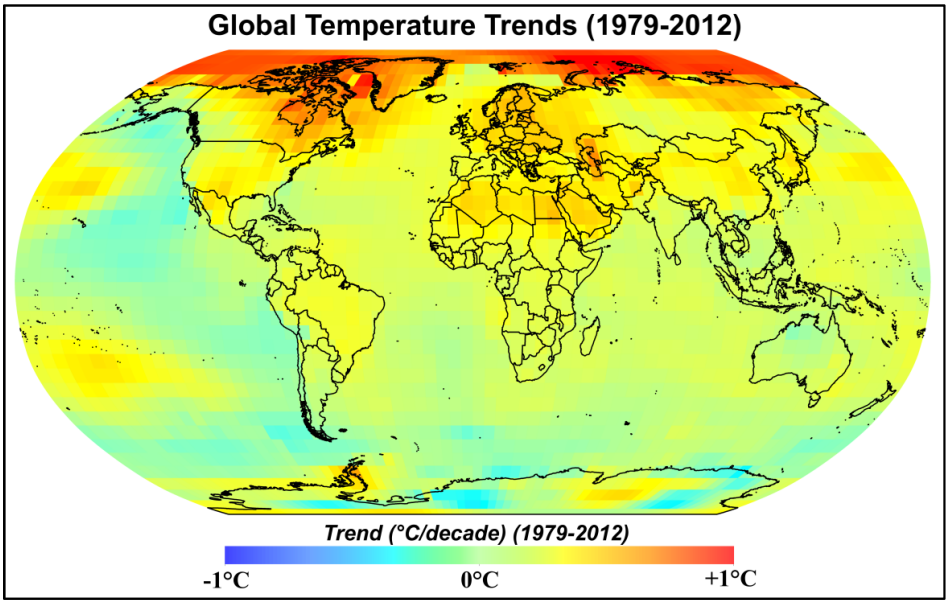

Figure 1-1: Spatial distribution of global temperature trends (°C/decade) over the period 1979-2012. Data are presented from the hybrid global temperature analysis of Cowtan and Way (2014).

Changes in the terrestrial cryosphere, and in particular glaciers and permafrost, have been observed throughout the Arctic and subarctic in Canada (Brown et al. 2012; Derksen et al. 2012). Projected high latitude warming will have substantial impacts on northern environmental systems (Woo et al. 1992) with climate models predicting a reduction of permafrost area ranging from 15% to 87% (Slater and Lawrence 2013). Recent work in the southern Yukon and northern B.C. (James et al. 2013) suggests that nearly half of the permafrost sites originally found by Brown (1967) in 1964 have since thawed and continued regional warming is projected to lead to further permafrost degradation in the coming decades (Bonnaventure and Lewkowicz 2011). In eastern Canada, rapid changes in ground surface/subsurface temperatures have been observed in the Québec portion of Labrador-Ungava (Payette et al. 2004; Thibault and Payette 2009) with the bulk of these changes occurring over the past decade (Allard et al. 2012a). The recent record of climate for eastern Labrador-Ungava shows that air temperatures have by 1.2°C over the past 30 years (Way and Viau 2015) and satellite remote sensing has shown that ground surface temperatures have also increased (Hachem et al. 2009; Comiso and Hall 2014).

The Permafrost Map of Canada (Heginbottom et al. 1995) shows the southernmost limit of lowland discontinuous permafrost in Labrador close to the 50°N parallel. Changes in the distribution and thickness of permafrost in the region are likely underway but these cannot be quantified at present because, apart from surveys completed several decades ago (Brown 1975; Brown 1979), there is little information on the current distribution and depth of permafrost. A paucity of field observations of permafrost characteristics and temperature has been a major concern for modelling past, present and future permafrost conditions in the region. Due to this knowledge gap, the extent of regional permafrost degradation is largely unknown, and with significant mineral and resource development projected for the region, it is important that additional local information is collected. Major resource projects include north-south ferroducts (New Millennium Development), mining of uranium (Paladin Energy) and rare earth minerals (Quest Rare Earth Minerals), hydro-electric development (Nalcor Energy), and the potential extension of the road network northwards. These projects will require significant infrastructure development for both the exploitation of resources and access to remote areas. It is therefore important from an engineering perspective to understand which areas are most vulnerable to future permafrost degradation as a means of avoiding structural damage (Smith and Riseborough 2010; Doré et al. 2016). Furthermore, the Labrador region includes two alpine national parks (Torngat Mountains National Park, Mealy Mountains Park Reserve) undergoing rapid environmental changes (Fraser et al. 2011; Brown et al. 2012; McLennan et al. 2012; Simms and Ward 2013; Jacobs et al. 2014; Way et al. 2015; Barrand et al. 2017) with little current

knowledge of permafrost dynamics inside their boundaries or how these changes may impact local ecosystems.

The main objective of this dissertation was to establish contemporary conditions of permafrost in the Labrador region of northeastern Canada and to model the distribution of permafrost at high resolution across the region's complex terrain. This information will improve our understanding of how past climate changes have impacted, and future changes will impact, perennially frozen ground in Labrador. To achieve this overall objective, baseline permafrost conditions were established using field-based data in conjunction with environmental and climate modelling. Disentangling the complex interactions between these ecological variables and their scale-dependency (from sub grid-cell to regional scales) was attempted along coastal-continental gradients throughout Labrador. This research has augmented our knowledge of the dynamics of sporadic and discontinuous permafrost in the Canadian Subarctic and Arctic, and should lead to an improved understanding of the importance of microclimate and regional topographic controls on permafrost distribution. This research also aims to inform assessments of permafrost vulnerability to change in the face of rapid climate warming and should assist the development of local mitigation practices which may reduce future infrastructure damage in the region.

1.2 Background literature

1.2.1 Permafrost fundamentals and zonation

Permafrost is defined thermally as ground that remains at or below 0°C for two consecutive years (Van Everdingen 2005c). Using a thermal definition, as opposed to 'frozen ground', reflects the fact that permafrost does not necessarily contain ice. Permafrost is overlain by a layer of seasonally frozen ground which freezes and thaws each year called the active layer. At the intersection between the base of the active layer and the top of permafrost a transition zone termed the transient layer is found. This transition zone may contain thaw uncomformities reflecting previous periods of exceptional active layer thaw which penetrated the top of permafrost (Shur et al. 2005). The depth at which seasonal variations in air temperature cease to impact ground temperatures (or decline below detectable limits [<0.1°C]) is termed the depth of zero annual amplitude (DZAA) and the temperature at that depth is the mean annual ground temperature (MAGT). Where thermal monitoring does not extend to the DZAA the convention is to use the annual average ground temperature of the deepest measurement (Smith et al. 2005).

The geographic distribution of permafrost is typically categorized at the broad (continental) scale into the following four zones (Heginbottom et al. 1995):

(a) Continuous zone: Permafrost is largely ubiquitous in this zone except for example beneath major bodies of water and newly exposed land surfaces. Mean annual air temperatures in this zone are typically below -6°C to -8°C with 90-100% of the land surface being underlain by permafrost;

(b) Extensive discontinuous zone: Permafrost is widespread in this zone but may not exist under unfavourable local conditions; 50-90% of the land surface is underlain by permafrost;

(c) Sporadic discontinuous zone: Permafrost is found under suitable local environmental and topoclimatic conditions with 10-50% of the land surface underlain by permafrost;

(d) Isolated patches zone: Permafrost is largely limited to organic terrain (Shur and Jorgenson, 2007) and found only at specific sites with suitable local environmental and topoclimatic conditions with 0-10% of the surface underlain by permafrost. Despite the widespread usage of the isolated patches class on permafrost maps, meaningful interpretation of this class can be challenging because it combines areas with nearly no permafrost (e.g. 0.01% of land area) with areas that have frequent small patches of permafrost (e.g. 9.9% of land area) into the same category.

1.2.2 The near-surface permafrost system

Smith and Riseborough (1996; 2002) and Riseborough (2004) presented the temperature at the top of permafrost (TTOP) model, a numerical model that summarizes the nature of air-to-ground coupling and ground thermal conditions in northern environments (Figure 1-2). TTOP refers to the temperature at the top of the permafrost located at the base of the active layer which includes the base of seasonal freezing in non-permafrost terrain. This simplified framework accounts for differences between air and ground surface temperatures through the surface offset which is calculated using transfer functions (n-factors) that estimate the influence of snow thickness and vegetation cover on ground surface temperatures according to Smith and Riseborough (1996; 2002). The average offset between air temperatures and ground surface temperatures in the winter is termed the nival offset and summarizes the influence of snow cover. The offset between ground surface temperatures and temperatures at the top of permafrost is termed the thermal offset (Burn and Smith 1988) and is strongly influenced by the thermal conductivities of subsurface materials and the number of thawing degree days at the ground surface (Smith and Riseborough 1996; 2002). Beneath the permafrost table, the variation in ground temperature with depth is far smaller and is largely a result of the geothermal flux and the thermal properties of the surficial geology. This simple conceptualized framework is useful for modelling the interactions between air and ground temperatures but can be problematic when considering the transient effects of rapid environmental change (Riseborough 2007).

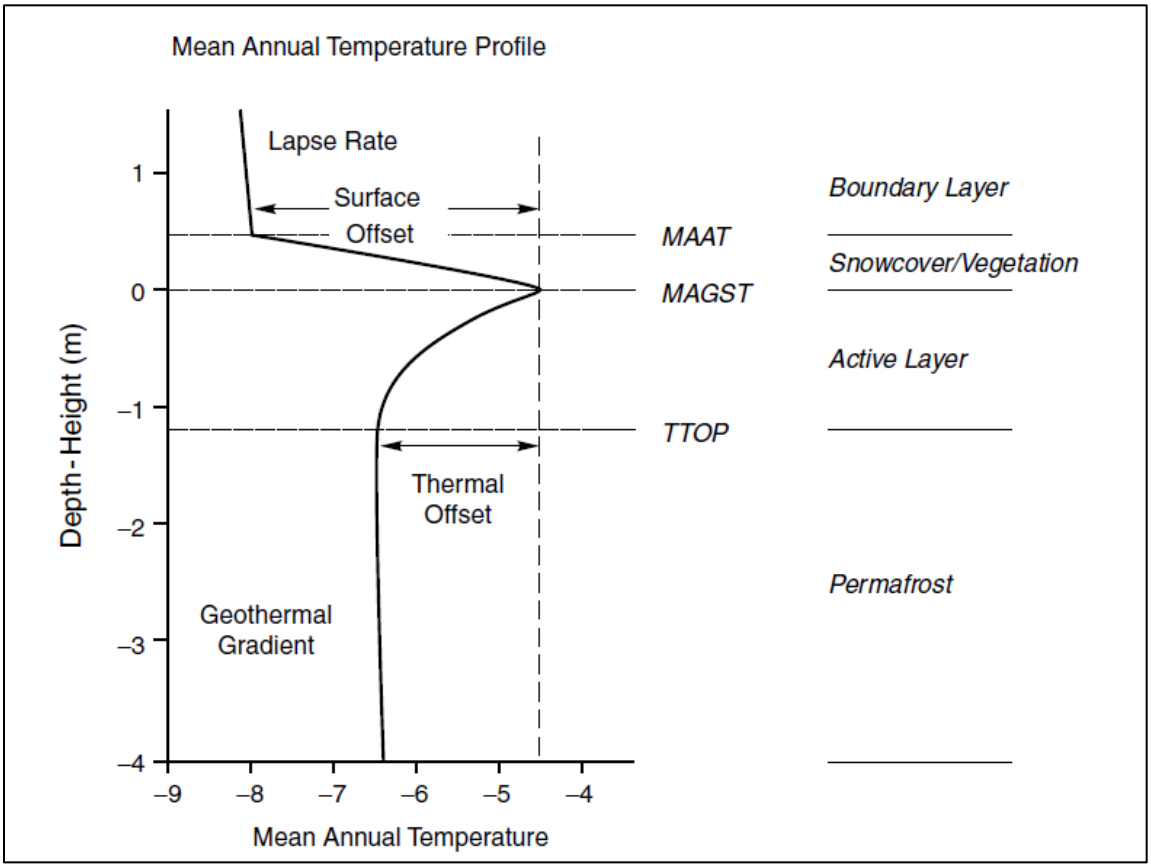

Figure 1-2: Idealized diagram of air-to-ground relations described by Smith and Riseborough (1996) and Smith and Riseborough (2002) in the formulation of the temperature at the top of permafrost (TTOP) model. From Smith and Riseborough (2002).

1.2.3 Permafrost formation and preservation

The broad permafrost zones discussed in *Section 1.2.2* relate to concepts introduced by Shur and Jorgenson (2007) that delineate the controls on permafrost formation and preservation. *'Climate-driven'* permafrost coincides with the continuous zone and therefore forms in almost all portions of the landscape. Hydrological systems such as rivers and large lakes that do not freeze to the bottom are largely associated with the absence of permafrost and open or through-going taliks often develop beneath and around these features. *'Climate-driven, ecosystem modified'* permafrost occurs within the zone of continuous permafrost where vegetation succession has altered the surface landscape leading to changes in permafrost conditions such as thinner/thicker active layers and warmer/colder permafrost. An example of 'climate-driven, ecosystem modified' permafrost occurs when a thick organic mat develops at the surface through ecological succession leading to thinner active layer depths. *'Climate-driven, ecosystem protected'* permafrost developed under a previous climate regime where conditions favoured the development of permafrost relatively ubiquitously across the landscape. Later stages of ecological succession have allowed permafrost to remain stable despite the development of a less favourable climate regime. The removal of overlying ecosystem components results in permafrost equilibrating with the less favourable climate conditions leading to thicker active layers and potential talik development in some cases.

'Ecosystem-driven' permafrost occurs when permafrost is formed directly as a result of ecological succession preconditioning the subsurface conditions towards a favourable permafrost environment. An example of this process is when late-successional ecosystems with thick organic covers provide large thermal offsets (Smith and Riseborough 2002) that allow for permafrost to develop under unfavourable climate conditions. *'Ecosystem-protected'* permafrost is similar to 'climate-driven, ecosystem protected' permafrost in that the permafrost formed under prior climate conditions that were more favourable to permafrost than current conditions. The development of late-successional surface environments allows for permafrost to remain stable under climatic conditions which would otherwise cause permafrost to thaw (Jorgenson et al. 2010). 'Ecosystem-protected' permafrost is very sensitive to perturbations and therefore can be completely thawed as a result of removal of surface cover or additional warming (Shur and Jorgenson 2007; Jorgenson et al. 2010).

1.3 Study area

The focus area of the Labrador Permafrost Project for *in situ* field investigations and modelling encompasses the region bounded by 50-61°N and 55-70°W. Although corresponding to portions of both Labrador and northeastern Québec, this region is referred to in this thesis as Labrador or eastern Labrador-

Ungava. This region also contains portions of the indigenous land claims zones designated for the Inuit of Nunatsiavut and the Inuit of Nunavik (Figure 1-3). Land claims negotiations are currently ongoing for the Innu of northeastern Québec/Labrador and a land claims proposal has been submitted for southeastern Labrador by the Nunatukavut Community Council.

1.3.1 The physical landscape of Labrador

Labrador is part of the Canadian Shield, and comprises numerous moderately high plateaus and mountain chains that reach the highest elevations in continental Canada east of the Rockies in the Torngat Mountains (~1650 m a.s.l. [1] in Figure 1-4). Distinct alpine regions are found throughout much of Labrador including near the Harp Lake Complex (~750 m a.s.l. [2]), the Red Wine Mountains (850 m a.s.l. [3]), the Mealy Mountains (1130 m a.s.l. [4]), the Romaine Hills (950 m a.s.l. [5]) and the Groulx Mountains (~1000 m a.s.l. [6]) (Figure 1-4). Lowlands are present in coastal locations along the Labrador Sea, the Ungava coastline and the Gulf of St. Lawrence and are also found along river valleys which dissect the landscape deep into the Labrador interior.

At the Last Glacial Maximum, Labrador was covered by the Laurentide ice sheet (LIS) (Dyke 2004). Early geomorphic work suggested that the LIS did not cover the uppermost reaches of the Torngat Mountains but newly developed techniques show that these areas were most likely covered by thin, cold-based ice (Marquette et al. 2004). The deglaciation of Labrador began in southeastern Labrador by 11 ka BP with the coastal areas near Makkovik being deglaciated by 9 ka BP and the north coast of Labrador beginning to be deglaciated at 8 ka BP. By 7 ka BP, most of northern Labrador and areas surrounding Lake Melville were deglaciated with the main LIS being centered near Schefferville (Dyke 2004). Continued deglaciation led to the separation of the LIS into two main ice bodies by 6 ka BP with the larger located in the uplands of Nunavik and the smaller ice mass located near Schefferville. By 5 ka BP, Labrador was completely deglaciated with the exception of small residual ice masses in upland areas. According to Viau and Gajewski (2009) and Gajewski (2015), Labrador was characterized by a mid-Holocene thermal maximum with a maximum intensity in summer warmth occurring ~4000 to 3000 years before present. Neoglacial cooling began soon after the Holocene thermal maximum (Viau and Gajewski 2009) but summer temperatures remained warmer than present until ~800 years ago allowing the treeline to migrate northwards (Lamb 1985; Payette 2007; Gennaretti et al. 2014; Naulier et al. 2015).

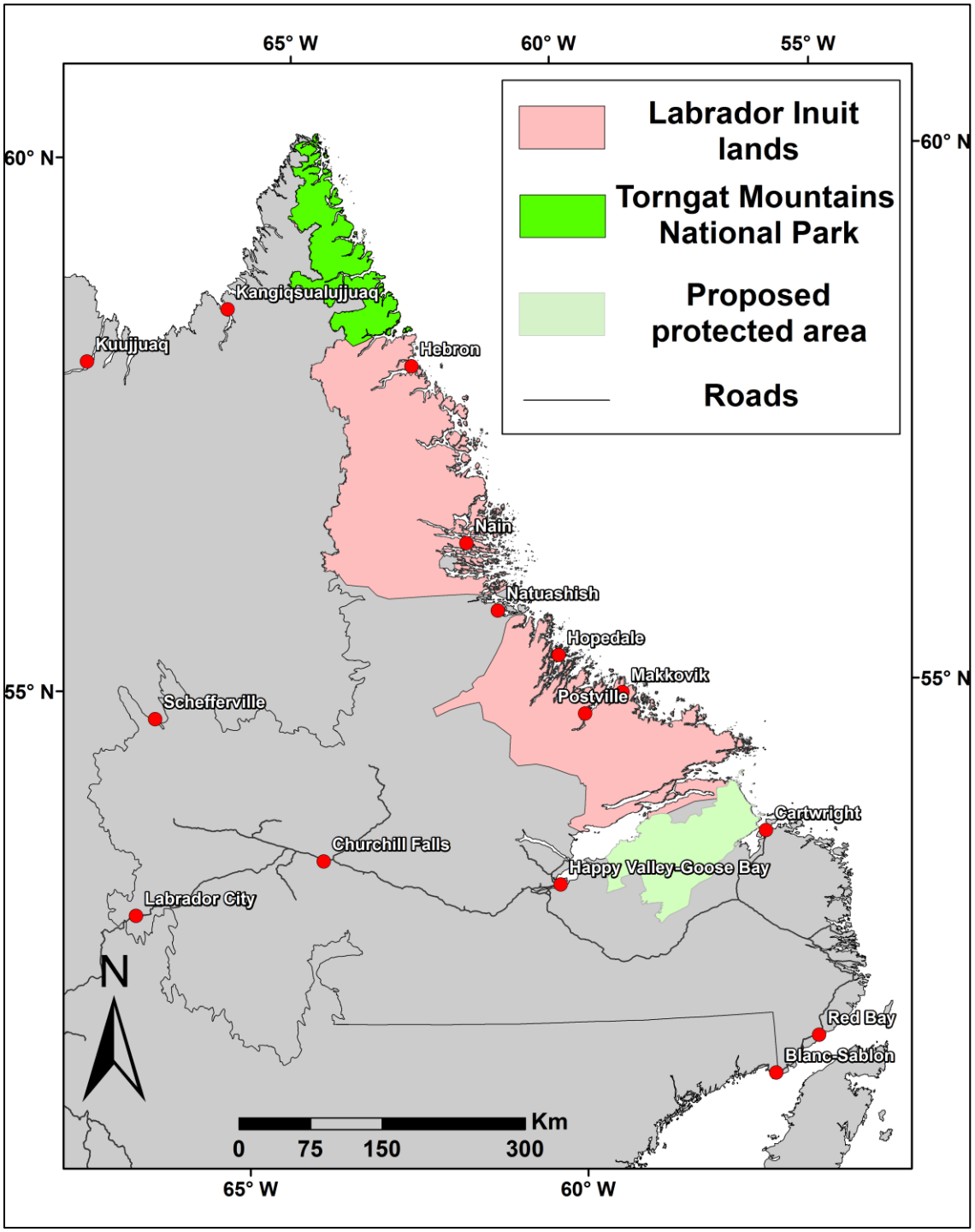

Figure 1-3: Study area map showing the largest communities, major roads and large lakes in eastern Labrador-Ungava. Land areas depicted on map comprise the approximate extent considered as Labrador for the purposes of field and modelling investigations in this study.

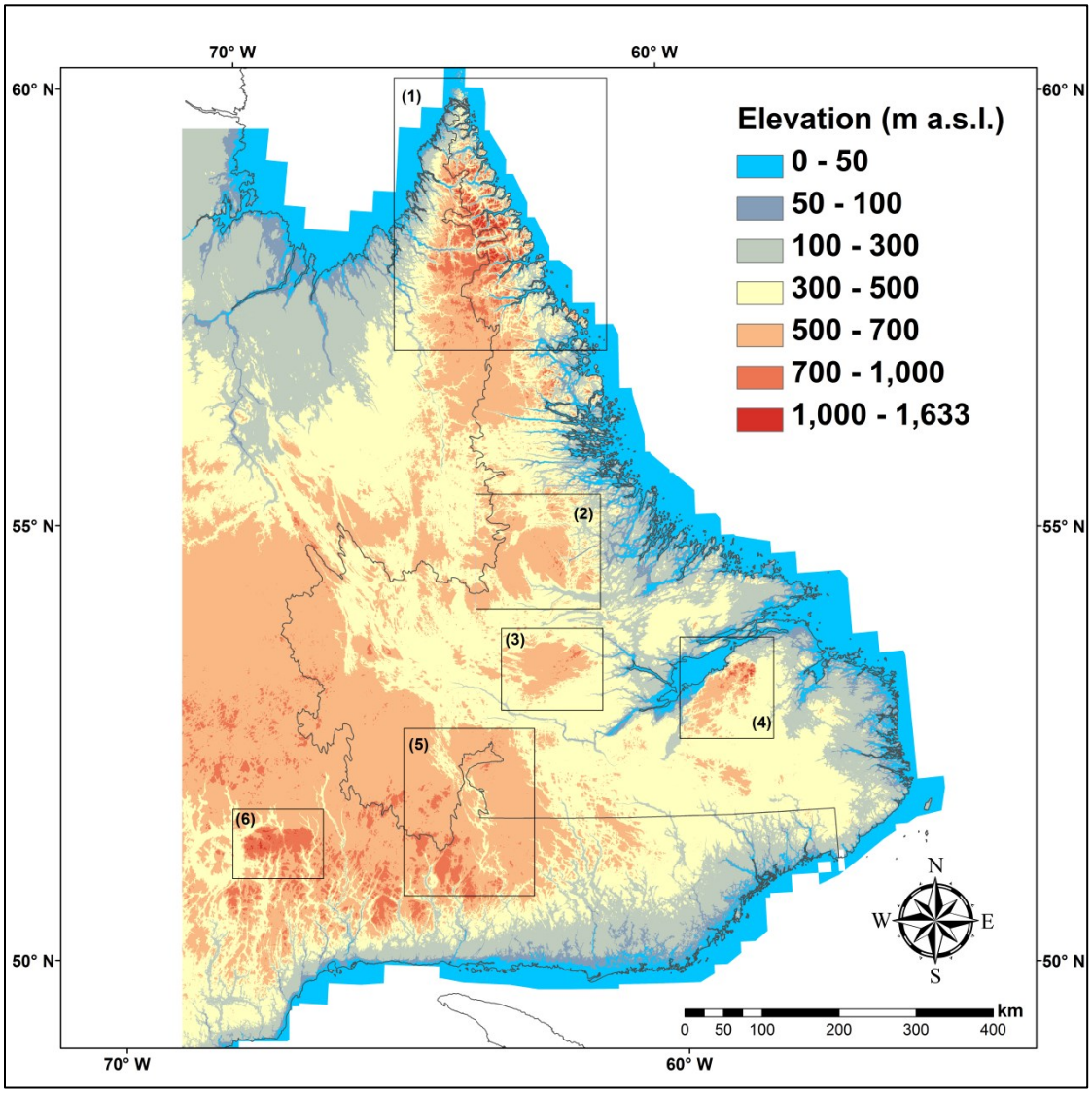

Figure 1-4: Digital elevation model of the eastern Labrador-Ungava region reclassified according to major elevation classes. Grey boxes depict mountainous regions described in *Section 1.3.1*. Distinct alpine regions highlighted on the map include: the Harp Lake Complex (~750 m a.s.l. [2]), the Red Wine Mountains (850 m a.s.l. [3]), the Mealy Mountains (1130 m a.s.l. [4]), the Romaine Hills (950 m a.s.l. [5]) and the Groulx Mountains (~1000 m a.s.l. [6]) (Figure 1-4).

At the landscape scale, Labrador's glacial history resulted in extensive areas of drumlins, eskers, megaflutes, megalineations, moraines and ribbed moraines which demarcate both the former position of the LIS and the evolution of ice sheet deglaciation (Clark et al. 2000). In upland zones, such as the Mealy and Red Wine Mountains, landscapes are glacially-scoured with rounded hills and large incised river valleys. In the Torngat Mountains, differential patterns of glacial erosion have formed deep U-shaped valleys at low elevations adjacent to mountain-tops that are relatively uneroded due to the presence of non-erosive cold-based ice at the LGM (Staiger et al. 2005). Across much of eastern Labrador-Ungava, the surficial geology consists of till blankets and veneers with small areas of glacio-fluvial and glacio-lacustrine surface covers along the Québec north shore and southern Labrador (Figure 1-5). Undivided exposed bedrock is the primary surface cover for most of the upland coastal and mountainous environments in eastern Labrador-Ungava. However, at lowland coastal sites, where marine invasions were extensive, glacio-marine and marine sediments are present, particularly along Ungava Bay and near the mouth of Lake Melville in central Labrador (Figure 1-5). The post-glacial marine limit varies from 150 m a.s.l. in southeast Labrador to 0 m a.s.l. at the northernmost tip of Labrador (Occhietti et al. 2011). Consequently, post-glacial marine deposition is most prevalent along the east coast in lowland environments, at the mouth of Lake Melville, and in southern Labrador near the Strait of Belle Isle. Due to elevated topography in much of coastal Labrador, the extent of marine invasion was less extensive than in the lowland-dominated coastline bordering Ungava Bay (Occhietti et al. 2011) .

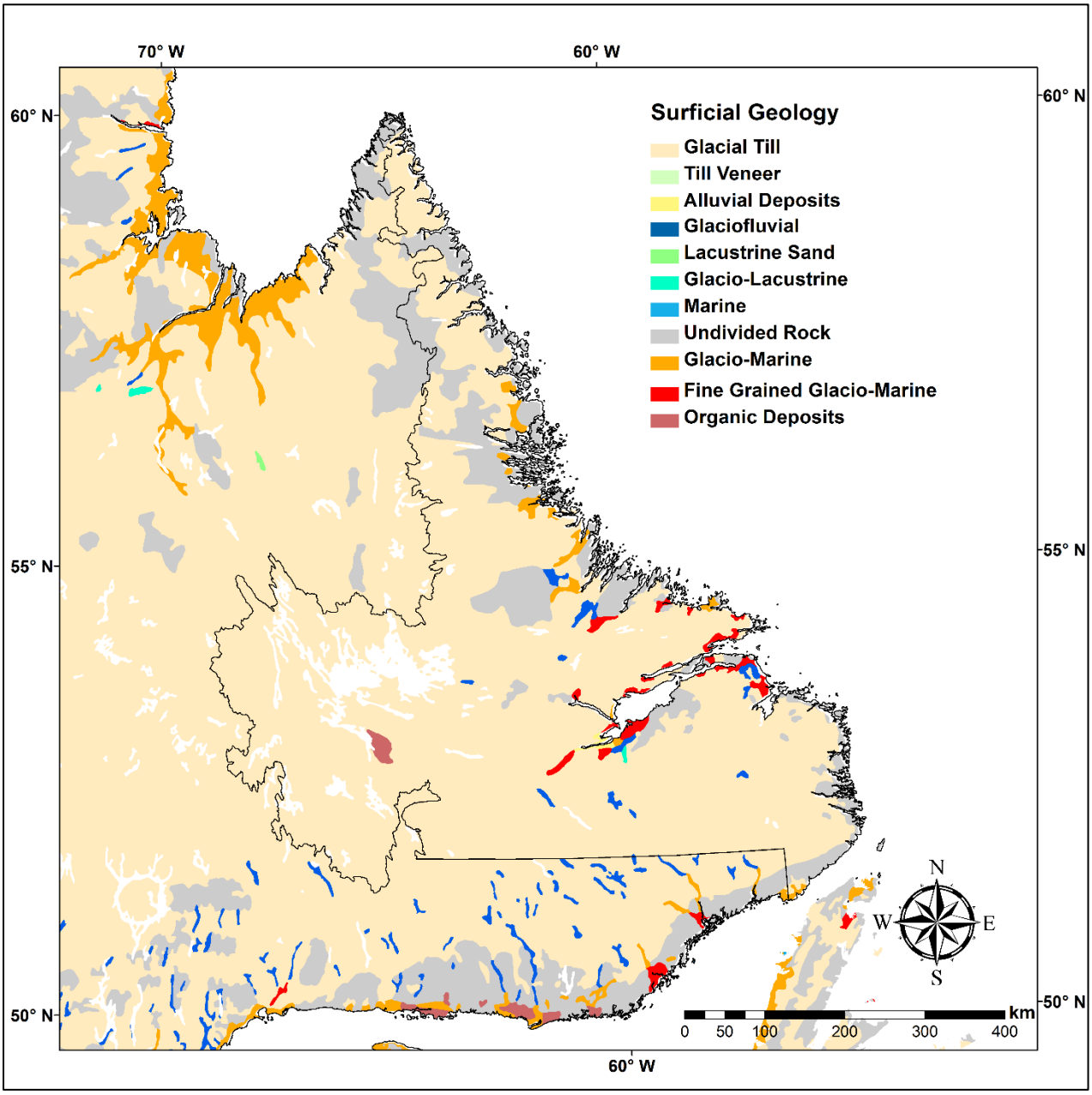

Figure 1-5: Surficial geology of the eastern Labrador-Ungava provided by the Geological Survey of Canada at a 1: 5,000,000 scale (Fulton 1995).

1.3.2 The climate of Labrador

Labrador is one of the most climatically sensitive regions in Canada, primarily because of the influence of the cold Labrador Sea current to the east and the warm Gulf Stream to the south (Banfield and Jacobs 1998). Labrador's climate is strongly associated with changes to northwest Atlantic sea surface temperatures and large-scale climatic oscillations (D'Arrigo et al. 2006) making the region prone to considerable interannual variability in air temperature (Way and Viau 2015). Regional air temperatures are also very sensitive to the impacts of volcanic eruptions, esspecially on atmospheric circulation (Way and Viau 2015). The regional climate of Labrador is dominated by the Labrador Current that transports cold arctic water south and cools the east coast and western Newfoundland. The position of the Arctic air masses and the Canadian Polar Trough in addition to the seasonal sea ice cover in the Hudson's Bay and the Hudson Strait create conditions which allow deep penetration of cold air into the interior of Labrador during winter and spring. Seasonal sea ice cover along the Labrador coastline typically begins to form in the month of December and does not dissipate until late May or early June. Consequently, sea surface temperatures along the Labrador coastline remain cold during the summer and do not warm up until the fall, affecting air temperature patterns in these seasons.

A century-long warming trend is apparent in the meteorological records for the region showing that average air temperatures increased by ~1.8°C from 1850 to 2016 (Figure 1-6) with the largest temperature increase occurring in the winter (2.0°C) and the smallest occurring in the spring (1.0°C). Previous publications had not identified a significant warming trend in Labrador over much of the 20th century (Jacobs et al. 1996; Banfield and Jacobs 1998). However, rapid regional warming began at the end of the 20th century and has continued to present (Brown et al. 2012; Way and Viau 2015). This trend is largely driven by anthropogenic climate change but varies on decadal timescales due to natural climate variability induced by anomalous atmospheric circulation patterns, sea surface temperatures in the North Atlantic and volcanic eruptions (Way and Viau 2015) (see Figure 1-6). Correspondingly, many climate models have difficulty simulating the degree of variability present in the region's climate (Way and Viau 2015). Due to rapid warming, the 0°C mean annual air temperature isotherm has been displaced northward by ~200 km over the past century.

Owing to a lack of long-term data on snowfall in Labrador and northeastern Québec it is not possible to characterize century-scale trends for snow conditions the region. However, Brown et al (2012) note that between 1950/1951 and 2006/2007 decreases in snow cover duration ranging from -4 days to -17 days have been noted in central Labrador and northern Québec. Further analysis is required for a more comprehensive assessment of the state of snow and its variability through time in the region.

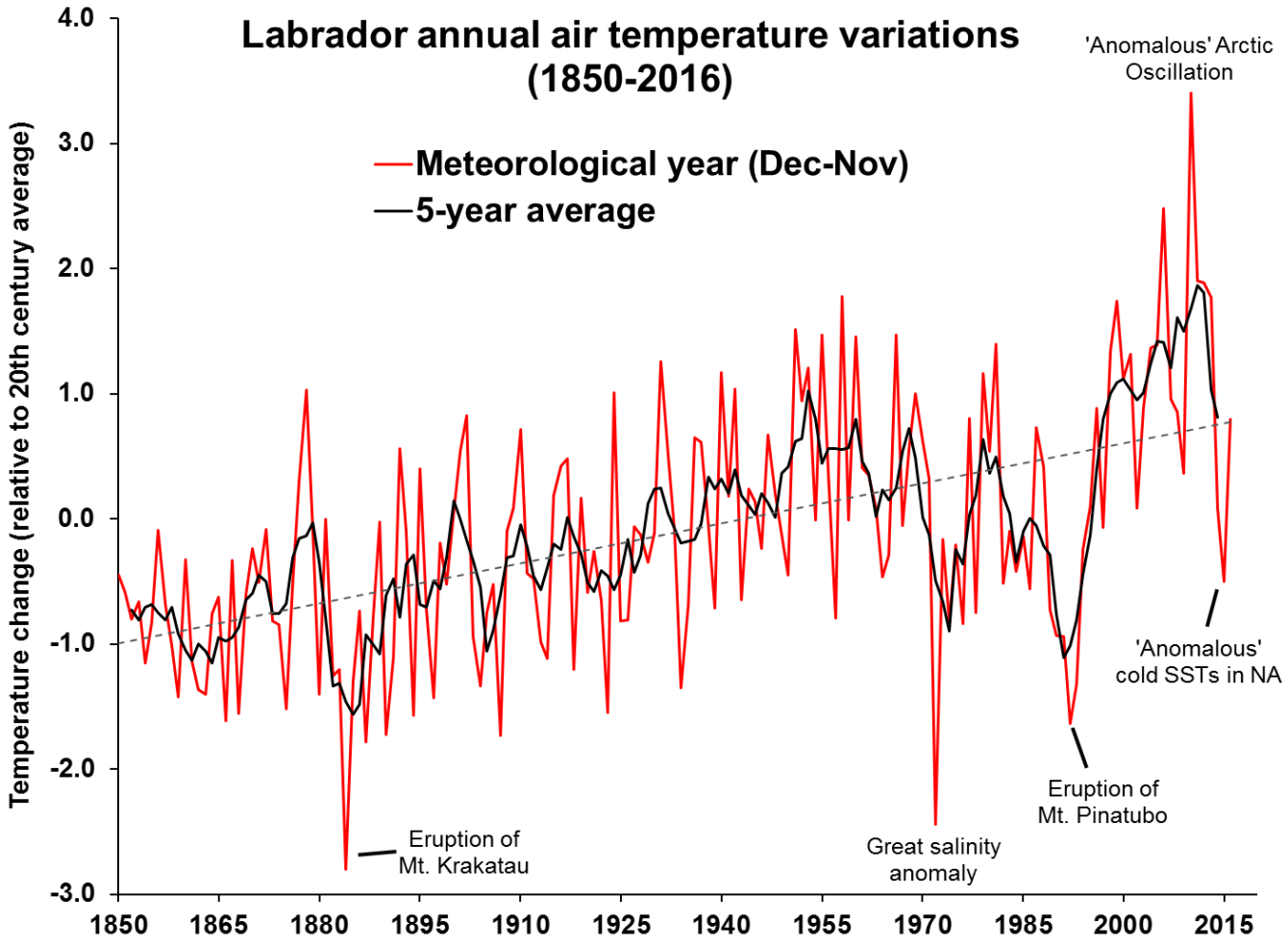

Figure 1-6: Labrador-wide annual average air temperature variations (1850-2016) updated from Way and Viau (2015). Labelled features indicate large deviations from the long-term trend associated with volcanic eruptions (Mt. Krakatau, Mt. Pinatubo), oceanic conditions (Great salinity anomaly, 'Anomalous' cold sea surface temperatures [SSTs] in the North Atlantic [NA]) and atmospheric teleconnections ('Anomalous' Arctic Oscillation).

1.3.3 The forests of Labrador

Biogeographically, Labrador encompasses many different vegetation biomes ranging from Subarctic deciduous forests to Arctic Cordilleran tundra (Figure 1-7). Wetlands cover ~5% of Labrador's land area with string bogs found throughout the interior and raised bogs in southeastern coastal areas (Roberts et al. 2006). Due to the presence of highland areas in both the coastal and continental portions of Labrador it can be difficult to interpret the true position of the Arctic treeline (Figure 1-8). The northernmost trees in Labrador are found where the Koroc River valley (Québec) meets the Labrador border at 58.7°N but upright trees are typically absent in most areas north of ~57°N (Elliott and Short 1979). In the interior of Labrador, the position of the elevational tree line varies with latitude and continentality, roughly occurring at 825 m a.s.l. near Labrador City at 53°N and declining towards the north and east. Along the outer Labrador coast, tree cover is limited, with areas of tundra as far south as 50°N due to shorter, cooler growing seasons and windy conditions (Roberts et al. 2006) (Figure 1-8). The northernmost trees consist of Eastern Larch and Black Spruce stands, although farther south along the coast the forest is typically composed of White Spruce (Payette 2007). In southern Labrador, forests are dominated by White and Black Spruce with some local areas being dominated by Balsam Fir, Jack Pine, Tamarack, and Birch stands (Payette 1993).

Labrador's postglacial vegetation history included periods of moderate boreal forest expansion and contraction in concert with centennial-scale variations in regional climate and fire regimes. During the Holocene Hypsithermal (~4000 BP), forests in Labrador reached elevations approximately 70 m above present tree line and likely attained their maximum latitudinal extent. However, northwards expansion was partially constrained by mountainous terrain in northern Labrador (Lamb 1985; Payette 1993; Payette 2007). Forest contraction likely occurred during the Little Ice Age following fires and other disturbances, and climate deterioration over this period did not permit forest regrowth at higher elevations (Payette 2007). Although recent regional warming has resulted in observations of treeline migration (Simms and Ward 2013), the expansion of contemporary forest cover northwards and to high elevations in Labrador is limited by insects, seedling recruitment and local geomorphology (Payette 2007; Trant et al. 2011; Trant and Hermanutz 2014; Jameson et al. 2015; Trant et al. 2015). In contrast, shrub cover in northern Labrador has dramatically increased (Fraser et al. 2011; Ju and Masek 2016). This shrub expansion has occurred primarily at low elevations in the southern section of Torngat Mountains National Park (Fraser et al. 2011).

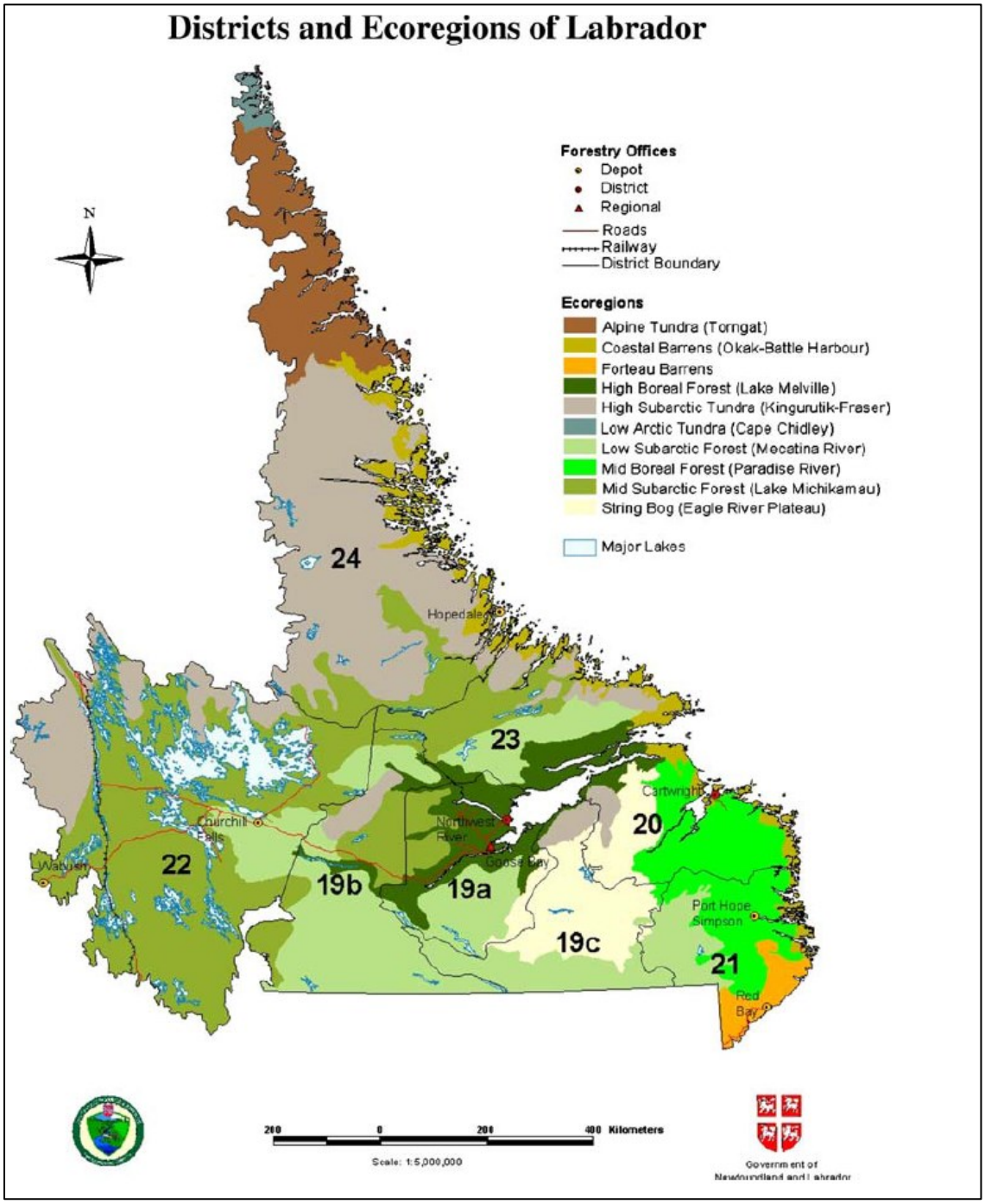

Figure 1-7: Spatial distribution of forest ecoregions of Labrador (from Roberts et al. 2006).

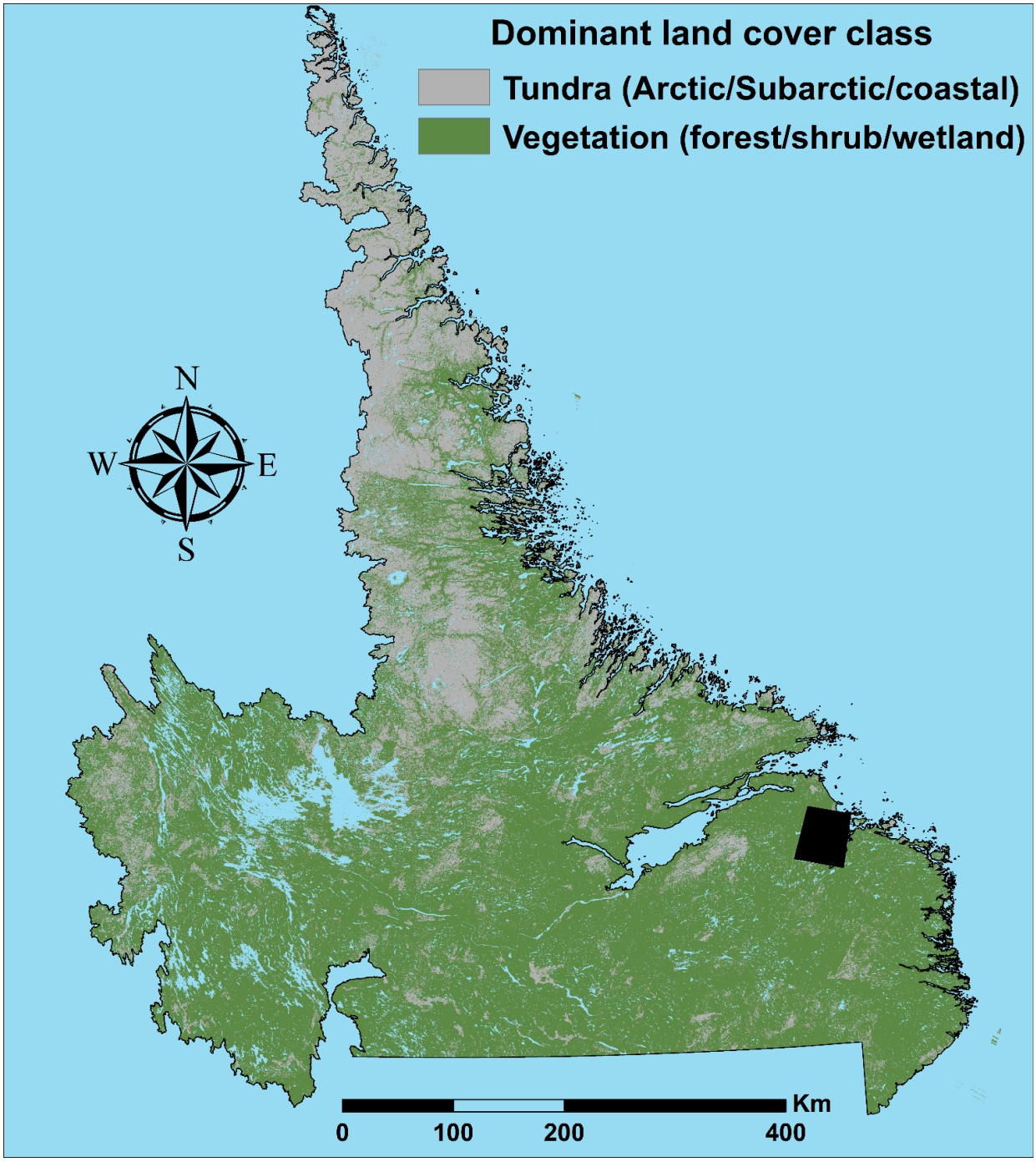

Figure 1-8: Distribution of vegetated and tundra dominated environments in Labrador according to a recently developed high resolution vegetation classification (Olthof et al. 2015). Note: Areas for which suitable satellite imagery were not available are shown in black.

1.3.4 History of observations of permafrost in Labrador

The presence of permafrost has been noted during resource development and exploration in Labrador but these observations have not previously been compiled into a comprehensive inventory. A review of the extant scientific and technical literature suggests that permafrost patches exist throughout all major climatic regions in Labrador under various vegetation types. Regional summaries are provided below and have also been compiled into maps depicting identified permafrost sites in non-wetland (Figure 1-9) and wetland (Figure 1-10) environments.

Western Labrador

Permafrost was encountered frequently in upland tundra zones at Schefferville during the establishment of iron ore mining operations in the 1950s, with thicknesses exceeding 120 m in the highest terrain north of Schefferville (Ives 1960; Nicholson 1979). Permafrost was found to be widespread above 680 m a.s.l. in areas which remain windblown in the winter, while below that elevation only relict bodies of permafrost were observed. Permafrost was encountered to a thickness of 60 m at elevations above 830 m a.s.l. about 200 km south of Schefferville during mining operations in Labrador City and Wabush Lake (Ives 1960; Andrews 1961). Palsas were also noted above 750 m a.s.l. on Mount Wright, 25 km from Labrador City, but these were inferred to have been destroyed by mining operations several decades ago (Brown 1979).

Permafrost with a thickness exceeding 5.5 m was encountered during excavations of a peatland mound in a small wetland along the route of the electrical transmission line from Twin Falls to Labrador City (Andrews 1961). A large body of permafrost was also encountered during the construction of the Northern Lands Company railway ~6 km west of the junction with the Québec North Shore and Labrador (QNS&L) railway at an elevation of 535 m a.s.l. (Andrews 1961). Frozen ground was found in the near-surface (upper 2 m) and was continuous across a 500 m transect (Andrews 1961). Railway construction projects such as the QNS&L encountered permafrost at various locations but details were only recorded at problematic sites where additional railroad maintenance was required (Pryer 1963). Sorted patterned ground and polygonal cracks were also observed on summits reaching 900 m a.s.l. north of Sept-Iles, while palsas were found above 800 m a.s.l. (Brown 1979). Palsas were also found at other locations throughout the Laurentian Scarp at similar elevations in areas north of Sept-Iles.

Central Labrador

The first observations of permafrost in central Labrador were of fields of palsas in coastal wetlands near Rigolet and Double Mer (Hustich 1939). According to Belcher (1949), permafrost was also encountered in poorly-drained sand terraces near Goose Bay during the construction of the military base. However, over the past 60 years there have been no other permafrost sites documented in the areas adjacent to Goose Bay. Roger Brown's 1960-era surveys of permafrost conditions in Labrador noted additional examples of palsas in wetlands 60 km northeast of Goose Bay and on Neivisik Island in Lake Melville (Brown 1975; Brown 1979). While investigating the Mealy Mountains, Brown also noted sorted patterned ground features and polygonal cracks at 1080 m a.s.l. which he inferred to be indicative of permafrost. The existence of permafrost in the Mealy Mountains has since been confirmed by Jacobs et al. (2014) at 995 m a.s.l. where a mean ground temperature of -1.9°C was measured at 1 m depth between 2001 and 2009. Further west, near Churchill Falls, bodies of permafrost 8 m thick were encountered on the floor of Bonnell Canyon (360 m a.s.l.) on the steep-sided Unknown River valley (Andrews 1961). In the 1960s, Brown (1975; 1979) also noted tree-covered retrogressive thaw slumps on north-facing slopes along the same river valley. Isolated patches of permafrost were also encountered in glacial tills during construction of the reservoir for the Churchill Falls hydroelectric plant on islands in Lobstick Lake and Ossokmanuan Lake (Brown 1979).

Coastal Labrador

Permafrost in the barren lands of coastal Labrador has been described at some locales but detailed field investigations and mapping of permafrost has not been undertaken. The existence of permafrost in the coastal barrens ecoregion has typically been recognized by the presence of palsas which are found in as far south as Blanc Sablon (Roberts et al. 2006). Palsas in coastal Labrador have been used by the Inuit of Labrador to keep meat fresh by storing it beneath layers of exposed peat (*Patricia Way, personal communication*). The earliest reports of palsas in coastal Labrador were by Hustich (1939) and Wenner (1947) who identified several palsa fields in the regions around Cartwright and Rigolet. During airborne field surveys of the southeastern Labrador coastline in the 1960s, palsas and peat plateaus were recorded for Red Bay, with larger palsa fields near the community of Cartwright and on nearby Huntington Island (Brown 1975; 1979). Other palsas located at Blanc Sablon were described in detail by Dionne (1984) and Dionne and Richard (2006). Palsas in this area were also investigated with geophysics by Séguin and Dionne (1992) and have been instrumented by Le Centre D'Études Nordiques with a temperature monitoring borehole that is still active (Allard et al. 2014). Along the north shore of Québec, organic

mounds reaching 1.75 m in height have been noted between Sept-Iles and Blanc-Sablon. No evidence of frost is found in these mounds and they are inferred as having been formed following forest fires due to differential deposition of organic debris and frost heaving of stones in some cases (Dionne and Gérardin 1988). Brown's surveys (1975; 1979) represent the most comprehensive assessment to date of permafrost in southeastern Labrador but describe the presence of permafrost at only a few sites along the coast.

A joint ecological survey conducted over three years in the late 1970s by the Newfoundland Department of Forest Resources and Lands, and the Lands Directorate of Environment Canada noted numerous palsas in lowland coastal areas in eastern Labrador (Figure 1-10). In total, the ELS identified 142 sub-regions where palsas formed a large proportion of the landscape with these areas primarily occurring along the north shore of Lake Melville and Groswater Bay near Double Mer and Rigolet. The ELS also documented large palsa fields along the outer Labrador Sea coastline from Sandwich Bay to Makkovik. The presence of permafrost near some of these sites was also noted by Brown (1975; 1979) who also identified retrogressive thaw slumps on south-facing river valleys near Rigolet, although these features have not been relocated. Further north along the coastal barrens, mapping during construction of the National Topographic Database identified numerous palsa fields north of Nain and on several of the islands (Natural Resources Canada, various dates). At the northernmost end of the coastal barrens in Okak, palsas were also described by Elias (1982) who excavated a 2.15 m high feature with small shrubs on top. Overall the existing literature suggests that nearly all permafrost patches in coastal Labrador, at least towards the south, exist as palsas and peat plateaus within the coastal barrens (Roberts et al. 2006).

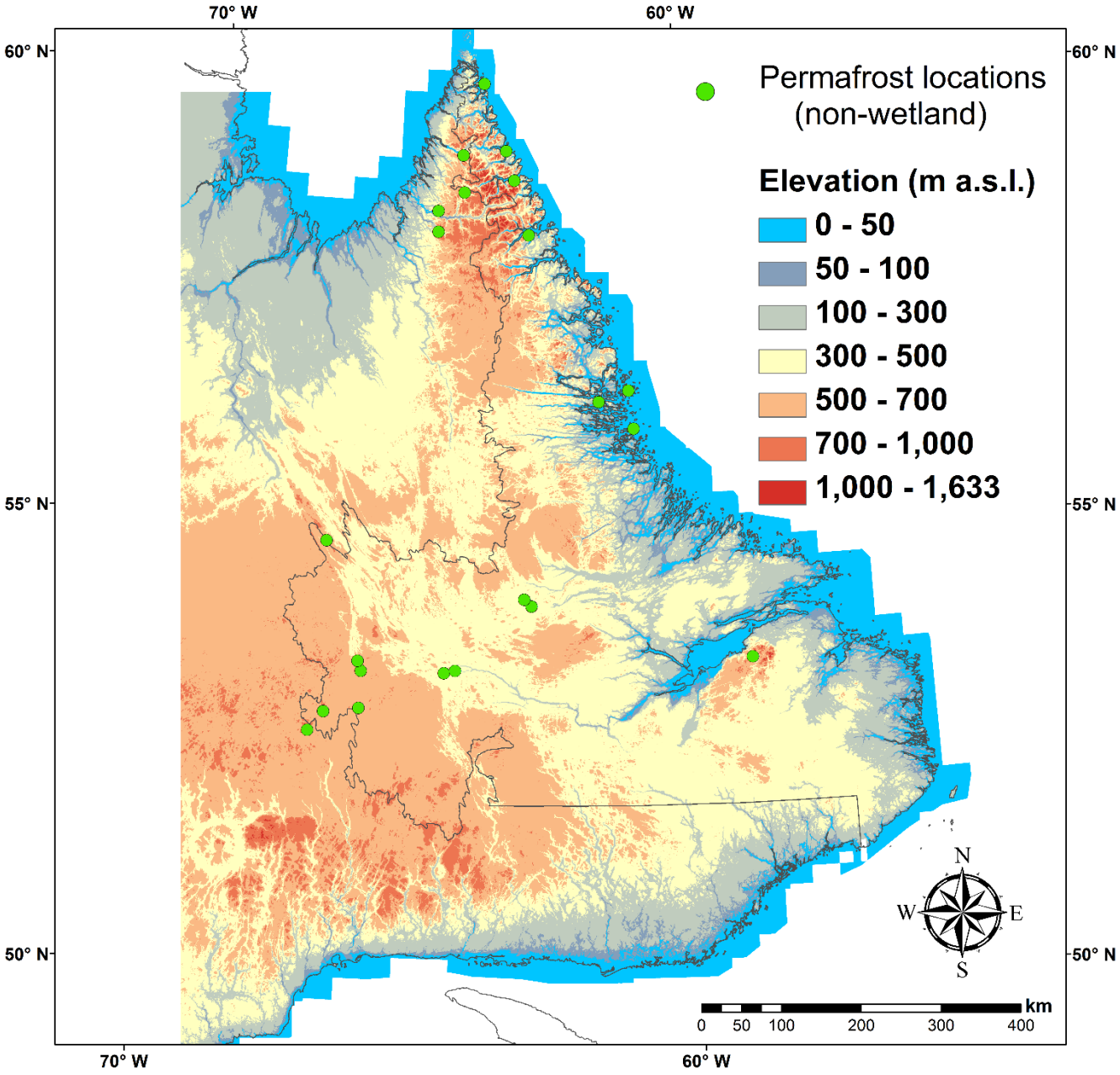

Figure 1-9: Composite map of non-wetland permafrost observations assembled from various historical sources discussed in the text.

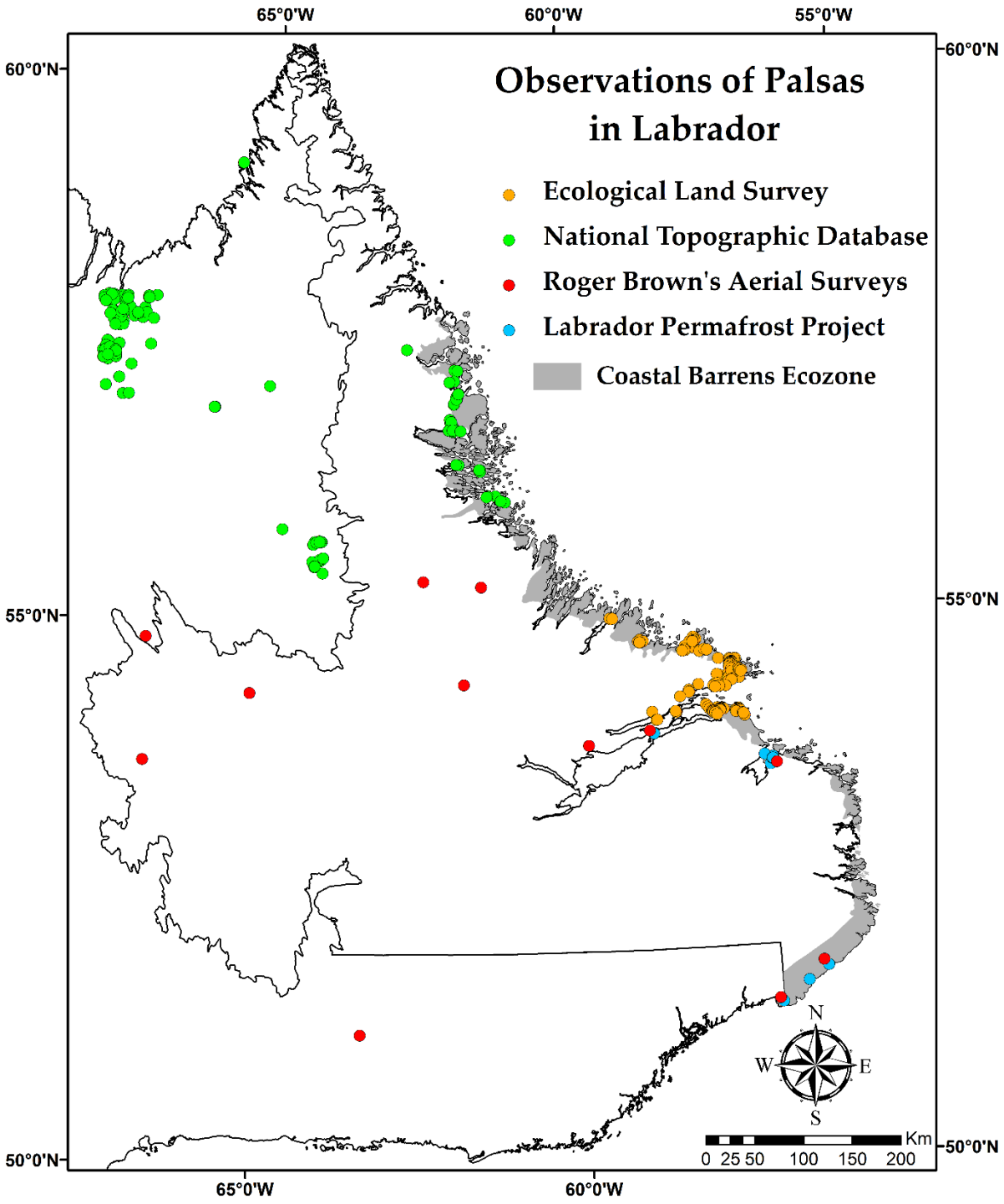

Figure 1-10: Composite map of palsas in the eastern Labrador-Ungava, including observations made as part of the current thesis.

Northern Labrador

Permafrost in the interior region of northern Labrador, which generally extends from north of Schefferville to inland from Nain, is amongst the least well-documented in the Labrador-Ungava region According to the National Topographic Database (Natural Resources Canada) there are numerous palsa fields west of Mistasin Lake, northwest of Border Beacon and to the southeast of Kuujjuaq. A high density of palsas were also mapped to the northeast of Kangiqsualujjuaq. Archeological investigations of abandoned Inuit settlements spanning the northern coastline revealed permafrost at Avayalik Island (Jordan 1980) and adjacent to Inuit dwellings at Komaktorvik Fiord, Iglosiatik Island, Oakes Bay and Nachvak Fiord (Woollett 2010; Butler 2011). Palsas were mapped by Natural Resources Canada in the organic soils north of Nain and on several of the coastal islands during the creation of the National Topographic Database. Soil sampling confirmed the presence of permafrost at five sites on mountain summits between Saglek Fiord and the community of Kangiqsualujjuaq, but did not encounter near-surface permafrost at another eight sites (Hendershot 1984; Hendershot 1985). Ground temperatures in several permafrost boreholes near Kangiqsualujjuaq were monitored from 1988-2014 (Allard et al. 2014). Temperatures are between -1°C and -2°C and active layers exceed three metres (Smith et al. 2010).

The existence of rock glaciers and ice-cored moraines in the Torngat Mountains was noted by Way et al. (2014). A preliminary inventory (Way and Lewkowicz 2014) found more than 150 talus derived or glacier-derived rock glaciers implying widespread permafrost (Figure 1-11). Surprisingly, excavations of seven gelifluction lobes along the coast on the south shore of Nachvak Fiord encountered no near-surface permafrost (Evans and Rogerson 1988). Permafrost was, however, encountered during waterjet drilling at the establishment of a Parks Canada thermal monitoring station near Ramah Bay but dataloggers show that this ground has remained unfrozen since the original installation of the monitoring apparatus (*Darroch Whitaker, personal communication, January 2016*). Deep active layers caused by coarse surficial sediment and exposed bedrock found throughout the Torngat Mountains make permafrost detection and monitoring difficult in the absence of geomorphic indicators.

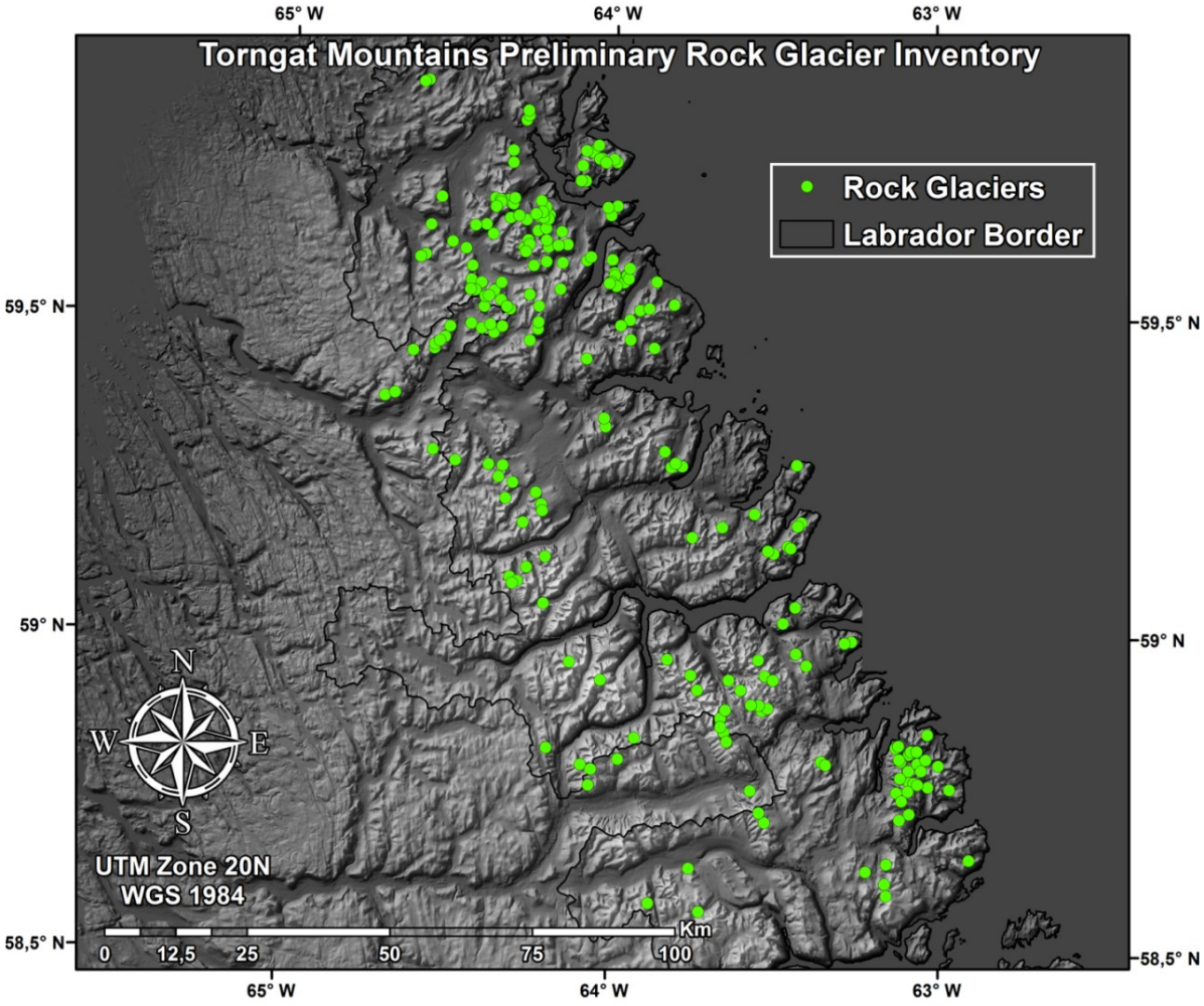

Figure 1-11: Spatial distribution of rock glaciers in the Torngat Mountains identified during preliminary mapping from SPOT5 satellite imagery (Way and Lewkowicz 2014).

Characterizations of regional permafrost distribution

The earliest map depicting permafrost limits in Labrador was produced by Brown (1960) using interpolated air temperature isotherms from active climate stations. Later field measurements by Ives (1960) and Andrews (1961) found that the southern limit of discontinuous permafrost was at least 200 km farther south. Field surveys in the late 1960s (Brown 1975; 1979) confirmed this finding, with the southernmost observations of permafrost noted at 51°N (Figure 1-12). After these early surveys, most field-based permafrost investigations in Labrador-Ungava focused on the Québec portion, with the easternmost studies occurring in Schefferville (Nicholson 1979; Granberg 1989) and Blanc Sablon (Dionne 1984; Dionne and Richard 2006). Permafrost distribution maps produced by Ives (1979), Allard and Seguin (1987), Heginbottom et al. (1995), Allard et al. (2012a) and Gruber (2012), all suggest that the southern fringe of the isolated patches permafrost zone in Labrador coincides with approximately 50°N, but differ considerably in their predictions for other parts of the region (Figure 1-13). Southeastern Labrador, for example, is within the isolated patches permafrost zone according to Heginbottom et al. (1995), whereas Payette (2001) shows it as sporadic discontinuous permafrost. A recent global topoclimatic permafrost map developed suggests that the portions of this area closest to the coast do not exhibit permafrost (Gruber 2012). Substantial differences in permafrost zonation predictions also exist for the northern interior along the Québec-Labrador border where permafrost transitions from isolated patches to the continuous zone over a distance of about 200 km (Figure 1-13). It is evident that the various physiographic and topographic contrasts in Labrador, including mountain ranges (see Figure 1-5), make an accurate delineation of permafrost distribution a significant challenge.

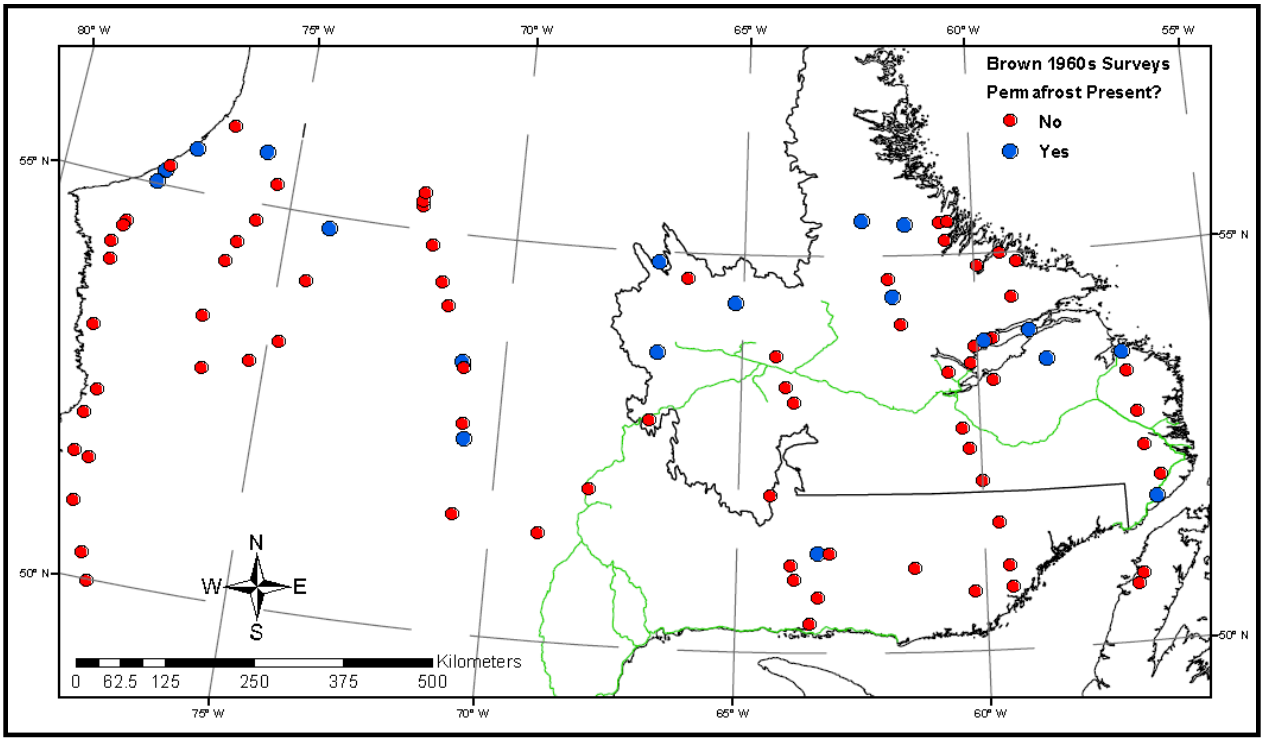

Figure 1-12: Map of southern Labrador-Ungava showing the distribution of sites visited by Brown (1975; 1979) during permafrost investigations in the 1960s.

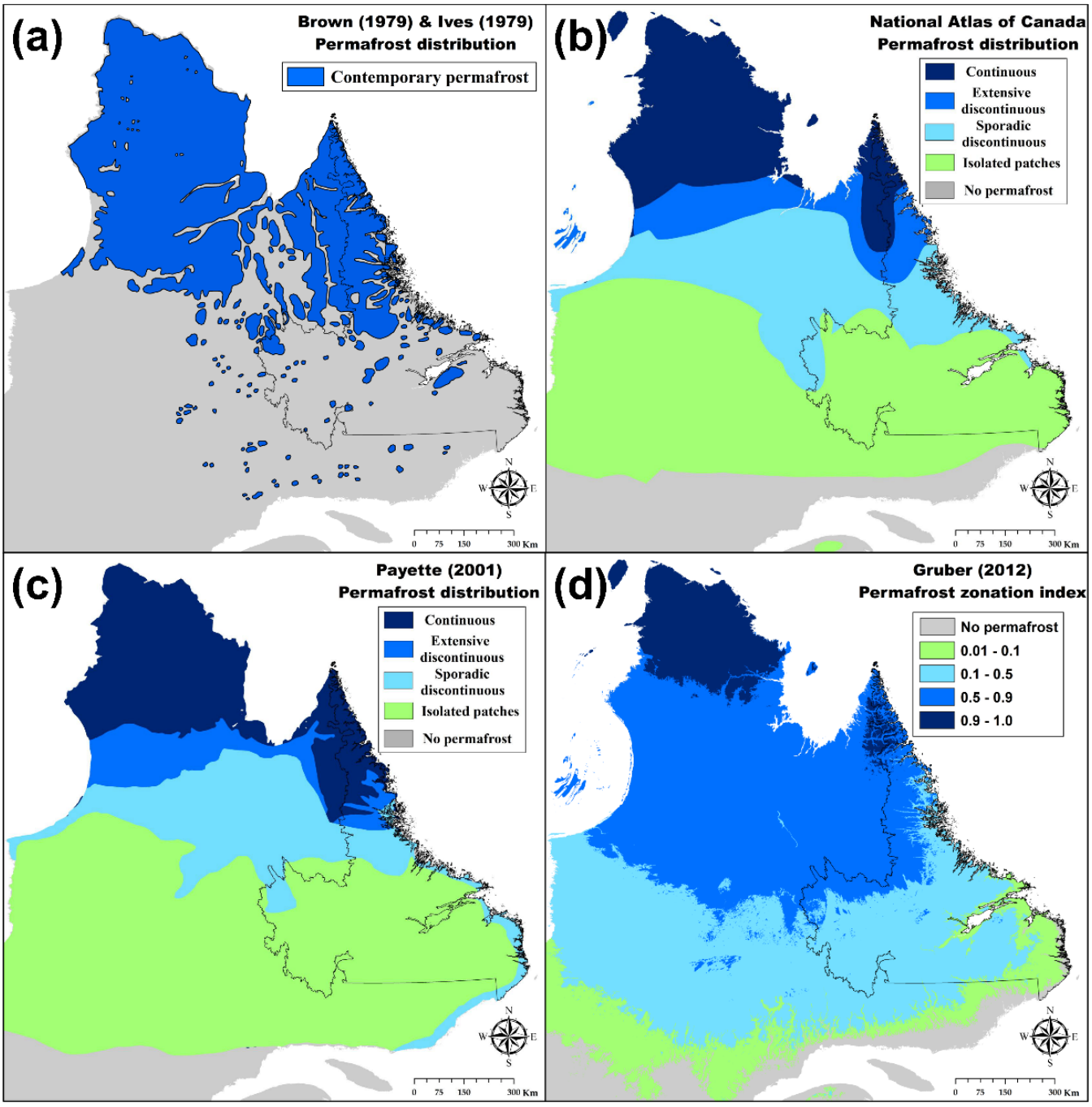

Figure 1-13: A subset of four existing maps of permafrost distribution in the eastern Labrador-Ungava region compiled by Way and Lewkowicz (2016). The maps shown were originally constructed by Ives (1979), Heginbottom et al. (1995), Payette (2001) and Gruber (2012).

1.4 Research methods

This section reviews the main methods used during the thesis research for permafrost detection, characterization, monitoring, and modelling. Specific details for individual study sites are given in the articles that constitute Chapters 2 to 6.

1.4.1 Frost-table probing, pit digging and instantaneous ground temperature profiles

Permafrost research widely employs the use of metal frost probes to detect the presence of the frost table (Mackay 1977). A frozen layer is interpreted as occurring when the probe is prevented from penetrating deeper into the soil. However, relying on probing alone for verification of frozen ground can be problematic as subsurface rocks and clays can cause a similar rebound or refusal (Leverington 1995) and because penetration can occur into the top of permafrost when soils are ice-poor (Mackay 1977). In these cases, probing using a temperature sensor and identifying the position of the 0°C threshold has been shown to be a viable alternative for active layer depth measurement (Mackay 1995). Direct determination of the presence of frozen ground in organic soils has also been widely conducted through manually digging pits to the depth of frost probe penetration (Leverington 1995) and inserting a thermistor into the ground to determine its temperature (Lewkowicz and Ednie 2004). An alternative approach consists of collecting instantaneous ground temperature profiles that can then be extrapolated to greater depths to infer the absence or presence of a frozen layer (James et al. 2013). A variation of this methodology uses four thermistors placed on a dowel at selected increments (typically 20 cm) attached to a four channel logger that continuously measures and displays ground temperatures at each thermistor position after the dowel has been inserted into the ground (Lewkowicz and Way 2014). The most challenging factor influencing direct detection of permafrost is that frozen layers can be due to both seasonal and perennial frost, so probing must be undertaken as late as possible in the thaw season to reduce the probability of misinterpreting seasonally frozen ground as permafrost (Lewkowicz et al. 2011).

Due to the presence of coarse surficial cover and deep active layers in Labrador, standard field techniques used for the detection of late-summer (typically between August and September) frozen ground including frost probing to 120 cm and instantaneous ground temperature profiles were often difficult to interpret, particularly in the absence of pit digging which was deemed unfeasible. Fieldwork was aimed to be completed as late in the thaw season as possible but this was not always practical due to logistical considerations. Correspondingly, it is possible that some additional active layer thickening may have occurred after our site visits and also that some locations interpreted to have thin permafrost may have in fact been late-lying seasonal frost or *pereletok* (Van Everdingen 2005b).

1.4.2 DC electrical resistivity tomography

DC electrical resistivity tomography (ERT) is a widely-used geophysical technique which measures changes in the electrical resistivity of the subsurface by sending electrical current through the ground between sets of contact points (electrodes). ERT profiles recorded along a transect can therefore indicate differences in the hydrological and thermal characteristics of the subsurface because the ground's resistance to electrical current is highly correlated with these and other variables (Hauck 2013). Although ERT has been most commonly used in the mineral exploration industry, its application to permafrost environments has become more widespread, particularly in the discontinuous zone (Hauck et al. 2003; Lewkowicz et al. 2011; Hauck 2013; You et al. 2013). Frozen ground is generally more resistive to electrical current than unfrozen ground, and ERT profiles can reveal the contrast between the two states. The contrast between unfrozen and frozen ground is particularly evident where cold permafrost adjoins warm unfrozen ground because the unfrozen moisture content of the ground in the permafrost body is much lower than in the surrounding sediments (Hauck 2013).

The depth of electrical penetration during ERT profiling depends on the spread of the electrode array and its survey length (excluding roll-along surveys) with typical penetration values for a standard 80 m transect being 12 m. ERT surveys in Labrador used an ABEM Terrameter LS profiling system with a Wenner electrode array configuration (Lewkowicz et al. 2011; Lewkowicz and Way 2014). Resistivity measurements must be processed using inversion software. In this thesis, RES2DINV software (Loke and Barker 1996; Loke et al. 2003) was used with iterations stopped once the RMS error was less than 5% or until the modelled errors did not appreciably decline (<1%) between iterations. These conditions were most often satisfied at the 4^{th} or 5^{th} iteration but in some rare cases were met at the 3^{rd} or 6^{th} iterations. Resistivity profiles were topographically corrected using slope measurements taken in the field.

Although ERT is a useful technique for permafrost investigations, it must be used in conjunction with other data in order to validate the results as there is no universally applicable resistivity boundary for discriminating between unfrozen and frozen ground (Hauck 2013). For example, in glacio-marine sediments on the eastern Hudson's Bay coastline, Fortier et al. (2008) used a 1000 Ω.m limit to delineate between unfrozen and frozen ground along ERT profiles, whereas in the organic soils of the southern Yukon, Lewkowicz et al. (2011) used values as low as 300 Ω.m. Common problems for the interpretation of ERT profiles include the presence of coarse, dry sediments which can have similar resistivities to those of warm permafrost (Hilbich et al. 2009) and the presence of bedrock at depth which typically has very high resistivities similar to, or exceeding those of cold permafrost (Lewkowicz et al. 2011). Validation of

ERT profiles using standard field methods for permafrost investigations is considered to be a necessity for interpreting ERT results.

1.4.3 In situ climate stations

The establishment of small, cost-effective climate stations at localized study sites is a widely-used technique in permafrost research for determining baseline air, surface and ground conditions (Lewkowicz 2008; Lewkowicz et al. 2012). *In situ* climate stations have been shown to be useful for permafrost investigations in the southern Yukon where a standardized approach to measuring air temperature, ground surface temperature, ground temperature and snow depth has been developed (Lewkowicz 2008; Lewkowicz et al. 2012).

Modified versions of the climate stations used in the southern Yukon were deployed in Labrador for permafrost mapping and monitoring (Table 1-1). Each station (Figure 1-14) consists of two Onset Hobo Pro v2 temperature loggers (model no. U23-003; ±0.21°C accuracy) storing bi-hourly measurements taken by external thermistors in a radiation shield located between 190-235 cm above the ground depending on the inferred site's snow thickness, ~2 cm below the ground surface, and at two depths in the ground typically separated by 25 or 50 cm with the deepest being at the maximum penetration depth of a frost probe. The deepest thermistor is considered an approximation for the temperature at the top of permafrost (TTOP), particularly when probing encounters a frost table. At each station, snow depth is approximated using data collected by vertical arrays of individual Maxim Integrated™ thermochron iButton temperature loggers (model no. DS1921G; ±1°C accuracy) placed at various intervals (typically 10 cm, 20 cm, 30 cm, 40 cm, 50 cm, 60 cm, 80 cm, 100 cm, 140 cm, 180 cm). This low-cost method allows snow depth to be estimated by comparing temperatures recorded at different heights along the array with the iButtons covered by snow which show less diurnal temperature variability than exposed iButtons (Lewkowicz 2008). As part of the Labrador Permafrost Project, climate stations were deployed at a total of 40 sites in southern and central Labrador and eastern Québec, covering broad latitudinal, longitudinal and elevational gradients.

Figure 1-14: Example of a Labrador Permafrost Project monitoring station located along the Trans-Labrador Highway in eastern Labrador. Data being collected at this monitoring station include air temperature (215 cm height), ground surface temperature (1 cm depth), ground temperatures (70 cm & 120 cm depths) and snow depth.

1.4.4 Ground thermal monitoring

The impacts of climate change on permafrost are typically evaluated by long-term monitoring of ground temperatures in boreholes (Smith et al. 2005; Romanovsky et al. 2010; Throop et al. 2012). Thermal monitoring is also integral to the development of process-based numerical models that can be used to evaluate the transient effects of changing environmental conditions (Zhang et al. 2003). Ground temperatures are most reliable for thermal modelling when they are measured at depths which exceed the depth of zero annual amplitude (Romanovsky et al. 2010). However, such boreholes are often expensive to drill and may be logistically implausible in many environments. A cost-effective means of drilling shallow boreholes is to use water-jet drilling to penetrate ice-rich permafrost and then case the hole with PVC tubing. Thermistor cables linked to data loggers (typically Hobo or RBR) can then be placed at selected depths within the tubing to produce annual temperature profiles (Figure 1-15). Five boreholes were drilled in this way in southeastern Labrador, to a maximum depth of 5.7 m and each was instrumented with Hobo V2 loggers which recorded bi-hourly temperatures (model no. U23-003; ±0.21°C accuracy). Although the boreholes are quite shallow, some extend through the permafrost and/or reach the depth of zero annual amplitude.

Where waterjet drilling is logistically unfeasible, shallow ground temperatures can also be used to characterize permafrost conditions using data loggers placed at depths ranging from 50 cm to 125 cm. This technique is particularly useful in coarser soils and at sites with deep active layers. This approach was widely employed across Labrador using Maxim Integrated™ thermochron iButton temperature loggers (model no. DS1922L; ± 0.5°C) placed in 1.9 cm diameter CPVC tubes inserted into the ground to their deepest attainable depths. The loggers were left in place for 12 months or more to allow annual ground temperature to be calculated, and hence to assess the likelihood of permafrost presence or absence at greater depths.

Figure 1-15: Photograph of covered borehole established at Cartwright, NL using water-jet drilling during the summer field season of 2014.

1.4.5 Spatial modelling of input climate data

Modelling of permafrost conditions across large spatial domains requires accurate climate datasets at a high spatial resolution. These climate datasets are typically derived from interpolating weather station data and are used in a variety of environmental applications ranging from climate research to forest sciences (Harris et al. 2014). Early generations of air temperature maps used for permafrost boundary delineation often used isotherms estimated from active meteorological stations (e.g. Brown 1960). However, these maps typically did not consider the elevation and coastal gradients present at the regional scale. Recent developments in computational capacity coupled with increases in available meteorological station data and environmental datasets (e.g. digital elevation models, satellite skin temperatures) have led to the development of topoclimatic datasets for a wide variety of areas ranging from the entire globe to the local-scale (Hijmans et al. 2005; Hopkinson et al. 2012a; Aznar et al. 2013; Kilibarda et al. 2014; Oyler et al. 2015). Although there are a variety of spatial interpolation techniques which have been employed for temperature data, the most commonly used methods employ multivariate forms of kriging or thin plate splines. Prior pan-Canadian work has evaluated thin plate splines as being a reliable approach for interpolation at the regional scale (Price et al. 2000; Milewska et al. 2005) with generated climate data available at a 10 km resolution (Hutchinson et al. 2009). In a follow-up study, Hopkinson et al. (2012a) showed that optimization of spatial models could be done through the incorporation of shorter climate stations that did not meet length requirements for climate normal calculations. Way and Bonnaventure (2015) recently tested this hypothesis in the sparse meteorological network of Labrador-Ungava showing that infilling techniques, when used on short climate records, improved the accuracy of simple spatial models in the region.

Infilling techniques with advanced interpolation approaches to the historical climate station network across Labrador allowed for the creation of gridded climate datasets (Chapter 2) that were used as inputs for spatial modelling of permafrost conditions (Chapter 6).

1.4.6 Spatial modelling of temperatures at the top of permafrost (TTOP)

Spatial modelling of permafrost conditions has been undertaken across the Northern Hemisphere using a variety of approaches that enable calculation of permafrost temperatures, distribution and/or susceptibility to future climate change (e.g. Gruber 2012; Gisnås et al. 2013; Pastick et al. 2015; Westermann et al. 2015a). Permafrost modelling across space is typically completed using analytical, numerical or empirical models (Singh et al. 2011). The first two approaches are based on simplifications of physical processes whereas the last uses field data with statistical modelling to characterize specific parameters (e.g. permafrost distribution). Although there are advantages and disadvantages with each

general approach, analytical models have been most widely-employed to permafrost environments because they require fewer inputs than numerical models and unlike empirical models, are based on physical principles.

The temperature at the top of permafrost model (TTOP) was used in this thesis and refers to the temperature at the base of the active layer where it meets the top of permafrost or base of seasonal freezing in seasonally frozen ground. TTOP is an analytical model developed by Smith and Riseborough (1996) and discussed in detail by Smith and Riseborough (2002) and Riseborough (2004). TTOP uses minimal climatic and environmental inputs to estimate the equilibrium temperature at the top of permafrost at local-to-regional spatial scales. The TTOP model is simplified and hence uses climatic parameters, air-to-ground transfer functions and ground characteristics to estimate the temperature at the top of permafrost by estimating a site's nival, surface and thermal offsets. The standard formulation of the TTOP model is given in **EQ. 1-1**.

EQ. 1-1

$$T_{Top} = \frac{(\frac{k_T}{k_F} n_T I_{TA} - n_F I_{FA})}{P}$$

$where$:

$T_{Top} = Temperature\ at\ the\ top\ of\ permafrost\ (°C)$;

$k_T = Thermal\ conductivity\ of\ thawed\ ground\ (Wm^{-1}K^{-1})$;

$k_F = Thermal\ conductivity\ of\ frozen\ ground\ (Wm^{-1}K^{-1})$;

$n_T = Scaling\ factor\ between\ air\ and\ surface\ thawing\ index$;

$n_F = Scaling\ factor\ between\ air\ and\ surface\ freezing\ index$;

$I_{TA} = Cumulative\ air\ thawing\ degree\ days\ (°Cs)$;

$I_{FA} = Cumulative\ air\ freezing\ degree\ days\ (°Cs)$;

$P = Period\ (typically\ 365\ days)$.

The TTOP model assumes stationary conditions in terms of the underlying climate and therefore reflects equilibrium rather than transient conditions. As a result, it can produce errors of up to 1°C under transient conditions, particularly when TTOP values approach 0°C (Riseborough 2007). TTOP errors are maximized when stronger climate trends occur and as time progresses, particularly between 50 and 100 years from an initial state. However, multi-year averaging of results can reduce the errors associated with year-to-year variability in TTOP values (Riseborough 2007). Errors in TTOP values are also introduced

with the development of near-surface taliks, in particular when the talik is relatively thin (<10 m). These errors largely relate to the simplified nature of the TTOP model which does not consider ground heat flows and permafrost established during previous climatic conditions.

Due to the latent heat required to melt ground ice, the TTOP model is less likely to be accurate where permafrost is ice-rich and/or ecosystem-protected but has been shown to be a robust estimator of permafrost conditions (and limits) where permafrost is ice-poor and/or contemporary (Riseborough 2004; Riseborough 2007). The TTOP model is computationally efficient compared to transient models such as the northern ecosystem soil temperature model (Zhang et al. 2003) and requires fewer inputs for permafrost estimation across large spatial domains (Riseborough et al. 2008). The implementation of a TTOP model across a large area requires gridded inputs which summarize the local near-surface air and ground climatological values, as well as surficial geology and vegetation information for parameterizing thermal conductivities and air-to-ground scaling factors (Smith and Riseborough 2002).

According to Smith and Riseborough (2002), the most important control on the limit between the continuous and discontinuous permafrost zones is nf (see Eq. 1-1) and the corresponding surface offset, whereas soil thermal conductivities and corresponding thermal offsets are the most important factors affecting permafrost presence at its southern limit. However, consistent techniques for widespread mapping of winter air-to-ground scaling factors have not been developed to date due to the heterogeneous nature of winter snow accumulation. Recent developments incorporating sub grid-cell snow cover variability into broader permafrost modelling are promising and may improve the parameterization of scaling factors (Gisnås et al. 2014). Thermal conductivities are also often difficult to model across broad areas due to the lack of detailed information on surficial geology in many high latitude environments. Typically, these values have been estimated from geologic maps or vegetation classification schemes (e.g. Gisnås et al. 2013; Gisnås et al. 2014; Westermann et al. 2015a).

TTOP modelling in Labrador (Chapter 6) used spatially modelled freezing and thawing degree-days derived in Chapter 2 as climatological inputs. Air-to-ground transfer functions (n-factors) were parameterized using data from a network of climate stations (*Section 1.4.3)*. N-factors and thermal properties of the ground (used to estimate the thermal offset) were spatially distributed at a high resolution across Labrador using land cover classifications, surficial materials maps and topographic indices.

1.5 Research objectives and thesis organization

This thesis is written in article format and each of the chapters represents a contribution towards the goal of increasing the current state of knowledge on the regional distribution and characteristics of

permafrost in Labrador. The specific thesis objectives addressed by each manuscript or publication are indicated below.

Objective 1: *Develop input climate products suitable for use in regional permafrost modelling*

Chapter 2 describes the creation of gridded climate datasets in support of permafrost modelling for all of Labrador-Ungava using the TTOP model. Building on previous work by Way and Bonnaventure (2015), this contribution develops a novel approach for processing and spatially interpolating monthly air temperature data across Labrador-Ungava for 1948-2014. This contribution also details a simplified method for generating annual freezing and thawing degree day totals from mean annual air temperature and annual temperature range datasets derived from the monthly air temperature grids. This contribution is primarily a methodological study but key findings include the derivation of gridded air temperature products for Labrador-Ungava with an overall accuracy (± 0.8°C) that is better than previous efforts for eastern Canada. This contribution presents an approach to modelling air temperatures across the region that is open source, replicable and able to be updated regularly to support permafrost modelling and other initiatives. The climate grids generated from this analysis have been updated for 1948-2016 and are currently being used to support permafrost modelling initiatives in Nunavik (Centre D'Étude Nordiques), fisheries research in northern Labrador (Government of Newfoundland and Labrador) and climate trend analysis across all of Labrador-Ungava (Ouranos). Chapter 2 was published in the *International Journal of Climatology*.

Way, R. G., A. G. Lewkowicz, and P. P. Bonnaventure. 2017. Development of moderate-resolution gridded monthly air temperature and degree-day maps for the Labrador-Ungava region of northern Canada. International Journal of Climatology 37(1): 493–508. doi: 10.1002/joc.4721.

Objective 2: *Characterize contemporary peatland permafrost in southeastern coastal Labrador*

Chapter 3 is a description and analysis of peatland permafrost in the coastal barrens ecozone of southeastern Labrador. Permafrost is inferred to be very rare if not absent from southern Labrador in most maps due to the region's moderate climate (MAAT = ~0.5°C) and heavy regional snowfall totals. This study documents peatland permafrost in coastal environments between the southern shore of Lake Melville, NL (53.8°N) and Blanc Sablon, QC (51.4°N). Observations of permafrost conditions at seven sites were made using standard techniques and ERT, and ground temperatures were measured in instrumented boreholes in palsas and peat plateaus at five locations. Numerical modelling using the transient Northern Ecosystem Soil Temperature (NEST) model (Zhang et al., 2003) was used to estimate

permafrost sensitivity to future climate change for borehole sites in Cartwright, NL and Blanc Sablon, QC. The key result of this contribution is that permafrost features in the southern end of this show large thermal offsets which enable permafrost to persist where ground surface temperatures are positive. A clear north-south gradient in recorded ground temperatures is shown for peatland permafrost sites with palsas in southern Labrador having higher ground temperatures than at the northern end of the transect. Numerical modelling with NEST shows that permafrost at Cartwright, NL and Blanc Sablon, QC is projected to thaw by 2060 under most warming scenarios. Chapter 3 is expected to be submitted to *The Cryosphere*.

Way, R.G., Lewkowicz, A.G. and Zhang, Y. Contemporary coastal peatland permafrost in southeastern Labrador, northern Canada. To be submitted to The Cryosphere.

Objective 3: *Describe contemporary permafrost conditions in northern coastal Labrador*

Chapter 4 is a field investigation of permafrost conditions carried out using a combination of standard field methods and ERT within and around the community of Nain, Nunatsiavut, the northernmost community in Labrador. This chapter examines the extent of permafrost in the community of Nain and relates its occurrence and/or absence to local geomorphology, surficial cover and vegetation types. Key findings include the identification of contemporary permafrost bodies within Nain in both disturbed and undisturbed terrain including beneath and adjacent to sites of future infrastructure development. This contribution also provides evidence of structural subsidence in sections of Nain which is inferred to be due to permafrost thaw. Chapter 4 will be submitted for publication in the *Canadian Geotechnical Journal*. Preliminary data from Chapter 4 has been published in the Proceedings of GéoQuebec: 68th Canadian Geotechnical Conference and 7th Canadian Permaforst Conference.

Way, R.G. and Lewkowicz, A.G. Investigation of discontinuous permafrost in Nain, Nunatsiavut with DC electrical resistivity tomography. To be submitted to Canadian Geotechnical Journal.

Way, R. G., and A. G. Lewkowicz. 2015. Investigations of discontinuous permafrost in coastal Labrador with DC electrical resistivity tomography. In Proceedings of GéoQuebec: 68th Canadian Geotechnical Conference and 7th Canadian Permafrost Conference, 8. Québec City, Canada. doi: 10.13140/RG.2.1.1647.8803.

Objective 4: *Establish a permafrost monitoring program across Labrador and analyze collected data to support regional permafrost modelling using the temperature at the top of permafrost model*

Chapter 5 describes data collected at environmental monitoring stations established across Labrador by the Labrador Permafrost Project for the purposes of informing permafrost modelling across

the region. These stations were placed in a variety of environmental settings which included most ecozones in Labrador and are supplemented by data from other monitoring networks in the Torngat Mountains National Park in northern Labrador and the Mealy Mountains in eastern Labrador. Available field data from the 83 monitoring stations were used to analyze the interrelationships of variables in the temperature at the top of permafrost model. Key results include the identification of snow depth, not mean annual air temperature, as the strongest single determinant of mean temperatures at the top of permafrost (TTOP), with its variability in turn related to land cover class. A late-winter snow depth of 70 cm or less was inferred to be adequate for preventing the formation of permafrost at the monitoring sites meaning that permafrost was absent in forests and concurrently present in some tundra locations. Testing of several land cover datasets for permafrost model parameterization gave errors in ground surface temperature ranging from ±0.9-2.1°C. Chapter 5 is in revision for publication in *Permafrost and Periglacial Processes*.

Way, R. G., and A. G. Lewkowicz. in revision. Relations between environmental setting and TTOP parameters in Labrador, northeast Canada. Permafrost and Periglacial Processes.

Objective 5: *Determine historical and contemporary permafrost distribution across Labrador and northern Québec using the temperature at the top of permafrost*

The final manuscript in this dissertation (Chapter 6) built on Chapters 2 and 4 to create high resolution maps (250 m by 250 m) of ground temperatures across Labrador-Ungava for historic and contemporary climate periods using the analytical temperature at the top of permafrost (TTOP) model. To facilitate this goal, an open source Labrador-specific version of the TTOP model was developed using a novel n-factor parameterization scheme that compensates for regional differences in continentality, snowfall, and land cover and is transferable to other Subarctic environments. The Labrador-Ungava TTOP model was supported by analysis of station data from 29 air and ground climate monitoring stations located across Labrador and the gridded climate data developed in Chapter 2. Key results include model predictions of discontinuous permafrost even in northern Labrador, in contrast to existing permafrost maps and predictions of the existence of isolated bodies of mountaintop permafrost throughout southern Labrador. Modelled permafrost area at equilibrium was inferred to have increased from the middle of the 20th century to a potential peak in the 1990s (36% of the total land area) followed by a decline of 25% (95 000 km^2) between the 1990s and the most recent decade. Chapter 6 was published in the *Canadian Journal of Earth Sciences*. R v3.3 code for the implementation of the TTOP model is given in Appendix A4.

Way, R. G., and A. G. Lewkowicz. 2016. Modelling the spatial distribution of permafrost in Labrador–Ungava using the temperature at the top of permafrost. Canadian Journal of Earth Sciences 53(10): 1010–1028. doi: 10.1139/cjes-2016-0034.

1.6 Authorship and co-author contributions

I am the primary author of the five manuscripts presented in this thesis in Chapters 2, 3, 4, 5 and 6. The overall research plan, field data collection methodology and analysis approach was established by me in consultation with my supervisor Dr. Antoni Lewkowicz. Field data collection was undertaken by me, Dr. Antoni Lewkowicz and various field assistants throughout the project. Each of the contributions was generated with original ideas from me and guidance from Dr. Antoni Lewkowicz who is a co-author on each of the manuscripts. Dr. Philip P. Bonnaventure is a co-author on Chapter 2 in recognition of his contributions to the theoretical approach for modelling air temperatures employed in that manuscript. Dr. Yu Zhang is a co-author on Chapter 3 for providing numerical model simulations of permafrost conditions at Cartwright, NL and Blanc Sablon, QC using NEST. Each of the five manuscripts presented in this thesis were improved by commentary on earlier drafts from either research colleagues, conference attendees, anonymous reviewers and/or journal editors.

1.7 References

Allard, M., and M. K. Séguin. 1987. Le pergélisol au Québec nordique : bilan et perspectives. Géographie physique et Quaternaire 41(1): 141. doi: 10.7202/032671ar.

Allard, M., M. Lemay, C. Barrette, E. L'Hérault, D. Sarrazin, T. Bell, and G. Doré. 2012. Permafrost and climate change in Nunavik and Nunatsiavut: Importance for municipal and transportation infrastructures. In Nunavik and Nunatsiavut: From science to policy. An Integrated Regional Impact Study (IRIS) of climate change and modernization, 171–197.

Allard, M., D. Sarrazin, and E. L'Hérault. 2014. Borehole monitoring temperatures in northeastern Canada v. 1.2 (1988-2014). Scientific data. Nordicana D8. Centre D'Étude Nordiques.

Anderson, R. K., G. H. Miller, J. P. Briner, N. A. Lifton, and S. B. DeVogel. 2008. A millennial perspective on Arctic warming from 14C in quartz and plants emerging from beneath ice caps. Geophysical Research Letters 35: 01502.

Andrews, J. T. 1961. Permafrost in southern Labrador-Ungava. Canadian Geographer 5(3): 34–35.

Aznar, J.-C., E. Gloaguen, D. Tapsoba, S. Hachem, D. Caya, and Y. Bégin. 2013. Interpolation of monthly mean temperatures using cokriging in spherical coordinates. International Journal of Climatology 33(3): 758–769. doi: 10.1002/joc.3468.

Banfield, C. E., and J. D. Jacobs. 1998. Regional patterns of temperature and precipitation for Newfoundland and Labrador during the past century. The Canadian Geographer/Le Géographe canadien 42(4): 354–364.

Barrand, N. E., R. G. Way, T. Bell, and M. J. Sharp. 2017. Recent changes in area and thickness of Torngat Mountain glaciers (northern Labrador, Canada). The Cryosphere 11(1): 157–168. doi: 10.5194/tc-11-157-2017.

Belcher, D. J. 1949. The use of aerial photographs for pre-determining ground conditions in the Arctic and sub-Arctic regions of North America. Unpublished research report. Arctic Institute of North America.

Bonnaventure, P. P., and A. G. Lewkowicz. 2011. Modelling climate change effects on the spatial distribution of mountain permafrost at three sites in northwest Canada. Climatic Change 105(1–2): 293–312. doi: 10.1007/s10584-010-9818-5.

Brown, R., M. Lemay, M. Allard, N. E. Barrand, C. Barrette, Y. Bégin, T. Bell, M. Bernier, S. Bleau, D. Chaumont, Y. Dibike, A. Frigon, P. Leblanc, D. Paquin, M. J. Sharp, and R. Way. 2012. Climate variability and change in the Canadian Eastern Subarctic IRIS region (Nunavik and Nunatsiavut). In Nunavik and Nunatsiavut: From science to policy. An Integrated Regional Impact Study (IRIS) of climate change and modernization, 57–93.

Brown, R. J. 1979. Permafrost distribution in the southern part of the discontinuous zone in Quebec and Labrador. Géographie physique et Quaternaire 33(3–4): 279–289.

Brown, R. J. E. 1960. The distribution of permafrost and its relation to air temperature in Canada and the USSR. Arctic: 163–177.

Brown, R. J. E. 1967. Permafrost investigations in British Columbia and Yukon Territory. 253. Division of Building Research. National Research Council of Canada.

Brown, R. J. E. 1975. Permafrost Investigations in Quebec and Newfoundland (Labrador). Technical Paper 449. Ottawa, Ontario: National Research Council of Canada.

Burn, C. R., and C. A. S. Smith. 1988. Observations of the "thermal offset" in near-surface mean annual ground temperatures at several sites near Mayo, Yukon Territory, Canada. ARCTIC 41(2): 99–104. doi: 10.14430/arctic1700.

Butler, D. H. 2011. Exploring soilscapes and places inside labrador Inuit winter dwellings. Canadian Journal of Archaeology 35(1): 55–85.

Cawley, G. C., K. Cowtan, R. G. Way, P. Jacobs, and A. Jokimäki. 2015. On a minimal model for estimating climate sensitivity. Ecological Modelling 297: 20–25. doi: 10.1016/j.ecolmodel.2014.10.018.

Clark, C. D., J. K. Knight, and J. T. Gray. 2000. Geomorphological reconstruction of the Labrador sector of the Laurentide Ice Sheet. Quarternary Science Reviews 19(13): 1343–1366.

Comiso, J. C., and D. K. Hall. 2014. Climate trends in the Arctic as observed from space: Climate trends in the Arctic as observed from space. Wiley Interdisciplinary Reviews: Climate Change 5(3): 389–409. doi: 10.1002/wcc.277.

Cook, J., D. Nuccitelli, S. A. Green, M. Richardson, B. Winkler, R. Painting, R. Way, P. Jacobs, and A. Skuce. 2013. Quantifying the consensus on anthropogenic global warming in the scientific literature. Environmental Research Letters 8(2): 024024. doi: 10.1088/1748-9326/8/2/024024.

Cowtan, K., and R. G. Way. 2014. Coverage bias in the HadCRUT4 temperature series and its impact on recent temperature trends: Coverage Bias in the HadCRUT4 Temperature Series. Quarterly Journal of the Royal Meteorological Society 140(683): 1935–1944. doi: 10.1002/qj.2297.

D'Arrigo, R., R. Wilson, and G. Jacoby. 2006. On the long-term context for late twentieth century warming. Journal of Geophysical Research 111(D3). doi: 10.1029/2005JD006352.

Derksen, C., S. L. Smith, M. Sharp, L. Brown, S. Howell, L. Copland, D. R. Mueller, Y. Gauthier, C. G. Fletcher, A. Tivy, M. Bernier, J. Bourgeois, R. Brown, C. R. Burn, C. Duguay, P. Kushner, A. Langlois, A. G. Lewkowicz, A. Royer, and A. Walker. 2012. Variability and change in the Canadian cryosphere. Climatic Change 115(1): 59–88. doi: 10.1007/s10584-012-0470-0.

Dionne, J.-C. 1984. Palses et limite méridionale du pergélisol dans l'hemisphere nord: le cas de Blanc-Sablon, Québec. Géographie physique et Quaternaire 38(2): 165–184. doi: 10.7202/032550ar.

Dionne, J.-C., and V. Gérardin. 1988. Observations sur les buttes organiques de la Cote-Nord du golfe du Saint-Laurent, Québec. Géographie physique et Quaternaire 42(3): 289–301. doi: 10.7202/032737ar.

Dionne, J.-C., and P. J. H. Richard. 2006. Origine, Age et taux d'accrétion verticale de la tourbiere palses de Blanc-Sablon, basse Cote-Nord, Golfe du Saint-Laurent, Québec. Géographie physique et Quaternaire 60(2): 199–205. doi: 10.7202/016829ar.

Doré, G., F. Niu, and H. Brooks. 2016. Adaptation methods for transportation infrastructure built on degrading permafrost. Permafrost and Periglacial Processes 27(4): 352–364. doi: 10.1002/ppp.1919.

Dyke, A. S. 2004. An outline of North American deglaciation with emphasis on central and northern Canada. Developments in Quaternary Science 2(B): 373–424.

Elias, S. A. 1982. Paleoenvironmental Interpretation of Holocene Insect Fossils from Northeastern Labrador, Canada. Arctic and Alpine Research 14(4): 311. doi: 10.2307/1550794.

Elliott, D. L., and S. K. Short. 1979. The Northern Limit of Trees in Labrador: A Discussion. ARCTIC 32(3): 201–206. doi: 10.14430/arctic2620.

Evans, D. J., and R. J. Rogerson. 1988. A radiocarbon-dated gelifluction lobe in the Nachvak Fiord area, northern Labrador, Canada. Earth Surface Processes and Landforms 13(7): 657–662.

Fortier, R., M. Allard, S. Buteau, and F. Calmels. 2008. Internal structure and conditions of permafrost mounds at Umiujaq in Nunavik, Canada, inferred from field investigation and electrical resistivity tomography. Canadian Journal of Earth Sciences 45(3): 367–387. doi: 10.1139/E08-004.

Fraser, R. H., I. Olthof, M. Carrière, A. Deschamps, and D. Pouliot. 2011. Detecting long-term changes to vegetation in northern Canada using the Landsat satellite image archive. Environmental Research Letters 6(4): 045502. doi: 10.1088/1748-9326/6/4/045502.

Fulton, R. J. 1995. Surficial Materials of Canada. Geological Survey of Canada Map. Natural Resources Canada.

Gajewski, K. 2015. Quantitative reconstruction of Holocene temperatures across the Canadian Arctic and Greenland. Global and Planetary Change 128: 14–23. doi: 10.1016/j.gloplacha.2015.02.003.

Gennaretti, F., D. Arseneault, A. Nicault, L. Perreault, and Y. Begin. 2014. Volcano-induced regime shifts in millennial tree-ring chronologies from northeastern North America. Proceedings of the National Academy of Sciences 111(28): 10077–10082. doi: 10.1073/pnas.1324220111.

Gisnås, K., B. Etzelmüller, H. Farbrot, T. V. Schuler, and S. Westermann. 2013. CryoGRID 1.0: Permafrost distribution in Norway estimated by a spatial numerical model. Permafrost and Periglacial Processes 24(1): 2–19. doi: 10.1002/ppp.1765.

Gisnås, K., S. Westermann, T. V. Schuler, T. Litherland, K. Isaksen, J. Boike, and B. Etzelmüller. 2014. A statistical approach to represent small-scale variability of permafrost temperatures due to snow cover. The Cryosphere 8(6): 2063–2074. doi: 10.5194/tc-8-2063-2014.

Granberg, H. B. 1989. Permafrost mapping at Schefferville, Québec. Physical Geography 10(3): 249–269.

Gruber, S. 2012. Derivation and analysis of a high-resolution estimate of global permafrost zonation. The Cryosphere 6(1): 221–233. doi: 10.5194/tc-6-221-2012.

Hachem, S., M. Allard, and C. Duguay. 2009. Using the MODIS land surface temperature product for mapping permafrost: an application to northern Québec and Labrador, Canada. Permafrost and Periglacial Processes 20(4): 407–416. doi: 10.1002/ppp.672.

Harris, I., P. D. Jones, T. J. Osborn, and D. H. Lister. 2014. Updated high-resolution grids of monthly climatic observations–the CRU TS3. 10 Dataset. International Journal of Climatology 34(3): 623–642.

Hauck, C. 2013. New Concepts in Geophysical Surveying and Data Interpretation for Permafrost Terrain: Geophysical Surveying in Permafrost Terrain. Permafrost and Periglacial Processes 24(2): 131–137. doi: 10.1002/ppp.1774.

Hauck, C., D. Vonder Mühll, and H. Maurer. 2003. Using DC resistivity tomography to detect and characterize mountain permafrost. Geophysical prospecting 51(4): 273–284.

Heginbottom, J. A., M.-A. Dubreuil, and P. A. Harker. 1995. Canada – Permafrost. National Atlas of Canada, 5th Edition. Ottawa, Canada: Natural Resources Canada.

Helm, V., A. Humbert, and H. Miller. 2014. Elevation and elevation change of Greenland and Antarctica derived from CryoSat-2. The Cryosphere 8(4): 1539–1559. doi: 10.5194/tc-8-1539-2014.

Hendershot, W. H. 1984. A Comparison of some Upland and Valley Soils in the Ungava-Labrador Peninsula. Géographie physique et Quaternaire 38(3): 243. doi: 10.7202/032566ar.

Hendershot, W. H. 1985. Comparison of Canadian and American classification systems for some arctic soils of the Ungava-Labrador Peninsula. Canadian journal of soil science 65(2): 283–291.

Hijmans, R. J., S. E. Cameron, J. L. Parra, P. G. Jones, and A. Jarvis. 2005. Very high resolution interpolated climate surfaces for global land areas. International Journal of Climatology 25(15): 1965–1978. doi: 10.1002/joc.1276.

Hilbich, C., L. Marescot, C. Hauck, M. H. Loke, and R. Mäusbacher. 2009. Applicability of electrical resistivity tomography monitoring to coarse blocky and ice-rich permafrost landforms. Permafrost and Periglacial Processes 20(3): 269–284. doi: 10.1002/ppp.652.

Hopkinson, R. F., M. F. Hutchinson, D. W. McKenney, E. J. Milewska, and P. Papadopol. 2012. Optimizing Input Data for Gridding Climate Normals for Canada. Journal of Applied Meteorology and Climatology 51(8): 1508–1518. doi: 10.1175/JAMC-D-12-018.1.

Hustich, I. 1939. Notes on the coniferous forest and tree limit on the east coast of Newfoundland-Labrador. Acta Geographica 7(1): 5–77.

Hutchinson, M. F., D. W. McKenney, K. Lawrence, J. H. Pedlar, R. F. Hopkinson, E. Milewska, and P. Papadopol. 2009. Development and testing of Canada-wide interpolated spatial models of daily minimum-maximum temperature and precipitation for 1961–2003. Journal of Applied Meteorology and Climatology 48(4): 725–741. doi: 10.1175/2008JAMC1979.1.

Ives, J. D. 1960. Permafrost in central Labrador-Ungava. Journal of Glaciology 3(28): 789–790.

Ives, J. D. 1979. A proposed history of permafrost development in Labrador-Ungava. Géographie physique et Quaternaire 33(3–4): 233–244. doi: 10.7202/1000360ar.

Jacobs, J. D., A. R. Maarouf, and E. A. Perkins. 1996. The recent record of climate on the range of the George River Caribou Herd, Northern Québec and Labrador, Canada. Rangifer 16(4): 193–200.

Jacobs, J. D., S. Chan, and E. Sutton. 2014. Climatology of the Forest-Tundra Ecotone at a Maritime Subarctic-Alpine Site, Mealy Mountains, Labrador. ARCTIC 67(1): 28–42. doi: 10.14430/arctic4358.

James, M., A. G. Lewkowicz, S. L. Smith, and C. M. Miceli. 2013. Multi-decadal degradation and persistence of permafrost in the Alaska Highway corridor, northwest Canada. Environmental Research Letters 8(4): 045013. doi: 10.1088/1748-9326/8/4/045013.

Jameson, R. G., A. J. Trant, and L. Hermanutz. 2015. Insects can limit seed productivity at the treeline. Canadian Journal of Forest Research 45(3): 286–296. doi: 10.1139/cjfr-2014-0385.

Jordan, R. H. 1980. Preliminary Results from Archaeological Investigations on Avayalik Island, Extreme Northern Labrador. ARCTIC 33(3): 607–627. doi: 10.14430/arctic2586.

Jorgenson, M. T., V. Romanovsky, J. Harden, Y. Shur, J. O'Donnell, E. A. G. Schuur, M. Kanevskiy, and S. Marchenko. 2010. Resilience and vulnerability of permafrost to climate change. Canadian Journal of Forest Research 40(7): 1219–1236. doi: 10.1139/X10-060.

Ju, J., and J. G. Masek. 2016. The vegetation greenness trend in Canada and US Alaska from 1984–2012 Landsat data. Remote Sensing of Environment 176: 1–16. doi: 10.1016/j.rse.2016.01.001.

Kilibarda, M., T. Hengl, G. B. M. Heuvelink, B. Gräler, E. Pebesma, M. Perčec Tadić, and B. Bajat. 2014. Spatio-temporal interpolation of daily temperatures for global land areas at 1 km resolution. Journal of Geophysical Research: Atmospheres 119(5): 2294–2313. doi: 10.1002/2013JD020803.

Lamb, H. F. 1985. Palynological Evidence for Postglacial Change in the Position of Tree Limit in Labrador. Ecological Monographs 55(2): 241–258. doi: 10.2307/1942559.

Leverington, D. 1995. A field survey of late-summer depths to frozen ground at two study areas near mayo, Yukon Territory, Canada. Permafrost and Periglacial Processes 6(4): 373–379.

Lewkowicz, A. G. 2008. Evaluation of miniature temperature-loggers to monitor snowpack evolution at mountain permafrost sites, northwestern Canada. Permafrost and Periglacial Processes 19(3): 323–331. doi: 10.1002/ppp.625.

Lewkowicz, A. G., and M. Ednie. 2004. Probability mapping of mountain permafrost using the BTS method, Wolf Creek, Yukon Territory, Canada. Permafrost and Periglacial Processes 15(1): 67–80. doi: 10.1002/ppp.480.

Lewkowicz, A. G., and R. G. Way. 2014. Overview report for the Nunatsiavut Government on permafrost conditions in the Nain area. Technical report.

Lewkowicz, A. G., B. Etzelmüller, and S. L. Smith. 2011. Characteristics of discontinuous permafrost based on ground temperature measurements and electrical resistivity tomography, southern Yukon, Canada. Permafrost and Periglacial Processes 22(4): 320–342. doi: 10.1002/ppp.703.

Lewkowicz, A. G., P. P. Bonnaventure, S. L. Smith, and Z. Kuntz. 2012. Spatial and thermal characteristics of mountain permafrost, northwest Canada. Geografiska Annaler: Series A, Physical Geography 94(2): 195–213.

Loke, M. H., and R. D. Barker. 1996. Rapid least-squares inversion of apparent resistivity pseudosections by a quasi-Newton method. Geophysical prospecting 44(1): 131–152.

Loke, M. H., I. Acworth, and T. Dahlin. 2003. A comparison of smooth and blocky inversion methods in 2D electrical imaging surveys. Exploration Geophysics 34(3): 182–187. doi: 10.1071/EG03182.

Mackay, R. J. 1977. Probing for the bottom of the active layer. 77–1A. Geological Survey of Canada.

Mackay, R. J. 1995. Active layer changes (1968 to 1993) following the forest-tundra fire near Inuvik, N.W.T., Canada. Arctic and Alpine Research 27(4): 323–336.

Marquette, G. C., J. T. Gray, J. C. Gosse, F. Courchesne, L. Stockli, G. Macpherson, and R. Finkel. 2004. Felsenmeer persistence under non-erosive ice in the Torngat and Kaumajet mountains, Quebec and Labrador, as determined by soil weathering and cosmogenic nuclide exposure dating. Canadian Journal of Earth Sciences 41(1): 19–38. doi: 10.1139/e03-072.

McLennan, D. S., T. Bell, D. Berteaux, W. Chen, L. Copland, R. Fraser, D. Gallant, G. Gauthier, D. Hik, C. J. Krebs, I. H. Myers-Smith, I. Olthof, D. Reid, W. Sladen, C. Tarnocai, W. F. Vincent, and Y. Zhang. 2012. Recent climate-related terrestrial biodiversity research in Canada's Arctic national parks: review, summary, and management implications. Biodiversity 13(3–4): 157–173. doi: 10.1080/14888386.2012.720818.

Milewska, E. J., R. F. Hopkinson, and A. Niitsoo. 2005. Evaluation of geo-referenced grids of 1961–1990 Canadian temperature and precipitation normals. Atmosphere-Ocean 43(1): 49–75.

Naulier, M., M. M. Savard, C. Bégin, F. Gennaretti, D. Arseneault, J. Marion, A. Nicault, and Y. Bégin. 2015. A millennial summer temperature reconstruction for northeastern Canada using oxygen isotopes in subfossil trees. Climate of the Past 11(9): 1153–1164. doi: 10.5194/cp-11-1153-2015.

Nicholson, F. H. 1979. Permafrost spatial and temporal variations near Schefferville, Nouveau-Québec. Géographie physique et Quaternaire 33(3–4): 265–277. doi: 10.7202/1000363ar.

Occhietti, S., M. Parent, P. Lajeunesse, F. Robert, and E. Govare. 2011. Late Pleistocene–Early Holocene decay of the Laurentide Ice Sheet in Québec-Labrador. Developments in Quaternary Science 11: 601–630. doi: 10.1016/B978-0-444-53447-7.00047-7.

Olthof, I., R. Latifovic, and D. Pouliot. 2015. A medium resolution land cover map of Canada's forested regions from 2005-2010 SPOT 4/5 data. 4. doi: 10.4095/295751.

Oyler, J. W., A. P. Ballantyne, K. Jencso, M. Sweet, and S. W. Running. 2015. Creating a topoclimatic daily air temperature dataset for the conterminous United States using homogenized station data and remotely sensed land skin temperature. International Journal of Climatology 35(9): 2258–2279.

Pastick, N. J., M. T. Jorgenson, B. K. Wylie, S. J. Nield, K. D. Johnson, and A. O. Finley. 2015. Distribution of near-surface permafrost in Alaska: Estimates of present and future conditions. Remote Sensing of Environment 168: 301–315. doi: 10.1016/j.rse.2015.07.019.

Paul, F., C. Huggel, and A. Kääb. 2004. Combining satellite multispectral image data and a digital elevation model for mapping debris-covered glaciers. Remote Sensing of Environment 89(4): 510–518. doi: 10.1016/j.rse.2003.11.007.

Payette, S. 1993. The range limit of boreal tree species in Québec-Labrador: an ecological and palaeoecological interpretation. Review of Palaeobotany and Palynology 79(1): 7–30.

Payette, S. 2001. Les processus et les formes périglaciaires. In Écologie des tourbières du Québec-Labrador, 199–239. Québec City, Canada: Les Presses de l'Université Laval.

Payette, S. 2007. Contrasted Dynamics of Northern Labrador Tree Lines Caused by Climate Change and Migrational Lag. Ecology 88(3): 770–780. doi: 10.1890/06-0265.

Payette, S., A. Delwaide, M. Caccianiga, and M. Beauchemin. 2004. Accelerated thawing of subarctic peatland permafrost over the last 50 years. Geophysical Research Letters 31(18): L18208. doi: 10.1029/2004GL020358.

Price, D. T., D. W. McKenney, I. A. Nalder, M. F. Hutchinson, and J. L. Kesteven. 2000. A comparison of two statistical methods for spatial interpolation of Canadian monthly mean climate data. Agricultural and Forest meteorology 101(2): 81–94.

Pryer, R. W. 1963. Mine railroads in Labrador-Ungava. In Proceedings of the 1st International Conference on Permafrost, 503–508. 1287. Washington, USA: National Academy of Sciences and National Research Council Publication.

Riseborough, D. 2007. The effect of transient conditions on an equilibrium permafrost-climate model. Permafrost and Periglacial Processes 18(1): 21–32. doi: 10.1002/ppp.579.

Riseborough, D., N. Shiklomanov, B. Etzelmüller, S. Gruber, and S. Marchenko. 2008. Recent advances in permafrost modelling. Permafrost and Periglacial Processes 19(2): 137–156. doi: 10.1002/ppp.615.

Riseborough, D. W. 2004. Exploring the parameters of a simple model of the permafrost-climate relationship. PhD Thesis, Ottawa: Carleton University.

Roberts, B. A., N. P. P. Simon, and K. W. Deering. 2006. The forests and woodlands of Labrador, Canada: ecology, distribution and future management. Ecological Research 21(6): 868–880. doi: 10.1007/s11284-006-0051-7.

Romanovsky, V. E., S. L. Smith, and H. H. Christiansen. 2010. Permafrost thermal state in the polar Northern Hemisphere during the international polar year 2007-2009: a synthesis. Permafrost and Periglacial Processes 21(2): 106–116. doi: 10.1002/ppp.689.

Séguin, M. K., and J.-C. Dionne. 1992. Modélisation géophysique et caractérisation thermique du pergélisol dans les palses de Blanc-Sablon, Québec. 92–1E. Current Research. Geological Survey of Canada.

Serreze, M. C., and R. G. Barry. 2011. Processes and impacts of Arctic amplification: A research synthesis. Global and Planetary Change 77(1–2): 85–96. doi: 10.1016/j.gloplacha.2011.03.004.

Serreze, M. C., B. Raup, C. Braun, D. R. Hardy, and R. S. Bradley. 2017. Rapid wastage of the Hazen Plateau ice caps, northeastern Ellesmere Island, Nunavut, Canada. The Cryosphere 11(1): 169–177. doi: 10.5194/tc-11-169-2017.

Shur, Y., K. M. Hinkel, and F. E. Nelson. 2005. The transient layer: implications for geocryology and climate-change science. Permafrost and Periglacial Processes 16(1): 5–17. doi: 10.1002/ppp.518.

Shur, Y. L., and M. T. Jorgenson. 2007. Patterns of permafrost formation and degradation in relation to climate and ecosystems. Permafrost and Periglacial Processes 18(1): 7–19. doi: 10.1002/ppp.582.

Simms, É., and H. Ward. 2013. Multisensor NDVI-Based Monitoring of the Tundra-Taiga Interface (Mealy Mountains, Labrador, Canada). Remote Sensing 5(3): 1066–1090. doi: 10.3390/rs5031066.

Singh, V. P., P. Singh, and U. K. Haritashya, ed. 2011. Encyclopedia of Snow, Ice and Glaciers. Encyclopedia of Earth Sciences Series. Dordrecht: Springer Netherlands. doi: 10.1007/978-90-481-2642-2.

Slater, A. G., and D. M. Lawrence. 2013. Diagnosing Present and Future Permafrost from Climate Models. Journal of Climate 26(15): 5608–5623. doi: 10.1175/JCLI-D-12-00341.1.

Smith, M. W., and D. W. Riseborough. 1996. Permafrost monitoring and detection of climate change. Permafrost and Periglacial Processes 7(4): 301–309. doi: 10.1002/(SICI)1099-1530(199610)7:4<301::AID-PPP231>3.0.CO;2-R.

Smith, M. W., and D. W. Riseborough. 2002. Climate and the limits of permafrost: a zonal analysis. Permafrost and Periglacial Processes 13(1): 1–15. doi: 10.1002/ppp.410.

Smith, S. L., and D. W. Riseborough. 2010. Modelling the thermal response of permafrost terrain to right-of-way disturbance and climate warming. Cold Regions Science and Technology 60(1): 92–103. doi: 10.1016/j.coldregions.2009.08.009.

Smith, S. L., M. M. Burgess, D. Riseborough, and F. Mark Nixon. 2005. Recent trends from Canadian permafrost thermal monitoring network sites. Permafrost and Periglacial Processes 16(1): 19–30. doi: 10.1002/ppp.511.

Smith, S. L., V. E. Romanovsky, A. G. Lewkowicz, C. R. Burn, M. Allard, G. D. Clow, K. Yoshikawa, and J. Throop. 2010. Thermal state of permafrost in North America: a contribution to the international polar year. Permafrost and Periglacial Processes 21(2): 117–135. doi: 10.1002/ppp.690.

Staiger, J. K. W., J. C. Gosse, J. V. Johnson, J. Fastook, J. T. Gray, D. F. Stockli, L. Stockli, and R. Finkel. 2005. Quaternary relief generation by polythermal glacier ice. Earth Surface Processes and Landforms 30(9): 1145–1159. doi: 10.1002/esp.1267.

Suo, L., O. Helge Otterå, M. Bentsen, Y. Gao, and O. M. Johannessen. 2013. External forcing of the early 20th century Arctic warming. Tellus A 65(0). doi: 10.3402/tellusa.v65i0.20578.

Thibault, S., and S. Payette. 2009. Recent permafrost degradation in bogs of the James Bay area, northern Quebec, Canada. Permafrost and Periglacial Processes 20(4): 383–389. doi: 10.1002/ppp.660.

Throop, J., A. G. Lewkowicz, S. L. Smith, and C. R. Burn. 2012. Climate and ground temperature relations at sites across the continuous and discontinuous permafrost zones, northern Canada. Canadian Journal of Earth Sciences 49(8): 865–876. doi: 10.1139/e11-075.

Trant, A. J., and L. Hermanutz. 2014. Advancing towards novel tree lines? A multispecies approach to recent tree line dynamics in subarctic alpine Labrador, northern Canada. Edited by Ole Vetaas. Journal of Biogeography 41(6): 1115–1125. doi: 10.1111/jbi.12287.

Trant, A. J., R. G. Jameson, and L. Hermanutz. 2011. Persistence at the tree line: old trees as opportunists. Arctic: 367–370.

Trant, A. J., K. Lewis, B. H. Cranston, J. A. Wheeler, R. G. Jameson, J. D. Jacobs, L. Hermanutz, and B. M. Starzomski. 2015. Complex changes in plant communities across a Subarctic alpine tree line in Labrador, Canada. ARCTIC 68(4): 500. doi: 10.14430/arctic4528.

Van Everdingen, R. 2005b. Pereletok. Multi-language glossary of permafrost and related ground-ice terms. Boulder, Colorado, USA: National Snow and Ice Data Center.

Van Everdingen, R. 2005c. Permafrost. Multi-language glossary of permafrost and related ground-ice terms. Boulder, Colorado, USA: National Snow and Ice Data Center.Viau, A. E., and K. Gajewski. 2009. Reconstructing Millennial-Scale, Regional Paleoclimates of Boreal Canada during the Holocene. Journal of Climate 22(2): 316–330. doi: 10.1175/2008JCLI2342.1.

Way, R. G. 2015. Multidecadal Recession of Grinnell and Terra Nivea Ice Caps, Baffin Island, Canada. ARCTIC 68(1): 45. doi: 10.14430/arctic4461.

Way, R. G., and P. P. Bonnaventure. 2015. Testing a reanalysis-based infilling method for areas with sparse discontinuous air temperature data in northeastern Canada: Reanalysis-based infilling in northeastern Canada. Atmospheric Science Letters 16(3): 398–407. doi: 10.1002/asl2.574.

Way, R. G., and A. G. Lewkowicz. 2014. Modelling the distribution of permafrost in the Labrador region of northeastern Canada. In 4th European Conference on Permafrost. Evora, Portugal.

Way, R. G., and A. G. Lewkowicz. 2016. Modelling the spatial distribution of permafrost in Labrador–Ungava using the temperature at the top of permafrost. Canadian Journal of Earth Sciences 53(10): 1010–1028. doi: 10.1139/cjes-2016-0034.

Way, R. G., and A. E. Viau. 2015. Natural and forced air temperature variability in the Labrador region of Canada during the past century. Theoretical and Applied Climatology 121(3–4): 413–424. doi: 10.1007/s00704-014-1248-2.

Way, R. G., T. Bell, and N. E. Barrand. 2014. An inventory and topographic analysis of glaciers in the Torngat Mountains, northern Labrador, Canada. Journal of Glaciology 60(223): 945–956. doi: 10.3189/2014JoG13J195.

Way, R. G., T. Bell, and N. E. Barrand. 2015. Glacier change from the early Little Ice Age to 2005 in the Torngat Mountains, northern Labrador, Canada. Geomorphology 246: 558–569. doi: 10.1016/j.geomorph.2015.07.006.

Wenner, C. G. 1947. Pollen diagrams from Labrador. Geographiska Annaler 29(3–4): 137–373.

Westermann, S., T. I. Østby, K. Gisnås, T. V. Schuler, and B. Etzelmüller. 2015. A ground temperature map of the North Atlantic permafrost region based on remote sensing and reanalysis data. The Cryosphere 9(3): 1303–1319. doi: 10.5194/tc-9-1303-2015.

Woo, M., A. G. Lewkowicz, and W. R. Rouse. 1992. Response of the Canadian permafrost environment to climatic change. Physical Geography 13(4): 287–317. doi: 10.1080/02723646.1992.10642459.

Woollett, J. 2010. Oakes Bay 1: A Preliminary Reconstruction of a Labrador Inuit Seal Hunting Economy in the Context of Climate Change. Geografisk Tidsskrift-Danish Journal of Geography 110(2): 245–259. doi: 10.1080/00167223.2010.10669510.

You, Y., Q. Yu, X. Pan, X. Wang, and L. Guo. 2013. Application of electrical resistivity tomography in investigating depth of permafrost base and permafrost structure in Tibetan Plateau. Cold Regions Science and Technology 87: 19–26. doi: 10.1016/j.coldregions.2012.11.004.

Zhang, Y., W. Chen, and J. Cihlar. 2003. A process-based model for quantifying the impact of climate change on permafrost thermal regimes. Journal of Geophysical Research 108(D22). doi: 10.1029/2002JD003354.

CHAPTER 2: DEVELOPMENT OF MODERATE-RESOLUTION GRIDDED MONTHLY AIR TEMPERATURE AND DEGREE-DAY MAPS FOR THE LABRADOR-UNGAVA REGION OF NORTHERN CANADA

Abstract: Detailed climatological grids are needed for many applications, including permafrost prediction, ecological modelling and infrastructure planning. This study describes the creation of moderate-resolution gridded climate datasets covering the entire Labrador-Ungava region (50-63°N) for a series of climate indices including monthly air temperature, annual air temperature, freezing degree-days and thawing degree-days. Using a recently developed spatio-temporal infilling technique, temporally-consistent climate grids spanning the 1948-2014 period were derived at a monthly resolution. Comparison against within-sample and out-of-sample climate stations revealed thin plate spline smoothing as more accurate for modelling air temperatures than regression, kriging and co-kriging. Evaluation of derived air temperature grids across a wide range of environments and scenarios shows an overall accuracy of 0.8 ± 0.3 °C. Spatially distributed air temperatures were converted to thawing and freezing degree-days using an empirical transfer function that compensates for the impacts of continentality and coastal proximity. These climate datasets will form the basis of inputs for future ecological and environmental modelling in the eastern Labrador-Ungava region.

2.1 Introduction

A growing demand for high-resolution topoclimatic datasets has developed over the past decade for use in various environmental applications such as animal ecology (e.g. Hu and Jiang 2010), forest management (e.g. Evangelista et al. 2011), biodiversity assessment, agriculture (e.g. Lane and Jarvis 2007), and paleoclimate research (e.g. Fortin and Gajewski 2012; Ladd et al. 2015). The development of digital databases containing climate and topographic information has also dramatically increased the interest in developing topoclimatic datasets, resulting in numerous newly available products covering local to global spatial domains (Kriticos et al. 2012; Wang et al. 2012; e.g. Aalto et al. 2013; Harris et al. 2014; Kilibarda et al. 2014). The WorldClim dataset (Hijmans et al. 2005) is an example of a moderate resolution (1 km) topoclimatic dataset which has been widely used in research applications judging by its impressive citation count (6050 as of May 31st, 2015 according to Google Scholar). Topoclimatic products such as WorldClim typically use local climate station observations provided by major station data holders (e.g. Global Historical Climate Network; Global Summary of the Day) in conjunction with topographic information derived from high-resolution digital elevation models in a geostatistical framework to model climate across wide spatial domains. However, WorldClim, like many publically-available topoclimatic datasets, covers a finite temporal period making it unsuitable for examining change in climate variables through time. Consequently, topoclimatic datasets covering longer time periods have been developed for much of North America using additional climatologically relevant covariates to improve reconstructed fields (McKenney et al. 2011). The widespread availability of land surface temperature (LST) products from satellite sensors (e.g. MODIS) at a moderate resolution (1 km) has also shifted the spatial modelling community by allowing higher temporal resolution datasets (e.g. daily) to be created covering isolated or topographically complex regions (Kilibarda et al. 2014; Oyler et al. 2015).

Topoclimatic data are needed in permafrost research to simulate present ground temperature conditions and for modelling former and future climate conditions when assessing permafrost vulnerability to climatic change (Zhang et al. 2006; Bonnaventure et al. 2012; Fiddes et al. 2015). Topoclimatic products have been used in this manner for empirical-statistical spatial modelling of permafrost conditions in a number of areas including the southern Yukon and northwest British Columbia (Bonnaventure and Lewkowicz 2013), the Northwest Territories (Wright et al. 2003), southern Norway (Gisnås et al. 2013) and the eastern North Atlantic sector (Westermann et al. 2015a). More complex transient models use heat transfer equations and have been employed with gridded climate datasets for a variety of locations including Alaska (Jafarov et al. 2012), the Hudson's Bay lowlands (Zhang et al. 2012; Zhang 2013), Ivvavik National Park (Zhang et al. 2013) and southern Norway (Westermann et al. 2013). In permafrost

research, the widely-used temperature at the top of permafrost (TTOP) model (Smith and Riseborough 1996; Smith and Riseborough 2002) relies on input climate data in the form of freezing and thawing degree-days in the air at the standard height (~2 m). Spatial modelling of these indices from remote weather stations can be challenging when considering regions with topographic differences where surface lapse rates may be uncertain and/or where persistent local-scale meteorological conditions may exist. For example, Lewkowicz and Bonnaventure (2011) found in the southern Yukon that spatially variable surface lapse rates had to be taken into account to accurately model the regional distribution of permafrost.

The Labrador Permafrost Project was initiated in 2013 with the goal of characterizing permafrost conditions throughout the eastern Labrador-Ungava region where there is a paucity of baseline information on permafrost distribution, ground ice content and thickness. The Permafrost Map of Canada classifies most of this region as being within the discontinuous zone, from isolated patches along the 50th parallel to extensive discontinuous-to-continuous permafrost north of 58°N (Heginbottom et al. 1995). Understanding permafrost dynamics across such a broad spatial domain requires local climatological information that is not currently available. Furthermore, evaluating the impacts of historical and future climate change (Brown et al. 2012; Finnis 2013; Way and Viau 2015) on regional permafrost conditions requires information on historical and future climate scenarios. This study describes the creation of moderate resolution (1 km) gridded topoclimatic datasets covering the Labrador-Ungava region for monthly air temperature, annual temperature range, freezing degree-days and thawing degree-days for the period 1948-2014. These datasets will form the basis of climate inputs for future modelling with the long-term goal of producing a regional TTOP model of past, current and future permafrost distribution and conditions in eastern Labrador-Ungava.

2.2 Study area

Labrador-Ungava stretches from the eastern coast of Hudson Bay (80° W) to the Atlantic Canadian Seaboard adjacent to the Labrador Sea (55° W) from 50° N to 63° N, and is affected climatologically by the offshore presence of arctic waters. The Labrador Current transports cold arctic water south bringing cooler summers along the east coast of Labrador (Banfield and Jacobs 1998) while Hudson Bay freezes over in the winter allowing deep penetration of cold-air into continental eastern Canada. As a consequence, annual surface air temperatures in the region are ~5 °C colder than at similar latitudes in western Canada (Hijmans et al. 2005). The landscape of the Labrador-Ungava region is typical of the Canadian Shield with relatively high plateaus and mountain chains that reach the highest elevations in continental Canada east of the Rockies in the Torngat Mountains (~1650 above sea level [a.s.l.]) (Figure 2-1). Other distinct

mountainous regions in the Labrador-Ungava include the Pingualuit National Park (650 m a.s.l.), the Harp Lake Complex (880 m a.s.l.), the Red Wine Mountains (880 m a.s.l.), the Mealy Mountains (1130 m a.s.l.), the Otish Mountains (1140 m a.s.l.), the Groulx Mountains (1080 m a.s.l.) and the Romaine Hills (960 m a.s.l.) (Figure 2-1). Prominent east-west and north-south regional climatic gradients account for mean annual air temperatures (MAATs) which vary from >1 °C in southeastern Labrador to <-8 °C in parts of the Torngat Mountains and northern Quebec. The region encompasses many different vegetation biomes, ranging from deciduous boreal forests in the south to Arctic tundra north of the tree-line at ~57 °N along the Labrador coast (Elliott and Short 1979). During the winter, extensive seasonal sea ice cover makes marine navigation into coastal regions of Labrador-Ungava almost impossible (Banfield and Jacobs 1998). The dynamic nature of the regional climate makes this region more difficult to evaluate in the context of global temperature reconstructions given the prominent role that natural variability can play in masking anthropogenic changes (Brown et al. 2012; Rapaić et al. 2015; Way and Viau 2015).

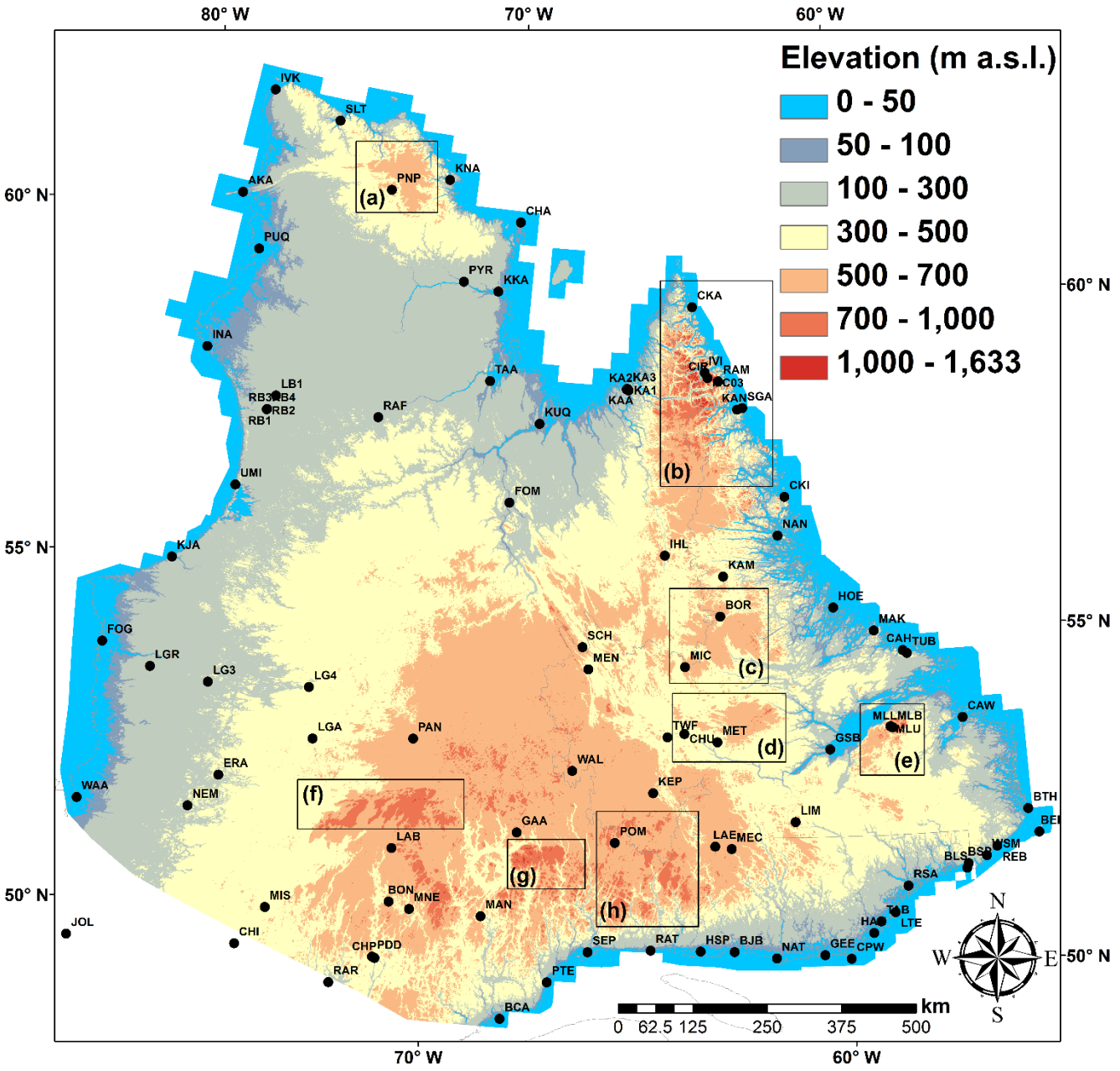

Figure 2-1: Distribution of climate stations used in this study superimposed on a digital elevation model from the National Topographic Database of the Labrador-Ungava region reclassified according to major elevation classes. Information on individual stations can be found in Table B1. Grey boxes depict mountainous regions mentioned in the text: (a) Pingualuit National Park; (b) the Torngat Mountains; (c) the Harp Lake Complex; (d) the Red Wine Mountains; (e) the Mealy Mountains; (f) the Otish Mountains; (g) the Groulx Mountains; and (h) the Romaine Hills.

2.3 Methods

Production of the climate variables developed in this study comprised the following five steps: (a) collection of raw monthly station air temperature data; (b) infilling of input monthly air temperature data; (c) spatial interpolation of air temperature data; (d) evaluation of output air temperature grids; and (e) conversion from air temperature to degree-days. The methodological approach employed at each step is described in detail in the following sections.

2.3.1 Assembly of climate data

Non-homogenized and homogenized monthly air temperatures for 97 climate stations (Figure 2-1) were collected from various official weather station sources including the National Climate Data Archive of Environment Canada (Vincent et al. 2012), the Berkeley Earth Surface Temperature Project (U.S.A) (Rohde et al. 2013a; Rohde et al. 2013b) and the Global Summary of the Day (GSOD) archive maintained by the National Climate Data Center. Supplemental data from four sites in western Labrador were provided by Hydro-Quebec through a data sharing agreement and data for six sites in the Torngat Mountains National Park were provided by Parks Canada. Station data was also made available for three sites by researchers in the Labrador Highlands Research group at Memorial University of Newfoundland (Chan 2010; Jacobs et al. 2014) and for eight sites by Centre D'Études Nordiques at Université Laval (CEN 2013; CEN 2014; Sarrazin and Allard 2014). Air temperature data from one climate station in northern Labrador (Kamestastin) (Trant et al. 2012) was provided by Dr. John Jacobs at Memorial University of Newfoundland. Summaries for the input stations used in spatial modelling of air temperatures across the Labrador-Ungava are available in Table B1. For degree-day modelling and evaluation, daily air temperature data available through Environment Canada were also collected from 48 stations using the Canadian Climate Data Scraping Tool (CCDST) (Bonifacio et al. 2015). For several datasets, daily air temperatures were aggregated to monthly means and monthly degree-day counts in the statistical analysis software R 3.0 using the *Zoo* package (Zeileis et al. 2015). Finally, climate normals (1971-2000/1981-2010) covering the Labrador-Ungava were also collected for 20 stations from Environment Canada (Hopkinson et al. 2012b) for the degree-day modelling described in *Section 2.3.5*.

2.3.2 Infilling of climate data

Recent work has shown that errors in spatial interpolation of air temperatures can be reduced through the inclusion of short, discontinuous climate series, particularly if methods of infilling are used to fill gaps in data coverage (Hopkinson et al. 2012b; Way and Bonnaventure 2015). Using a combination of

climate station data and atmospheric reanalysis over the period 1979-2012, Way and Bonnaventure (2015) showed that infilled air temperature data could be used to reliably estimate air temperatures at inactive climate stations throughout the Labrador-Ungava region. Evaluation of this methodology showed that the accuracy of the infilled climate series depends on the fidelity of the reference series used to guide infilling (atmospheric reanalysis) and the length of the climate station data. This study adopts the infilling methodology of Way and Bonnaventure (2015) to infill station data from the 97 input climate stations using a homogenized gridded anomaly product produced by the Berkeley Earth surface temperature product as a reference series. The Berkeley Earth product is derived using spatial interpolation and filtering of air temperature data collected from climate stations distributed all across the globe (Rohde et al. 2013a; Rohde et al. 2013b) and has been shown to provide reliable estimates of mean temperature anomalies in Labrador (Way and Viau 2015; Way et al. 2017b). Air temperatures are infilled to be spatially and temporally complete at a monthly resolution over the period 1948-2014 when Berkeley Earth's homogenized regional anomaly fields are well-constrained compared to local temperature series (Way et al. 2017b). Moreover, previous evaluation of the accuracy of infilling showed that the Berkeley Earth series provided lower mean absolute errors (MAE) than any of the reanalysis datasets tested in Way and Bonnaventure (2015).

2.3.3 Spatial interpolation of monthly air temperatures

Way and Bonnaventure (2015) showed that simple regression modelling of latitude, longitude and elevation against air temperature could explain >90 % of the spatial variability in air temperatures across Labrador-Ungava. Using a co-kriging approach, Aznar et al (2013) showed that air temperatures in the Labrador-Ungava are highly correlated at large distances and were reasonably correlated with climate model simulations for the area. This allowed them to produce air temperature grids at a 1 km resolution at a monthly temporal resolution over the period 1950-2000 (Aznar et al. 2013). Although both Aznar et al. (2013) and Way and Bonnaventure (2015) illustrated the applicability of different forms of spatial modelling in the Labrador-Ungava region, neither provided operationalized results that would be needed to facilitate modelling of current climate conditions. Several Canadian specific studies, however, have generated operationalized products at the national scale using climate station data incorporated in a Thin Plate Spline algorithm implemented using the ANUSPLIN software package (Hutchinson et al. 2009; Hopkinson et al. 2011; Hopkinson et al. 2012b).

Three spatial interpolation techniques (Regression Kriging, Thin Plate Spline smoothing, Co-Kriging) were evaluated for a test dataset for the purposes of evaluating the most appropriate approach for

operationalizing monthly air temperature mapping using geographic position (x, y) and elevation (m a.s.l.) as the only inputs. Spatial models were implemented primarily in the statistical analysis software R 3.0 using the *fields* (Nychka et al. 2015) and *raster* (Hijmans et al. 2015) packages with a digital elevation model from Canada's National Topographic Database for the region aggregated to a 1 km spatial resolution. Each of the spatial models was evaluated using climate normals averaged over the entire period of record for the infilled climate stations (n=97) (1948-2014). Four scenarios were designed to test the applicability of each of the three methods for modelling air temperatures. Under each of the scenarios, 24 out of the 97 sites were held-out and spatial models were derived for the full period (1948-2014) from the remaining 73 stations with evaluation statistics generated by comparing derived climate surfaces to both within-sample and out-of-sample stations. Each of the four held-out subsets was designed to test methods under a range of scenarios including holding-out mostly coastal stations, mostly continental stations and two random subsets (Figure 2-2).

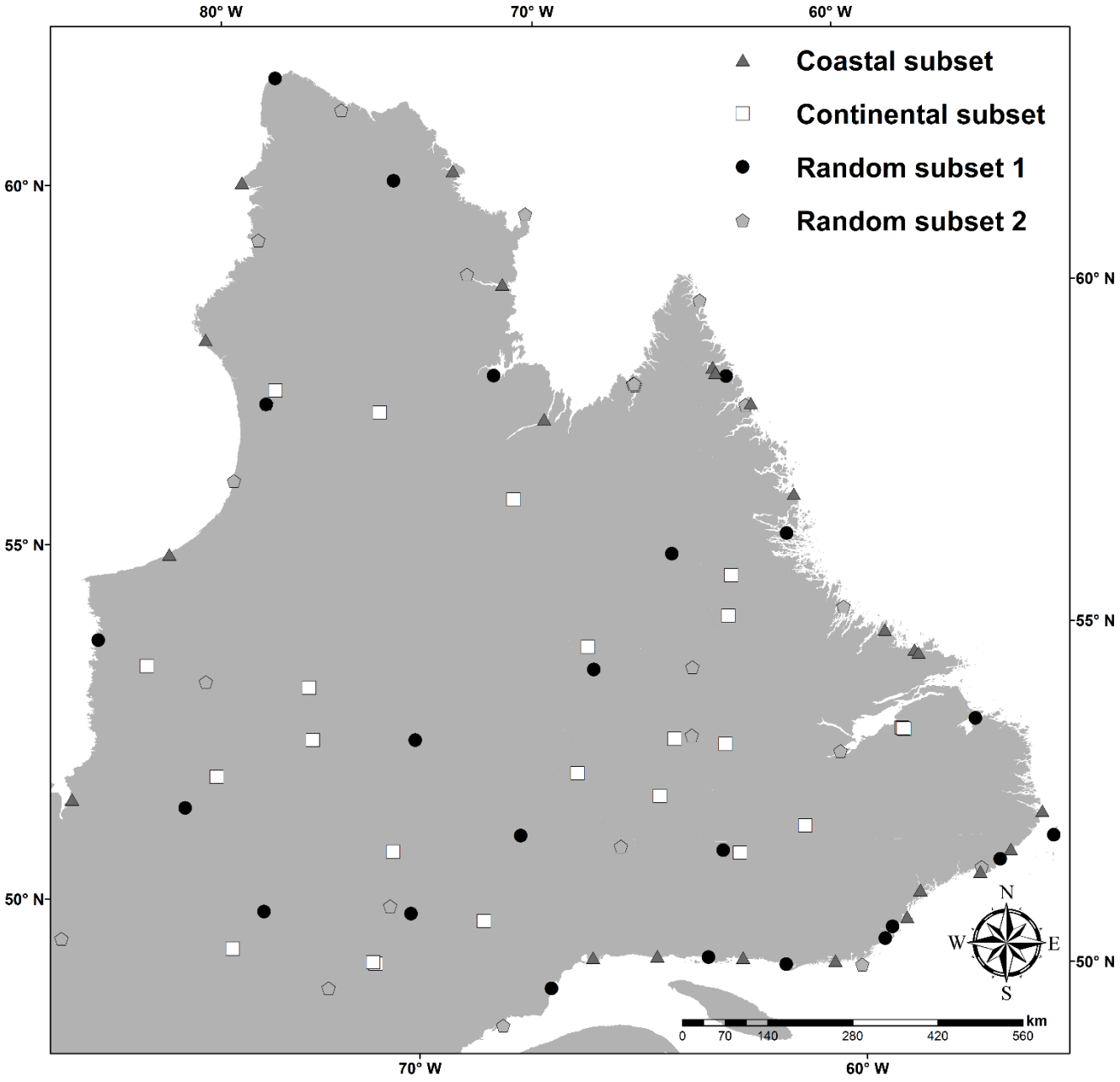

Figure 2-2: Spatial distribution of climate station subsets used in the evaluation of spatial modelling techniques. Under each scenario targeted subsets were withheld for comparison against modelled values derived from Regression Kriging, Thin Plate Spline smoothing or Co-Kriging.

2.3.4 Evaluation of selected interpolation method

Spatial interpolation of monthly air temperatures over the period (1948-2014) was evaluated using two alternative methods. The first method used leave-one-out cross validation to assess model performance in the absence of individual station observations. This method requires that observations for a given station are omitted at each time step and are then reconstructed from the remainder of the station data. This process was applied iteratively so that each individual station was omitted and subsequently reconstructed from the remaining observations for each of the 804 monthly time steps (see code in Appendix A1). The second approach compared additional stations (n=25) not included in the modelling algorithm because records were too short to meet the 36-month of continuous operation requirement for infilling. These stations consisted of six stations through which data is available via Environment Canada and 19 climate stations established as part of the Labrador Permafrost Project. Each of the latter group was located in undisturbed lowland or mountain sites in south-central Labrador with many sites paired at different elevations within close proximity of one other. Sites were established using Onset Hobo Pro v2 loggers (accuracy ± 0.2 °C, precision 0.02 °C) measuring surface air temperature at 1.9-2.4 m height above the ground in radiation screens (e.g. Lewkowicz 2008). By sampling the output climate grids during their respective overlapping time periods, the above stations can be directly compared to the spatial models generated in this study. Modelled and observed air temperatures were compared using standard evaluation statistics including mean absolute errors (MAE), root mean square errors (RMSE) and mean differences (e.g. Daly 2006). Spatial comparisons were also made with two alternative gridded products, the WorldClim product covering 1950-2000 (Hijmans et al. 2005) and the METEO1KM global daily air temperature product (Kilibarda et al. 2014) for the year 2011.

2.3.5 Conversion from air temperatures to degree-days

A variety of approaches have been used to generate cumulative freezing and thawing degree-day (FDD/TDD) products from air temperature data, with the most common being to directly aggregate daily data to the temporal interval needed for study. However, daily data are generally less readily available from major data providers and require more pre-processing to generate the desired products. Options for converting from monthly air temperatures to degree-days have typically included using simulated sine waves or infilling techniques (Allen 1976; Riseborough et al. 2012; Zhang et al. 2013). For permafrost-specific applications, Smith and Riseborough (1996; 2002) converted northern Canada climate station normals into freezing and thawing degree-days using a regression function considering only mean annual

air temperature. This approach provided reasonable results (±280 degree-days) when using a large set of climate normals distributed across Canada but it was not tested regionally (Smith and Riseborough 2002).

To test the applicability of converting degree-days directly from air temperatures, 1961-1990, 1971-2000 and 1981-2010 climate normals were collected for 20 Environment Canada climate stations located throughout northern Québec and Labrador. A comparison of accumulative degree-days and monthly air temperatures revealed that a simple 2nd order polynomial function can approximate this relation (r^2= 0.99); however, the statistical relation differs slightly among continental (temperature range: >35 °C), intermediate (temperature range: 30-35 °C) and coastal stations (temperature range: <30 °C) (Figure 2-3). This variability reflects the greater extremes experienced at more continental stations relative to coastal stations, resulting in higher cumulative degree-day totals for stations with greater temperature ranges (Figure 2-3).

Differential degree-day accumulation rates, as inferred from the observations, suggest that the original method proposed by Smith and Riseborough (1996; 2002) for degree-day conversion may produce errors across coastal-continental transitions. When tested on Labrador-Ungava data, the simple regression model comparing MAAT to cumulative degree-days provides a strong statistical association (TDD: r^2 >0.85; FDD: r^2 >0.87); however, the incorporation of an additional covariate (temperature range: T_{july} - T_{jan}) improves the results substantially (TDD: r^2 >0.99; FDD: r^2 >0.99). Given the small sample size (n=20), the robustness of this statistical association was tested by bootstrapping (1000 samples) with 95% of bias-corrected confidence intervals for r^2 falling between 0.979 and 0.993 for TDD and 0.996 to 0.999 for FDD. The mean absolute error for the two bias-adjusted regression models was 22 and 24 degree-days for TDD and FDD, respectively. On the basis of these relatively low errors, the above mentioned degree-day modelling approach was used to convert the air temperature grids produced in this study to annual degree-day maps. Regression coefficients were estimated using bootstrapping (n=1000) of the linear model with each coefficient derived from bias-adjusted coefficients

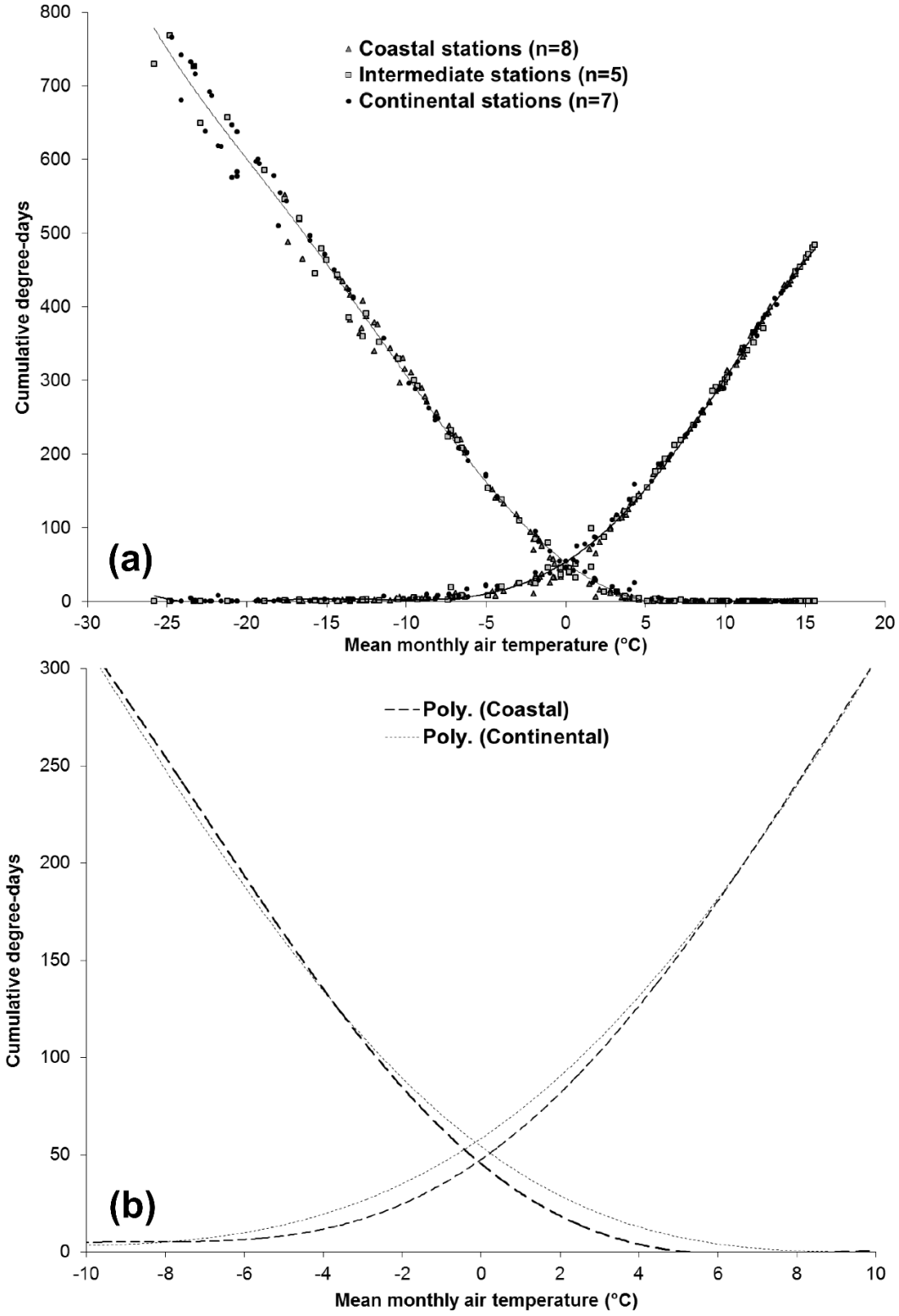

Figure 2-3: (a) Comparisons between observed mean monthly air temperatures and cumulative thawing and freezing degree-days for coastal, intermediate and continental stations. TDD line increase to the right and FDD line increases to the left. (b) Derived 5th and 6th order polynomial relations for both coastal and continental stations focusing on the area of divergence between the two statistical fits. Equations were as follows: Coastal fit: 1E-05x^6 - 1E-05x^5 - 0.006x^4 + 0.0103x^3 + 1.615x^2 - 16.573x + 45.261; Continental fit: -9E-05x^5 - 0.0024x^4 + 0.0282x^3 + 1.3037x^2 - 17.344x + 49.148.

2.4 Results and discussion

2.4.1 Evaluation of spatial interpolation methods

Mean absolute errors (MAEs) for each of the three spatial interpolation techniques were calculated from within-sample and out-of-sample station data in relation to four groupings of stations (coastal, continental, two random subsets; see Figure 2-2) over a long baseline climatology period (1948-2014). Within-sample results for each of the four groupings with 74 stations used gives MAEs of 0.46 °C, 0.30 °C, and 0.66 °C for Regression Kriging, Thin Plate Spline smoothing and Co-Kriging, respectively (Figure 2-4 a, b, c, d). The difference between the three approaches is greatest under the random subset 2 excluded scenario and least under random subset 1 excluded. Groups of stations with a subset of excluded coastal (n=24) and continental stations (n=24) both give much lower MAEs (better than 0.13 °C improvement) for Thin Plate Spline smoothing relative to Regression Kriging and Co-Kriging (Figure 2-4). Comparisons of the withheld stations under the four scenarios also show Thin Plate Spline smoothing as having the lowest overall MAE (0.61 °C) compared to Regression Kriging (0.64 °C) and Co-Kriging (0.68 °C) but the results are much closer than for the within-sample evaluation.

The out-of-sample coastal and continental station comparisons also support the slight improvement observed when using the Thin Plate Spline algorithm but the random subset results are more consistent across all methods (Figure 2-4 e, f, g, h). However, Regression Kriging outperforms Thin Plate Spline smoothing and Co-Kriging using the random subset 2 stations although the presence of several outliers could affect these results. Overall, across the four scenarios, within-sample comparisons typically have a lower MAE than out-of-sample results for Thin Plate Spline smoothing (~0.31 °C) and Regression Kriging (~0.18 °C) but show very little change for Co-Kriging (0.03 °C). The Thin Plate Spline's improved representation of the within-sample data coupled with the adequate performance against out-of-sample data suggests that in a full sample this technique will outperform both Regression Kriging and Co-Kriging. Overall, the methodological evaluation of within-sample and out-of-sample data indicate that Thin Plate Spline smoothing is the most consistently effective of the three techniques for spatial modelling of monthly air temperatures across the Labrador-Ungava region and was therefore selected for the remaining analysis. The implementation of the Thin Plate Spline used hereafter employs generalized cross validation to estimate the smoothing parameter, corrects for local degrees of freedom and scales independent variables into standardized units (see Nychka et al. 2015 for more details).

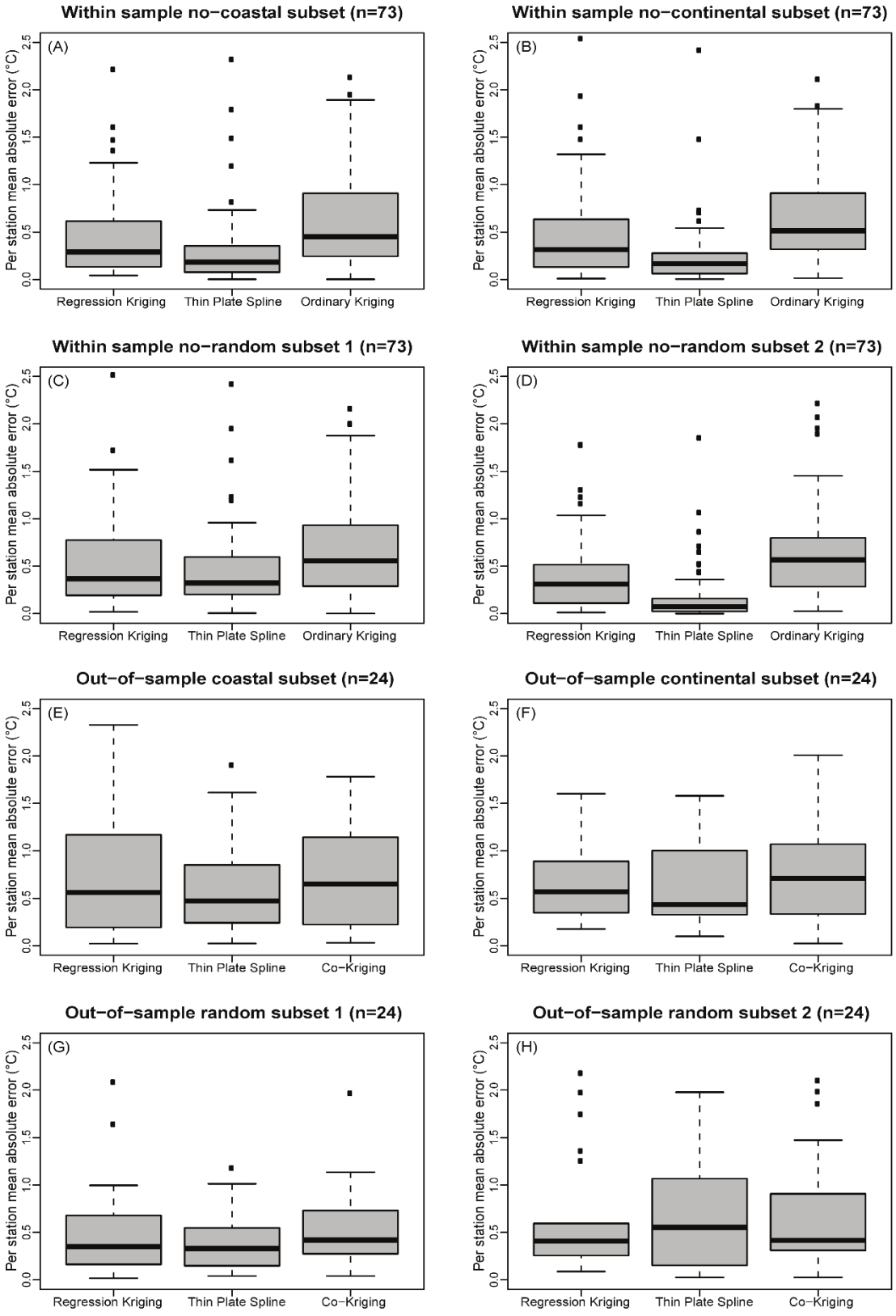

Figure 2-4: Comparison of mean absolute errors for selected spatial modelling techniques calculated by comparing modelled temperatures to within-sample (a, b, c, d) and withheld (e, f, g, h) observations for four scenarios each (coastal, continental and random subsets 1 & 2).

2.4.2 Spatial modelling assessment

Monthly air temperatures derived from Thin Plate Spline smoothing were assessed using leave-one-out cross validation and comparison against stations not included in modelling. Using the first approach, per station monthly MAE averaged 0.79 °C for the 97 stations with 50 % of the station MAEs being between 0.49 °C and 1.0 °C (Figure 2-5). Overall, ~75% of stations had MAEs lower than 1 °C. The root mean square error (RMSE) averaged across all stations was 0.95 °C with first and third quartiles of 0.59 °C and 1.19 °C, respectively. Mean differences on a per station basis averaged -0.01°C demonstrating no clear bias in the modelled values. However, compared to the original raw data (prior to infilling) the mean difference averaged on a per station basis was +0.15 °C indicating that modelled temperatures were on average slightly higher than those in the raw data. This bias, albeit small, arose because raw station data were infilled outside of a short (36 month) re-baselining period based on temperature anomalies from the Berkeley Earth product that had been adjusted for various inhomogeneities that artificially cooled the record in eastern Canada (Vincent et al. 2012; e.g. Rohde et al. 2013a). Evaluation of the spatial distribution of MAEs using Moran's I test for spatial autocorrelation (Moran 1950) suggested that errors (Figure 2-6) were distributed randomly (z-score: 0.17; p-value: 0.86). However, the largest MAEs were typically found along portions of the Labrador Sea coastline where interpolation is strongly influenced by stations in the interior, and in portions of the continental interior of Québec where station coverage is sparse. Temporally, MAEs showed no distinct trend through time (Figure B1) indicating the consistency of the selected interpolation approach (Thin Plate Spline smoothing) and the Berkeley-based infilling. The overall per station accuracy through time and space using the first method is estimated as 0.79 °C ± 0.28 °C. The second approach compares output grids and stations excluded from modelling (n=25). For the excluded stations, the average per station MAE was 0.77 ± 0.57°C with 50% of these stations having MAEs between 0.57 °C and 0.93 °C. These results have provided a very similar error estimate to the first approach for the stations examined (Figure 2-6).

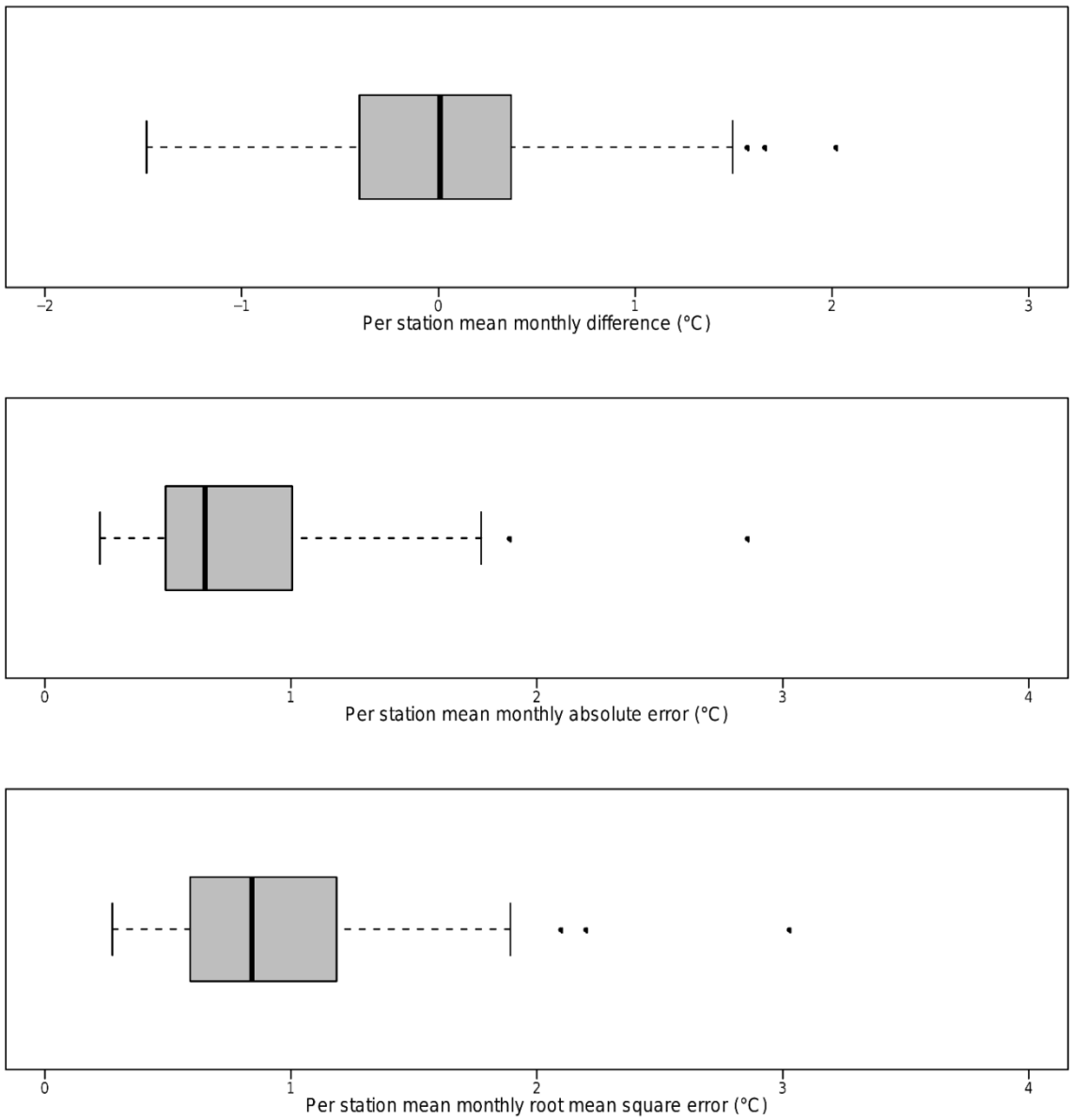

Figure 2-5: Summary statistics showing the results of leave-one-out cross validation at 97 stations located in the Labrador-Ungava region. Statistics include the mean difference (°C), mean absolute error (°C) and root mean square error (°C).

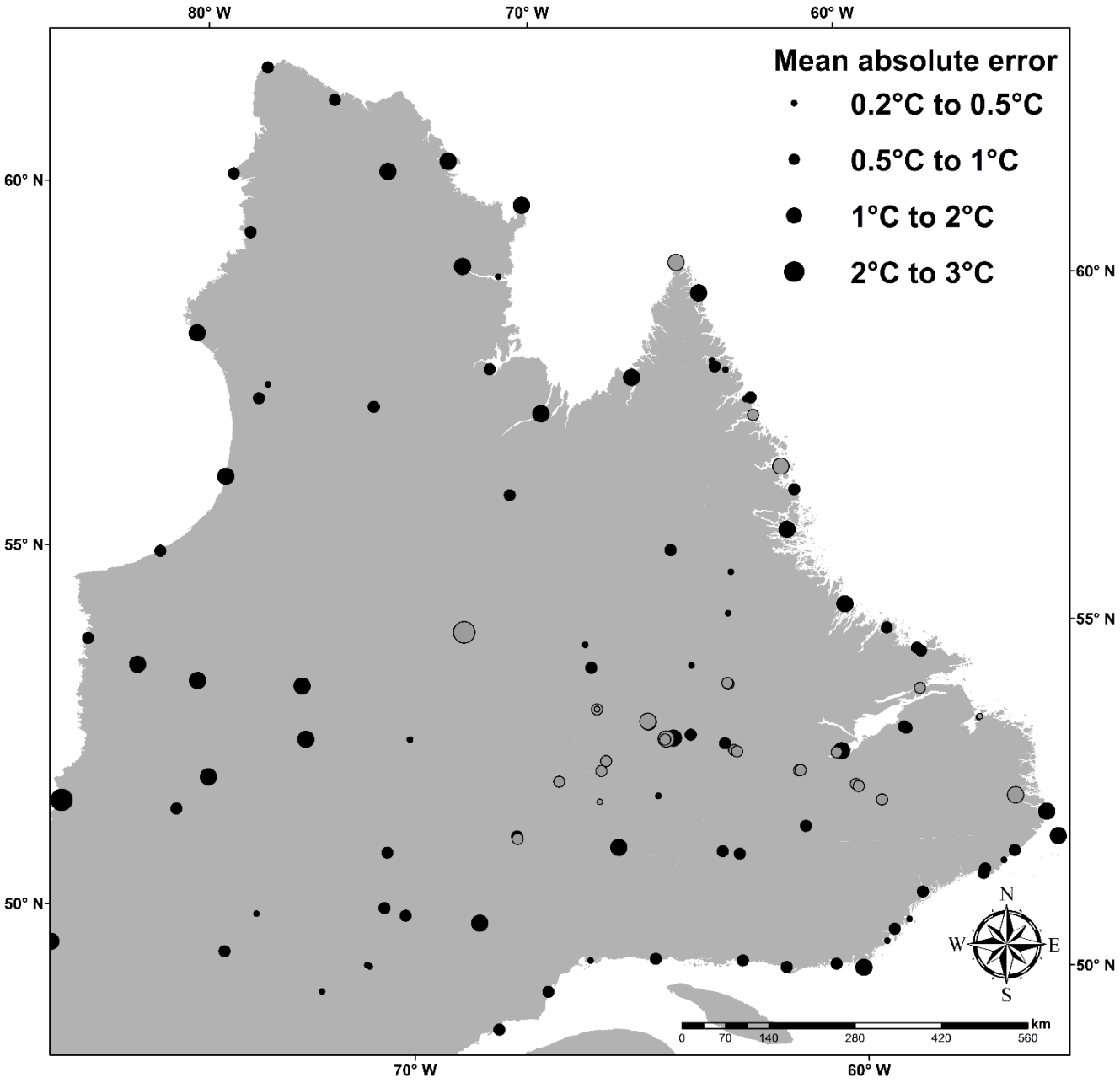

Figure 2-6: Spatial distribution of average per station mean absolute errors (°C) for 122 climate stations located across the Labrador-Ungava region. Grey dots show results for stations excluded from spatial modelling.

2.4.3 Spatial reconstructions of climate variables

Generated monthly air temperature climate grids showing the coldest (Figure 2-7 a) and warmest (Figure 2-7 b) Februaries in the Labrador-Ungava region illustrates the extreme spatial and temporal variability that characterize the region's climate. Spatial reconstructions of Labrador-Ungava air temperatures (aggregated to seasonal means) over the past 15 years are presented in Figure 2-8. The presence of seasonal sea ice cover on Hudson Bay and the position of the Arctic air masses allows for cold southeast trending winter temperatures (<-20 °C) to penetrate deep into the interior of Labrador-Ungava (Figure 2-8 a). The warmest parts of the landscape in the winter therefore correspond to coastal regions in the southeastern quadrant while the coldest portions are found in the upland portions of the continental interior. In the spring, the distribution of the coldest and warmest portions of the landscape shifts to being more latitudinally-controlled with higher temperatures found along the Labrador Sea coastline relative to Hudson's Bay (Figure 2-8 b). Elevation appears to control the air temperature distribution in summer with the coldest portions of the landscape restricted to high elevations in northern Québec and in the Torngat Mountains of northern Labrador where small mountain glaciers still persist (Way et al. 2014; Way et al. 2015) (Figure 2-8 c). Notably, the southeastern Labrador coastal region shifts from being the warmest region in the winter to one of the coldest regions in the summer reflecting the coastal influences of the cold Labrador Current to the east and the Gulf of St-Lawrence to the south. In the fall the lowest air temperatures are present at similar locations as in the summer, but include high elevations throughout the southern latitudes of the study area (Figure 8 d). The highest air temperatures during the fall occur in the coastal southeastern portion of Labrador and along the southern portions of the Hudson Bay coastline and are attributed to the thermal inertia of the adjacent waters which reach their highest temperature in the fall.

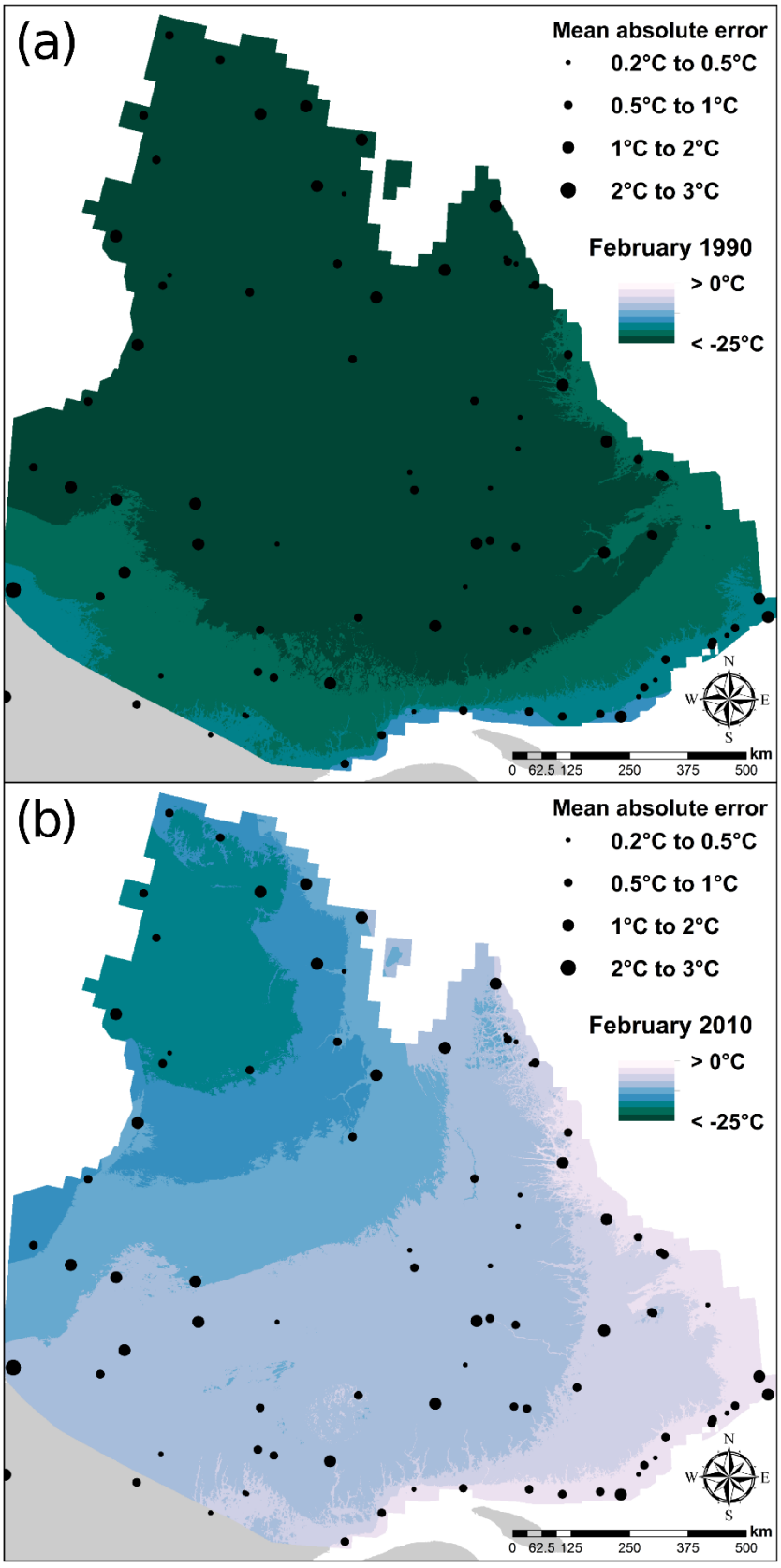

Figure 2-7: Example of monthly output grids for (a) the coldest and (b) the warmest Februaries reconstructed.

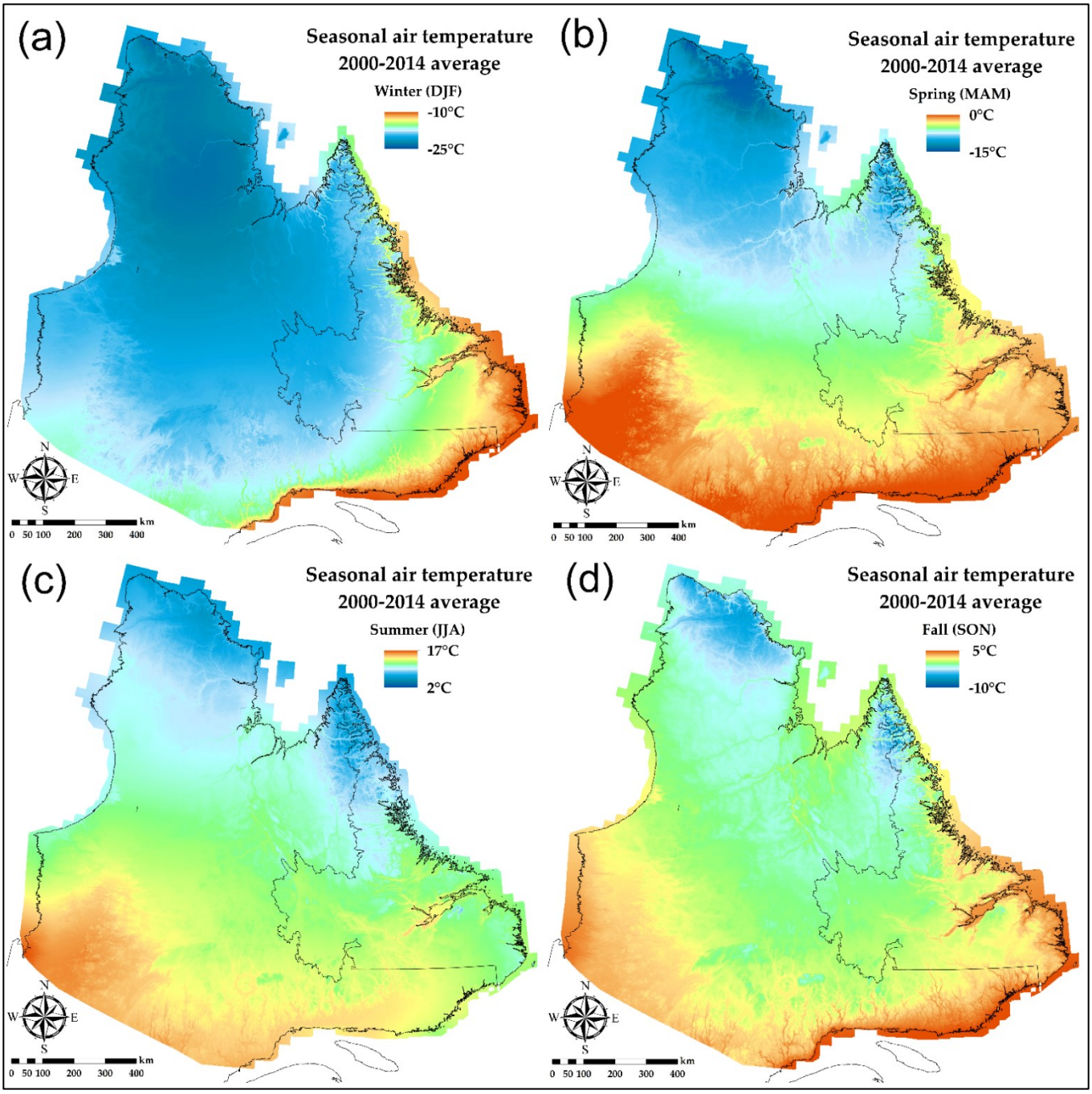

Figure 2-8: Spatial distribution of seasonal air temperatures modelled for the entire Labrador-Ungava region at a 1 km resolution over the period 2000-2014. Each map has a different absolute scale but shows the same temperature range (15°C) to facilitate visualization of seasonal temperature gradients across the region.

Mean annual air temperatures (MAAT) across much of the Labrador-Ungava region over the most recent period (2000-2014) are <-1 °C with much lower temperatures in the northern parts and at higher elevations (Figure 2-9 a). The warmest sectors are in the coastal areas of southeastern Labrador where MAAT exceeds 1 °C. The lowest MAAT (< -8 °C) occurs in the northernmost sections of Québec where the terrain is elevated and in the highest parts of the Torngat Mountains (Figure 2-9 a). Within the southern half of the region, relatively low MAATs occur as discrete areas within the Otish and Groulx Mountains and in the Mealy Mountains of eastern Labrador. Because of the deep penetration of low air temperatures in the winter and the relatively high summer air temperatures, the regions east of Hudson Bay including the continental interior have ranges of monthly average temperatures that exceed 34 °C (Figure 2-9 b). In contrast, the annual temperature range along the Labrador Sea coastline can be as little as 22 °C. The result is a clear coastal-continental gradient, with much of Labrador falling into zones between the highly maritime climatic regime of the coast and highly continental regime of interior Québec (Figure 2-9 b).

Coastal influences, particularly in Labrador, are also clearly identifiable in the degree-day maps developed for the region (Figure 2-9 c, d). Thawing degree-day counts are highest in southwestern Labrador-Ungava where the influences of elevation and water bodies are minimal, and lower in coastal regions, particularly in southeastern Labrador. Elevation is a clear control on the number of thawing degree-days with the lowest counts occurring in the upland regions of northern Québec and the Torngat Mountains (Figure 2-9 c). Other notable locations with lower degree-day counts include the Harp Lake Complex and Mealy Mountains where alpine terrain is widespread. By contrast, the freezing degree-day maps do not show the same pattern associated with elevation due to the deep cold air penetration in winter which affects both low and high elevations (Figure 2-9 d). Cumulative freezing degree-day and thawing degree-day patterns do not mirror each other. In the northern sector of Labrador, for example, thawing degree-days counts are amongst the lowest in the entire study area whereas freezing degree-days are comparable to much of northern Québec. In southeastern Labrador, thawing degree-day counts are low relative to much of the southern terrain while cumulative freezing degree-days are the lowest in all of the study area (Figure 2-9 c, d). Overall, the thawing and freezing degree-day maps show the persistent coastal influence on the region's climate, particularly in Labrador where coastal-continental contrasts occur over relatively short distances.

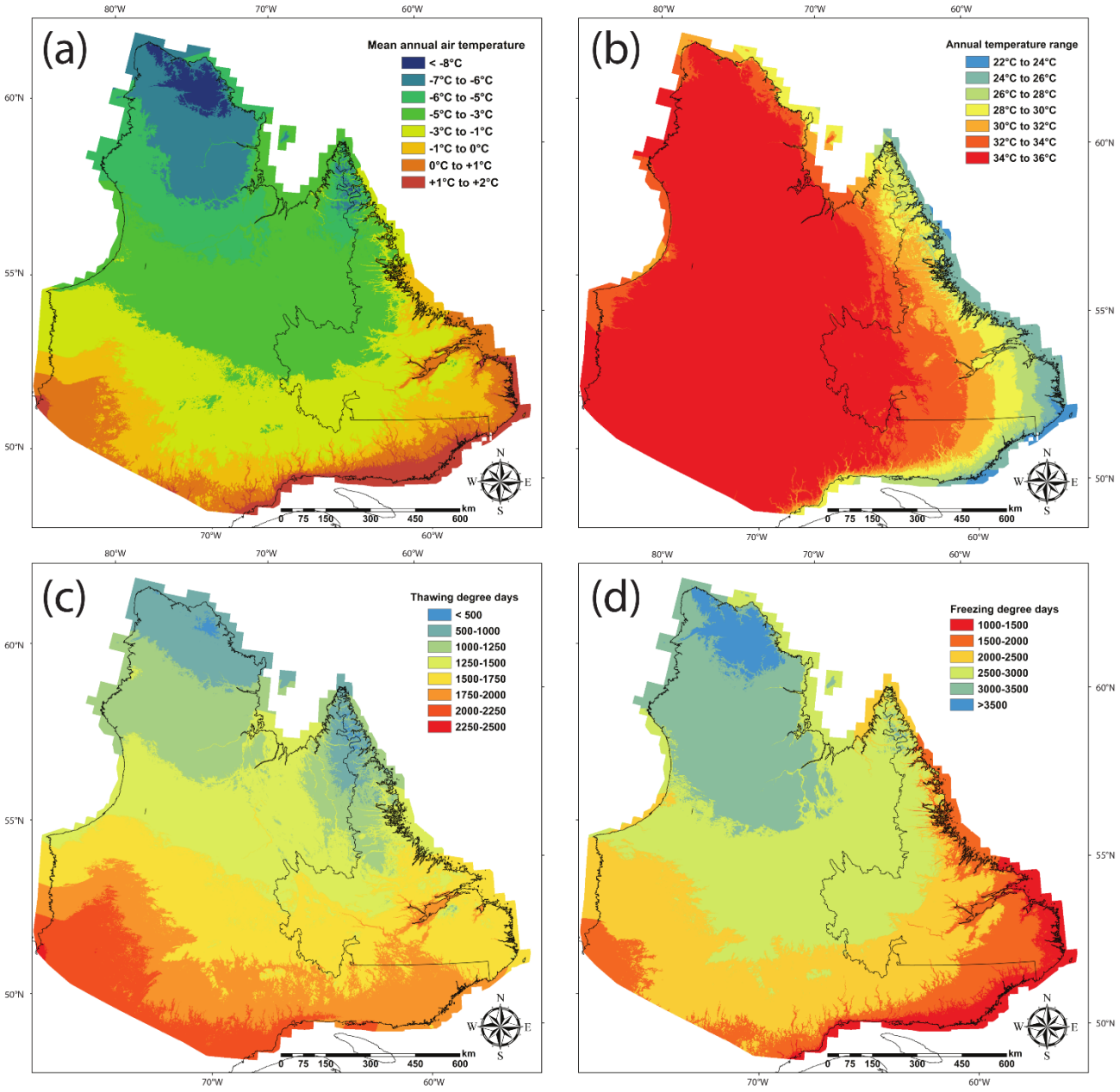

Figure 2-9: Climate variables derived from spatially modelled air temperatures across Labrador-Ungava. (a) Mean annual air temperature (°C) calculated by averaging monthly air temperature maps reclassified to show broad regional patterns; (b) Reclassified annual temperature range (°C) over the period 2000-2014 calculated by differencing July and January air temperatures; (c) Cumulative thawing degree-days over the 2000-2014 period calculated using empirically derived regression function that considers mean annual air temperature and annual temperature range; (d) Cumulative freezing degree-days over the 2000-2014 period calculated using empirically derived regression function that considers mean annual air temperature and annual temperature range.

2.4.4 Comparison with other studies

Tens of studies have produced air temperature grids over the last decade covering various scales ranging from local and regional (e.g. Daly et al. 2008; Wang et al. 2012) to global (e.g. Hijmans et al. 2005; Kilibarda et al. 2014). Methods for generating climate surfaces have rapidly increased in complexity from considering just geographic position and elevation (Hijmans et al. 2005) to climatologically-guided interpolation (Atkinson and Gajewski 2002; Daly et al. 2008) and advanced spatio-temporal kriging methods (Kilibarda et al. 2014; Kilibarda et al. 2015). Although topoclimatic products have been developed for a wide range of regions with various methods and means of assessing accuracy, the majority of recent studies use forms of Co-Kriging or Thin Plate Spline smoothing with mean absolute errors and root mean square errors being the most widely reported assessment statistic. In a Canada-wide study, Hutchinson et al (2009) used a Thin Plate Spline algorithm implemented through the ANUSPLIN software to produce Canada-wide daily air temperatures for both maximum and minimum temperatures. The mean absolute errors reported in that study (1.1-1.6°C) are slightly higher than those produced in this study, possibly due to the greater difficulty in interpolating maximum and minimum temperatures (Hutchinson et al. 2009). Another Canada-wide study by Hopkinson et al (2012b) provided MAEs of 0.36 °C and 0.66 °C at 48 (mostly low elevation and southern) withheld stations for interpolating 1971-2000 monthly climate normals using Thin Plate Spline smoothing. The authors noted that including infilled climate data improved spatial interpolation under most scenarios (Hopkinson et al. 2012b). A recent study by Oyler et al (2015) created a topoclimatic daily air temperature dataset for the entire lower 48 portion of the United States using a program developed to homogenize, infill and interpolate climate data through time and space across broad areas using additional information from MODIS LSTs. MAEs for annual minimum and maximum temperature were 0.78 °C and 0.56 °C, respectively, while the inclusion of MODIS LSTs did not improve interpolations uniformly across all months (Oyler et al. 2015), a result also found by Parmentier et al. (2015).

In the Labrador-Ungava region, two studies have produced spatial models of air temperature using remote sensing in conjunction with some form of either temporal or spatial interpolation (Hachem et al. 2009; Aznar et al. 2013). For example, Hachem et al. (2009) derived land surface temperatures across Labrador-Ungava for a brief period using the MODIS LST product with incomplete sampling compensated for with a form of temporal infilling based on a sinusoidal annual temperature wave. The results of this study indicated colder than expected temperatures across the Labrador-Ungava due to the impacts of water bodies and late-season snow patches which record lower land surface temperatures than surface air temperatures (Hachem et al. 2009). Using Co-Kriging, Aznar et al. (2013) used the Hachem et al. (2009)

LST data and the Canadian Regional Climate Model (CRCM 4.2.3) with climate station data collected at 202 weather stations to model monthly air temperatures over the period 1961-2000 at a 1 km resolution for the whole region. Elevation was not used as a covariate because LST maps were considered adequate representations of the spatial variability in air temperature patterns across the region. MAEs were 1.5 ± 1.2 °C using take-one-out cross-validation procedures over this period (Aznar et al. 2013).

We used an entirely different methodological approach with corresponding MAEs (0.79 ± 0.28 °C) approximately half of those of Aznar et al. (2013) despite covering a much longer period (1948-2014). Moreover, we used a larger elevation range for input stations and an infilling technique (Way and Bonnaventure 2015) to reduce spatio-temporal biases associated with interpolating from incomplete station records. We hypothesize that the absence of an elevation covariate contributes to the higher errors for Aznar et al. (2013), given that the within-sample and out-of-sample climate station data used in our study suggest an important role for this factor. As a final methodological comment, our study shows that under most scenarios Thin Plate Spline smoothing is a more accurate interpolator of air temperatures across the Labrador-Ungava region than Co-Kriging with the same covariates.

Our modelled MAAT surfaces were also compared to those generated for the region as part of the WorldClim project. To make the two products comparable, air temperatures were averaged over the period 1950-2000 to match WorldClim's temporal coverage (Hijmans et al. 2005). Given that many of the source datasets are similar and both WorldClim and this study use forms of Thin Plate Spline smoothing, the results are expected to be broadly similar. The mean difference between the two grids (this study minus WorldClim) is calculated to be -0.09 °C with a standard deviation of 0.55 °C, and the majority of this study's model results are within ± 0.5 °C of the WorldClim surfaces (Figure 2-10 a). Distinct differences between the two products are most noticeable along the southeastern coast of the Hudson Bay where this study produces higher air temperatures and in northern Québec where WorldClim temperatures are higher. Smaller areas of somewhat greater disagreement occur in mountainous regions in southwestern Labrador, in the interior of the Torngat Mountains and in coastal areas of central Labrador (Figure 2-10 a). Overall, this comparison shows that the spatial modelling employed in this study produces comparable results to WorldClim despite using a number of different input stations and an alternative implementation of Thin Plate Spline smoothing.

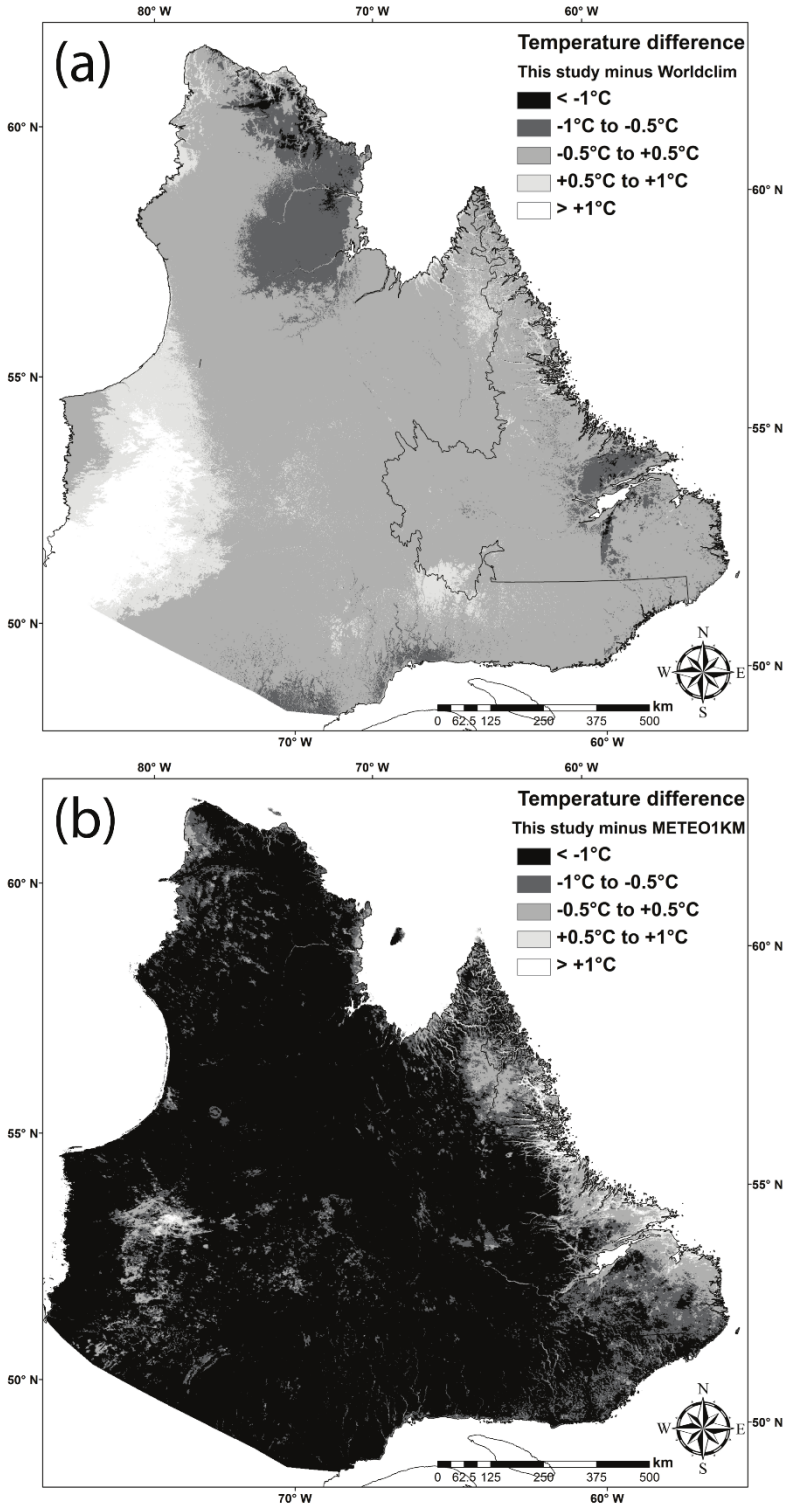

Figure 2-10: MAAT calculated in this study compared to published products: (a) comparison with the WorldClim product calculated over the period 1950-2000; and (b) comparison with the METEO1KM product calculated for the year 2011.

A comparison was also made for Labrador-Ungava between the results of this study and those of the METEO1KM product (Kilibarda et al. 2014). The METEO1KM is currently only available for the year 2011 at a daily resolution, so the product's daily air temperatures were first averaged over the entire year and then compared to the average of the 2011 results for this study. The METEO1KM results have a mean bias relative this study of +1.48 °C with a standard deviation of 0.69 °C. Spatially, this warm bias appears to exist throughout much of the interior Labrador-Ungava with some isolated pockets having comparable air temperatures to those presented in this study (Figure 2-10 b). Notably, this study presents higher air temperatures throughout much of coastal Labrador with some exceptions such as the Torngat Mountains where METEO1KM is higher. In the Mealy Mountains, the METEO1KM is much higher than observed values at upper elevations in particular (Figure 2-10 b). We note that a similar (too warm) pattern in the Mealy Mountains appears in the Aznar et al. (2013) and Hachem et al. (2009) which, like Kilibarda et al. (2014), use LST data in spatial interpolation.

2.4.5 Limitations of spatial reconstruction methodology

Some of the limitations associated with the spatial reconstructions presented in this study include that we develop a regional rather than local representation of air temperatures and degree-days and therefore do not account for local climate influences such as aspect, exposure, vegetation cover and proximity to lakes. Despite having high correlations at large distances, air temperatures can also exhibit spatial heterogeneity at the local scale as a result of synoptic patterns such as the persistence of deep cold air inversions in the interior in winter or in the Arctic-like coastal regions of Labrador during summer. Climatologically-aided interpolation techniques (e.g. Atkinson and Gajewski 2002; Daly et al. 2008) or the addition of more covariates into spatial modelling could, in theory, provide a more detailed representation of local climate conditions. For example, the local-scale impact of large inland lakes and seasonal sea ice cover in coastal zones might need to be explicitly incorporated in higher resolution topoclimatic modelling.

The generation of temporally complete, quality-controlled records of LST at a finer spatial scale (e.g. 250m, Metz et al. 2014) could be a means of adding supplemental spatial information which cannot be estimated from isolated weather stations; however, at this point there is not sufficient evidence that available MODIS LST products for the Labrador-Ungava (e.g. Hachem et al. 2009) are free of biases. Alternatively, from a geostatistical perspective it may be possible in the future to use LSTs in conjunction with additional covariates including this study's derived climatology field to further refine spatial air temperature maps at the local-scale. Monitoring stations established as part of the Labrador Permafrost

Project were selected on the basis of filling gaps in coverage of the current observational network and also to provide a detailed understanding of climatological conditions in the forest-tundra to alpine transitional environments. Once these stations (33 established to date) meet the criteria for inclusion established as part of this study (36 months continuous operation) they can be included in future iterations of spatial modelling, thereby providing a diverse spatial and elevational sampling of the Labrador portion of the region.

Finally, it is important to also note that the derived spatial models developed in this study are strongly dependent on the fidelity of the reference series (Berkeley Earth) used for infilling. Although the accuracy assessment suggests that Berkeley Earth was an appropriate choice, it is possible that its accuracy may vary prior to this study's start (1948) when station counts decline in northeastern Canada (Rapaić et al. 2015). The reliance of infilling on selected reference series is a limitation, in that Berkeley Earth may not adequately capture the spatial variability in temperature anomalies, but also an advantage because this study's methodology can be easily re-implemented if more accurate reference series become available. Temporal stability may also be a concern in the derived degree-day relations with mean annual air temperature and temperature range. This is particularly the case when projecting into the future when climate warming may affect the frequency of extreme events and their spatial character.

2.5 Summary and conclusion

This study presents the methodological framework for the creation of moderate resolution (1 km) air temperature and degree-day grids for the Labrador-Ungava region for the entire 1948-2014 period. Comparison between three commonly used interpolation techniques revealed Thin Plate Spline smoothing to be the most accurate means to spatially represent the patterns of air temperature in Labrador-Ungava using only three covariates (geographic position and elevation). The derived air temperature grids, evaluated across a wide range of environments and scenarios, have an overall accuracy of 0.79 ± 0.28 °C on a per month basis illustrating a higher accuracy than other recent studies. They qualitatively show regional patterns that agree with climatological characteristics in the region caused by the combined influences of Arctic air masses and coastal proximity. Comparisons between air temperatures and cumulative degree-days show a predictable pattern of greater cumulative degree-days in the spring and fall seasons in continental sites compared to coastal sites. This relation can be used in an empirically-derived regression function to accurately convert air temperature maps (mean annual air temperature & temperature range) to annual freezing and thawing degree-day counts. More work is needed to better fully

characterize the influence of local-scale synoptic processes on air temperatures across the Labrador-Ungava region but this study presents a step towards achieving this goal.

Acknowledgements

The authors would like to thank all the organizations and individuals who have made climate data available for the Labrador-Ungava. In particular, we would like to thank Dr. John Jacobs of Memorial University of Newfoundland and Dr. Darroch Whitaker of Parks Canada for making weather station available for the Mealy Mountains, Kamestastin and the Torngat Mountains. We would like to thank Hydro Québec for making data from a number of climate stations available for this study. The authors would like to thank Steven Mosher for help with various programming and theoretical issues related to this project. RGW would like to acknowledge financial support from NSERC, the Association of Canadian Universities for Northern Studies and the University of Ottawa. Funding for instrumentation and fieldwork was provided by the University of Ottawa, NSERC and the Northern Scientific Training Program.

2.6 References

Aalto, J., P. Pirinen, J. Heikkinen, and A. Venäläinen. 2013. Spatial interpolation of monthly climate data for Finland: comparing the performance of kriging and generalized additive models. Theoretical and Applied Climatology 112(1–2): 99–111. doi: 10.1007/s00704-012-0716-9.

Allen, J. C. 1976. A modified sine wave method for calculating degree days. Environmental Entomology 5(3): 388–396.

Atkinson, D. E., and K. Gajewski. 2002. High-Resolution Estimation of Summer Surface Air Temperature in the Canadian Arctic Archipelago. Journal of Climate 15(24): 3601–3614. doi: 10.1175/1520-0442(2002)015<3601:HREOSS>2.0.CO;2.

Aznar, J.-C., E. Gloaguen, D. Tapsoba, S. Hachem, D. Caya, and Y. Bégin. 2013. Interpolation of monthly mean temperatures using cokriging in spherical coordinates. International Journal of Climatology 33(3): 758–769. doi: 10.1002/joc.3468.

Banfield, C. E., and J. D. Jacobs. 1998. Regional patterns of temperature and precipitation for Newfoundland and Labrador during the past century. The Canadian Geographer/Le Géographe canadien 42(4): 354–364.

Bonifacio, C., T. E. Barchyn, C. H. Hugenholtz, and S. W. Kienzle. 2015. CCDST: A free Canadian climate data scraping tool. Computers & Geosciences 75: 13–16. doi: 10.1016/j.cageo.2014.10.010.

Bonnaventure, P. P., and A. G. Lewkowicz. 2011. Modelling climate change effects on the spatial distribution of mountain permafrost at three sites in northwest Canada. Climatic Change 105(1–2): 293–312. doi: 10.1007/s10584-010-9818-5.

Bonnaventure, P. P., and A. G. Lewkowicz. 2013. Impacts of mean annual air temperature change on a regional permafrost probability model for the southern Yukon and northern British Columbia, Canada. The Cryosphere 7(3): 935–946. doi: 10.5194/tc-7-935-2013.

Bonnaventure, P. P., A. G. Lewkowicz, M. Kremer, and M. C. Sawada. 2012. A permafrost probability model for the southern Yukon and northern British Columbia, Canada. Permafrost and Periglacial Processes 23(1): 52–68. doi: 10.1002/ppp.1733.

Brown, R., M. Lemay, M. Allard, N. E. Barrand, C. Barrette, Y. Bégin, T. Bell, M. Bernier, S. Bleau, D. Chaumont, Y. Dibike, A. Frigon, P. Leblanc, D. Paquin, M. J. Sharp, and R. Way. 2012. Climate variability and change in the Canadian Eastern Subarctic IRIS region (Nunavik and Nunatsiavut). In Nunavik and Nunatsiavut: From science to policy. An Integrated Regional Impact Study (IRIS) of climate change and modernization, 57–93.

CEN. 2013. Environmental data from Boniface river region in Nunavik, Quebec, Canada, v. 1.1 (1988-2013). Scientific data 7. Nordicana D. Centre D'Étude Nordiques.

CEN. 2014. Environmental data from the Blanc-Sablon station, Quebec, Canada, v. 1.0 (1990-2012). Scientific data 5. Nordicana D. Centre D'Étude Nordiques.

Chan, S. 2010. Regional and Local Climatology of a Subarctic Alpine Treeline, Mealy Mountains, Labrador. MSc Thesis, St. John's, Newfoundland and Labrador: Memorial University of Newfoundland.

Daly, C. 2006. Guidelines for assessing the suitability of spatial climate data sets. International Journal of Climatology 26(6): 707–721. doi: 10.1002/joc.1322.

Daly, C., M. Halbleib, J. I. Smith, W. P. Gibson, M. K. Doggett, G. H. Taylor, J. Curtis, and P. P. Pasteris. 2008. Physiographically sensitive mapping of climatological temperature and precipitation across the conterminous United States. International Journal of Climatology 28(15): 2031–2064. doi: 10.1002/joc.1688.

Elliott, D. L., and S. K. Short. 1979. The Northern Limit of Trees in Labrador: A Discussion. ARCTIC 32(3): 201–206. doi: 10.14430/arctic2620.

Evangelista, P. H., S. Kumar, T. J. Stohlgren, and N. E. Young. 2011. Assessing forest vulnerability and the potential distribution of pine beetles under current and future climate scenarios in the Interior

West of the US. Forest Ecology and Management 262(3): 307–316. doi: 10.1016/j.foreco.2011.03.036.

Fiddes, J., S. Endrizzi, and S. Gruber. 2015. Large-area land surface simulations in heterogeneous terrain driven by global data sets: application to mountain permafrost. The Cryosphere 9(1): 411–426. doi: 10.5194/tc-9-411-2015.

Finnis, J. 2013. Projected impacts of climate change for the province of Newfoundland and Labrador. Technical report. St. John's, Newfoundland and Labrador: Office of Climate Change, Energy Efficiency and Emissions Trading, Provincial Government of Newfoundland and Labrador.

Fortin, M.-C., and K. Gajewski. 2012. Potential problems with the use of gridded climate data in regional quantitative paleoenvironmental studies from data-poor regions. Journal of Paleolimnology 48(3): 641–650. doi: 10.1007/s10933-012-9639-9.

Gisnås, K., B. Etzelmüller, H. Farbrot, T. V. Schuler, and S. Westermann. 2013. CryoGRID 1.0: Permafrost distribution in Norway estimated by a spatial numerical model. Permafrost and Periglacial Processes 24(1): 2–19. doi: 10.1002/ppp.1765.

Hachem, S., M. Allard, and C. Duguay. 2009. Using the MODIS land surface temperature product for mapping permafrost: an application to northern Québec and Labrador, Canada. Permafrost and Periglacial Processes 20(4): 407–416. doi: 10.1002/ppp.672.

Harris, I., P. D. Jones, T. J. Osborn, and D. H. Lister. 2014. Updated high-resolution grids of monthly climatic observations–the CRU TS3. 10 Dataset. International Journal of Climatology 34(3): 623–642.

Heginbottom, J. A., M.-A. Dubreuil, and P. A. Harker. 1995. Canada – Permafrost. National Atlas of Canada, 5th Edition. Ottawa, Canada: Natural Resources Canada.

Hijmans, R. J., S. E. Cameron, J. L. Parra, P. G. Jones, and A. Jarvis. 2005. Very high resolution interpolated climate surfaces for global land areas. International Journal of Climatology 25(15): 1965–1978. doi: 10.1002/joc.1276.

Hijmans, R. J., J. van Etten, J. Cheng, M. Mattiuzzi, M. Sumner, J. A. Greenberg, O. P. Lamigueiro, A. Bevan, E. B. Racine, A. Shortridge, and M. R. J. Hijmans. 2015. raster (version 2.5-2). Geographic Data Analysis and Modeling.

Hopkinson, R. F., D. W. McKenney, E. J. Milewska, M. F. Hutchinson, P. Papadopol, and L. A. Vincent. 2011. Impact of Aligning Climatological Day on Gridding Daily Maximum–Minimum Temperature and Precipitation over Canada. Journal of Applied Meteorology and Climatology 50(8): 1654–1665. doi: 10.1175/2011JAMC2684.1.

Hopkinson, R. F., M. F. Hutchinson, D. W. McKenney, E. J. Milewska, and P. Papadopol. 2012. Optimizing input data for gridding climate normals for Canada. Journal of Applied Meteorology and Climatology 51(8): 1508–1518. doi: 10.1175/JAMC-D-12-018.1.

Hu, J., and Z. Jiang. 2010. Predicting the potential distribution of the endangered Przewalski's gazelle: Potential distribution of Przewalski's gazelle. Journal of Zoology 282(1): 54–63. doi: 10.1111/j.1469-7998.2010.00715.x.

Hutchinson, M. F., D. W. McKenney, K. Lawrence, J. H. Pedlar, R. F. Hopkinson, E. Milewska, and P. Papadopol. 2009. Development and testing of Canada-wide interpolated spatial models of daily minimum-maximum temperature and precipitation for 1961–2003. Journal of Applied Meteorology and Climatology 48(4): 725–741. doi: 10.1175/2008JAMC1979.1.

Jacobs, J. D., S. Chan, and E. Sutton. 2014. Climatology of the Forest-Tundra Ecotone at a Maritime Subarctic-Alpine Site, Mealy Mountains, Labrador. ARCTIC 67(1): 28–42. doi: 10.14430/arctic4358.

Jafarov, E. E., S. S. Marchenko, and V. E. Romanovsky. 2012. Numerical modeling of permafrost dynamics in Alaska using a high spatial resolution dataset. The Cryosphere 6(3): 613–624. doi: 10.5194/tc-6-613-2012.

Kilibarda, M., T. Hengl, G. B. M. Heuvelink, B. Gräler, E. Pebesma, M. Perčec Tadić, and B. Bajat. 2014. Spatio-temporal interpolation of daily temperatures for global land areas at 1 km resolution. Journal of Geophysical Research: Atmospheres 119(5): 2294–2313. doi: 10.1002/2013JD020803.

Kilibarda, M., M. P. Tadić, T. Hengl, J. Luković, and B. Bajat. 2015. Global geographic and feature space coverage of temperature data in the context of spatio-temporal interpolation. Spatial Statistics 14: 22–38. doi: 10.1016/j.spasta.2015.04.005.

Kriticos, D. J., B. L. Webber, A. Leriche, N. Ota, I. Macadam, J. Bathols, and J. K. Scott. 2012. CliMond: global high-resolution historical and future scenario climate surfaces for bioclimatic modelling. Methods in Ecology and Evolution 3(1): 53–64. doi: 10.1111/j.2041-210X.2011.00134.x.

Ladd, M., R. G. Way, and A. E. Viau. 2015. The impact of using different modern climate data sets in pollen-based paleoclimate reconstructions of North America. Quaternary Science Reviews 112: 78–85. doi: 10.1016/j.quascirev.2015.01.020.

Lane, A., and A. Jarvis. 2007. Changes in climate will modify the geography of crop suitability: agricultural biodiversity can help with adaptation. SAT ejournal 4(1): 1–12.

Lewkowicz, A. G. 2008. Evaluation of miniature temperature-loggers to monitor snowpack evolution at mountain permafrost sites, northwestern Canada. Permafrost and Periglacial Processes 19(3): 323–331. doi: 10.1002/ppp.625.

McKenney, D. W., M. F. Hutchinson, P. Papadopol, K. Lawrence, J. Pedlar, K. Campbell, E. Milewska, R. F. Hopkinson, D. Price, and T. Owen. 2011. Customized spatial climate models for North America. Bulletin of the American Meteorological Society 92(12): 1611–1622.

Metz, M., D. Rocchini, and M. Neteler. 2014. Surface temperatures at the continental scale: tracking changes with remote sensing at unprecedented detail. Remote Sensing 6(5): 3822–3840. doi: 10.3390/rs6053822.

Moran, P. A. P. 1950. Notes on Continuous Stochastic Phenomena. Biometrika 37(1/2): 17–23. doi: 10.2307/2332142.

Nychka, D., R. Furrer, J. Paige, and S. Sain. 2015. fields (version 8.3-6). Tools for Spatial Data.

Oyler, J. W., A. P. Ballantyne, K. Jencso, M. Sweet, and S. W. Running. 2015. Creating a topoclimatic daily air temperature dataset for the conterminous United States using homogenized station data and remotely sensed land skin temperature. International Journal of Climatology 35(9): 2258–2279.

Parmentier, B., B. J. McGill, A. M. Wilson, J. Regetz, W. Jetz, R. Guralnick, M.-N. Tuanmu, and M. Schildhauer. 2015. Using multi-timescale methods and satellite-derived land surface temperature for the interpolation of daily maximum air temperature in Oregon. International Journal of Climatology 35(13): 3862–3878. doi: 10.1002/joc.4251.

Rapaić, M., R. Brown, M. Markovic, and D. Chaumont. 2015. An evaluation of temperature and precipitation surface-based and reanalysis datasets for the Canadian Arctic, 1950–2010. Atmosphere-Ocean 53(3): 283–303. doi: 10.1080/07055900.2015.1045825.

Riseborough, D. W., S. Wolfe, and C. Duchesne. 2012. Simplified climate statistics for permafrost modeling: Yellowknife case study. In Proceedings of the 10th International Conference on Permafrost, 335–340. Salekhard, Russia.

Rohde, R., R. A. Muller, R. Jacobsen, E. Muller, and C. Wickham. 2013a. A new estimate of the average earth surface land temperature spanning 1753 to 2011. Geoinformatics & Geostatistics: An Overview 1(1). doi: 10.4172/2327-4581.1000101.

Rohde, R., R. Muller, R. Jacobsen, S. Perlmutter, and S. Mosher. 2013b. Berkeley Earth temperature averaging process. Geoinformatics & Geostatistics: An Overview 1(2). doi: 10.4172/2327-4581.1000103.

Sarrazin, D., and M. Allard. 2014. Environmental data from the Kangiqsualujjuaq region in Nunavik, Quebec, Canada, v. 1.1 (1988-2013). Scientific data 14. Nordicana D. Centre D'Étude Nordiques.

Smith, M. W., and D. W. Riseborough. 1996. Permafrost monitoring and detection of climate change. Permafrost and Periglacial Processes 7(4): 301–309. doi: 10.1002/(SICI)1099-1530(199610)7:4<301::AID-PPP231>3.0.CO;2-R.

Smith, M. W., and D. W. Riseborough. 2002. Climate and the limits of permafrost: a zonal analysis. Permafrost and Periglacial Processes 13(1): 1–15. doi: 10.1002/ppp.410.

Trant, A. J., J. D. Jacobs, and T. Sable. 2012. Teaching and learning about climate change with Innu Environmental Guardians. Polar Geography 35(3–4): 229–244. doi: 10.1080/1088937X.2012.682229.

Vincent, L. A., X. L. Wang, E. J. Milewska, H. Wan, F. Yang, and V. Swail. 2012. A second generation of homogenized Canadian monthly surface air temperature for climate trend analysis. Journal of Geophysical Research: Atmospheres 117(D18): n/a-n/a. doi: 10.1029/2012JD017859.

Wang, T., A. Hamann, D. L. Spittlehouse, and T. Q. Murdock. 2012. ClimateWNA - High-Resolution Spatial Climate Data for Western North America. Journal of Applied Meteorology and Climatology 51(1): 16–29. doi: 10.1175/JAMC-D-11-043.1.

Way, R. G., and P. P. Bonnaventure. 2015. Testing a reanalysis-based infilling method for areas with sparse discontinuous air temperature data in northeastern Canada: Reanalysis-based infilling in northeastern Canada. Atmospheric Science Letters 16(3): 398–407. doi: 10.1002/asl2.574.

Way, R. G., and A. E. Viau. 2015. Natural and forced air temperature variability in the Labrador region of Canada during the past century. Theoretical and Applied Climatology 121(3–4): 413–424. doi: 10.1007/s00704-014-1248-2.

Way, R. G., T. Bell, and N. E. Barrand. 2014. An inventory and topographic analysis of glaciers in the Torngat Mountains, northern Labrador, Canada. Journal of Glaciology 60(223): 945–956. doi: 10.3189/2014JoG13J195.

Way, R. G., T. Bell, and N. E. Barrand. 2015. Glacier change from the early Little Ice Age to 2005 in the Torngat Mountains, northern Labrador, Canada. Geomorphology 246: 558–569. doi: 10.1016/j.geomorph.2015.07.006.

Way, R. G., F. Oliva, and A. E. Viau. 2017. Underestimated warming of northern Canada in the Berkeley Earth temperature product. International Journal of Climatology 37(4): 1746–1757. doi: 10.1002/joc.4808.

Westermann, S., T. V. Schuler, K. Gisnås, and B. Etzelmüller. 2013. Transient thermal modeling of permafrost conditions in Southern Norway. The Cryosphere 7(2): 719–739. doi: 10.5194/tc-7-719-2013.

Westermann, S., T. I. Østby, K. Gisnås, T. V. Schuler, and B. Etzelmüller. 2015. A ground temperature map of the North Atlantic permafrost region based on remote sensing and reanalysis data. The Cryosphere 9(3): 1303–1319. doi: 10.5194/tc-9-1303-2015.

Wright, J. F., C. Duchesne, and M. M. Côté. 2003. Regional-scale permafrost mapping using the TTOP ground temperature model. In Proceedings of the 8th International Conference on Permafrost, 1241–1246. Zürich, Switzerland.

Zeileis, A., G. Grothendieck, J. A. Ryan, F. Andrews, and A. Zeileis. 2015. zoo (version 1.7-12). S3 Infrastructure for Regular and Irregular Time Series.

Zhang, Y. 2013. Spatio-temporal features of permafrost thaw projected from long-term high-resolution modeling for a region in the Hudson Bay Lowlands in Canada. Journal of Geophysical Research: Earth Surface 118(2): 542–552. doi: 10.1002/jgrf.20045.

Zhang, Y., W. Chen, and J. Cihlar. 2003. A process-based model for quantifying the impact of climate change on permafrost thermal regimes. Journal of Geophysical Research 108(D22). doi: 10.1029/2002JD003354.

Zhang, Y., W. Chen, and D. W. Riseborough. 2006. Temporal and spatial changes of permafrost in Canada since the end of the Little Ice Age. Journal of Geophysical Research 111(D22). doi: 10.1029/2006JD007284.

Zhang, Y., J. Li, X. Wang, W. Chen, W. Sladen, L. Dyke, L. Dredge, J. Poitevin, D. McLennan, H. Stewart, S. Kowalchuk, W. Wu, G. P. Kershaw, R. K. Brook, and C. R. Burn. 2012. Modelling and mapping permafrost at high spatial resolution in Wapusk National Park, Hudson Bay Lowlands. Canadian Journal of Earth Sciences 49(8): 925–937. doi: 10.1139/e2012-031.

Zhang, Y., X. Wang, R. Fraser, I. Olthof, W. Chen, D. Mclennan, S. Ponomarenko, and W. Wu. 2013. Modelling and mapping climate change impacts on permafrost at high spatial resolution for an Arctic region with complex terrain. The Cryosphere 7(4): 1121–1137. doi: 10.5194/tc-7-1121-2013.

CHAPTER 3: CHARACTERISTICS AND EVOLUTION OF COASTAL PEATLAND PERMAFROST IN SOUTHEASTERN LABRADOR, CANADA

Abstract

Palsas and peat plateaus, accompanying permafrost up to 8 m thick, are present in the coastal barrens of southeastern Labrador despite high regional snowfall totals and a relatively warm climate which includes areas exceeding 0°C mean annual air temperature. Mean ground temperatures recorded at the top of permafrost in peatlands varied from -0.7°C at the southernmost site (latitude 51.4°N) to -2.3°C at the northernmost location (latitude 54°N) with shallow active layers (40-60 cm) throughout. Permafrost was inferred to be absent in wetland, forested and forest-tundra areas inland, notwithstanding average air temperatures lower than at the coast. An analysis of future permafrost dynamics at two of the sites using a range of climate scenarios shows complete permafrost disappearance from a southern site between 2044-2054 under all RCP scenarios. At a northern site, permafrost is predicted to be slightly more resilient, persisting beyond 2100 under the optimistic RCP2.6 or disappearing between 2063-2096 under two faster warming scenarios. Evidence of historical peatland permafrost degradation combined with these modelling results indicate that permafrost is unlikely to persist in the southeastern Labrador coastal region beyond the end of this century.

3.1 Introduction

Recent studies have suggested that significant degradation of frozen peatlands may occur over the next century in response to projected regional warming, this will modify ecosystem properties and change landscape development processes (Tarnocai 2006; 2009). Projected changes to peatland permafrost in the future are expected to result in a net increase in atmospheric organic carbon which will impact the global carbon cycle and magnify the longwave radiative forcing of the greenhouse effect (Schuur et al. 2015). However, recent work by Cooper et al (2017) suggests that the potential for methane releases from thawing peatlands in response to warming may be overstated in earlier work.

Perennially frozen peatlands often represent the southernmost occurrences of lowland permafrost making them useful for examining the historical and future evolution of permafrost in a region (Smith and Riseborough 2002). Peatland permafrost in the discontinuous zone is typically associated with peat covered mounds that are heaved relative to adjacent unfrozen terrain. These features are typically subdivided into palsas, which are usually unvegetated peat covered mounds between 0.5-7 m high and 2-100 m long, and peat plateaus, which are elevated flat-topped peat surfaces; both landforms result from ice segregation processes (Seppälä 1982; Gurney 2001; Seppälä 2011). Palsas form in an otherwise unfrozen peatland due to localized snow redistribution caused by wind-scouring of local micro topography which allows deeper frost penetration and greater heat escape from the ground in winter (Seppälä 1982; 2011). The resultant frost heave due to the formation of segregated ice in the underlying sediments creates an elevated ground surface which promotes drying of the near-surface peat layers in the summer, reducing the thermal conductivity of the peat and diminishing heat transfer into the ground (An and Allard 1995; Allard and Rousseau 1999; Seppälä 2011). The palsa grows during successive freezing cycles until the freezing plane reaches non frost-susceptible material, or surface energy exchanges are altered due to climate warming, cracking of the overlying peat cover or increased vegetation growth trapping snow. Peat plateaus form due to a similar process as palsas but occur when more extensive areas of peatlands are well-drained, allowing for less heat penetration in the summer, and larger areas of frost heave and wind-scouring in the winter (Zoltai 1972; Zoltai and Tarnocai 1975). The degradation of peat plateaus typically includes the development of hydrological pathways which dissect the plateau and accumulate snow in the winter thereby accelerating permafrost thaw. For both palsas and peat plateau, the near-surface peat layers are critical to permafrost formation, unlike lithalsas which form entirely in mineral soils (Wolfe et al. 2014).

Degradation of peatland permafrost in Canada has been reported from the eastern coast of Hudson's Bay (Thibault and Payette 2009) and on its southwest coast in northern Ontario (Ou et al. 2016a; Ou et al. 2016b). A 49% decrease in palsa area and a concurrent increase in collapse scar area was observed between

1957-1983 in northern Québec, near Hudson Bay, and a further 33% reduction in permafrost was observed between 1983-1993 (Laprise and Payette 1988; Laberge and Payette 1995). Similarly, Payette et al. (2004) noted palsa and peat plateau degradation in a part of northern Québec from 82% coverage (1957) to 13% (2003). Several papers have described palsas and other periglacial features in southeastern Labrador and the adjacent north shore of the Gulf of St Lawrence (Hustich 1939; Brown 1975; Brown 1979; Dionne 1984; Dionne and Gérardin 1988; Dionne and Richard 2006; Roberts et al. 2006). However, systematic measurement or analysis of peatland permafrost in the region has only been completed in a small area near Blanc Sablon, QC (Dionne 1984; Dionne and Richard 2006). Regional-scale modelling suggests that considerable permafrost thaw may have occurred over the past 50 years (Way and Lewkowicz 2016), coinciding with a period of rapidly increasing regional air temperatures (Way and Viau 2015). However, the absence of direct field or remote sensing data on peatland permafrost in southeastern Labrador means that it has not been possible to evaluate whether permafrost continues to persist in these marginal environments, or to determine the evolution of peatland permafrost in the region under a warming climate.

This study aims to characterize the state of contemporary peatland permafrost in a variety of locations in southeastern Labrador and easternmost Québec, from the southernmost limits of the isolated patches zone to the southern limit of the sporadic discontinuous zone. Isolated patches of peatland permafrost are described using a combination of field techniques, ground temperature monitoring and UAV photography. In addition, the susceptibility of permafrost bodies to future environmental change is analyzed using 1-dimensional thermal modelling (Zhang et al. 2003) in order to assess permafrost persistence.

3.1.1 Regional setting

For the purposes of this study, the southeastern coast of Labrador comprises areas of the coastal barrens ecozone south of Rigolet, NL and extends across the Labrador-Québec border as far as Blanc Sablon, QC (Figure 3-1a). Regional vegetation cover in this ecozone is sparse forest-and shrub-tundra on exposed outer coasts but also includes thick Black Spruce, Tamarack and White Spruce forests in sheltered areas and farther inland (Roberts et al. 2006). Peat deposits and wetlands are found throughout the region with plateau string bogs clustered in the interior and raised bogs in the coastal zone due to regional moisture and physiographic controls on bog development (Foster and Glaser 1986; Foster et al. 1988; Glaser 1992). Surficial materials consist primarily of exposed rock and bedrock covered by glacial tills on outer coasts. Inland the surficial cover is primarily glacial till and diamicton with scattered glaciofluvial sediments (Fulton 1995). Marine and glaciomarine sediments, deposited during Holocene high stands, are found

predominantly near Blanc Sablon and in areas north of Cartwright because of a relatively high marine limit at the former location and widespread lowland terrain at the latter (Figure 3-1b).

Annual air temperatures during the period of observation (2013-2016) were within ±0.1°C of the long-term mean (1948-2016) (data from Way and Viau 2015). Regional climate grids (100 m res.) show mean annual air temperatures (2013-2016) at sea level declining with increasing latitude from +1.0°C near Blanc Sablon, QC to -0.5°C north of Cartwright, NL (Figure 3-1a) (Way et al. 2017a). High elevation plateaus and mountainous zones, including the proposed Mealy Mountains National Park, exhibit lower annual air temperatures (Figure 3-1a). Mean cold-season (December to April) snow depth averages 109 cm at Cartwright (1981-2010) but only 24 cm at Blanc Sablon (1981-2010) (Environment and Climate Change Canada, 2017). A regional composite of data from several homogenized Environment Canada meteorological stations in southeastern Labrador compiled by Way and Viau (2015) shows that annual air temperatures in the region have increased by 1.8°C between 1917-2016.

Palsa bogs in Labrador are considered to have cultural value as locations for storing komatiks (towing sleds), berry picking (cloudberries) and cooling meat beneath the surface peat layers (Patricia Way, *personal communication*). The elevated surfaces of palsas and peat plateau have also been regularly used by indigenous and settler trappers as locations to establish fox traps (Gary Bird, *personal communication*).

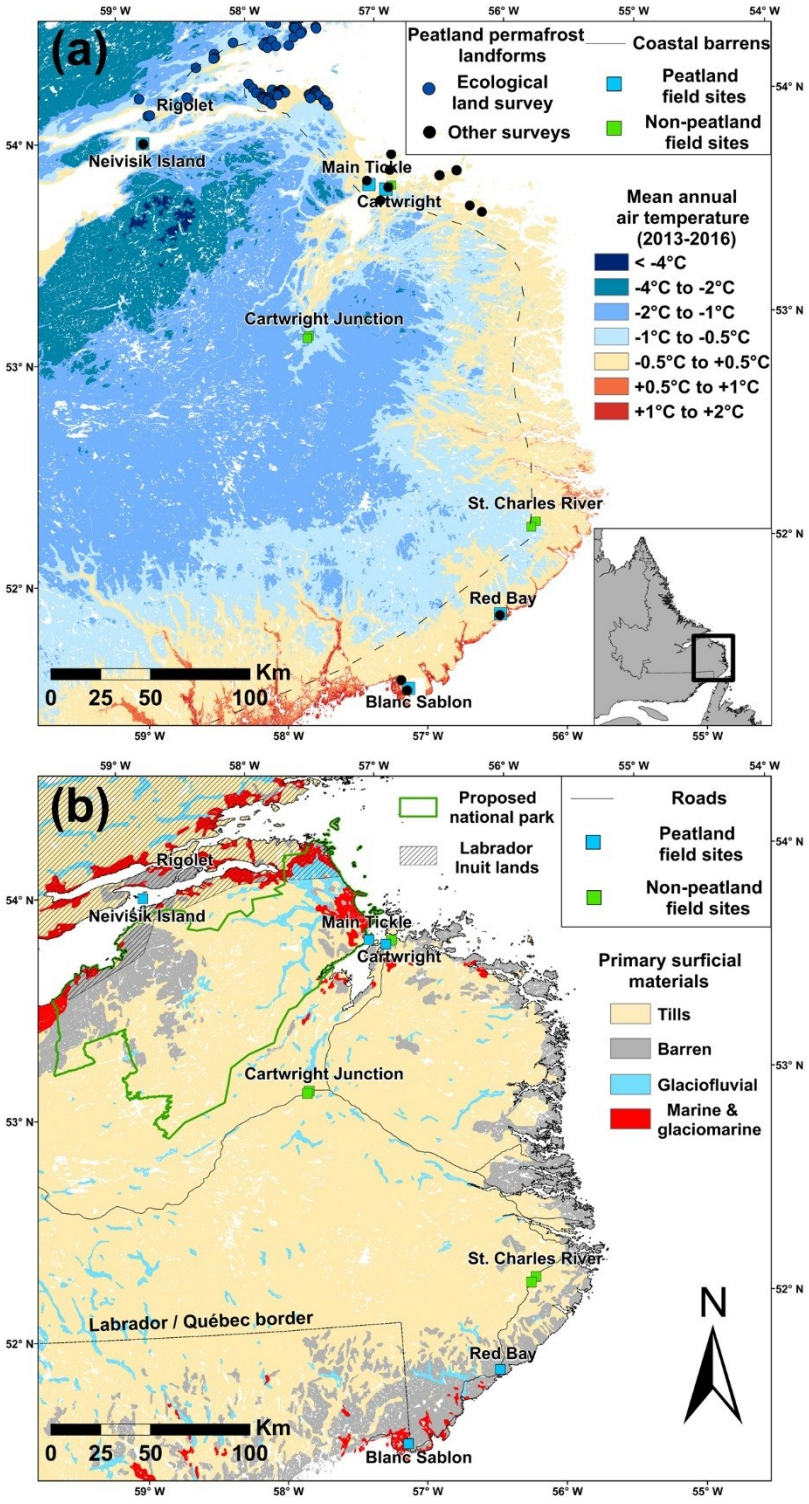

Figure 3-1: (a) Location of peatland and non-peatland study sites in southeastern Labrador with peatland permafrost landforms mapped by various studies. Sites are superimposed on a map showing the spatial distribution of mean annual air temperatures (2013-2016) (Way et al. 2017a). The boundary of the coastal barrens ecozone (Roberts et al. 2006) is shown as grey line following the coast from south to north. (b) Location of peatland and non-peatland study sites in southeastern Labrador with Labrador Inuit lands and the proposed Mealy Mountains National Park outlined. Sites are superimposed on a map showing surficial materials throughout southeastern Labrador according to Fulton (Fulton 1995).

3.2 Methods

Field investigations were undertaken at five peatland sites (Table 3-1 and Figure 3-1) where monitoring stations were established to characterize local air and ground temperatures to a maximum depth of 5.7 m. Methods included geophysical surveys using DC electrical resistivity tomography, UAV aerial photography (Figure 3-2) and thaw depth measurement by probing. Information on a variety of permafrost relevant environmental parameters including air temperature, ground surface temperature, ground temperatures (50-120 cm depths) and snow depth were also available from inland and coastal monitoring stations previously established in the Labrador Permafrost Project (Way and Lewkowicz *in revision*).

Monitoring stations established at the five study sites measured shielded air temperature (190-235 cm heights; because of deep regional snow covers), ground surface temperature (~2-3 cm beneath the surface) and shallow ground temperature (50-120 cm depths) using Onset Hobo Pro V2 (accuracy ± 0.2°C) and/or Maxim Integrated high-resolution ibutton loggers (accuracy ± 0.5°C). Corrections for differing sensor types are described in Way and Lewkowicz (*in revision*). For shallow ground temperatures, the deepest thermistor was placed at the maximum depth of probe penetration and was considered to be an approximation of the base of the annual freeze-thaw layer. Snow depth at monitoring stations was measured using vertically arranged low-resolution ibutton loggers (e.g. Lewkowicz 2008) installed at various heights (typically 10, 20, 30, 40, 50, 60, 80, 100, 140 and 180 cm). Ibutton data were used to calculate daily snow heights using an empirical threshold established from correlations between the daily temperature ranges at various heights (see Way and Lewkowicz *in revision*). Uncertainties increased at higher snow depths due to the decreased vertical resolution of the sensors but this issue had little impact on results for most of peatland sites where the snowpack was shallow.

Boreholes (Table 3-2) were drilled using the waterjet method and were cased with 1-inch PVC pipe. The base of the permafrost was not reached at two boreholes (WJD01 and WJD05) due to limited water supply. Ground temperatures were recorded bi-hourly with Onset Hobo V2 loggers (± 0.2°C) and thermistors placed typically at six depths in the borehole. Temperatures at WJD01 were measured with five high resolution ibutton loggers (± 0.5°C) attached at different depths on a wooden dowel. Ground temperatures presented for four of the five boreholes are reported for the second full year of record to reduce any influence of waterjet drilling on recorded temperatures. However, due to a later drill date for one borehole (WJD05), the available data were for the first year after drilling with the most thermally disturbed early part of the record eliminated and infilling performed using cross-correlation between borehole depths and against the monitoring station at Cartwright (AMET13) to generate a full annual average.

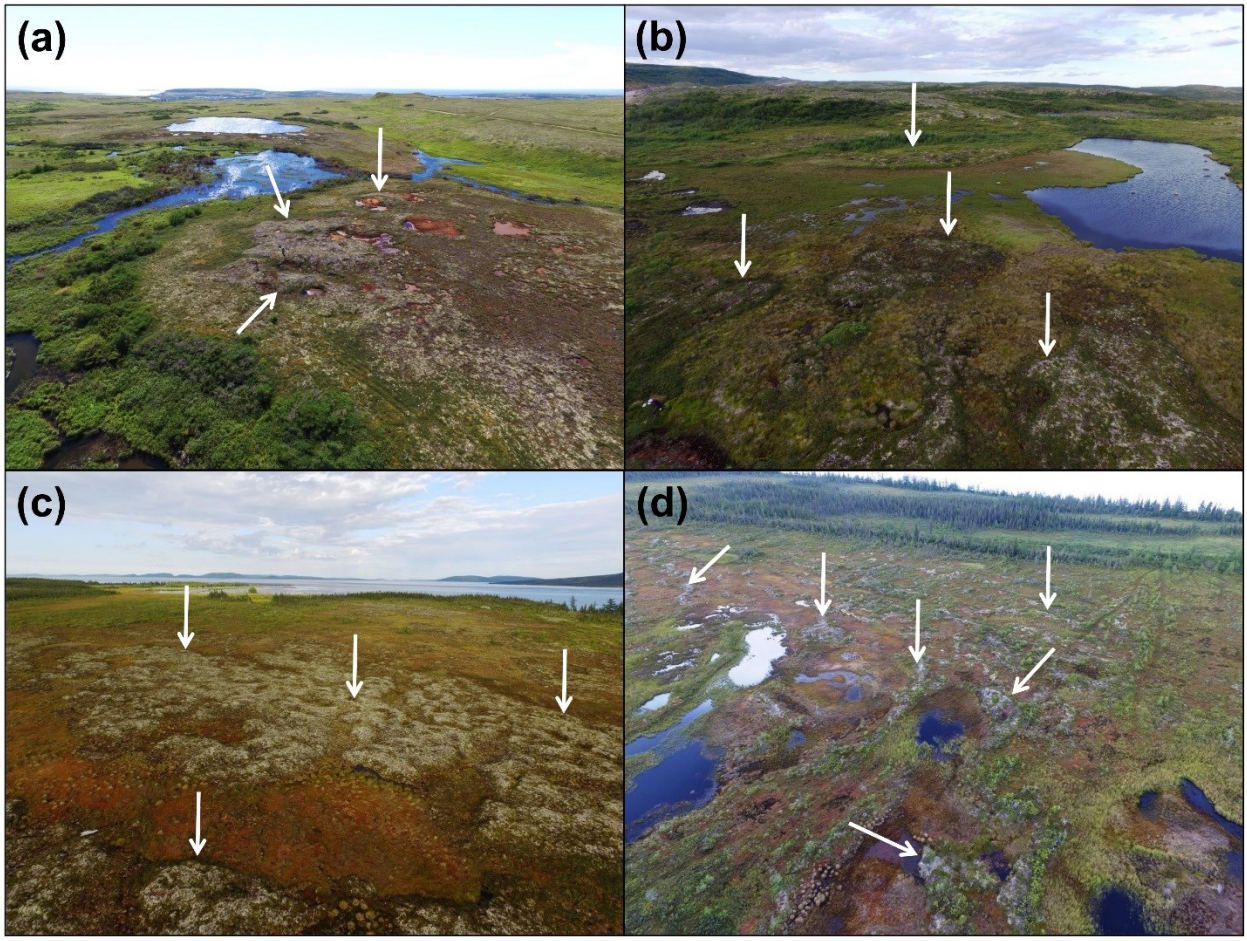

Figure 3-2: Low altitude UAV imagery of peatland permafrost sites at (a) Blanc Sablon, QC; (b) Red Bay, NL; (c) Main Tickle, NL; and (d) Neivisik Island, NL. White arrows point to examples of palsa and peat plateau in each image.

Table 3-1: Site information and field data collected (2013-2016).

Site location(s)	Latitude	Longitude	Elevation	Local geomorphology	Description of field data collection	ERT ID
Blanc Sablon, QC	51.4565°N	57.1185°W	115 m a.s.l.	Palsa field	ERT survey (n=2); climate monitoring station; borehole	1 & 2
Blanc Sablon, QC	51.4577°N	57.1219°W	143 m a.s.l.	Barren hilltop	Ground temperature logger (n=2)	
Red Bay, NL	51.7589°N	56.4135°W	72 m a.s.l.	Palsa field	ERT survey (n=1); climate monitoring station; borehole	3
Red Bay, NL	51.7581°N	56.4143°W	77 m a.s.l.	Peat-covered bedrock	ERT survey	4
St. Charles River, NL	52.1611°N	56.0977°W	217 m a.s.l.	Dense forest	Climate monitoring station	
St. Charles River, NL	52.1385°N	56.1347°W	333 m a.s.l.	Low-shrub tundra	Climate monitoring station	
Cartwright Junction, NL	53.0640°N	57.6796°W	190 m a.s.l.	Open forest	Climate monitoring station	
Cartwright Junction, NL	53.0739°N	57.6649°W	302 m a.s.l.	Barren hilltop	Climate monitoring station	
Cartwright, NL	53.7037°N	57.0098°W	5-10 m a.s.l .	Palsa fields	ERT survey (n=7); climate monitoring station; borehole (n=2)	5 to 11
Cartwright, NL	53.7255°N	56.9641°W	158 m a.s.l.	Barren hillslope	Climate monitoring station	
Main Tickle, NL	53.7357°N	57.1331°W	9 m a.s.l.	Peat plateau	ERT survey (n=2); climate monitoring station; borehole	12 & 13
Neivisik Island, NL	53.9851°N	58.8358°W	12 m a.s.l.	Palsa field	Climate monitoring station	
Neivisik Island, NL	53.9851°N	58.8358°W	3-12 m a.s.l.	Open forest	Ground temperature logger (n=2)	

Table 3-2: Temperature monitoring boreholes.

Borehole ID	Elevation (m)	Location	Date established	Measurement depths (m)	Logger type
WJD01	11	Cartwright, NL	2014.08.09	0.25; 0.5; 1.5; 2.15	Ibutton
WJD02	14	Cartwright, NL	2014.07.23	0.5; 1.0; 2.0; 3.0; 4.25; 5.7	Hobo Pro V2
WJD03	115	Blanc Sablon, QC	2014.08.05	0.25; 0.5; 1.0; 2.0; 3.0; 4.2	Hobo Pro V2
WJD04	75	Red Bay, NL	2014.08.06	0.25; 0.5; 1.0; 2.0; 3.0; 4.25	Hobo Pro V2
WJD05	8	Main Tickle, NL	2015.09.09	0.75; 1.0; 1.25; 1.73	Hobo Pro V2

DC electrical resistivity tomography (ERT) surveys were undertaken with an ABEM Terrameter LS profiling system with 30 cm steel nails for electrodes arranged in a Wenner configuration. Electrode spacing was 0.5, 1 or 2 m giving survey lengths of 40-160 m (longer where roll-along surveys were performed) and maximum penetration depths of approximately 6 m, 12 m or 25 m. RES2DINV software was used to invert the measured resistivities (Loke and Barker 1996; Loke et al. 2003) with the robust inversion method. Inversion proceeded until the fifth iteration or until the RMS error dropped below 5%, whichever came first. Prior to inversion, ERT profiles were topographically corrected using a handheld GPS (Garmin Oregon 450t) to obtain site elevations and a Brunton compass was used to obtain relative elevations. Modelled resisitivities are presented as model blocks with low sensitivity areas (< 0.1) faded to reflect the uncertainties of these sections of the modelled profile. The spacing of the electrodes and the inversion process mean that model blocks are larger near the ends of a profile than beneath its centre, reducing the detail in these portions. The frost table was probed at 1 or 2 m intervals along each ERT transect using a 120-cm long titanium probe. Surface vegetation cover was also described in the field, and aerial photography was acquired using a DJI Phantom 3 Professional quadracopter.

ERT has been widely used for detecting permafrost bodies and estimating permafrost thickness in Canada (Lewkowicz et al. 2011; Way and Lewkowicz 2015; Briggs et al. 2016; Douglas et al. 2016; Minsley et al. 2016), Scandinavia (Kasprzak 2015; Sjöberg et al. 2015), the European Alps (Hauck 2013) and the Tibetan Plateau (You et al. 2013). ERT is effective for permafrost characterization because frozen ground typically resists electrical current much more than unfrozen ground, and measurements of subsurface resistivities can effectively reveal differences between the two states (Hauck 2013). There is no universally applicable resistivity boundary for discriminating between unfrozen and frozen ground, therefore validation of ERT results with standard field methods and/or boreholes is required (Hauck 2013). For example, in the glacio-marine sediments on the eastern Hudson's Bay coastline, Fortier et al. (2008) used a boundary of approximately 1000 Ω.m to delineate between unfrozen and frozen ground, whereas in the organic soils of north-western North America, values near 300 Ω.m have been used as an unfrozen/frozen limit (Lewkowicz et al. 2011; Briggs et al. 2016; Minsley et al. 2016). Other issues with the interpretation of ERT data include the presence of coarse sediments, which have similar resistivities to those of warm permafrost (e.g. Hilbich et al. 2009), and the frequent presence of near-surface bedrock which can exhibit high resistivities similar to those of cold permafrost (Lewkowicz et al. 2011).

One-dimensional numerical modelling was undertaken for two instrumented borehole sites on palsas at Cartwright and Blanc Sablon using the finite-element Northern Ecosystem Soil Temperature model (NEST) (e.g. Zhang 2003; Zhang et al. 2013; Zhang 2013). NEST has been widely-used for transient

permafrost modelling and has been shown to be effective for modelling change in peatland permafrost features in northern Manitoba (Zhang 2013) and the Hudson's Bay lowlands of northern Ontario (Ou et al. 2016a; Ou et al. 2016b). The model was calibrated to recorded ground temperatures using climate data from 1900 to present and then run into the future using multi-model means derived from ensemble projections for RCPs 2.6, 4.5 and 8.5 for 2016-2100 (van Vuuren et al. 2011). Past climate data were accessed from Environment Canada for Cartwright (1938-2016) and Blanc Sablon (1976-2016) (Vincent et al. 2012). Input data from 1901 to the start of station observations were comprised of interpolated daily temperature data (10 km res.) from the Canadian Forest Service (Hutchinson et al. 2009). The year 1900 was infilled with the 1901 data for each month for model initialization purposes. The model was calibrated using daily observations from two boreholes with permafrost (WJD02 & WJD03) for the period 2014-2016. Snow drifting and leaf area index parameters were tuned so that modelled near-surface soil layer temperatures were comparable to observations and these parameters were kept constant. The former index was set to assume virtually no snow accumulation on the tops of palsas through the winter which correspondingly results in little to no influence from historical variability in snow characteristics at these sites. Soil profile properties were estimated from observations during waterjet drilling (e.g. peat thickness of 1.2 m) and depth to bedrock was based on the ERT survey results (see *Section 3.3*).

3.3 Results

Field results are presented from south to north for the five peatland permafrost sites and are summarized in Tables 3-3 and Table B2.

Table 3-3: Description of ERT surveys and inferred permafrost thicknesses.

ERT ID	Length / Mean spacing	Vegetation description (highest to lowest coverage)	Inferred maximum permafrost thickness
1	100 m / 1 m	Exposed peat, ground lichen cover, short grasses, low shrubs	6 m
2	50 m / 0.5 m	Exposed peat, ground lichen cover and short grasses	6 m
3	80 m / 1 m	Sedges & grasses, medium shrubs, ground lichen cover, exposed peat	3.5 m
4	80 m / 1 m	Exposed peat, sedges and grasses, ground lichen cover	6 m - bedrock possibly frozen deeper
5	240 m / 2 m	Medium shrubs, exposed peat, short sedges & grasses, ground lichen cover	5.4 m
6	80 m / 2 m	Ground lichen cover, medium shrubs, short sedges & grasses, exposed peat	3.9 m
7	120 m / 2 m	Ground lichen cover, exposed peat, low shrubs, short grasses	5.2 m
8	40 m / 1 m	Ground lichen cover, short grasses, exposed peat	4.8 m
9	40 m / 1 m	Ground lichen cover, exposed peat, short grasses, low shrubs	3.7 m
10	80 m / 2 m	Short sedges & grasses, ground lichen cover, exposed peat	3.7 m
11	40 m / 1 m	Short sedges & grasses, ground lichen cover, exposed peat	~.9 m
12	160 m / 2 m	Ground lichen cover, exposed peat, short grasses, medium shrubs	8 m - bedrock possibly frozen deeper
13	100 m / 1 m	Ground lichen cover, exposed peat, short sedges & grasses	8 m - bedrock possibly frozen deeper

3.3.1 Field observations

Blanc Sablon, QC

Two ERT profiles (1 & 2) were completed approximately 3.5 km north of the community (Table 3-3). Profile 1 (100 m roll-along survey) was run across a series of 0.4-1.4 m high mounds which were mostly covered by ground lichens but included one mound that had exposed peat due to wind abrasion and large cracks at the surface (Figure 3-3). Profile 2 used a closer electrode spacing perpendicular to the first profile and across the mound that included the monitoring station and a 4.25 m deep borehole (WJD03) (Figure 3-2a; Figure 3-3b). Surface cover along profile 2 was primarily ground lichens although areas of wetter depressions had some surface water pooling and low grasses and sedges were more frequent near the beginning of the profile. ERT results for profile 1 showed higher resistivity values (> 600 Ω.m) extending to depths of 3.4 m (P1), 4.5 m (P2) and 4.3 m (P4) beneath the surface of the elevated mounds (Figure 3-3a). At P3, higher resistivity values reached the base of the profile at 12 m. Lower resistivity values (< 400 Ω.m) were typically found in the near-surface layer and in depressions between each mound; however, much lower resistivityies (< 150 Ω.m) were measured beneath higher resistivity layers at P1 and P4. Frost tables were encountered on all of the elevated mounds with a median thaw depth of 63 cm on September 11, 2015 (Figure 3-3a). Full frost probe penetration was possible in depressions and on all portions of the transect without mounds. At several of these locations, however, 15-30 cm thick frozen ground was present approximately 40 cm below the surface but with some effort, the probe could be pushed through this layer to its full length. Air temperatures at the monitoring station and borehole adjacent to 51 m along the profile averaged -0.4°C, the near-surface temperature was +0.8°C and the ground temperature at 1 m was -0.7°C. The lowest thermistor at a depth of 4.25 m recorded an average temperature of +0.06°C while that at 3 m depth was -0.1°C, indicating that the base of permafrost was most likely found between 3.5 m and 4.2 m depth depending on how extrapolation is done (Figure 3-3c).

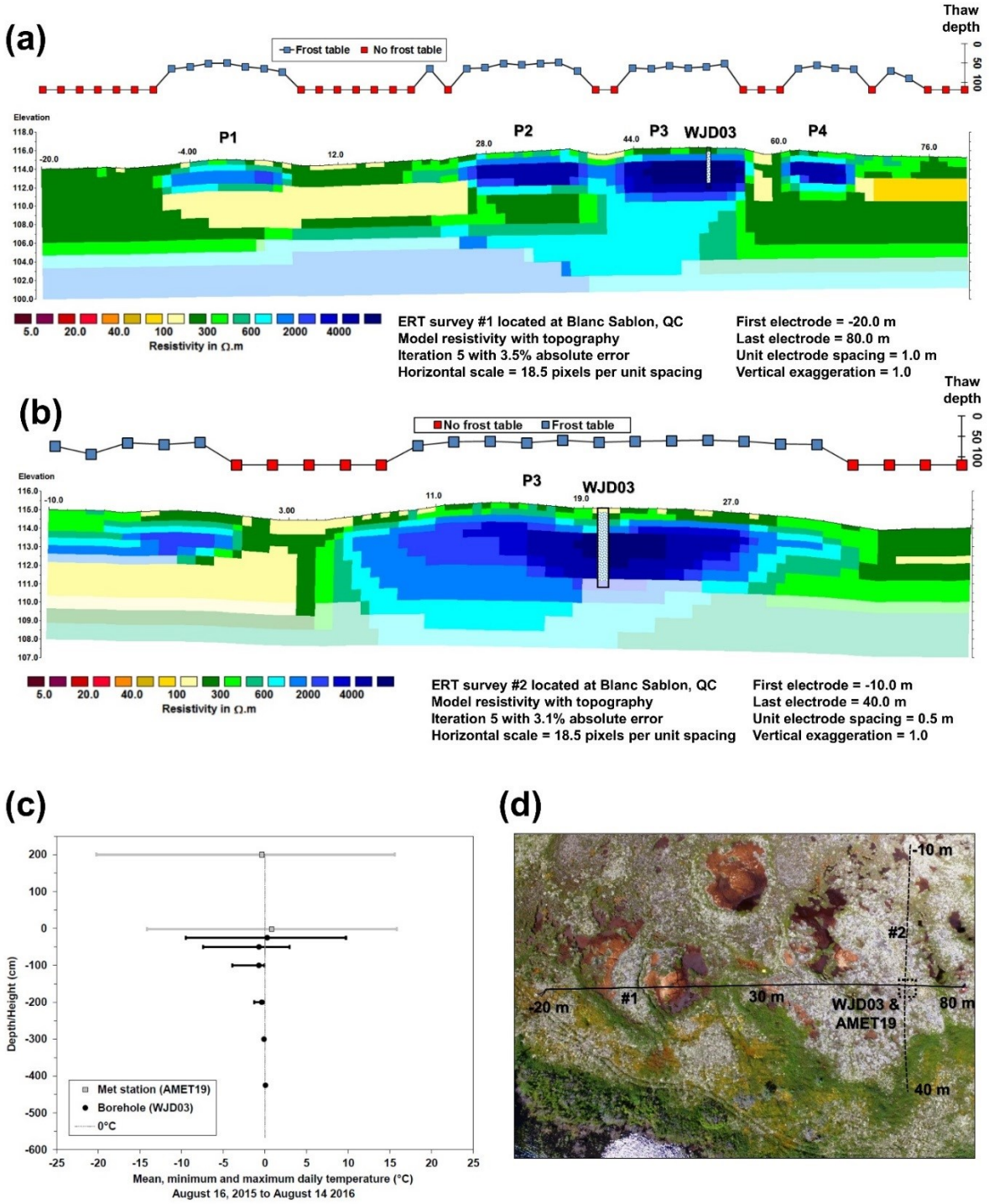

Figure 3-3: Field investigations of permafrost conditions at Blanc Sablon, QC. (a) Inferred thaw depths and modelled resistivities from co-located frost probing and ERT profile #1. Approximate location of temperature borehole is indicated on the ERT survey and depths with permafrost in the borehole are denoted by hatching; (b) Inferred thaw depths and modelled resistivities from co-located frost probing and ERT profile #2. Approximate location of temperature borehole is indicated on the ERT survey and depths with permafrost in the borehole are denoted by hatching; (c) Ground temperatures measured at monitoring station AMET19 and temperature borehole WJD03 located on ERT profile #1; (d) Low altitude UAV imagery of the site. Black lines delimit the approximate location of the ERT survey lines and text shows the start and end points.

Combining the ERT, frost probing and borehole data, the mounds are palsas and the boundary between frozen and unfrozen ground is inferred to be between 500-800 Ω.m. Accordingly, permafrost thicknesses along the profile were inferred to be 2.8 m (P1), 3.9 m (P2) and 3.7 m (P4) (Table 3-3). Permafrost thickness beneath P3 was more challenging to interpret as profile 1 indicated high resistivity values extending to the base of the profile whereas co-located ground temperatures showed unfrozen ground at 425 cm. The higher resolution profile 2 showed low-sensitivity values at this depth (Figure 3-3b) beneath the borehole but high resistivity values nearby suggesting that frozen ground may extend deeper in the areas adjacent to the borehole. Considering the accuracy of the ground temperature loggers (± 0.2°C) and uncertainty in ERT values, the maximum permafrost thickness beneath P3 was estimated to be about 6 m. The thin layer of frozen ground found at some locations without mounds was interpreted to be a remnant of seasonal frost, but given the September survey date, it may have persisted throughout the thaw season and hence could be classified as *pereletok* (Van Everdingen 2005b).

Shallow ground temperatures were recorded at two upland tundra locations on an exposed hilltop approximately 250 m northwest of WJD03 and AMET13 (Table 3-1). Both sites were heavily wind-scoured with widespread patterned ground (sorted circles and steps). However, permafrost was not present according to ground temperatures which averaged 1.0°C and 0.6°C at depths of 35 cm and 62 cm, respectively.

Red Bay, NL

Profiles 3 and 4 were completed about 2 km north of Red Bay in a wetland close to the Trans Labrador Highway that exhibited several low mounds. Profile 3 was performed across the surface of four of these, terminating in an adjacent herbaceous wetland (Figure 3-2b; Figure 3-4). This profile ran across a monitoring station which included a 4.25 m deep borehole. The surface cover along profile 3 varied but was primarily composed of peaty mounds 0.3-1 m high with ground lichen cover and some exposed peat. Vegetation cover included sedges and grasses in wetter portions at the beginning and end of the profile, as well as small shrubs on the surface of peat mounds and in the herbaceous wetlands. Profile 4 ran perpendicular to profile 3, beginning amongst mounds in the wetland and ending upslope in drier peat-covered terrain (Figure 3-5). Little variability in surface cover was observed along this profile with exposed peat and lichen cover being most common, while low grasses and sedges were evident in the wetland which was intermixed with peat mounds at the start of the profile.

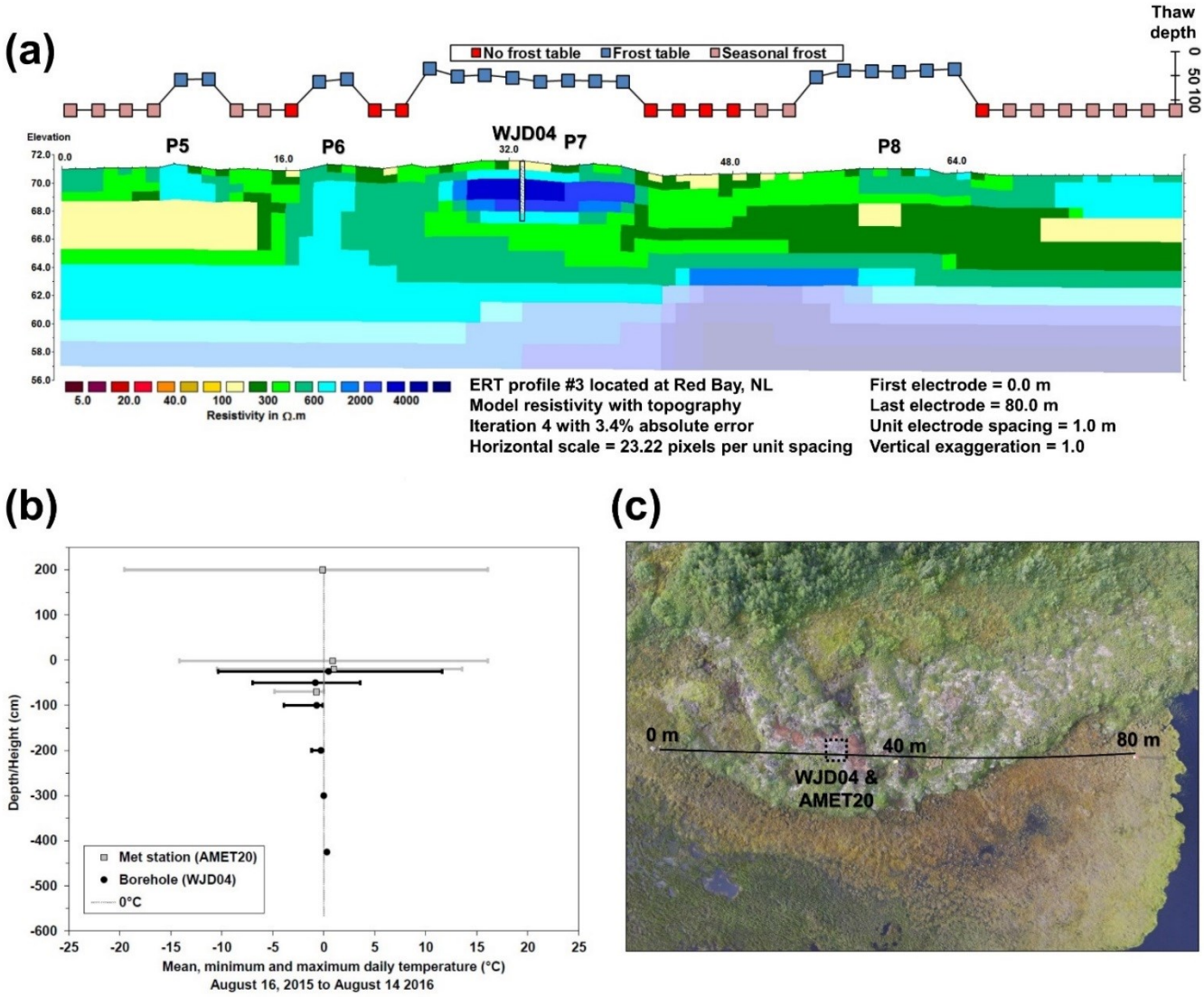

Figure 3-4: Field investigations of permafrost conditions at Red Bay, NL. (a) Inferred thaw depths and modelled resistivities from co-located frost probing and ERT profile #3. Approximate location of temperature borehole is indicated on the ERT survey and depths with permafrost in the borehole are denoted by hatching; (b) Ground temperatures measured at monitoring station AMET20 and temperature borehole WJD04 located along ERT profile #3; (c) Low altitude UAV imagery of the site. Black line delimits the approximate location of the ERT survey line and text shows the start and end points.

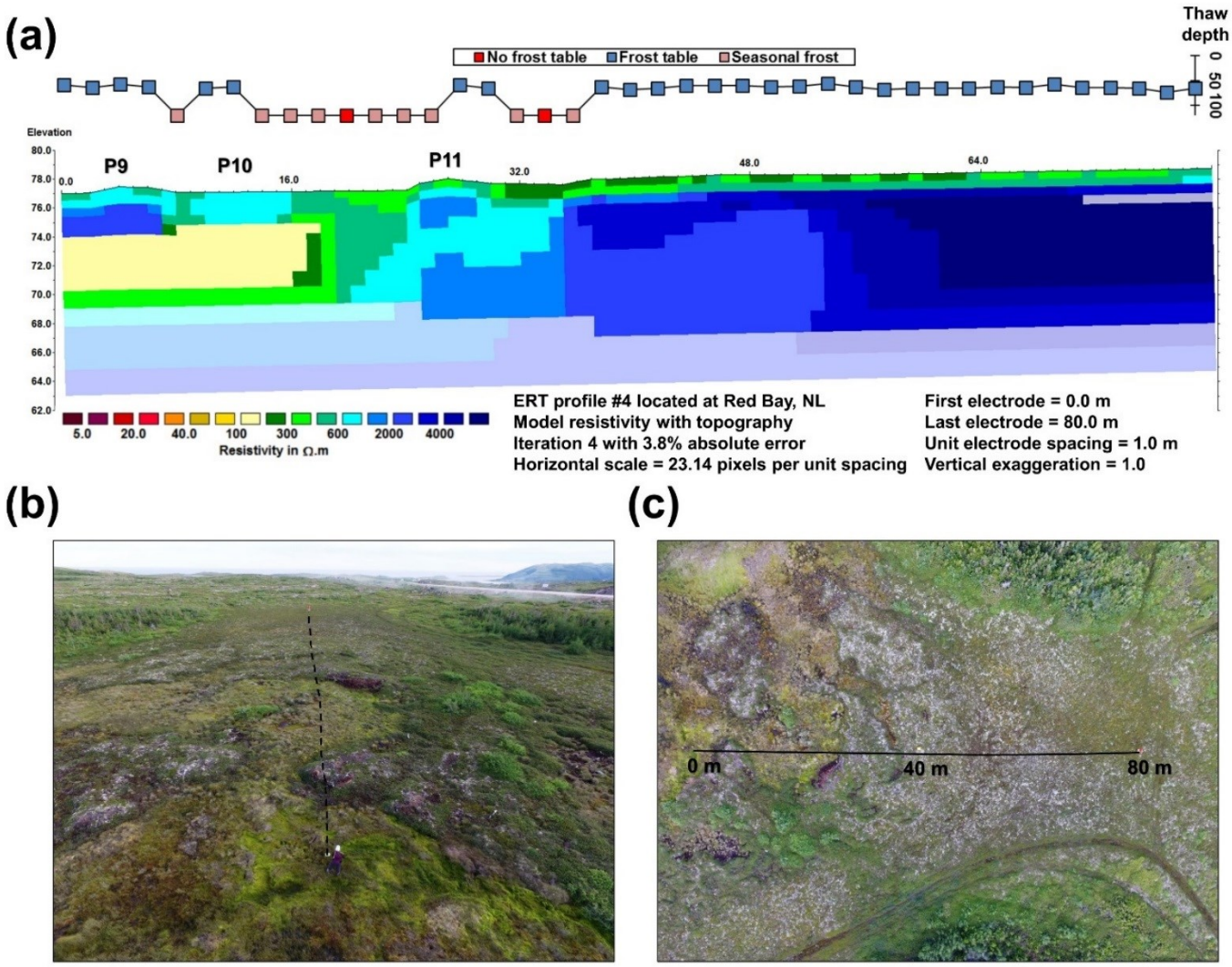

Figure 3-5: Field investigations of permafrost conditions at Red Bay, NL. (a) Inferred thaw depths and modelled resistivities from co-located frost probing and ERT profile #4; (b) Low altitude oblique photo upslope along ERT profile #4 from the approximate survey start point. Dotted black line delimits location of ERT survey line; (c) Low altitude UAV imagery of the site. Black line delimits the approximate location of the ERT survey line and text shows the start and end points.

ERT profile 3 (80 m long) showed moderate (> 300 Ω.m) to high (> 600 Ω.m) resistivities throughout the profile with the highest values (> 4000 Ω.m) beneath the four mounds (P5, P6, P7, P8), extending to depths of 2-4 m (Figure 3-4a) (Table 3-3; Table B2). Lower resistivities (< 200 Ω.m) were present at selected locations in the near-surface and at depth beneath P5 and P6, and between 42 to 53 m along the profile. Full frost probe penetration was possible in most areas adjacent to mounds whereas frost tables were encountered continuously beneath the elevated surface of each mound (median thaw depth: 54 cm on September 12, 2015) (Figure 3-4a). Probe refusal occurred between 1-14 m and 68-80 m due to a frozen soil layer (median depth: 60 cm); however, frost layers could eventually be penetrated although they were thick (30-40 cm). Surprisingly, these frost tables were even present in low vegetated areas covered by shallow standing water. The mean air temperature at the monitoring station was -0.1°C (August 2015 to August 2016) while ground temperatures averaged +0.9°C (near-surface), -0.7°C at 1 m, -0.1 at 3 m and +0.3°C at 4.2 m depth (Figure 3-4b). These results show permafrost is present between ~50 cm and ~3.5 m depth at the borehole location.

ERT survey results from profile 4 (80 m long) showed a high resistivity body (> 1000 Ω.m) across its second half with higher values also present to depths of 3-4 m beneath P9 and P10, and to the base of the profile at P11 (Figure 3-5a) (Table 3-3). Moderate resistivities (200-400 Ω.m) were present throughout the near-surface portions of the profile while lower resistivities (< 200 Ω.m) were present only in one section beneath P10. Frost probing resulted in refusal due to frozen layers beneath P9, P10 and P11 but not in areas between these mounds (median thaw depth: 63 cm) (Figure 3-5a). Frost tables were also encountered continuously along the gently sloping peat-covered area with a median thaw depth of 64 cm.

Considering the borehole data, frost probing and modelled resistivities from both profiles, the mounds were confirmed to be palsas and the boundary between frozen and unfrozen ground was between 500-800 Ω.m. Accordingly, permafrost thicknesses along profile 3 were inferred to be 1.9 m (P5), 2.7 m (P6), 4 m (P7) and 0.8 m (P8) (Table 3-3; Table B2). Ambiguity exists as to whether frozen ground exists at depth beneath P6 given the high resistivity values between 2-10 m depths (Figure 3-4a). On profile 4, permafrost was inferred to be at least 2.8 m thick beneath P9, 1.7 m thick at P10 and 4.6 m thick at P11. Along the peat covered slope between 38-80 m (Figure 3-5c), it was not possible to determine the thickness of permafrost because bedrock appears to be close to the surface upslope. However, given the frozen nature of the overlying peat and the ERT results, it is inferred that permafrost extends to the bedrock at this site with an unknown maximum thickness.

Cartwright, NL

A total of seven ERT surveys were completed across mounds in three raised bogs located in and around the community of Cartwright, NL (Tables 3-3; Table B2). Results are represented by two long surveys (profiles 5 and 7) (Figure 3-6), and a third shorter survey (profile 9) that traverses a monitored borehole (Figure 3-7). Profile 5 was completed about 200 m north of the main road in Cartwright in an elevated peat bog found inside the community (Figure 3-6c). This profile consisted of numerous small elevated peaty areas and six larger peat mounds ranging in height from 0.3-1.3 m. Surface cover along the profile was comprised primarily of ground lichen and exposed peat in the drier areas and low-to-medium height shrubs in the wetter zones. Towards the end of the profile the survey line entered medium-to-high shrubs and then White Spruce forest. Profile 7 was in another raised bog on the south side of Cartwright, 250 m from a housing development and 100 m from an ocean inlet (Figure 3-6d). This profile began in medium-to-high shrubs and scattered White Spruce trees and then traversed an elevated zone of dry peat for ~80 m which contained four 0.6-1.0 m high mounds separated by depressions. Like profile 5, surface cover was comprised primarily of ground lichen and exposed peat in the drier areas and small shrubs in the wetter areas. Profile 9 was located 100 m northeast of profile 5 in the same elevated peat bog (Figure 3-7c). This profile featured two peat mounds 0.3-0.6 m high with exposed peat and ground lichen evident at the surface and wetter depressions in between the two mounds covered by low shrubs and mosses.

ERT profile 5 (240 m long roll-along) showed a wide range of resistivities from less than 10 Ω.m in the near-surface layers at the start of the profile to values greater than 6000 Ω.m at depths below 15 m. Values beneath six peat mounds (P12-P17) were higher, ranging between 600 Ω.m and 4000 Ω.m (Figure 3-6a). Much lower resistivity (< 40 Ω.m) values were found at 1-12 m depth between 0 m and 40 m along the profile. Lower resistivities (< 300 Ω.m) were also present from 3-8 m depth between 58 and 164 m along the profile, including beneath the high resistivity layers associated with the mounds. Higher resistivities (> 4000 Ω.m) observed in the near-surface between 222 m and 240 m were inferred to be bedrock based on local geomorphology and the presence of similar values at depth sloping near the base of the entire profile (Figure 3-6a). Frost probing along profile 5 gave a median thaw depth of 45 cm (July 22, 2014) where a frost table was encountered. Frost tables were measurable along the profile wherever there were elevated peat mounds and also at some locations with slightly elevated dry peat (Figure 3-6a). Full probe penetration occurred wherever surface water was present or the peat was not dry.

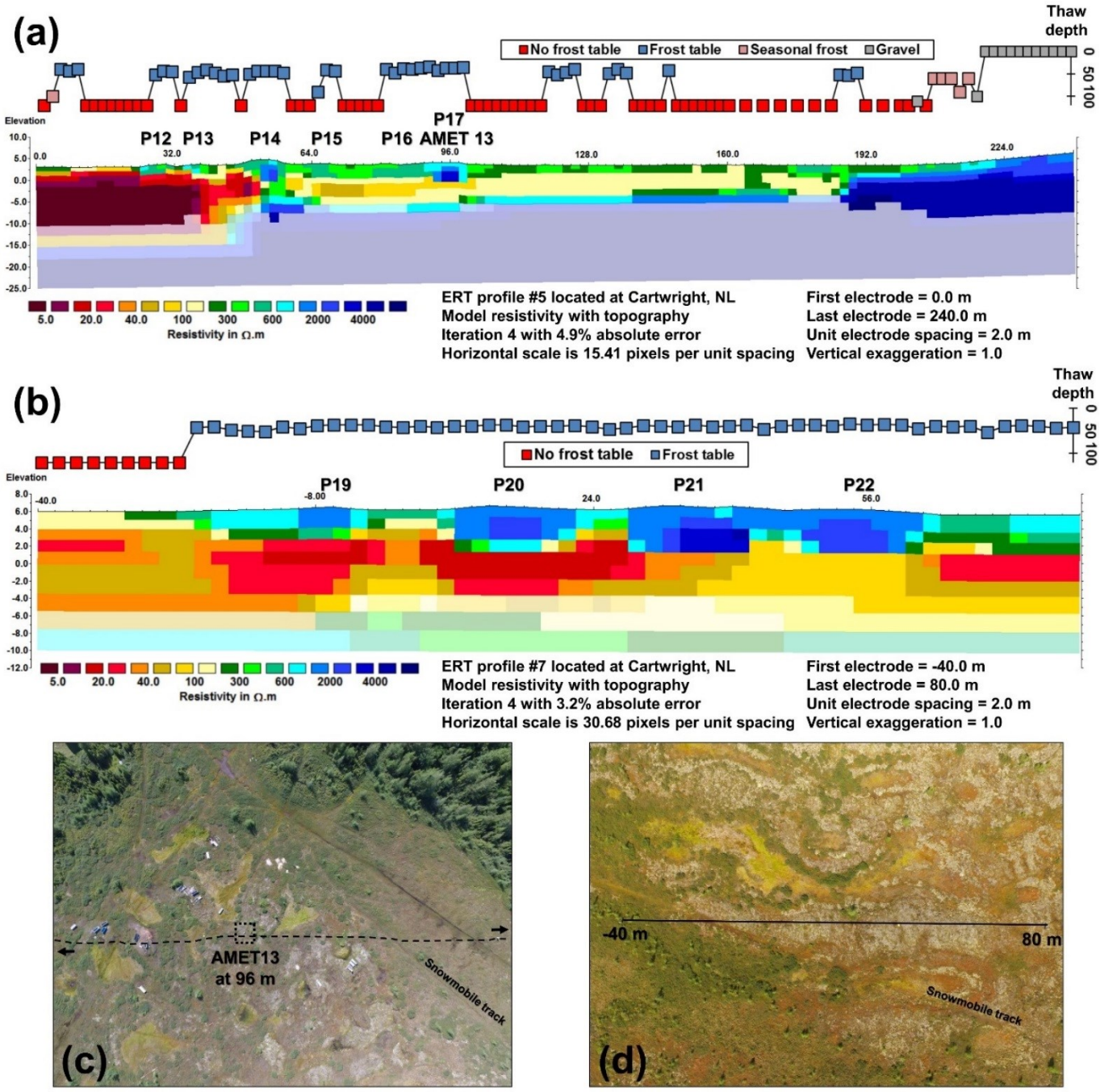

Figure 3-6: Field investigations of permafrost conditions at Cartwright, NL. (a) Inferred thaw depths and modelled resistivities from co-located frost probing and ERT profile #5; (b) Inferred thaw depths and modelled resistivities from co-located frost probing and ERT profile #7; (c) Low altitude UAV imagery of ERT profile #5. Black line delimits the approximate location of the ERT survey line and arrows point to location of start and end points; (d) Low altitude UAV imagery of ERT profile #7. Black line delimits the approximate location of the ERT survey line and text shows the start and end points.

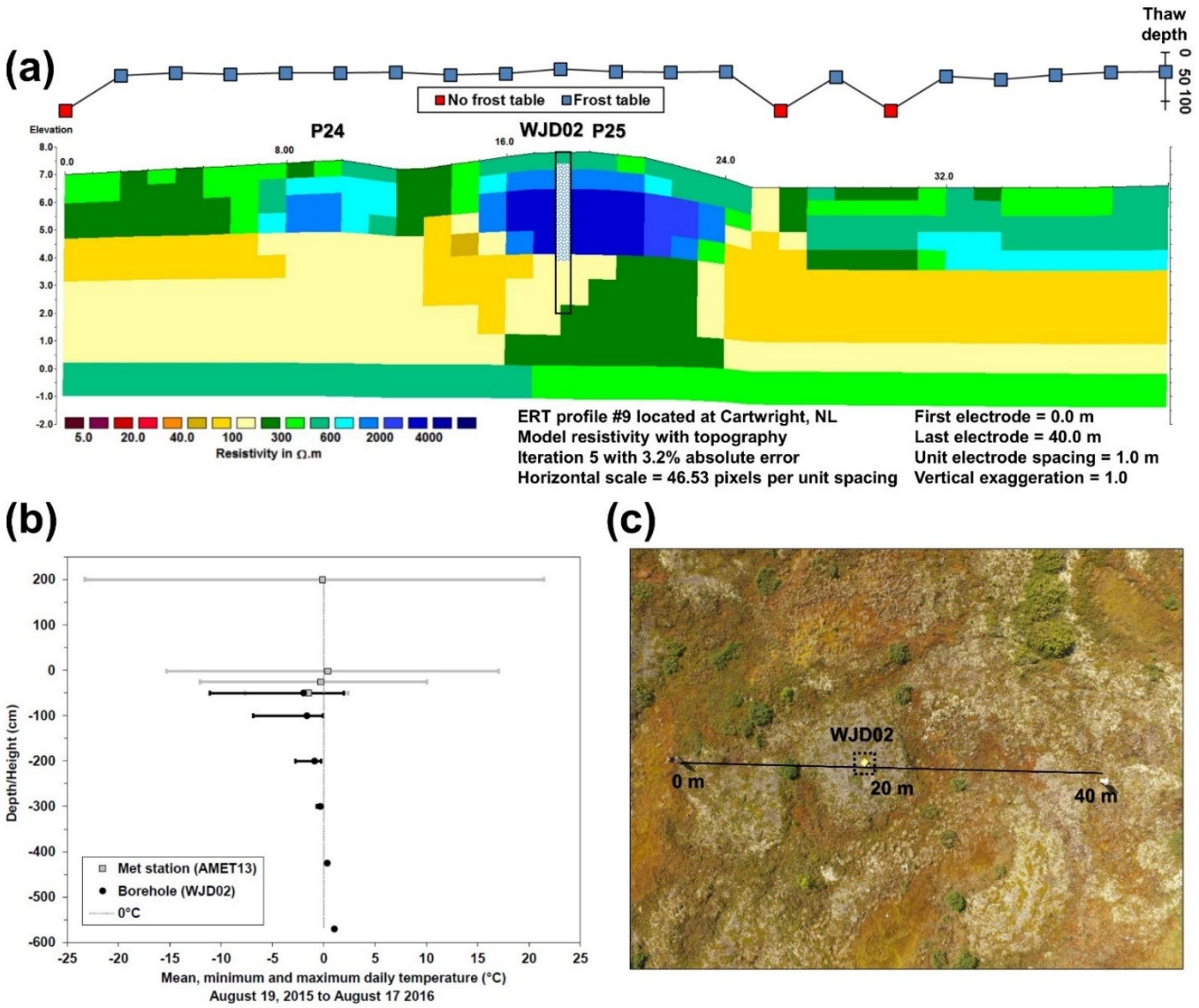

Figure 3-7: Field investigations of permafrost conditions at Cartwright, NL. (a) Inferred thaw depths and modelled resistivities from co-located frost probing and ERT profile #9. Approximate location of temperature borehole is indicated on the ERT profile and depths with permafrost in the borehole are denoted by hatching; (b) Ground temperatures measured at nearby monitoring station AMET13 and the temperature borehole WJD02 located along ERT profile #9; (c) Low altitude UAV imagery of the site. Black line delimits the approximate location of the ERT survey line and text shows the start and end points.

Higher resistivities were present in the near-surface and to a maximum depth of 5.5 m along profile 7 (100 m long roll-along), with the deepest areas of higher resistivities (> 1000 Ω.m) directly below four 0.5-1 m mounds (P19, P20, P21, P22) located on elevated and elongated peaty terrain (Figure 6b). A layer of low resistivities (< 50 Ω.m) was present beneath. Frost tables were encountered continuously between -22 m and 80 m with a median thaw depth of 40 cm (July 25, 2014).

At profile 9, resistivity values were moderate (200-400 Ω.m) to higher (> 1000 Ω.m) across the upper 3.5 m of profile 9 (40 m long) which traversed a borehole (Figure 3-7a). Below this, a 4 m thick near-continuous layer of predominantly lower resistivities (< 200 Ω.m) was present. Measurable frost tables were present in all but three spots along the profile. The median thaw depth at this site was 43 cm (July 24, 2014).

Ground temperatures recorded between August 2015 and August 2016 at the WJD02 borehole, located at 18 m on profile 7, averaged -2.0°C at 50 cm and -1.6°C at 100 cm (Figure 3-7b). Values at a depth of 3 m of -0.3°C and 4.25 m of +0.3°C indicated that the base of permafrost was approximately 3.6 m. A shallower borehole (WJD01) about 70 m to the southeast gave similar values down to its base at 2.15 m. Annual air temperature measured about 100 m away in the same palsa field was -0.1°C while the average surface temperature was +0.4°C.

Comparisons among the ERT profiles, the frost probing results and the borehole temperatures at Cartwright indicate that the mounds are palsas and places the resistivity boundary for frozen/unfrozen materials between 300-400 Ω.m. Based on this value, the thickest body of permafrost reached 5.4 m beneath mound P14 along profile 5 (Figure 3-6a) (Table 3-3 and Table B2). Maximum permafrost thicknesses beneath mounds along profile 7 ranged from 3.1 m (P19) to 5.2 m (P21) with thin permafrost or deep late-lying seasonal frost present continuously in the peat between the mounds (Figure 3-6b). At this location there is some uncertainty as to whether the four palsas represent individual features or local high points on one larger feature. On profile 9, the borehole and ERT results suggested a maximum permafrost thickness of ~3.5 m. These results agree with observations during waterjet drilling when frozen ground was noted until at least 3.25 m depth (Figure 3-7a).

In all the profiles at Cartwright, permafrost was detected only beneath the palsa surfaces and adjacent elevated (dry) peaty terrain, although late-lying seasonal frost (possibly *pereletok*) was widespread in some areas. Annual ground temperatures at or close to TTOP (60 to 125 cm depths) at three non-palsa locations (i.e. lacking dry surface peat) around Cartwright (coastal tundra [n=1]; wetland [n=2]) ranged from 0.7°C to 2.3°C showing that permafrost was absent.

Main Tickle, NL

Profiles 12 and 13 were undertaken across a dissected peat plateau complex (0.5-1.0 m high) located 9 km northwest of Cartwright on the northern shore of an inlet of the Atlantic Ocean (Sandwich Bay) adjacent to an area locally known as Main Tickle (Figure 3-2c, Figures 3-8 and 3-9). The plateau (Figures 3-8c and 3-9b) covered approximately 4 ha within a raised bog that also contained other smaller peat mounds 0.5-1 m high. The peat plateau was noticeably dissected and consisted of hummocky terrain with elevated plateau interspersed with saturated depressions. Profile 12 (160 m long) began in a transition from low forest to moderately high shrubs and progressed onto the peat bog and across the peat plateau, terminating in a grassy wetland with shallow surface water (Figure 3-8c). Surface cover on the peat plateau mostly comprised ground lichen and exposed peat whereas depressions were typically grass and lichen-covered, and saturated. A borehole and monitoring station were located at 100 m along this profile on the elevated peat plateau. However, the borehole could only be drilled to 1.7 m due to a lack of nearby surface water in September 2015. Return of material during drilling indicated 1.0-1.5 m of peat overlying grey fine sand to coarse silt. ERT profile 13 (100 m roll-along) ran perpendicular to profile 12, traversing most of the peat plateau (Figure 3-9b). Surface cover was similar to that on profile 12 with lichens and exposed peat on the peat plateau and typically grasses and other herbaceous vegetation in the saturated depressions forming the dissected portions of the plateau.

Resistivities were higher (> 1000 Ω.m) except in the near surface and extended to the base of the profile (Figure 3-8a). A much higher resistivity (> 4000 Ω.m) sloping surface was present at depth across 75% of the profile. This feature was interpreted as being due to bedrock which was exposed near the start of the profile. Probing indicated the presence of a frost table nearly continuously between 32-160 m along the profile with a median thaw layer thickness of 58 cm (September 9, 2015) (Figure 3-8a). Probe penetration was greater towards the end of the profile which terminated in an area of shallow surface water which nevertheless overlay frozen ground. After infilling, the mean air temperature at the monitoring station was calculated to be -1.0°C (August 2015 to August 2016) while ground temperatures averaged -0.3°C (near-surface), -1.4°C at 1 m, and -0.7 at 1.73 m depth (Figure 3-8b). These results show that permafrost is present between at least ~0.7 m (maximum temperature < 0°C) and 1.73 m depth at the borehole but it likely extends deeper at this location. Although indicative of relatively cold permafrost, these borehole temperatures should be interpreted with caution as they were infilled using cross correlation and may include some residual thermal effects of waterjet drilling.

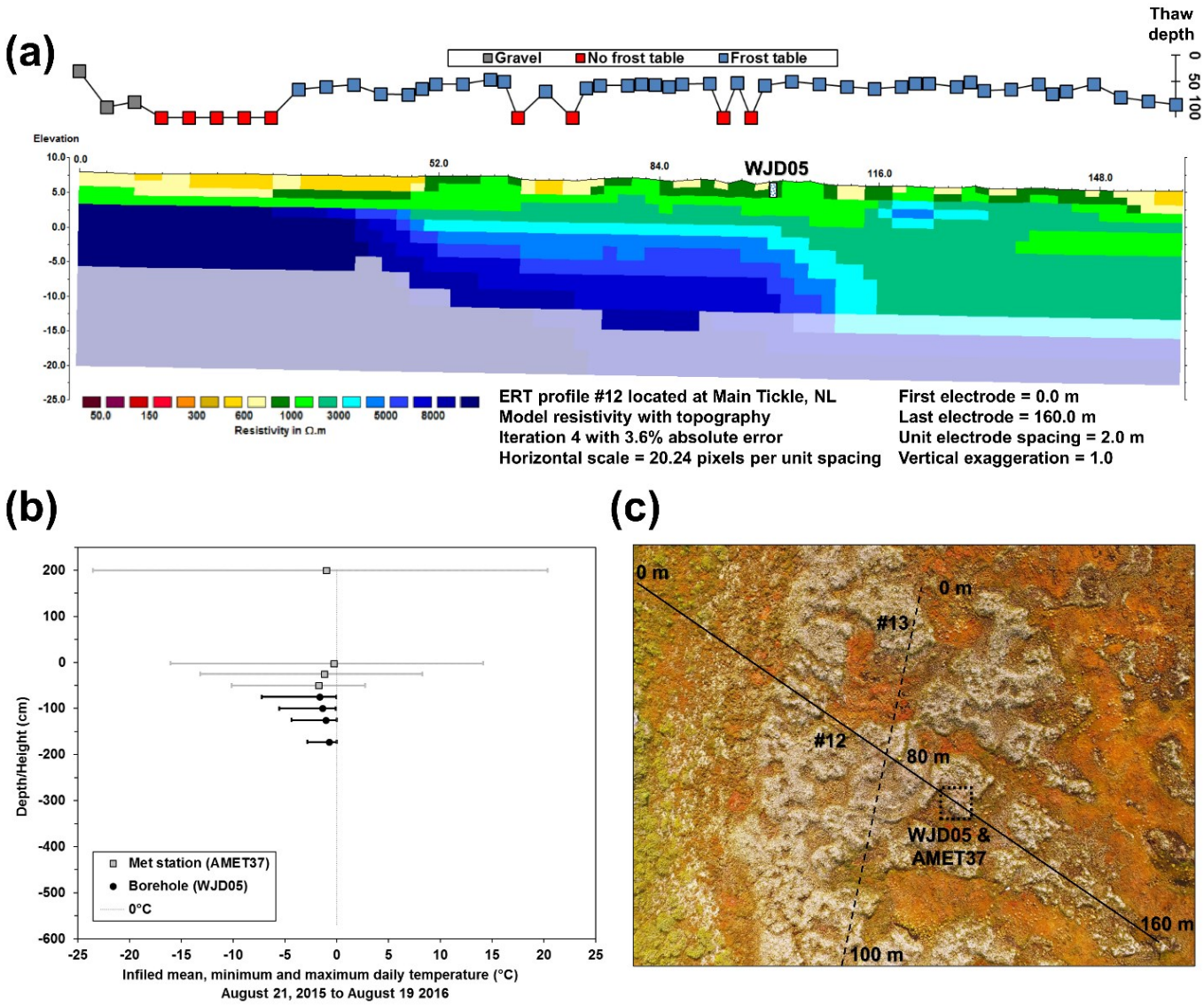

Figure 3-8: Field investigations of permafrost conditions at Main Tickle, NL. (a) Inferred thaw depths and modelled resistivities from co-located frost probing and ERT profile #12. Approximate location of temperature borehole is indicated on the ERT survey and depths with permafrost in the borehole are denoted by hatching; N.B. The colour scale used differs from that in the other figures to differentiate between zones of high resistivity. Consequently, some zones that would appear blue in Figures 3-8 are green on this modified scale but still inferred to be frozen; (b) Ground temperatures measured at monitoring station AMET37 and the temperature borehole WJD05 located along ERT profile #12; (c) Low altitude UAV imagery of the site. Black line delimits the approximate location of the ERT survey line and text shows the start and end points.

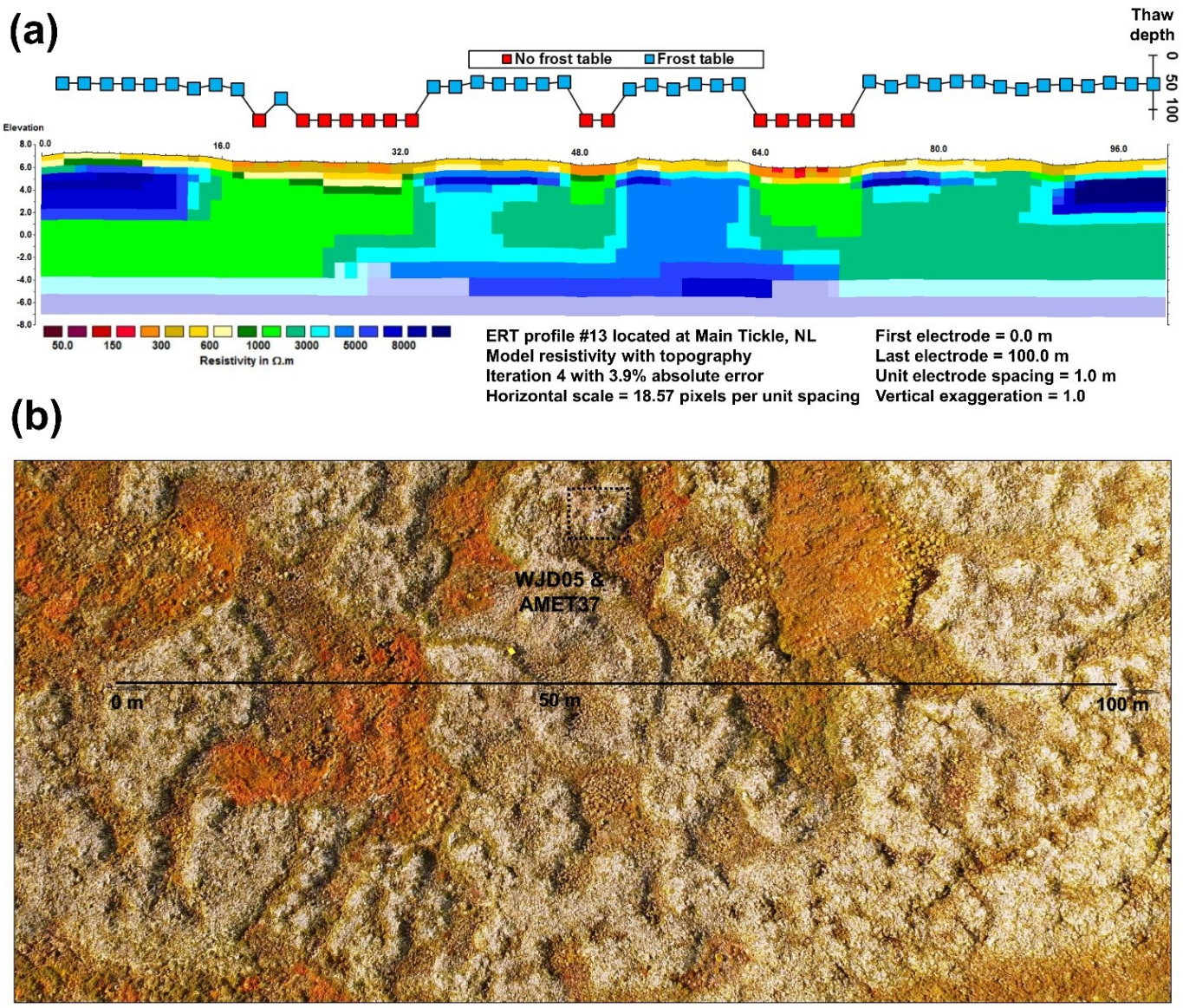

Figure 3-9: Field investigations of permafrost conditions at Main Tickle, NL. (a) Inferred thaw depths and modelled resistivities from co-located frost probing and ERT profile #13; N.B. The colour scale used differs from that in the other figures to differentiate between zones of high resistivity. Consequently, some zones that would appear blue in Figures 3-8 are green on this modified scale but still inferred to be frozen; (b) Low altitude UAV imagery of the site. Black line delimits the approximate location of the ERT survey line and text shows the start and end points.

Along profile 13, resistivities were uniformly higher (> 1000 Ω.m) than at the same depths in profile 12 but the more detailed near-surface parts of the profile showed lower values (< 300 Ω.m and as low as 20 Ω.m) between the elevated peat sections (Figure 3-9a). Resistivities were also lower at depth between the elevated parts of the peat plateau, but still > 1000 Ω.m. A higher resistivity zone (> 5000 Ω.m) at 8 m below the surface occurred in the centre of the profile at the intersection with profile 12 and is interpreted as a continuation of the bedrock surface (Figure 3-9a). Frost probing along profile 13 showed shallow thaw depths (median: 53 cm on September 9, 2015) on the peat plateau and full penetration in depressions (Figure 3-9b).

Permafrost at Main Tickle was interpreted to be widespread beneath the peat plateau along profiles 12 and 13 based on the ERT results, frost probing and ground temperature data. The boundary for delineating between frozen and unfrozen ground used at this site was 400-800 Ω.m but interpretation was complicated by the likely presence of high resistivity bedrock whose thermal state is unknown. Permafrost may be absent between 0-28 m of profile 12 given the lack of a frost table and the probable presence of near-surface bedrock (Figure 3-8a). However, permafrost was inferred to be present throughout the remainder of this profile including below shallow surface waters near its end. Permafrost was also inferred to be ubiquitous along profile 13, reaching bedrock at a depth of about 8 m. On both profiles, the surface unfrozen layer exceeded probe length in surface depressions in the plateau but the resistivity values remained much higher beneath, suggesting the presence of permafrost. The lower resistivity values in these zones probably represent higher unfrozen water contents in sediments whose temperatures are close to 0°C.

Neivisik Island, NL

Mounds, interpreted as palsas, were common throughout the peatland visited on Neivisik Island, but were lower, smaller in areal extent, and more elongated than those observed at the other field sites (Figure 3-2d). Many of the palsas were partially covered by low shrubs and showed evidence of degradation, with surface cracks, exposed peat, and uneven terrain. Thermokarst ponds were also common within the bog (Figure 3-2d). Vegetation cover at this site was more extensive than at other investigated peat bogs with small-to-medium shrubs evident on the surface of many of the mounds.

Ground temperatures recorded from August 2014 to August 2016 on a 1 m high mound about 500 m from the coast in the centre of the island averaged -0.9°C at 15 cm depth and -2.3°C at 55 cm depth. Frost probing at a variety of locations in the peatland showed thaw depths between 40 and 60 cm for peat mounds with complete probe penetration at non-elevated peat covered or vegetated surfaces. Average

ground temperatures (50-100 cm depths) measured at two other sites on the island without a dry peat surface (low shrub [n=1]; wetland [n=1]) were 2.9°C and 1.5°C, respectively. These results confirm that the peat mounds were palsas and that permafrost is unlikely to occur on Neivisik Island where palsas are absent.

3.3.2 Peatland permafrost ground ice content

Palsa height and permafrost thickness can be used to calculate average excess ice fractions (EICs) (e.g. Lewkowicz et al. 2011) using **EQ. 3-1.**

EQ. 3-1

$$\boldsymbol{Excess\ ice\ fraction} = \frac{\boldsymbol{Mound\ height\ (m)}}{\boldsymbol{Permafrost\ thickness\ (m)}}$$

EICs calculated for the palsas examined in southeastern Labrador ranged from 0.1 to 0.6 with a median value of 0.17 (n=27) (Figure 3-10). The peat plateau at Main Tickle was not included in this calculation because of the difficulty in establishing the maximum permafrost thickness at this site but given the relatively low height of the peat plateau and thick permafrost, the EICs would likely be lower than 0.15. These values suggest mean excess ice contents lower than those typically found in the southern Yukon (0.2-0.4) (Lewkowicz et al. 2011) but higher than those calculated for palsas in northern Sweden (<0.03-0.25) by Sjöberg et al. (2015) (Figure 3-10).

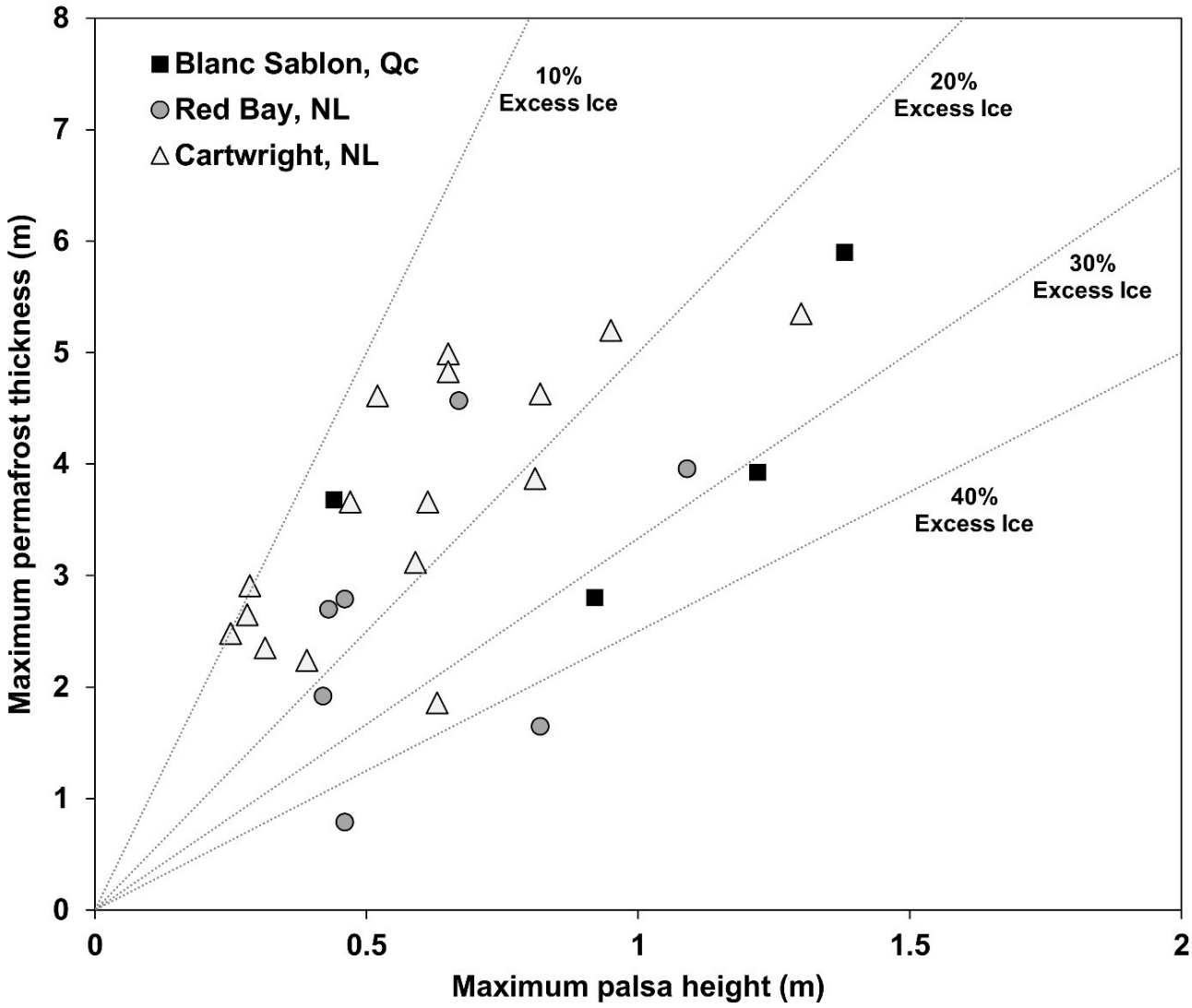

Figure 3-10: Comparison between maximum palsa height and inferred maximum permafrost thickness calculated for palsas surveyed in this study. Dotted lines depict the association between maximum palsa height and inferred maximum permafrost thickness for excess ice quantities of 10%, 20%, 30% and 40%.

3.3.3 Ground temperature modelling

Daily ground temperatures were modelled for the Blanc Sablon (WJD03) and Cartwright (WJD02) boreholes for 2014-2016. Following calibration, modelled daily ground temperatures for 2014-2016 were in good agreement with the measured temperatures at the shallowest depths: WJD02 at 55 cm, n=755; r^2=0.94; mean difference: -0.1°C; mean absolute difference: 0.75°C; and WJD03 at 25 cm, n=734; r^2=0.94; mean difference: -0.13°C; mean absolute difference: 0.84°C. The overall fit to observed ground temperatures was good at most depths and reproduced the large observed thermal offsets of -2.7°C (Blanc Sablon) and -1.7°C (Cartwright) and the thin permafrost at both locations. To achieve these results, however, modelled geothermal heat fluxes at the sites had to be set to 0.54 W m^{-2} (Blanc Sablon) and 1.02 W m^{-2} (Cartwright). These fluxes are an order of magnitude larger than those typically used at non-peatland sites (Zhang 2013) and may reflect advective and vertical heat flow from surrounding unfrozen terrain and water bodies rather than being the true geothermal heat flows. A similar parameterization of geothermal heat fluxes was required for modelling permafrost mounds in northern Québec (Buteau et al. 2004).

Modelled permafrost thickness declined from nearly 5 m at both sites in 1900 to about 3.8 m at Blanc Sablon and 2.5 m at Cartwright in 2016. This decrease was continuous at Cartwright whereas periods of permafrost thinning and re-aggradation were modelled for Blanc Sablon (Figure 3-11a). Modelling results show complete permafrost degradation under all RCP scenarios at Blanc Sablon: by 2044 under an aggressive warming scenario (RCP8.5) and by 2054 under RCP2.6 which requires significant climate change mitigation measures (Figure 3-11a). There is greater variation in modelling results for Cartwright (Figure 3-11b). Permafrost degrades completely by 2063 under RCP 8.5 whereas under the RCP 4.5 scenario, thin permafrost persists until nearly the end of the 21st century. Finally, under RCP2.6, permafrost with an estimated thickness of 1.6 m remains in 2100 and no degradation occurs during the preceding 30 years (Figure 3-11b).

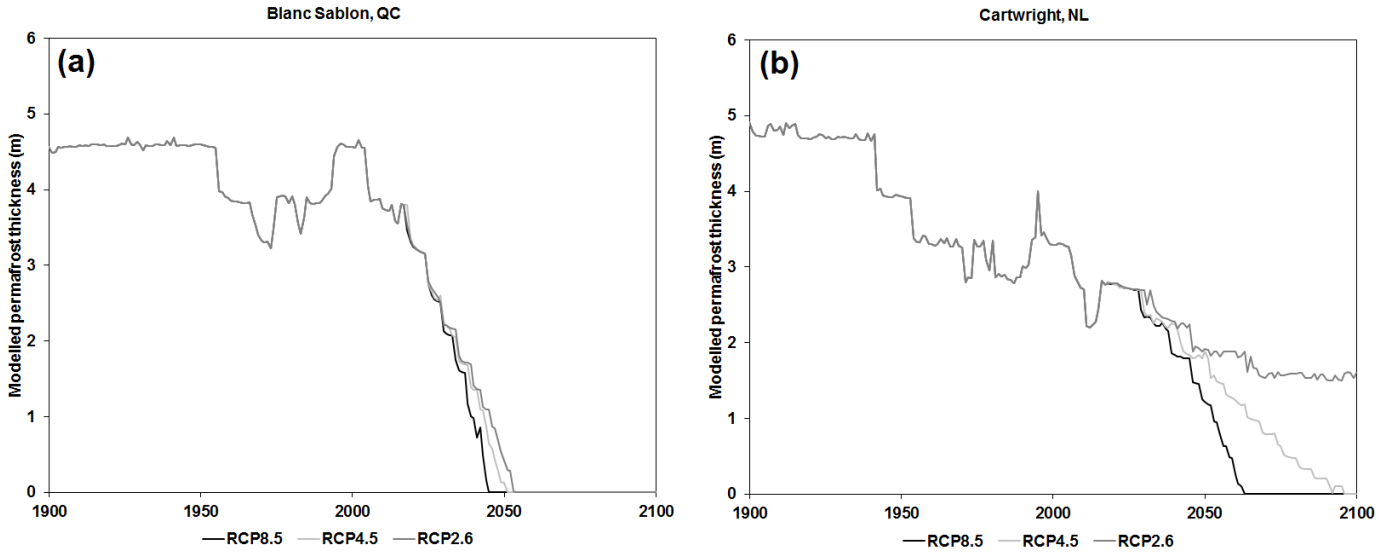

Figure 3-11: Historical and future permafrost thicknesses modelled with NEST (Zhang et al. 2003) covering the period 1900-2100 for (a) Blanc Sablon, QC; (b) and Cartwright, NL. Modelled permafrost thicknesses are shown for three representative carbon pathways (RCP2.6; RCP4.5; RCP8.5).

3.4 Discussion

3.4.1 Southeastern Labrador palsas and peat plateaus

The palsas examined have heights of 0.3-1.5 m which places them at the low end of the circumarctic range of palsa heights (Van Everdingen 2005a), reflecting thin permafrost and moderate excess ice contents. Inferred permafrost thicknesses beneath individual palsas varied from ~80 cm to ~650 cm although thicknesses exceeding 15 m were inferred beneath the peat plateau at Main Tickle. Their vegetation cover is generally limited to lichens with exposed peat during degradational phases due to wind abrasion, as is particularly evident at Blanc Sablon (Figure 3-2a; Figure 3-3d). Peat thicknesses was not directly measured but was estimated during waterjet drilling as between 1-1.5 m at the Cartwright, Main Tickle and Red Bay boreholes and as 1.5-2 m at Blanc Sablon.

Measured snow depths suggest minimal accumulation on any of the palsas with a median late-winter snow depth of 15 cm (range: 5-25 cm) (Way and Lewkowicz in revision). Given that regional late-winter snow accumulation commonly exceeds 100 cm, the palsas must be heavily wind scoured in the winter, an observation confirmed by local observers (Gary Bird, *personal communication*). These findings accord with results from northern Scandinavia where a snow depth of about 50 cm or less was required for palsa formation (Seppälä 2011). Low shrubs including Labrador Tea and Blueberry bushes were present on palsas at Red Bay and Neivisik Island. Given high snowfalls in southeastern Labrador, the presence of tall shrubs would likely capture enough snow to lead to the eventual thaw of these permafrost landforms.

Ground temperatures recorded at TTOP on the peatland permafrost features varied from -0.7°C at the southernmost site (Blanc Sablon) to -2.3°C at the northernmost one (Neivisik Island) showing a clear latitudinal gradient (Figure 3-12). These are relatively low values given MAAT > 0°C, and therefore reflect small surface offsets and large thermal offsets. Although the latter could be caused by the slow transient response of ground temperatures to recent regional warming (Jorgenson et al. 2010; Lewkowicz et al. 2016; Morse et al. 2016), we favour the explanation that these large offsets are due to differences in frozen and unfrozen thermal conductivities resulting from thick peat found in the well-drained raised bogs (Seppälä 2011). This inference is supported by very shallow thaw depths, ranging from 37-65 cm (median: 46 cm). Such offsets allow permafrost to persist even where the MAAT is > 1°C (Jorgenson et al. 2010).

The shallow thaw depths observed contradict broader scale models (e.g. Smith and Riseborough 2002; Zhang et al. 2008b) which predict thick active layers (1-2 m) at the southern end of the discontinuous zone. However, these do not consider that permafrost in this zone, where present, is typically in peatlands which are not represented well on most national scale surficial maps used as modelling inputs.

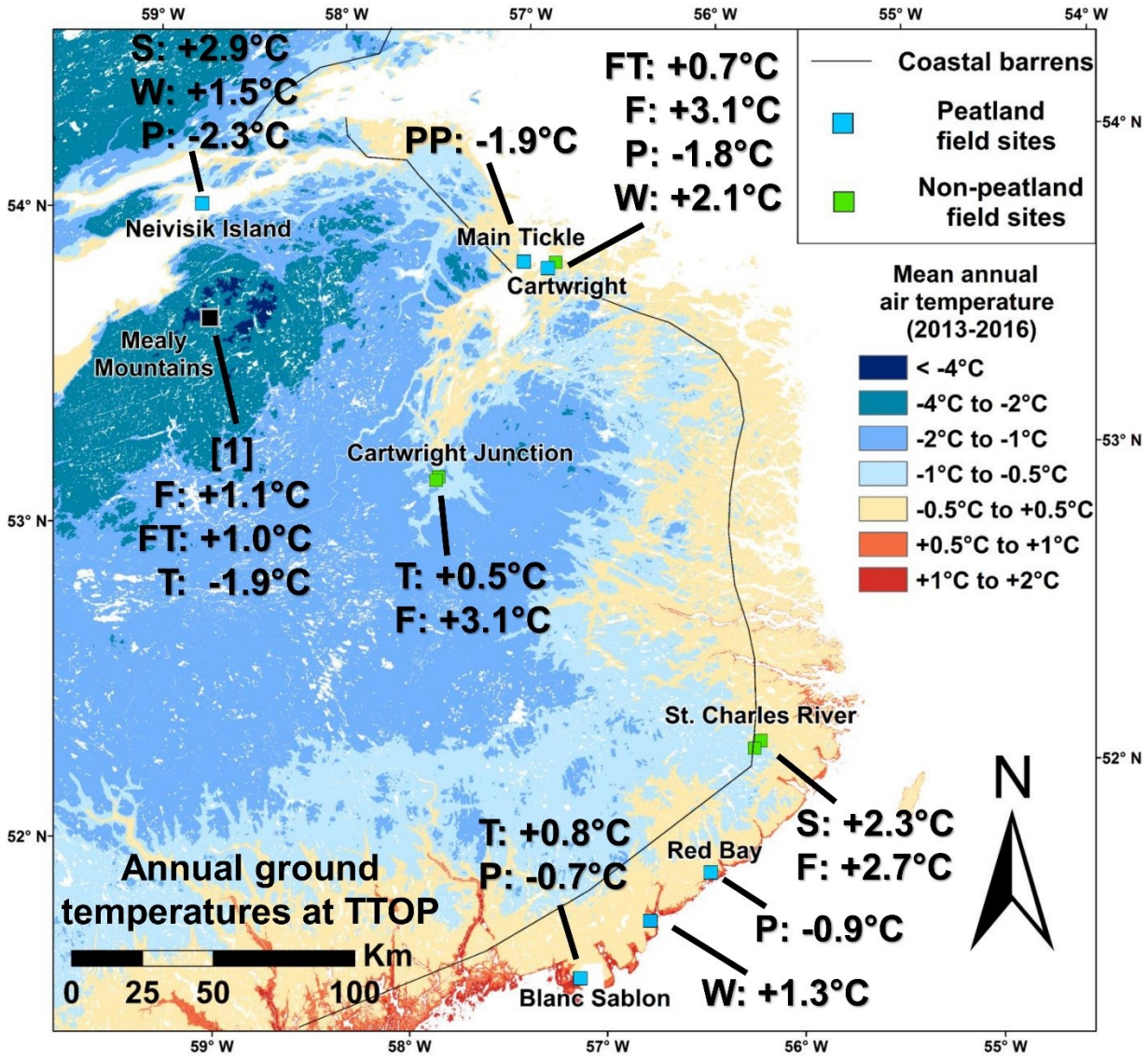

Figure 3-12: Spatial distribution of shallow ground temperatures observed at University of Ottawa monitoring locations across southeastern Labrador between 2013-2016. Letters denote primary land cover class at each location including: F – Forest; P – Palsa; PP – Peat Plateau; S – Shrub; T – Tundra; and W – Wetland. At Cartwright, ground temperatures for palsas were averaged from three nearby sites. Location indicated by [1] shows data from the Mealy Mountains collected by Jacobs et al (2014) between 2001-2009.

There is evidence that peatland permafrost in southeastern Labrador has degraded over that past half-century. For example, palsas at Cartwright were 1.5 m high and peat plateaus were > 60 m long and > 6 m wide in 1968 (Brown 1975; 1979). Currently, palsas and peat plateau do not exceed 1 m in height and permafrost-cored terrain appears to cover a much smaller part of the landscape than 50 years ago. Similarly, palsas and peat plateaus at Neivisik Island were 1.8 m high and covered most of the bog in 1968 (Brown 1975, 1979), whereas there are currently no mounds greater than 1 m high or with long axes >20 m, and many collapse scars and thermokarst ponds (Figure 3-2c). Degradational features on palsas were also evident at Blanc Sablon and Cartwright where several mounds exhibited large cracks exposing their interiors. Analyses of ground temperature data recorded intermittently between 1991-2012 (with a data gap from 1998-2004) at a palsa field north of Blanc Sablon by Allard et al. (2014) show that temperatures at 50 cm depth increased over this time period to the point where average ground temperatures regularly exceed 0°C (Figure B2). These data support recent modelling studies (Way and Lewkowicz 2016) and the general field interpretation that regional permafrost thaw has occurred.

3.4.2 Permafrost in southeastern Labrador

A detailed inventory of palsas and peat plateau in the study area would require high resolution aerial photography and/or satellite imagery to characterize inaccessible sites, with sub-meter resolution imagery needed to identify the very small palsas found in many areas (Borge et al. 2017). Furthermore, many small mounds identified throughout the study area had seasonal frost or possibly *pereletok* and could be misclassified as small palsas due to their similar morphology and height. A preliminary analysis of Google Earth™ imagery suggests that peatland permafrost features may exist at several other locations in the coastal barrens between Blanc Sablon and Cartwright. For example, Brown (1975; 1979) visited palsas north of Red Bay by helicopter although these features have not been relocated since originally described.. Satellite imagery also shows widespread thermokarst ponds in the region, including on the northernmost tip of the island of Newfoundland. Archeological investigations at L'Anse aux Meadows (51.6°N) described the excavation of a palsa including the characterization of frozen layers beneath thick surface peat (Henningsmoen 1977). Given the similar geographic setting and climate to sites at the southern end of the transect examined in this study, there is no reason *a priori* that palsas could not persist in northernmost parts of Newfoundland.

Permafrost at the southern end of the Labrador transect was restricted to very isolated patches in peatlands and ground temperature data at monitoring stations showed a larger differences (median: 1.8°C) between temperatures at the ground surface and those recorded at the top of permafrost compared to other

land cover types (Way and Lewkowicz in revision). These results suggest that peatland permafrost of southeastern Labrador is ecosystem protected (Shur and Jorgenson 2007) and only tenable due to large thermal offsets caused by thick peat accumulations (e.g. Jorgenson et al. 2010; Lewkowicz et al. 2016). The limited extent and small size of palsas in the southernmost parts of Labrador suggest that permafrost can persist only under a very narrow range of environmental conditions and that these features were most likely formed under an earlier cold period such as the Little Ice Age (e.g. Dionne and Richard 2006; Tremblay et al. 2014). Towards the northern end of the study transect, permafrost was observed to be more widespread with larger patch sizes, thicker permafrost bodies and more frequent occurrences near Cartwright and Main Tickle (Figure 3-12). At the latter site, wetland terrain adjacent to the peat plateau remained frozen near the end of the thaw season.

The peatland permafrost features were all found in areas considered to be coastal barrens with MAATs between -0.5°C and +1.0°C (2013-2016). Colder areas inland and at higher elevation were noticeably absent of permafrost mounds, a pattern noted elsewhere for much colder portions of Labrador (Brown, 1979; Way and Lewkowicz, in revision) (Figure 3-12). The -1°C MAAT threshold commonly used in northern Scandinavia (e.g. Vorren 2017) for delimiting the upper climatic boundary for palsa formation is too low for Labrador. However, a recent inventory found isolated patches of peatland permafrost in Finnmark at MAATs as high as +1°C although features were most frequently observed at MAATs between -2°C and -4°C (Borge et al. 2017).

Peatland permafrost in southeastern Labrador has a unique geographic distribution in which it is not present inland where MAATs are lower while it exists in low-elevation coastal areas where MAATs commonly exceeded 0°C. One-dimensional numerical simulations by Riseborough (2004) showed that, when all other inputs are equal, ground temperatures should be lower in areas with smaller temperature ranges, such as at coastal sites. Furthermore, several other factors likely contribute to the persistence of peatland permafrost near the coast. First, seasonal sea ice can promote near-surface temperature inversions that cool the ground in the winter and spring in many areas adjacent to the coast (Maxwell 1981; Atkinson and Gajewski 2002; Smith and Bonnaventure 2017). Second, melting sea ice and ocean-atmosphere contrasts promote coastal fog and persistent cloudiness in summer, leading to Arctic-like temperatures in many parts of coastal Labrador (Maxwell 1981; Way et al. 2014; Way et al. 2017a). Finally, persistent high winds and frequent winter melt events likely modify snow properties (e.g. density) which increase winter heat exchange between the ground and the atmosphere (Derksen et al. 2014). In addition, windy conditions influence snow redistribution and enhance wind scouring which reduce the insulating effect of snow cover on ground temperatures. It has been hypothesized by Dionne (1984) that palsas found at several

locations north of Blanc Sablon may be relic features that have persisted in the area since the Little Ice Age due to coastal effects, including persistent cloudiness. Evidence supporting this hypothesis includes coring done on palsas at Blanc Sablon, QC by Dionne and Richard (2006), and near the James Bay hydroelectric development in northwestern Québec by Temblay et al (2014) which used peat dating techniques to estimate the timing of permafrost formation at these sites as being during the Little Ice Age.

Despite the coastal climate, permafrost was not encountered at monitoring sites in upland tundra, forest tundra, low shrubs, and thick Black and White Spruce forest in the coastal transect (Figure 3-11). The absence of permafrost beneath wind-scoured tundra hilltops in the vicinity of Blanc Sablon, Cartwright Junction and Cartwright (up to 302 m a.s.l.) demonstrates that permafrost cannot now exist in mineral soils in southeastern Labrador at low elevations. However, cooler climatic conditions during the mid-20th century or the Little Ice Age may have allowed permafrost to exist in mineral and organic soils outside of peatlands (Way and Lewkowicz 2016). Relict polygonal terrain near Blanc Sablon which dates from the Little Ice Age (Dionne 1983) lend support to this inference. Contemporary mountain permafrost is present in some high elevation tundra environments (> 600 m a.s.l.) in the Mealy Mountains (Figure 3-12) (Brown 1979; Jacobs et al. 2014) and is inferred to exist in high elevation tundra areas farther south based on spatial modelling (Way and Lewkowicz 2016).

The thermal modelling results indicate that peatland permafrost will thaw in most of southeastern Labrador in the 21st century, with southern sites losing frozen ground by about 2050. Farther north, responses depend on the RCP scenario and there is the possibility of permafrost persistence if RCP 2.6 is followed. However, the modelling considered only vertical fluxes whereas isolated patches of peatland permafrost may undergo degradation via two-dimensional or three-dimensional processes including advective heat transfer, wind abrasion of surface peat and block collapse into adjacent standing water, all of which may accelerate the rate of permafrost loss. Therefore, the modelling results are likely to be optimistic in terms of permafrost persistence.

3.5 Conclusion

This study shows the contemporary existence of peatland permafrost in the coastal region of southeastern Labrador along a transect of approximately 300 km, from 51.5°N to 54°N. Palsas and peat plateaus are present in localized lowland portions of the landscape at the southern end of the transect and become more widespread towards the northern end. Despite spanning a mean annual air temperature gradient ranging from +1.0°C (south) to –1.5°C (north), permafrost thicknesses are similar at the five peatlands examined. However, ground temperatures recorded at the top of permafrost show a clear

latitudinal trend suggesting that other factors (local drainage, surficial materials) may be limiting permafrost thicknesses at several of the northern sites.

Results from air and ground temperature monitoring stations located in a variety of environmental settings suggest that at the southern end of the transect near Blanc Sablon, QC, permafrost can only occur where a sufficiently thick peat cover is present. At the northern end of the transect near Main Tickle, NL, ERT profiling indicated permafrost presence in non-peat covered areas adjacent to a large peat plateau indicating that the climate at this site remains suitable for permafrost preservation under a greater variety of conditions. At most sites, however, monitoring station data showed permafrost to be absent from non-peatland environments and peatland climate data showed a large thermal disequilibrium with surface climate conditions (Smith and Riseborough 2002; Jorgenson et al. 2010). The absence of permafrost in inland peatlands suggests that the coastal influences play an important role in promoting lower ground temperatures in the region.

One-dimensional numerical modelling for palsas at Cartwright, NL and Blanc Sablon, QC using downscaled data from representative carbon pathways suggests that permafrost may disappear from both sites by 2065 under business as usual warming scenarios (RCP8.5). Given the sensitivity of southeastern Labrador palsas to future changes and potential disturbances, more effort should be made to locate, characterize and monitor these ecosystem-protected permafrost environments.

3.6 References

Allard, M., and L. Rousseau. 1999. The internal structure of a palsa and peat plateau in the Riviere Boniface region, Québec: Inferences on the formation of ice segregation mounds. Géographie physique et Quaternaire 53(3): 373–387.

Allard, M., D. Sarrazin, and E. L'Hérault. 2014. Borehole monitoring temperatures in northeastern Canada v. 1.2 (1988-2014). Scientific data. Nordicana D8. Centre D'Étude Nordiques.

An, W., and M. Allard. 1995. A mathematical approach to modelling palsa formation: Insights on processes and growth conditions. Cold Regions Science and Technology 23(3): 231–244.

Atkinson, D. E., and K. Gajewski. 2002. High-Resolution Estimation of Summer Surface Air Temperature in the Canadian Arctic Archipelago. Journal of Climate 15(24): 3601–3614. doi: 10.1175/1520-0442(2002)015<3601:HREOSS>2.0.CO;2.

Bajzak, D. 1973. Bio-physical land classification of the Lake Melville Area, Labrador. Land classification report N-X-88. St. John's, Newfoundland and Labrador: Newfoundland Forest Research Centre.

Borge, A. F., S. Westermann, I. Solheim, and B. Etzelmüller. 2017. Strong degradation of palsas and peat plateaus in northern Norway during the last 60 years. The Cryosphere 11(1): 1–16. doi: 10.5194/tc-11-1-2017.

Briggs, M. A., S. Campbell, J. Nolan, M. A. Walvoord, D. Ntarlagiannis, F. D. Day-Lewis, and J. W. Lane. 2016. Surface Geophysical Methods for Characterising Frozen Ground in Transitional Permafrost Landscapes: Surface Geophysical Methods for Characterising Frozen Ground. Permafrost and Periglacial Processes. doi: 10.1002/ppp.1893.

Brown, R. J. 1979. Permafrost distribution in the southern part of the discontinuous zone in Quebec and Labrador. Géographie physique et Quaternaire 33(3–4): 279–289.

Brown, R. J. E. 1975. Permafrost Investigations in Quebec and Newfoundland (Labrador). Technical Paper 449. Ottawa, Ontario: National Research Council of Canada.

Buteau, S., R. Fortier, G. Delisle, and M. Allard. 2004. Numerical simulation of the impacts of climate warming on a permafrost mound. Permafrost and Periglacial Processes 15(1): 41–57. doi: 10.1002/ppp.474.

Cooper, M. D. A., C. Estop-Aragonés, J. P. Fisher, A. Thierry, M. H. Garnett, D. J. Charman, J. B. Murton, G. K. Phoenix, R. Treharne, S. V. Kokelj, S. A. Wolfe, A. G. Lewkowicz, M. Williams, and I. P. Hartley. 2017. Limited contribution of permafrost carbon to methane release from thawing peatlands. Nature Climate Change 7(7): 507–511. doi: 10.1038/nclimate3328.

Derksen, C., J. Lemmetyinen, P. Toose, A. Silis, J. Pulliainen, and M. Sturm. 2014. Physical properties of Arctic versus subarctic snow: Implications for high latitude passive microwave snow water equivalent retrievals. Journal of Geophysical Research: Atmospheres 119(12): 2013JD021264. doi: 10.1002/2013JD021264.

Dionne, J.-C. 1983. Réseaux reliques de polygones de tourbe, moyenne et basse Côte-Nord du Saint-Laurent, Québec. Géographie physique et Quaternaire 37(2): 127. doi: 10.7202/032510ar.

Dionne, J.-C. 1984. Palses et limite méridionale du pergélisol dans l'hemisphere nord: le cas de Blanc-Sablon, Québec. Géographie physique et Quaternaire 38(2): 165–184. doi: 10.7202/032550ar.

Dionne, J.-C., and V. Gérardin. 1988. Observations sur les buttes organiques de la Cote-Nord du golfe du Saint-Laurent, Québec. Géographie physique et Quaternaire 42(3): 289–301. doi: 10.7202/032737ar.

Dionne, J.-C., and P. J. H. Richard. 2006. Origine, Age et taux d'accrétion verticale de la tourbiere palses de Blanc-Sablon, basse Cote-Nord, Golfe du Saint-Laurent, Québec. Géographie physique et Quaternaire 60(2): 199–205. doi: 10.7202/016829ar.

Douglas, T. A., M. T. Jorgenson, D. R. N. Brown, S. W. Campbell, C. A. Hiemstra, S. P. Saari, K. Bjella, and A. K. Liljedahl. 2016. Degrading permafrost mapped with electrical resistivity tomography, airborne imagery and LiDAR, and seasonal thaw measurements. GEOPHYSICS 81(1): WA71-WA85. doi: 10.1190/geo2015-0149.1.

Fortier, R., M. Allard, S. Buteau, and F. Calmels. 2008. Internal structure and conditions of permafrost mounds at Umiujaq in Nunavik, Canada, inferred from field investigation and electrical resistivity tomography. Canadian Journal of Earth Sciences 45(3): 367–387. doi: 10.1139/E08-004.

Foster, D. R., and P. H. Glaser. 1986. The raised bogs of south-eastern Labrador, Canada: classification, distribution, vegetation and recent dynamics. Journal of Ecology 74(1): 47–71.

Foster, D. R., H. E. Wright, M. Thelaus, and G. A. King. 1988. Bog development and landform dynamics in central Sweden and south-eastern Labrador, Canada. Journal of Ecology 76(4): 1164–1185.

Fulton, R. J. 1995. Surficial Materials of Canada. Geological Survey of Canada Map. Natural Resources Canada.

Glaser, P. H. 1992. Raised Bogs in Eastern North America--Regional Controls for Species Richness and Floristic Assemblages. The Journal of Ecology 80(3): 535. doi: 10.2307/2260697.

Gurney, S. D. 2001. Aspects of the genesis, geomorphology and terminology of palsas: perennial cryogenic mounds. Progress in Physical Geography 25(2): 249–260.

Hauck, C. 2013. New Concepts in Geophysical Surveying and Data Interpretation for Permafrost Terrain: Geophysical Surveying in Permafrost Terrain. Permafrost and Periglacial Processes 24(2): 131–137. doi: 10.1002/ppp.1774.

Henningsmoen, K. E. 1977. Pollen-analytical investigations in the L'Anse aux Meadows area, Newfoundland. In The Discovery of a Norse Settlement in America, 289–340. Oslo: Universitetsforlaget.

Hilbich, C., L. Marescot, C. Hauck, M. H. Loke, and R. Mäusbacher. 2009. Applicability of electrical resistivity tomography monitoring to coarse blocky and ice-rich permafrost landforms. Permafrost and Periglacial Processes 20(3): 269–284. doi: 10.1002/ppp.652.

Hustich, I. 1939. Notes on the coniferous forest and tree limit on the east coast of Newfoundland-Labrador. Acta Geographica 7(1): 5–77.

Hutchinson, M. F., D. W. McKenney, K. Lawrence, J. H. Pedlar, R. F. Hopkinson, E. Milewska, and P. Papadopol. 2009. Development and testing of Canada-wide interpolated spatial models of daily minimum-maximum temperature and precipitation for 1961–2003. Journal of Applied Meteorology and Climatology 48(4): 725–741. doi: 10.1175/2008JAMC1979.1.

Jacobs, J. D., S. Chan, and E. Sutton. 2014. Climatology of the Forest-Tundra Ecotone at a Maritime Subarctic-Alpine Site, Mealy Mountains, Labrador. ARCTIC 67(1): 28–42. doi: 10.14430/arctic4358.

Jorgenson, M. T., V. Romanovsky, J. Harden, Y. Shur, J. O'Donnell, E. A. G. Schuur, M. Kanevskiy, and S. Marchenko. 2010. Resilience and vulnerability of permafrost to climate change. Canadian Journal of Forest Research 40(7): 1219–1236. doi: 10.1139/X10-060.

Kasprzak, M. 2015. High-resolution electrical resistivity tomography applied to patterned ground, Wedel Jarlsberg Land, south-west Spitsbergen. Polar Research 34(0). doi: 10.3402/polar.v34.25678.

Laberge, M.-J., and S. Payette. 1995. Long-Term Monitoring of Permafrost Change in a Palsa Peatland in Northern Quebec, Canada: 1983-1993. Arctic and Alpine Research 27(2): 167. doi: 10.2307/1551898.

Laprise, D., and S. Payette. 1988. Évolution récente d'une tourbière à palses (Québec subarctique): analyse cartographique et dendrochronologique. Canadian Journal of Botany 66(11): 2217–2227.

Lewkowicz, A. G. 2008. Evaluation of miniature temperature-loggers to monitor snowpack evolution at mountain permafrost sites, northwestern Canada. Permafrost and Periglacial Processes 19(3): 323–331. doi: 10.1002/ppp.625.

Lewkowicz, A. G., B. Etzelmüller, and S. L. Smith. 2011. Characteristics of discontinuous permafrost based on ground temperature measurements and electrical resistivity tomography, southern Yukon, Canada. Permafrost and Periglacial Processes 22(4): 320–342. doi: 10.1002/ppp.703.

Lewkowicz, A. G., O. Bellehumeur-Génier, C. M. Miceli, and S. L. Smith. 2016. Change in discontinuous permafrost in the Alaska Highway corridor examined by repeated electrical resistivity tomography and ground temperature monitoring, northwest Canada. In Proceedings of the 10th International Conference on Permafrost. Potsdam, Germany.

Loke, M. H., and R. D. Barker. 1996. Rapid least-squares inversion of apparent resistivity pseudosections by a quasi-Newton method. Geophysical prospecting 44(1): 131–152.

Loke, M. H., I. Acworth, and T. Dahlin. 2003. A comparison of smooth and blocky inversion methods in 2D electrical imaging surveys. Exploration Geophysics 34(3): 182–187. doi: 10.1071/EG03182.

Maxwell, J. B. 1981. Climatic regions of the Canadian Arctic Islands. ARCTIC 34(3): 225–240.

Minsley, B. J., N. J. Pastick, B. K. Wylie, D. R. N. Brown, and M. Andy Kass. 2016. Evidence for nonuniform permafrost degradation after fire in boreal landscapes. Journal of Geophysical Research: Earth Surface 121(2): 320–335. doi: 10.1002/2015JF003781.

Morse, P. D., S. A. Wolfe, S. V. Kokelj, and A. J. R. Gaanderse. 2016. The occurrence and thermal disequilibrium state of permafrost in forest ecotopes of the Great Slave Region, Northwest Territories, Canada. Permafrost and Periglacial Processes 27(2): 145–162. doi: 10.1002/ppp.1858.

Ou, C., B. Leblon, Y. Zhang, A. LaRocque, K. Webster, and J. McLaughlin. 2016a. Modelling and mapping permafrost at high spatial resolution using Landsat and Radarsat images in northern Ontario, Canada: Part 1 – model calibration. International Journal of Remote Sensing 37(12): 2727–2750. doi: 10.1080/01431161.2016.1157642.

Ou, C., A. LaRocque, B. Leblon, Y. Zhang, K. Webster, and J. McLaughlin. 2016b. Modelling and mapping permafrost at high spatial resolution using Landsat and Radarsat-2 images in Northern Ontario, Canada: Part 2 – regional mapping. International Journal of Remote Sensing 37(12): 2751–2779. doi: 10.1080/01431161.2016.1151574.

Payette, S., A. Delwaide, M. Caccianiga, and M. Beauchemin. 2004. Accelerated thawing of subarctic peatland permafrost over the last 50 years. Geophysical Research Letters 31(18): L18208. doi: 10.1029/2004GL020358.

Riseborough, D. W. 2004. Exploring the parameters of a simple model of the permafrost-climate relationship. PhD Thesis, Ottawa: Carleton University.

Roberts, B. A., and A. W. Robertson. 1980. Palsa bogs, sand dunes, salt marshes, environmentally sensitive habitats in the coastal region southeastern Labrador. In Proceedings of workshop on research in the Labrador coastal and offshore region, 245–263. St. John's, Newfoundland and Labrador.

Roberts, B. A., N. P. P. Simon, and K. W. Deering. 2006. The forests and woodlands of Labrador, Canada: ecology, distribution and future management. Ecological Research 21(6): 868–880. doi: 10.1007/s11284-006-0051-7.

Schuur, E. A. G., A. D. McGuire, C. Sch?del, G. Grosse, J. W. Harden, D. J. Hayes, G. Hugelius, C. D. Koven, P. Kuhry, D. M. Lawrence, S. M. Natali, D. Olefeldt, V. E. Romanovsky, K. Schaefer, M. R. Turetsky, C. C. Treat, and J. E. Vonk. 2015. Climate change and the permafrost carbon feedback. Nature 520(7546): 171–179. doi: 10.1038/nature14338.

Séguin, M. K., and J.-C. Dionne. 1992. Modélisation géophysique et caractérisation thermique du pergélisol dans les palses de Blanc-Sablon, Québec. 92–1E. Current Research. Geological Survey of Canada.

Seppälä, M. 1982. An experimental study of the formation of palsas. In Proc. 4th Can. Permafrost Conf, 36–42.

Seppälä, M. 2011. Synthesis of studies of palsa formation underlining the importance of local environmental and physical characteristics. Quaternary Research 75(2): 366–370. doi: 10.1016/j.yqres.2010.09.007.

Shur, Y. L., and M. T. Jorgenson. 2007. Patterns of permafrost formation and degradation in relation to climate and ecosystems. Permafrost and Periglacial Processes 18(1): 7–19. doi: 10.1002/ppp.582.

Sjöberg, Y., P. Marklund, R. Pettersson, and S. W. Lyon. 2015. Geophysical mapping of palsa peatland permafrost. The Cryosphere 9(2): 465–478. doi: 10.5194/tc-9-465-2015.

Smith, M. W., and D. W. Riseborough. 2002. Climate and the limits of permafrost: a zonal analysis. Permafrost and Periglacial Processes 13(1): 1–15. doi: 10.1002/ppp.410.

Smith, S. L., and P. P. Bonnaventure. 2017. Quantifying Surface Temperature Inversions and Their Impact on the Ground Thermal Regime at a High Arctic Site. Arctic, Antarctic, and Alpine Research 49(1): 173–185. doi: 10.1657/AAAR0016-039.

Tarnocai, C. 2006. The effect of climate change on carbon in Canadian peatlands. Global and Planetary Change 53(4): 222–232. doi: 10.1016/j.gloplacha.2006.03.012.

Tarnocai, C. 2009. The impact of climate change on Canadian peatlands. Canadian Water Resources Journal 34(4): 453–466.

Thibault, S., and S. Payette. 2009. Recent permafrost degradation in bogs of the James Bay area, northern Quebec, Canada. Permafrost and Periglacial Processes 20(4): 383–389. doi: 10.1002/ppp.660.

Tremblay, S., N. Bhiry, M. Lavoie, and A. de Vernal. 2014. Long-term dynamics of a palsa in the sporadic permafrost zone of northwestern Quebec (Canada). Canadian Journal of Earth Sciences 51(5): 500–509. doi: 10.1139/cjes-2013-0123.

Van Everdingen, R. 2005a. Palsa. Multi-language glossary of permafrost and related ground-ice terms. Boulder, Colorado, USA: National Snow and Ice Data Center.

Van Everdingen, R. 2005b. Pereletok. Multi-language glossary of permafrost and related ground-ice terms. Boulder, Colorado, USA: National Snow and Ice Data Center.

Vincent, L. A., X. L. Wang, E. J. Milewska, H. Wan, F. Yang, and V. Swail. 2012. A second generation of homogenized Canadian monthly surface air temperature for climate trend analysis. Journal of Geophysical Research: Atmospheres 117(D18): n/a-n/a. doi: 10.1029/2012JD017859.

Vorren, K.-D. 2017. The first permafrost cycle in Færdesmyra, eastern Finnmark, Norway? Norsk Geografisk Tidsskrift - Norwegian Journal of Geography: 1–8. doi: 10.1080/00291951.2017.1316309.

van Vuuren, D. P., J. Edmonds, M. Kainuma, K. Riahi, A. Thomson, K. Hibbard, G. C. Hurtt, T. Kram, V. Krey, J.-F. Lamarque, T. Masui, M. Meinshausen, N. Nakicenovic, S. J. Smith, and S. K. Rose. 2011. The representative concentration pathways: an overview. Climatic Change 109(1–2): 5–31. doi: 10.1007/s10584-011-0148-z.

Way, R. G., and A. G. Lewkowicz. in revision. Relations between environmental setting and TTOP parameters in Labrador, northeast Canada. Permafrost and Periglacial Processes.

Way, R. G., and A. G. Lewkowicz. 2015. Investigations of discontinuous permafrost in coastal Labrador with DC electrical resistivity tomography. In Proceedings of GéoQuebec: 68th Canadian Geotechnical Conference and 7th Canadian Permafrost Conference, 8. Québec City, Canada. doi: 10.13140/RG.2.1.1647.8803.

Way, R. G., and A. G. Lewkowicz. 2016. Modelling the spatial distribution of permafrost in Labrador–Ungava using the temperature at the top of permafrost. Canadian Journal of Earth Sciences 53(10): 1010–1028. doi: 10.1139/cjes-2016-0034.

Way, R. G., and A. E. Viau. 2015. Natural and forced air temperature variability in the Labrador region of Canada during the past century. Theoretical and Applied Climatology 121(3–4): 413–424. doi: 10.1007/s00704-014-1248-2.

Way, R. G., T. Bell, and N. E. Barrand. 2014. An inventory and topographic analysis of glaciers in the Torngat Mountains, northern Labrador, Canada. Journal of Glaciology 60(223): 945–956. doi: 10.3189/2014JoG13J195.

Way, R. G., A. G. Lewkowicz, and P. P. Bonnaventure. 2017a. Development of moderate-resolution gridded monthly air temperature and degree-day maps for the Labrador-Ungava region of northern Canada. International Journal of Climatology 37(1): 493–508. doi: 10.1002/joc.4721.

Wolfe, S. A., C. W. Stevens, A. J. Gaanderse, and G. A. Oldenborger. 2014. Lithalsa distribution, morphology and landscape associations in the Great Slave Lowland, Northwest Territories, Canada. Geomorphology 204: 302–313. doi: 10.1016/j.geomorph.2013.08.014.

You, Y., Q. Yu, X. Pan, X. Wang, and L. Guo. 2013. Application of electrical resistivity tomography in investigating depth of permafrost base and permafrost structure in Tibetan Plateau. Cold Regions Science and Technology 87: 19–26. doi: 10.1016/j.coldregions.2012.11.004.

Zhang, Y. 2003. A process-based model for quantifying the impact of climate change on permafrost thermal regimes. Journal of Geophysical Research 108(D22). doi: 10.1029/2002JD003354.

Zhang, Y. 2013. Spatio-temporal features of permafrost thaw projected from long-term high-resolution modeling for a region in the Hudson Bay Lowlands in Canada. Journal of Geophysical Research: Earth Surface 118(2): 542–552. doi: 10.1002/jgrf.20045.

Zhang, Y., W. Chen, and J. Cihlar. 2003. A process-based model for quantifying the impact of climate change on permafrost thermal regimes. Journal of Geophysical Research 108(D22). doi: 10.1029/2002JD003354.

Zhang, Y., W. Chen, and D. W. Riseborough. 2008. Transient projections of permafrost distribution in Canada during the 21st century under scenarios of climate change. Global and Planetary Change 60(3–4): 443–456. doi: 10.1016/j.gloplacha.2007.05.003.

Zhang, Y., X. Wang, R. Fraser, I. Olthof, W. Chen, D. Mclennan, S. Ponomarenko, and W. Wu. 2013. Modelling and mapping climate change impacts on permafrost at high spatial resolution for an Arctic region with complex terrain. The Cryosphere 7(4): 1121–1137. doi: 10.5194/tc-7-1121-2013.

Zoltai, S. C. 1972. Palsas and peat plateaus in central Manitoba and Saskatchewan. Canadian Journal of Forest Research 2(3): 291–302.

Zoltai, S. C., and C. Tarnocai. 1975. Perennially frozen peatlands in the western Arctic and Subarctic of Canada. Canadian Journal of Earth Sciences 12(1): 28–43.

CHAPTER 4: INVESTIGATIONS OF DISCONTINUOUS PERMAFROST IN NAIN, NUNATSIAVUT WITH DC ELECTRICAL RESISTIVITY TOMOGRAPHY

Abstract

The characteristics of permafrost bodies within the coastal Labrador community of Nain, Nunatsiavut were examined using a combination of standard field methods and DC electrical resistivity tomography (ERT). Permafrost was inferred to be present at numerous sites within the community under both fine and coarse surficial covers. Permafrost thicknesses up to 18 m were interpreted within marine deposits at the coast with thicknesses up to 9 m at a nearby forested site. Localized talik formation was inferred for several sites proximate to buildings affected by subsidence and was correlated with low resistivity values in the ERT profiles. The identification of permafrost bodies in Nain proved challenging due to the absence of links to surface geomorphic features, a frequently coarse surficial cover, deep active layers, and anthropogenic disturbance, all of which complicate interpretation of geophysical data. These results indicate highly heterogeneous permafrost conditions in this part of coastal Labrador making it difficult to predict how ecosystems and permafrost in the region may respond to future changes in climate.

4.1 Introduction

Projected warming of northern Canada over the next century is expected to rapidly thaw permafrost along the southern boundary of the discontinuous zone (Woo et al. 1992; Zhang et al. 2008b). Consequently, careful planning and adaptation measures are required to avoid future structural damage to infrastructure in these regions (Nelson et al. 2001; Smith and Riseborough 2010; Hong et al. 2014). In the Labrador region of northeastern Canada, there is limited information on the current distribution and physical characteristics of permafrost owing to a paucity of permafrost-specific field studies in the past few decades. However, a century-long regional warming trend (Brown et al. 2012; Way and Viau 2015) has likely impacted local permafrost characteristics (Way and Lewkowicz 2016) and satellite records collected over the last three decades show regional ground surface temperatures are warming (Hachem et al. 2009; Comiso and Hall 2014).

Comprehensive field studies in the 1960s and 1970s along the northwestern Labrador/Quebec border detailed the distribution of permafrost in the vicinity of Schefferville (e.g. Nicholson 1979), but there is much less information available on permafrost in the coastal regions along the Labrador Sea (Brown 1979). Existing maps depict permafrost zones in coastal Labrador as spanning from no permafrost near 51°N to continuous permafrost at 58°N (Heginbottom et al. 1995) (Figure 4-1). The impact of permafrost degradation on this region is expected to be medium overall, due to a projected moderate soil thermal response and a low soil physical response to warming, but there remains considerable uncertainty at finer spatial scales (Smith and Burgess 2004). A key aim of the Labrador Permafrost Project is to improve the state of knowledge on permafrost in coastal Labrador and to evaluate its future susceptibility to change.

Here we report on the first local permafrost investigations, conducted in late-July 2014, in and around the community of Nain, NL at the northern end of the sporadic discontinuous zone. The main goal of this research was to test the applicability of DC electrical resistivity surveys (ERT) and standard field methods used in northwestern Canada for permafrost detection in coastal Labrador where surficial materials tend to be coarse grained. A particular focus was placed on describing contemporary permafrost bodies in areas where building subsidence may be caused by degrading discontinuous permafrost (Allard et al. 2012a; Lewkowicz and Way 2014).

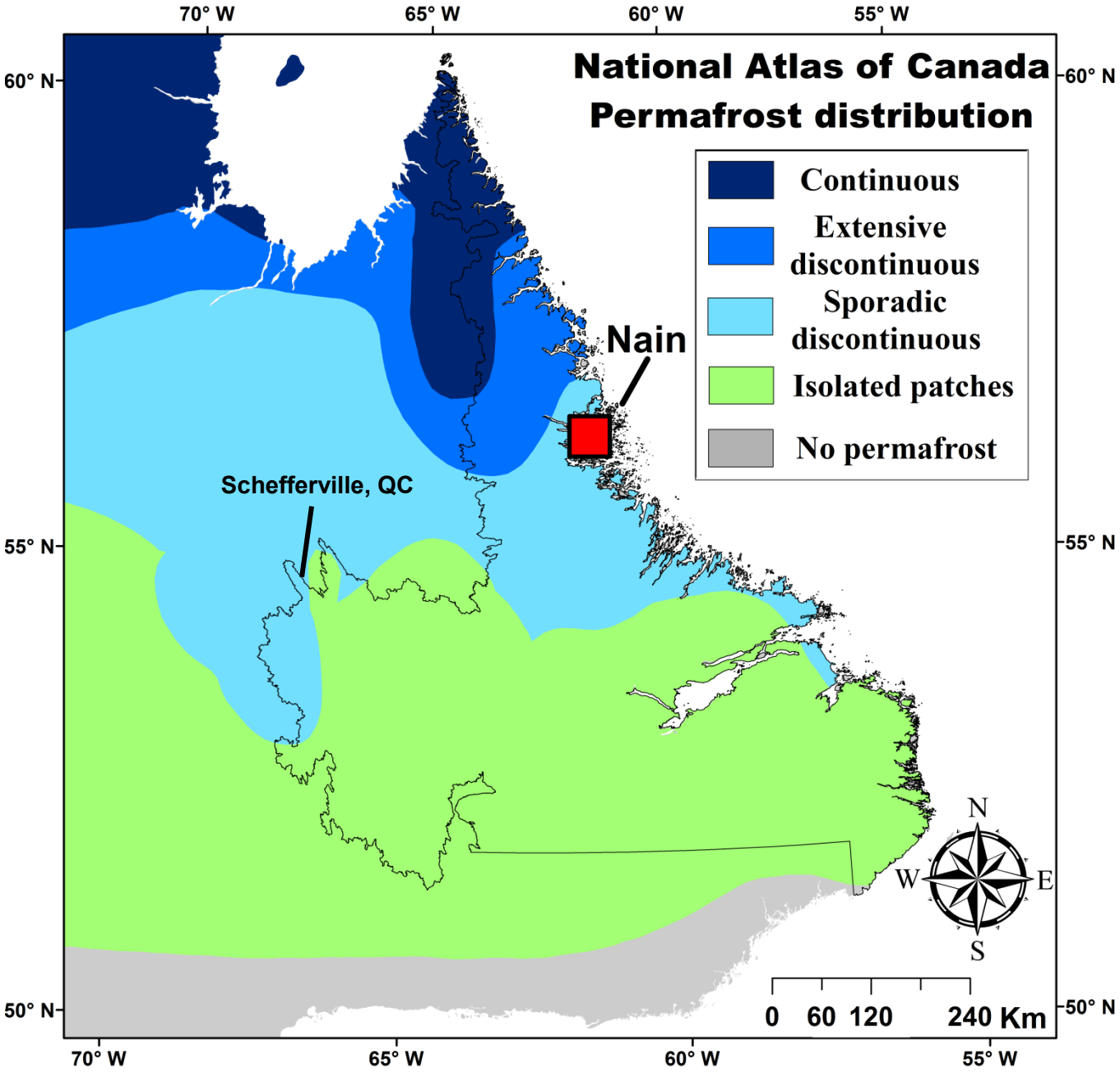

Figure 4-1: Permafrost zonation in the Labrador region of northeastern Canada as defined by the National Atlas of Canada (Heginbottom et al. 1995). The red square depicts the site of field investigations at Nain, NL.

4.2 Study Area

The community of Nain is located in the Nunatsiavut land claim zone on the Labrador Sea coastline fringing the coastal barrens ecozone (Roberts et al. 2006). According to the Permafrost Map of Canada (Heginbottom et al. 1995), Nain is located at the northern section of the sporadic discontinuous permafrost zone (Figure 4-1) but there are no published studies analyzing permafrost anywhere in northern Labrador. Permafrost was reported during port construction at Voisey's Bay 10 km southwest of Nain (Voisey's Bay Nickel Corporation 1997) and during archeological investigations on outer islands 40-50 km east of Nain (Woollett 2010; Butler 2011). Vegetation cover in the region is sparse forest-tundra on wind-exposed coasts but thick forest consisting of Black Spruce, Tamarack and White Spruce occurs at lower elevations in more sheltered areas. At elevations above ~120 m a.s.l. the vegetation cover is predominantly forest-tundra with isolated patches of forest occurring up to ~200 m a.s.l.

Nain has a subarctic climate with a mean annual air temperature of -2.5°C (1981-2010) and cool summers averaging 9.2°C (Table 4-1). The mean cold-season snow thickness averages 68 cm (1981-2010) with a maximum mean monthly snow depth of 92 cm in March (Table 4-1). The presence of seasonal sea ice cover along the Labrador coast affects Nain by producing more continental winter and spring conditions than would be expected given its coastal location (Way et al. 2017a). In the ice-free summers, this coastal proximity produces relatively cold summer conditions throughout northern Labrador (Maxwell 1981; Banfield and Jacobs 1998; Way et al. 2017a).

Surficial deposits in the Nain area include Holocene marine sediments up to elevations of ~15 m a.s.l. in addition to widespread glacial tills in various stages of reworking (Occhietti et al. 2011). In Nain, medium-to-fine-grained marine clays are frost-susceptible and may contain excess ice, making their presence a concern for the construction of community infrastructure where permafrost is present (Bell et al. 2011). A recent housing survey found that near-surface layers of fine-grained marine sediments were a major contributor to housing issues at Nain, NL including structural damage due to ground settling and movement (Bell et al. 2011). Drilling done in support of Nunatsiavut Government initiatives at a number of sites in the community in 2012 and 2014 could give additional information regarding local surficial materials but to date these data have not been released publicly.

Table 4-1: Climate normals (1981-2010) for Nain (Environment Canada, 2016).

Nain, Labrador	Jan	Feb	Mar	Apr	May	Jun	Jul	Aug	Sep	Oct	Nov	Dec	Year
Mean air temperature (°C)	-17.6	-17.4	-12.5	-4.6	1.5	6.4	10.1	11.0	7.5	2.1	-4.4	-11.8	-2.5
Mean daily maximum (°C)	-13.5	-13.0	-7.5	0.0	5.6	11.0	14.9	15.8	11.5	5.1	-1.3	-8.1	1.7
Mean daily minimum (°C)	-21.6	-21.8	-17.4	-9.1	-2.5	1.8	5.3	6.1	3.4	-1.0	-7.5	-15.4	-6.6
Thawing degree days	0.6	0.6	1.3	13.7	71.0	192.7	314.4	341.2	224.2	79.9	7.3	0.7	1247.6
Freezing degree days	551.0	488.3	387.5	151.7	23.7	0.1	0.0	0.0	0.0	15.8	141.0	375.8	2134.9
Total precipitation (mm)	83.8	70.9	73.6	71.1	57.0	83.4	98.6	71.5	81.9	74.2	77.6	81.9	925.4
Mean snow depth (cm)	60.0	75.0	92.0	84.0	24.0	0.0	0.0	0.0	0.0	1.0	15.0	42.0	33.0
Days with snow	31.0	28.2	31.0	29.7	21.5	1.7	0.0	0.0	0.1	6.4	24.7	30.4	204.6

4.3 Methods

4.3.1 DC electrical resistivity tomography surveys

Investigation of local permafrost conditions in the community of Nain used standard field techniques (frost probing and temperature monitoring) and DC electrical resistivity tomography (ERT) (Lewkowicz et al. 2011) (Figure 4-2). ERT is a widely-used geophysical technique that determines the electrical resistivity of the subsurface by sending electrical current into the ground between pairs of electrodes with a terrameter measuring the voltage drop in the subsurface. Resistivity measurements recorded along a transect can be used to infer differences in the hydrological and thermal characteristics of subsurface materials because frozen ground is generally much more resistive to electrical current than unfrozen ground (Hauck 2013). The application of ERT to permafrost investigation has become more common in the last decade, particularly in mountain permafrost, extensive discontinuous and continuous permafrost environments (Hauck et al. 2003; Lewkowicz et al. 2011; You et al. 2013; Oldenborger and LeBlanc 2015; Sjöberg et al. 2015; Briggs et al. 2016; Douglas et al. 2016).

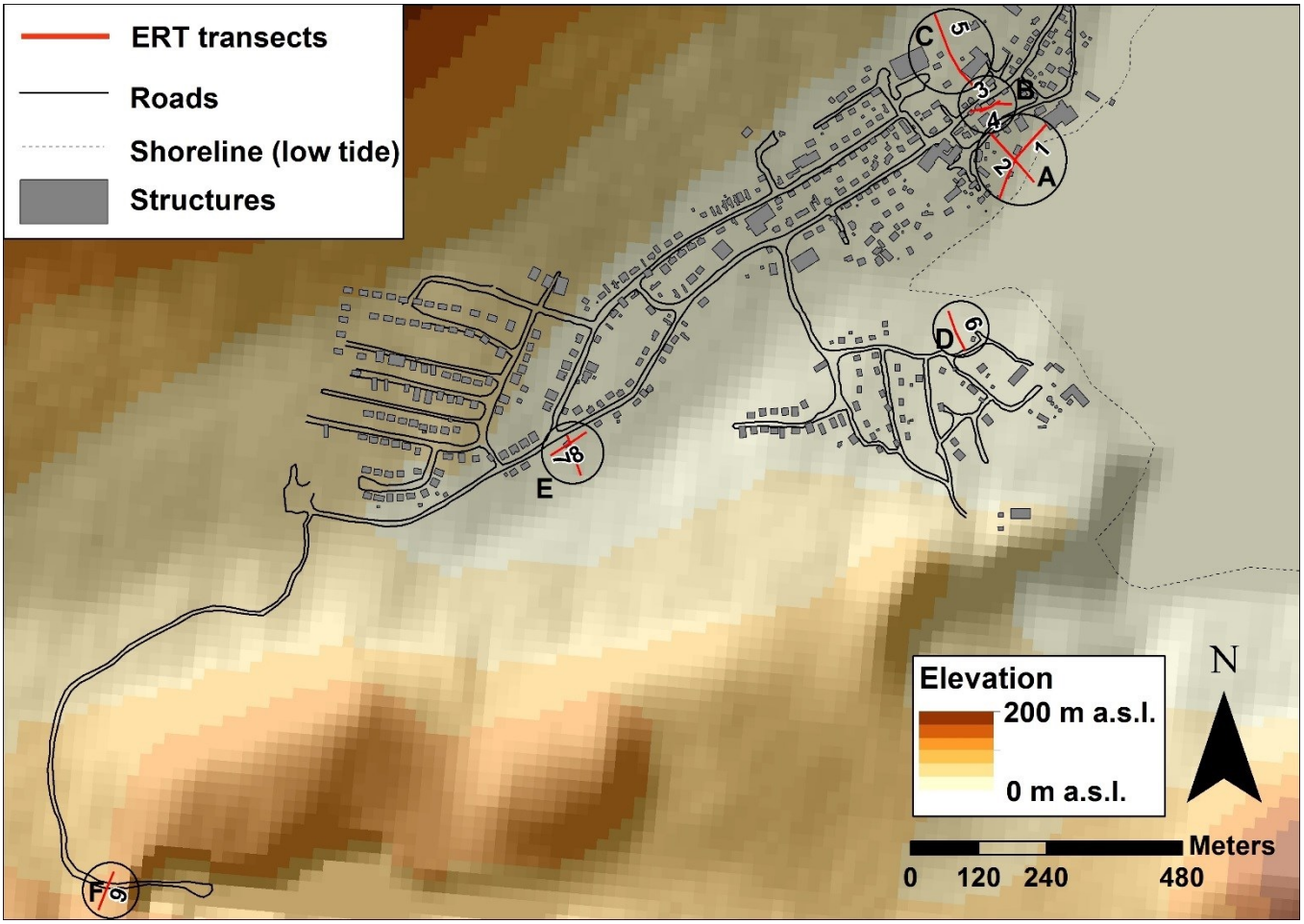

Figure 4-2: Location of field investigations undertaken in the Nain area in July 2014. Survey locations are overlain on a digital elevation model (National Topographic Database) created by Natural Resources Canada and aggregated to ~50 m resolution. Labels correspond to the survey IDs which are also found in Table 4-2 and described in the text. Note: Black circles correspond to general locations described in the text and from north to south are locations C, B, A, D, E and F. Marine sediments are inferred to occur up to approximately 20 m a.s.l. according to regional mapping done by Bell et al (2011).

ERT surveys were undertaken with an ABEM Terrameter LS using electrodes set out in a Wenner array configuration with either a 1 m or 2 m spacing. The depth of electrical penetration during ERT profiling depends on the spread of the electrode array and its survey length (excluding roll-along surveys) with the typical depth for a 80 m transect being 12 m. Resistivity data were processed using the RES2DINV software (Loke and Barker 1996; Loke et al. 2003) using the robust inversion method for up to a maximum of five iterations or until the modelled pseudosection's root mean square error did not decline more than 1% from the prior iteration. Resistivity profiles were topographically corrected using surface slope measurements along the profiles collected with a Brunton compass and elevation values from profile endpoints using a digital hand-held GPS (e.g. Lewkowicz et al. 2011). Areas of the model with a sensitivity of less than 0.1 were left in place for visualization purposes but were interpreted with caution due to the higher uncertainties with these layers. They are faded in the ERT tomograms. Near surface ground freezing conditions were investigated along the ERT profiles by frost table probing with a 120 cm long titanium probe (e.g. Lewkowicz et al. 2011; James et al. 2013). At sites where the presence of clasts made probing uncertain, instantaneous ground temperature profiles were recorded continuously with an Onset Hobo Pro v2 logger (accuracy ± 0.5°C) for 15 minutes after attaching four thermistors to a wooden dowel at 20 cm increments and inserting it into the ground. Temperature profiles were used to estimate whether the frost table was present within 2 m of the ground surface through interpolation of temperature at the four depths (e.g. James et al. 2013) using either logarithmic or exponential best fits.

Observations of vegetation characteristics and surficial cover were recorded at each ERT survey site. Geotechnical borehole logs were also made available by the Nunatsiavut Government for two field sites (Stantec 2012). This ground truth information permitted calibration of ERT results in areas of coarse surficial cover where results of probing and temperature profiles can be ambiguous. Validation of ERT results with field methods and boreholes was required because there is no universally applicable resistivity boundary for discriminating between unfrozen and frozen ground (Hauck 2013). For example, in the glacio-marine sediments on the eastern Hudson's Bay coastline, Fortier et al (2008) used a frozen/unfrozen boundary of 1000 Ω.m whereas in the organic soils of north-western North America, Lewkowicz et al (2011), Briggs et al (2016) and Minsley et al (2016) used values near 300 Ω.m. Additional problems with the interpretation of ERT profiles include the presence of dry unfrozen coarse sediments, which may show resistivities similar to those of warm permafrost (e.g. Hilbich et al. 2009), and the presence of bedrock at depth which can exhibit high resistivities similar to those of cold permafrost (Lewkowicz et al. 2011).

4.4 Results

A total of nine ERT surveys were completed at six separate locations (Figure 4-2) in and around the community of Nain, NL in a variety of environmental settings (Figure 4-3). Descriptions and survey results are summarized for each location and are presented below and in Table 4-2.

Table 4-2: Details of DC electrical resisitivity tomography surveys for Nain, NL.

Survey no.	Elevation	Length and spacing	Maximum penetration depth	Inferred permafrost thickness	Field observations
1	6.0 to 4.3 m a.s.l.	160 m and 2 m	26 m	17.5 m in centre	Boreholes (n=3) and probing
2	9.0 to 3.3 m a.s.l.	120 m and 2 m	23 m	15.5 m in centre	Boreholes (n=3)
3	8.0 to 7.3 m a.s.l.	80 m and 2 m	15 m	>15 m with ~8 m talik	Structural subsidence
4	7.0 to 4.8 m a.s.l.	40 m and 1 m	7.5 m	2.5 m	Structural subsidence
5	14.0 to 25.5 m a.s.l.	160 m and 2 m	26 m	9.0 m	Probing with or without thermistor
6	1.0 to 5.7 m a.s.l.	80 m and 2 m	15 m	2 m on upslope	Probing with or without thermistor
7	28.0 to 17.5 m a.s.l.	76 m and 2 m	15 m	5.5 m downslope	Probing with or without thermistor
8	23.0 to 28.75 m a.s.l.	80 m and 2 m	15 m	Permafrost absent	Probing with or without thermistor
9	95.0 to 109.7 m a.s.l.	80 m and 2 m	15 m	Uncertain (shallow bedrock)	Probing with or without thermistor

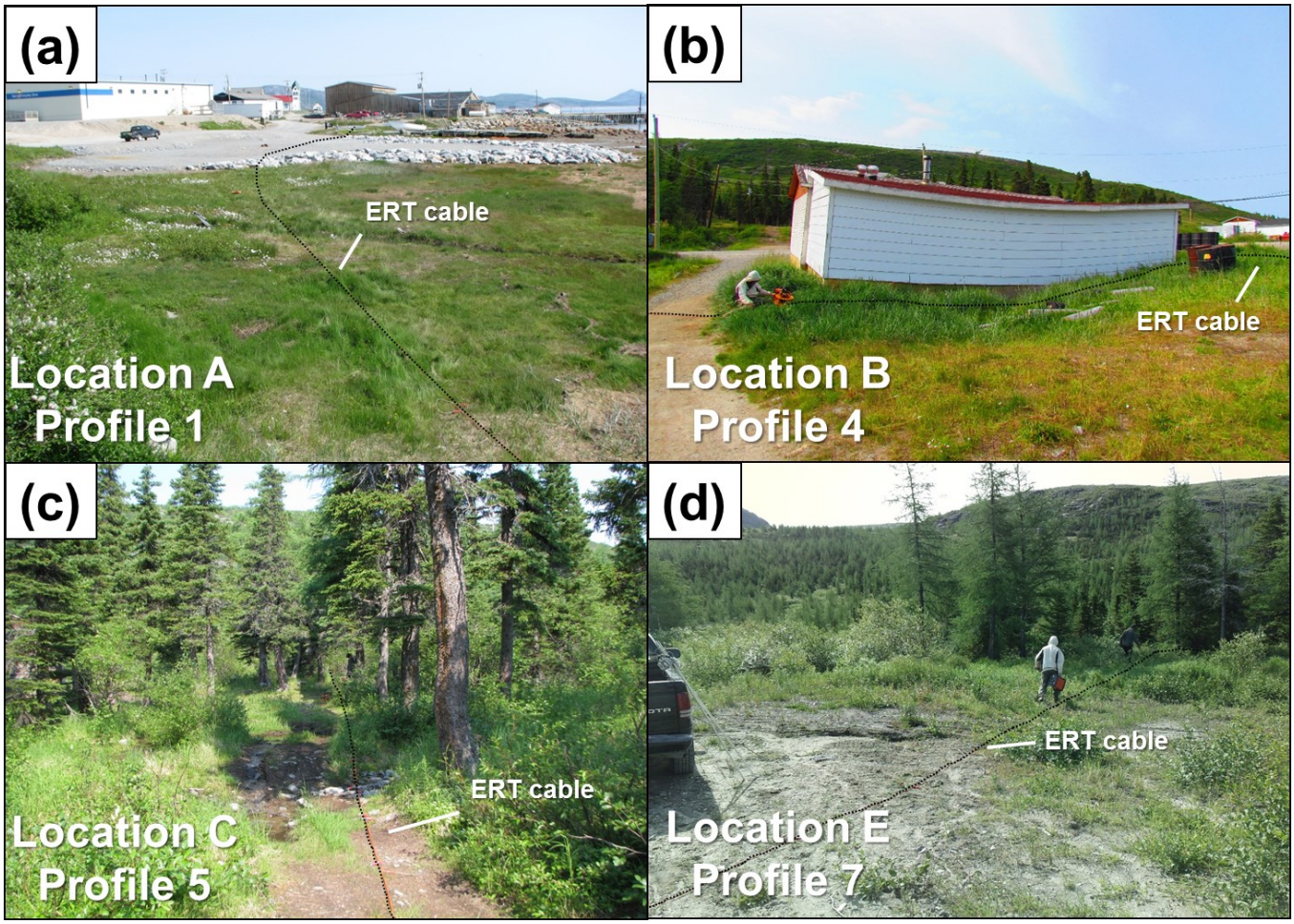

Figure 4-3: Ground photography of selected field sites at Nain, NL. (a) Photograph of ERT survey 1 which includes the gravel pad and adjacent coastal zone situated at the proposed Torngâsok Cultural Centre construction site (location A); (b) Structural subsidence at Puffin Snacks convenience store (location B) and adjacent ERT survey lines (3 and 4) which were co-located along the building's rear wall; (c) Forested upslope zone (location C) with a small walking trail located along survey 5 in Nain, NL; and (d) Cleared lot for a multiplex housing development and adjacent forest cover (location E) which includes the site of ERT profile 7. Note: Black dotted lines on all ground photographs show the approximate location of ERT survey lines.

Location A (surveys 1 & 2)

Location A was on the northern shoreline of Nain, NL and included a gravel pad covering the construction site of the future Torngâsok Cultural Centre (Figure 4-3a). Profile 1 was taken parallel to the shoreline across poorly drained substrate with its central location traversing the widest portion of the gravel pad (Figure 4-2). The shoreline included sections covered by low sedges and grasses with sandy silts evident in the near-surface and thin organic cover found between -40 m and 54 m along the profile (Figure 4-4a). Between 56 and 122 m, the profile traversed disturbed areas including the gravel pad and construction site (Figure 4-3a), and grassy regrowth and areas of bare ground were found between 124 m and 160 m although gravel surfaces were again prevalent near the end of the profile. Shallow surface streams were apparent at 28-30 m and again at 146 m along the profile. Profile 2 was perpendicular to the shoreline beginning adjacent to an abandoned fire station in a gravel lot and ending in the high tide zone (Figure 4-2). This profile was mostly unvegetated with the building lot occurring between 40 and 58 m followed by a zone of sand between 20 and 36 m and then a gravel road between 78 and 96 m. The gravel pad for the Torngâsok Cultural Centre construction site occurred between 98 and 132 m, and the shoreline environment (between 134-160 m) included boulders, surface clays and silts, and short grasses at a few locations (Figure 4-4b). Surficial materials along both profiles were assumed to be of marine or glaciomarine origin based on local surficial mapping (Bell et al. 2011).

The ERT surveys at location A exhibited a complex pattern of modelled resistivities that ranged from 10 to 10,000 Ω.m. On profile 1, values were lowest in the near surface in the first 60 m of the profile and below a depth of 10 m in the first 90 m of the profile. Two areas of high resistivities were present at depths of 2-7 m near the start of the profile, and from near the surface to depths of up to 15 m from 68 m to 148 m beneath another grassed area and the gravel pad (Figure 4-4a). Frost tables, confirmed by instantaneous temperature measurements, were present between 26 m and 50 m (median thaw depth: 70 cm) while full probe penetration was possible between -40 m and 24 m and (Figure 4-4a). Frost probing was not possible over the gravel pad between 56-110 m but was possible between 112-160 m with no detectable frost table occurring in this section (either full penetration or rejection from coarse materials). Instantaneous ground temperatures at 20 m on the profile, where a thick layer of low resistivities is present, led to an estimated temperature at 2 m of +1.2°C.

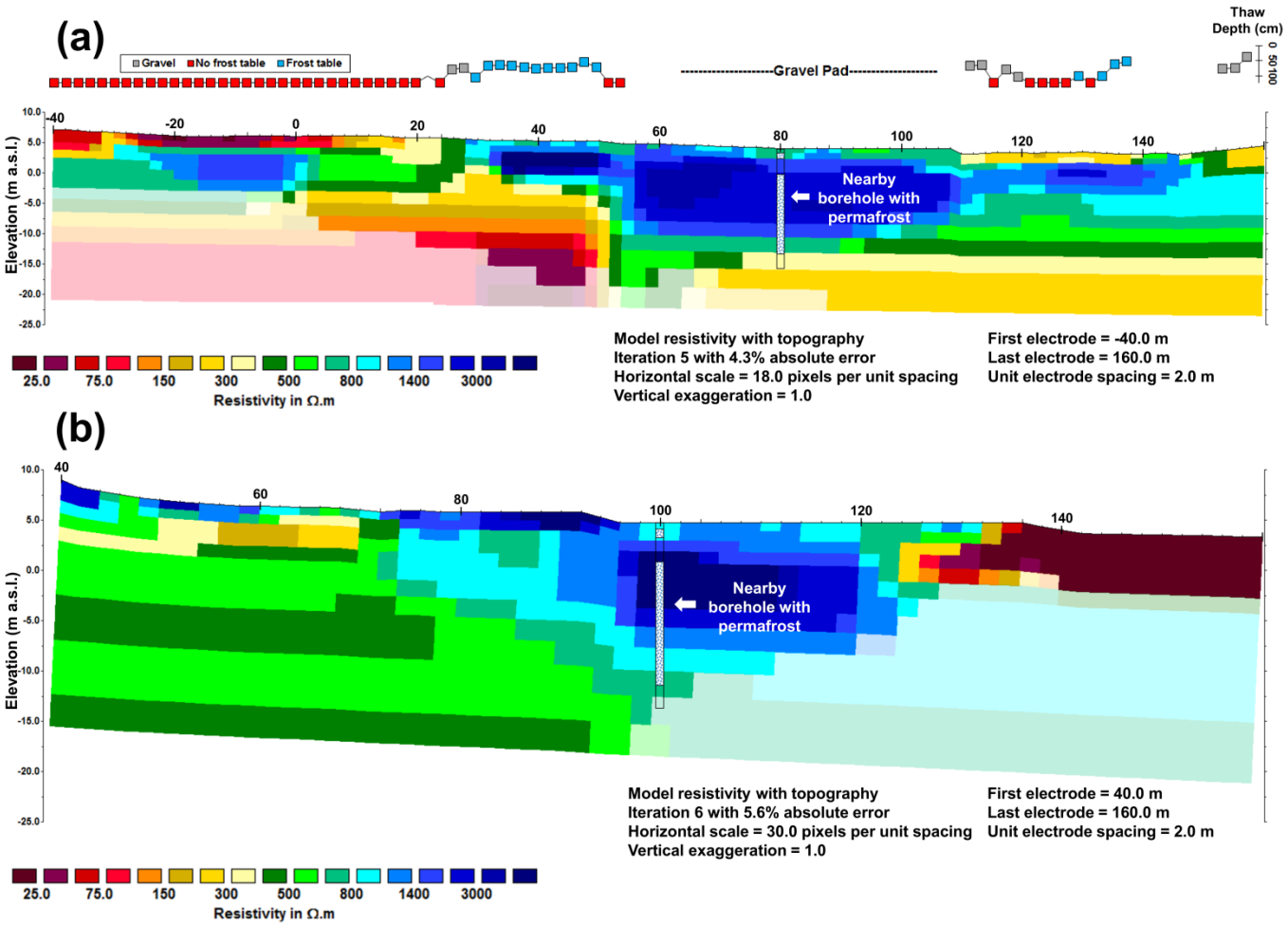

Figure 4-4: Field investigations of permafrost conditions at location A. (a) ERT profile results and inferred thaw depths from frost probing for survey 1; and (b) ERT profile results for survey 2. Note: the position and depth of boreholes drilled by Stantec (2012) near the ERT profiles are superimposed on the transects with permafrost indicated by white and blue checkered pattern.

Profile 2 showed modelled resitivities between 10 to 10,000 Ω.m with the lowest values observed in the near-surface and the highest values found below 6 m depth (Figure 4-4b). Resistivity values between 500 and 3000 Ω.m were observed in the upper 2 m between 40-86 m along the profile and values greater than 1000 Ω.m were found in these upper layers between 88-132 m. Lower resitivities (< 75 Ω.m) were found in the upper 6 m between 134 m and 160 m with greater depths showing low sensitivity values. At depths between 2 and 20 m below the surface, values less than 600 Ω.m were consistently present at 40-74 m along the profile. Farther along the profile between 90-120 m modelled resistivities above 1000 Ω.m were consistently observed to depths of ~17 m below the surface.

Three boreholes drilled close to profiles 1 and 2 during geotechnical investigations of the Torngâsok Cultural Centre construction site (Stantec 2012) confirmed the presence of frozen ground beneath the gravel pad with a maximum thickness of 18 m. The borehole data and frost table probing were used to determine a frozen ground boundary which was estimated as above 800 Ω.m. Permafrost was therefore interpreted as present throughout most of profile 1 and the centre of profile 2. On profile 1, 4-6 m thick permafrost was inferred to occur with a thick active layer between -30 and 2 m along the profile. Permafrost was again inferred to occur between 28 m and 148 m with a maximum thickness of 17.5 m in agreement with the co-located borehole measurements (Stantec 2012). On profile 2, permafrost 14 to 16 m thick was inferred to occur between 96 and ~120 m along the profile similar to observations from the nearby boreholes (Stantec 2012) with thinner permafrost between 74 and 92 m (Table 4-2).

Location B (surveys 3 & 4)

Location B was positioned directly upslope of location A and ran adjacent to a convenience store (Puffin Snacks), across an open yard and two gravel paths (Figure 4-2). Puffin Snacks showed apparent longitudinal structural subsidence (Figure 4-3b) so surveys parallel to the building were done at two electrode spacings enabling deeper penetration on the longer 80 m survey (survey 3) and more detail in the near-surface in the shorter 40 m survey (survey 4) (Figure 4-2; Table 4-2). Survey 3 began on a disturbed lot that consisted of compacted sand and gravel and continued across a gravel road then along the back of Puffin Snacks. The profile then traversed a small gravel trail and ended in an empty lot that contained short grasses which were interpreted as post-disturbance regrowth. The shorter 40 m survey (#4) began directly adjacent to the end of the Puffin Snacks convenience store and ended just after the gravel road at the beginning of the empty revegetated lot (Figure 4-2). Surficial materials in this section of the community were considered to be marine or glaciomarine according to Bell et al (2011).

Modelled resistivity values along profile 3 showed considerable variability in the near upper 2.5 m of the profile with values ranging from 300 to >2000 Ω.m. The highest resistivities in these upper layers occurred between 22-30 m along the profile and again between 46-74 m. At greater depths (2.5-13 m), modelled resistivities ranged from less than 150 Ω.m between 26-50 m along the profile and greater than 1000 Ω.m from 46-80 m (Figure 4-5a). The most conspicuous feature in this profile was the contrast between the higher resistivity surface layer adjacent to Puffin Snacks (Figure 4-5a) and the lower resistivity feature directly beneath at depths between 2.5 and 8.5 m. In contrast, higher resistivity layers extended from the surface to the base of the tomogram between 46-80 m along the profile. The modelled resistivity values in survey 4 were similar to those in survey 3 where they overlapped (from 16 m to 56 m on survey 3) (Figure 4-5b), with higher modelled resistivities (800 > Ω.m) in the upper 2-3 m and lower modelled resistivities beneath (< 150 Ω.m) adjacent to Puffin Snacks. The highest resistivities (> 3000 Ω.m) in survey 4 profile occurred between 24 and 34 m to a maximum depth of 2.5 m beneath the surface (Figure 4-5b).

In the absence of suitable surficial materials for frost probing, the resistivity boundary (800 Ω.m) from location 1 (100 m downslope) was used to differentiate between frozen and unfrozen ground although some coarser tills observed in the near-surface layers make suggest the boundary could be higher in those layers. Using this approximate boundary for survey 3, frozen ground was inferred to be present in the upper 3 m adjacent to a portion of Puffin Snacks convenience store (21-30 m) and between 45-54 m and 61-72 m. From 45-72 m of the profile a low resistivity feature (< 300 Ω.m) at 2.5-8 m depths was followed by high resistivities (> 1000 Ω.m) again below 8 m depth. Results from survey 4 generally support the above interpretations where the two surveys overlapped. Accordingly, location B was inferred to have near surface frozen ground (either seasonal or perennial) beneath portions of Puffin Snacks and some adjacent terrain with permafrost beneath. Between 22-30 m high resistivity values were inferred to be either deep season frost, coarse materials or thin permafrost whereas between 46-60 m permafrost was inferred to be present in portions of the near-surface and at depths exceeding the maximum penetration of the survey (~16 m) with an unfrozen zone found between 2 and 7 m below the surface (Figure 4-5a). Along survey 3 between 60 and 64 m frozen ground was inferred to be present and extended to the base of the survey.

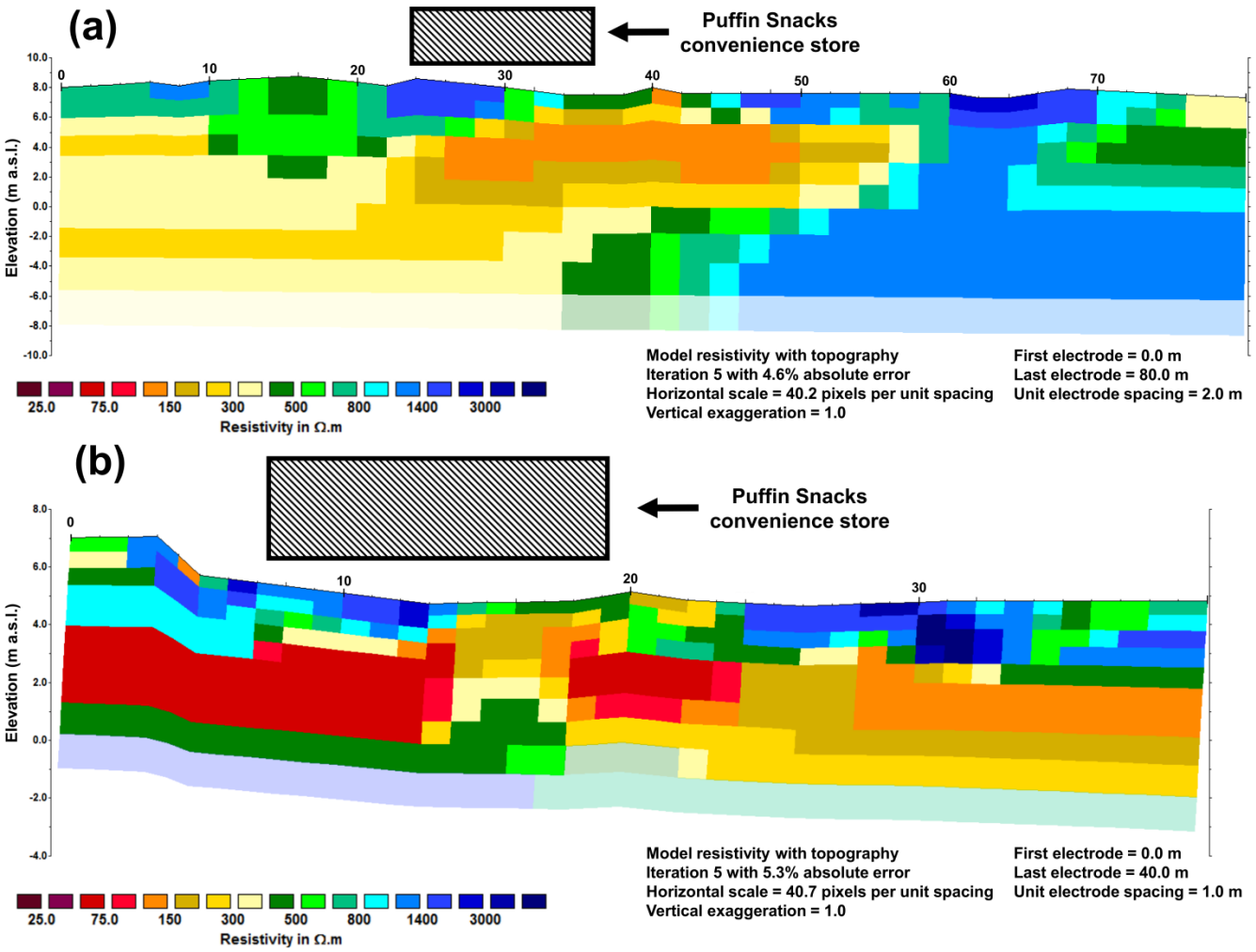

Figure 4-5: Field investigations of permafrost conditions at location B. (a) ERT profile results for survey 3; and (b) ERT profile results for survey 4. The approximate position of the Puffin Snacks convenience store is shown on both profiles for interpretation purposes. Note: probing was not possible due to clasts or gravel.

Location C (survey 5)

Location C was north of locations A and B on a forested hillslope that was relatively undisturbed apart from a small trail (Figure 4-2; Figure 4-3c). Survey 5 was 160 m long and began at the end of a building lot and proceeded upslope ~12 m terminating in undisturbed forest (Table 4-2). The terrain along this survey between 0 and 48 m consisted of gravel and compacted sandy silt with a small stream running parallel to the survey a few meters away. Between 50 and 66 m the survey followed a trail that proceeded into open forest consisting of Balsam Fir, White Spruce and Tamarack. The trail comprised compacted silt and organic materials with small grasses and short shrubs along its periphery. Between 68 to 118 m along the survey the dominant ecotone became open forest with periodic occurrences of small streams, standing water and small mounds of organic materials. At 120 m the terrain was undisturbed with a mixture of small shrubs (Labrador Tea, Dwarf Birch, Willows) and open forest cover including some Birch that continued to the end of the profile. Surficial mapping showed the survey area as primarily covered by colluvial deposits (Bell et al. 2011).

Survey (#5) results showed a higher resistivity layer (1200 Ω.m to 3800 Ω.m) in the upper 5-10 meters nearly continuously between 10 and 148 m along the survey (Figure 4-6a). Lower resistivities (< 1200 Ω.m) were observed in the upper 10 m between 0-10 m along the survey and at depths between 10 m and 26 m throughout the profile. A conspicuous body of 700-1000 Ω.m resistivity values in the centre of the profile extended down to the base of the survey. Frost table probing was not possible at the beginning or end of the survey due to coarse near-surface materials (Figure 4-6a). Probing results elsewhere suggested frost table presence between 52 m and 96 m (median thaw depth: 67 cm), and 124 and 144 m (median thaw depth: 40 cm) whereas full probe penetration was mostly possible between 98-120 m (Figure 4-6a). The ground temperature measured ~128 m along the profile was 0.6°C at 45 cm depth with a steep vertical gradient between measurement depths (5 cm = 27.0°C; 25 cm = 9.7°C; 45 cm = 0.6°C). Frozen ground was inferred to be present no deeper than 80 cm at the time of the survey, assuming an exponential relation. Frozen ground observed in the field at this site coincided with near-surface modelled resistivities greater than 1200 Ω.m so this value was adopted for interpreting permafrost thicknesses (Figure 4-6a). Permafrost was correspondingly inferred to be nearly continuous along the profile with a maximum thickness of 8.5 m at ~86 m along the profile. The area of moderate resistivity values at depth in the centre of the profile were inferred to be due to bedrock and/or a change in surficial materials, but could also represent warm permafrost (Figure 4-6a).

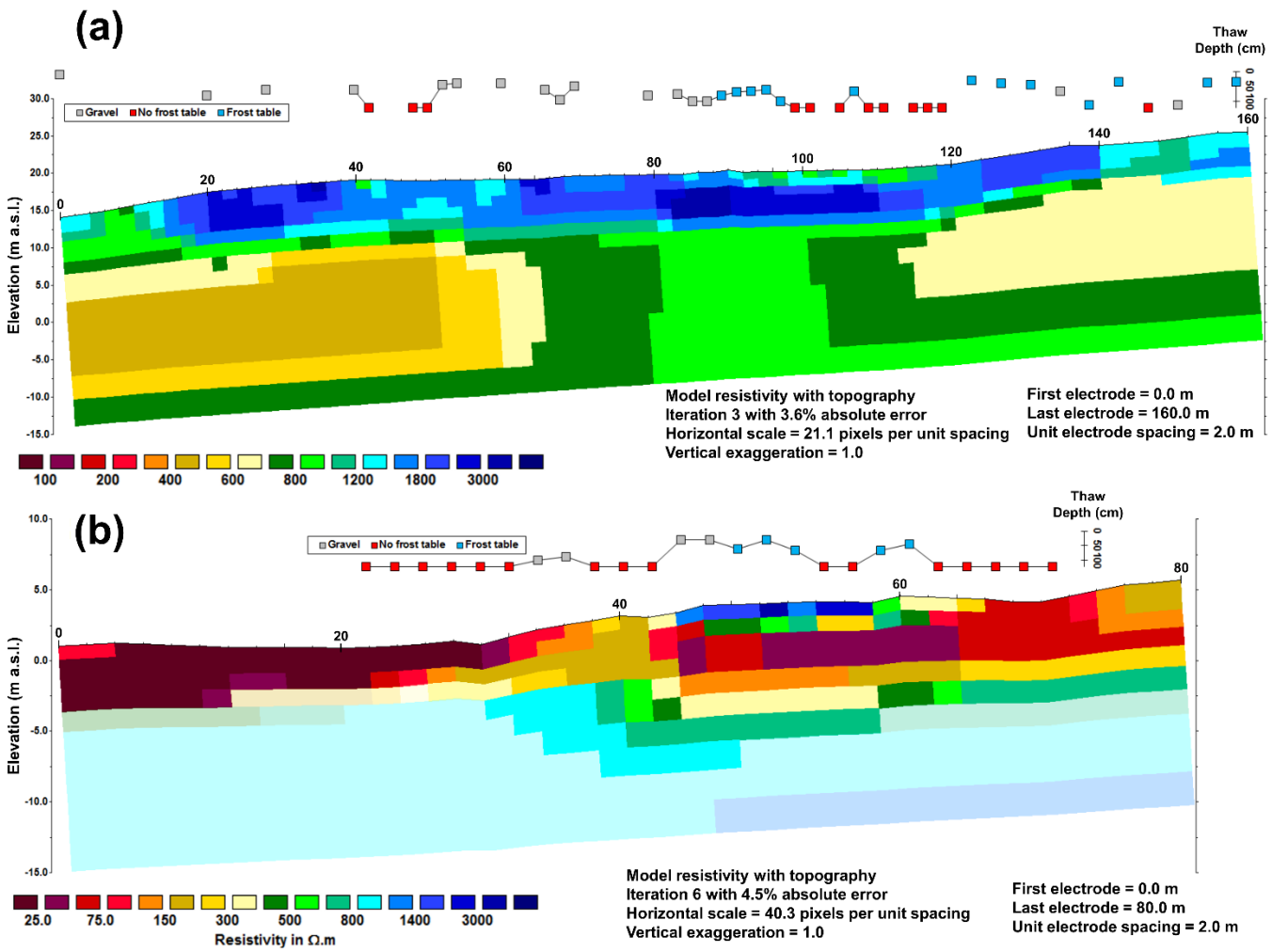

Figure 4-6: Field investigations of permafrost conditions at locations C and D. (a) ERT profile results and inferred thaw depths from frost probing for survey 5; and (b) ERT profile results and inferred thaw depths from frost probing for survey 6. Note: the resistivity scales differ for the two profiles. Probing was not possible due to clasts or gravel in parts of the profiles without an indication of frost table depth.

Location D (survey 6)

ERT profile 6 was positioned 350 m southwest of location A on the opposite side of the coastal inlet (Figure 4-2). Profile 6 began in a sandy tidal zone, followed a vegetated surface upslope and ended in a patch of open forest. The first 18 m of the survey was unvegetated with surficial materials composed of coarse and fine sands with several small ponds of water apparent at the surface. At 20 m along the survey, grasses and sedges and a clayish substrate were observed at the surface. Dwarf Birch and Willow shrubs with surface mosses began at 32 m and continued until 62 m when a zone of Balsam Fir and Tamarack forest began. In the latter section, understorey cover was primarily Willows and grasses. The survey ended on a gravel road between 72 and 80 m along the survey (Figure 4-2). The dominant surficial materials in this section of the community are marine or glaciomarine (Bell et al. 2011).

Resistivity values were low within the upper 4 m (< 400 Ω.m) of survey 6 except between 44 m and 59 m where the top 2 m exhibited values exceeding1200 Ω.m (Figure 4-6b). Resistivities were < 100 Ω.m beneath this high value anomaly. Resistivities also appeared to be high at depths of 5 m or more across the entire profile, but these represent low sensitivity portions of the tomogram. Frost probing revealed no frozen ground in the upper 120 cm between 1-44 m and 64-80 m (Figure 4-6b). However, frozen ground was detected at some locations between 46-62 m with a median thaw depth of 46 cm (Figure 4-6b). Instantaneous ground temperature measurements also indicated that frozen ground should exist in the top 1 m adjacent to the profile at 38 m and 48 m. Using the frozen ground boundary from marine deposits at location A (e.g. greater than 800 Ω.m), frozen ground was inferred to occur to a maximum depth of ~1.5 m in the near surface. The limited thickness of the frozen ground, and mid-summer survey dates suggest that the ground at this site was either deep late-lying seasonal frost or very thin permafrost (Table 4-2). Lower resistivity values (< 100 Ω.m) observed just below the frozen ground layer indicate unfrozen conditions. The higher values at depth may be an artefact of the inversion, degrading permafrost, or most likely, bedrock.

Location E (surveys 7 & 8)

Location E was located about 1 km southwest of location A and was the site of a future multiplex development that had been cleared of vegetation in anticipation of building construction (Figure 4-2). Profile 7 was 76 m long and began at the lot's entrance and proceeded down a forested slope behind the lot ending at a small stream (Figure 4-3d) (Table 4-2). Profile 8 was an 80 m survey run across the cleared lot's width and included thick shrubs intermixed with open forest adjacent to the lot between 0-16 m and again between 48 and 80 m. The downslope profile (#7) began in the coarse sands and gravels of the

cleared lot (0-18 m) with vegetation cover composed primarily of medium to high shrubs beginning at 18 m along the profile. Open forest (Tamarack, Balsam Fir) cover began at 22 m and continued until near the end of the profile where the forest cover opened at 54 m and transitioned to medium height (0.5-1.0 m) Dwarf Birch shrubs until the end of the profile. The profile ended at 76 m at a small stream with adjacent saturated areas. The surficial cover was coarse throughout the profile with a thin organic cover, typically less than 10 cm. Surficial deposits in this section of the community are primarily glacial till over shallow bedrock (Bell et al. 2011).

Resistivities on profile 7 were generally highest in the upper 7 m with values of ~2000 Ω.m between 16-38 m along the profile and >4000 Ω.m after ~42 m along the profile (Figure 4-7a). Higher resistivities (> 4000 Ω.m) were also found at depths between 2.5-5 m below the surface in the first 14 m of the profile. Resistivity values were generally low (< 600 Ω.m) at depths exceeding 7 meters, but these values are less certain because of low sensitivities (Figure 4-7a). ERT survey 8 running across the lot showed moderate to higher (800-4000 Ω.m) modelled resistivities in the upper 2.5 m of the profile (Figure 4-7b). At depths between 2.5 and 12 m higher modelled resistivities (> 4000 Ω.m) occurred between 42-80 m and sloped parallel to the surface (Figure 4-7b). Modelled resistivities greater than 1600 Ω.m but less than 5000 Ω.m were observed between 0 and 16 m at depths between 2.5 and 12 m. Lower modelled resistivities (< 1200 Ω.m) were found at these depths between 16 and 42 m. The same pattern of resistivities continued to the base of the profile but these areas have low sensitivity.

Due to the disturbed nature of the lot and the coarse surficial deposits, frost probing was not useful in identifying a frost table as probe refusal often occurred at shallow depths along both profiles. However, full probe penetration was possible at several locations between 1-36 m and 70-74 m along profile 7 but not between 38-68 m (Figure 4-7a). An instantaneous temperature reading was taken 7 m away from profile 7 at approximately 66 m along the profile. The depth of this measurement was shallow (~40-80 cm) but was indicative of frozen ground present in the near-surface (0.05°C). On profile 8, the sloping highly resistive surface was interpreted as being bedrock due to the higher modelled resisitivities and relatively even surface. Considering the coarser glacial tills, the ERT profile results, the ambiguous frost probing data and the instantaneous temperature data, the resistivity boundary between unfrozen and frozen conditions was inferred to be ~4000 Ω.m for both profiles. Correspondingly, permafrost was inferred to possibly exist between 42 m and 70 m along profile 7 with a maximum thickness of 5.5 m. Permafrost may also exist along sections of profile 8, but the likely presence of bedrock, disturbed surface cover and lack of independent validation makes it difficult to assess this with confidence.

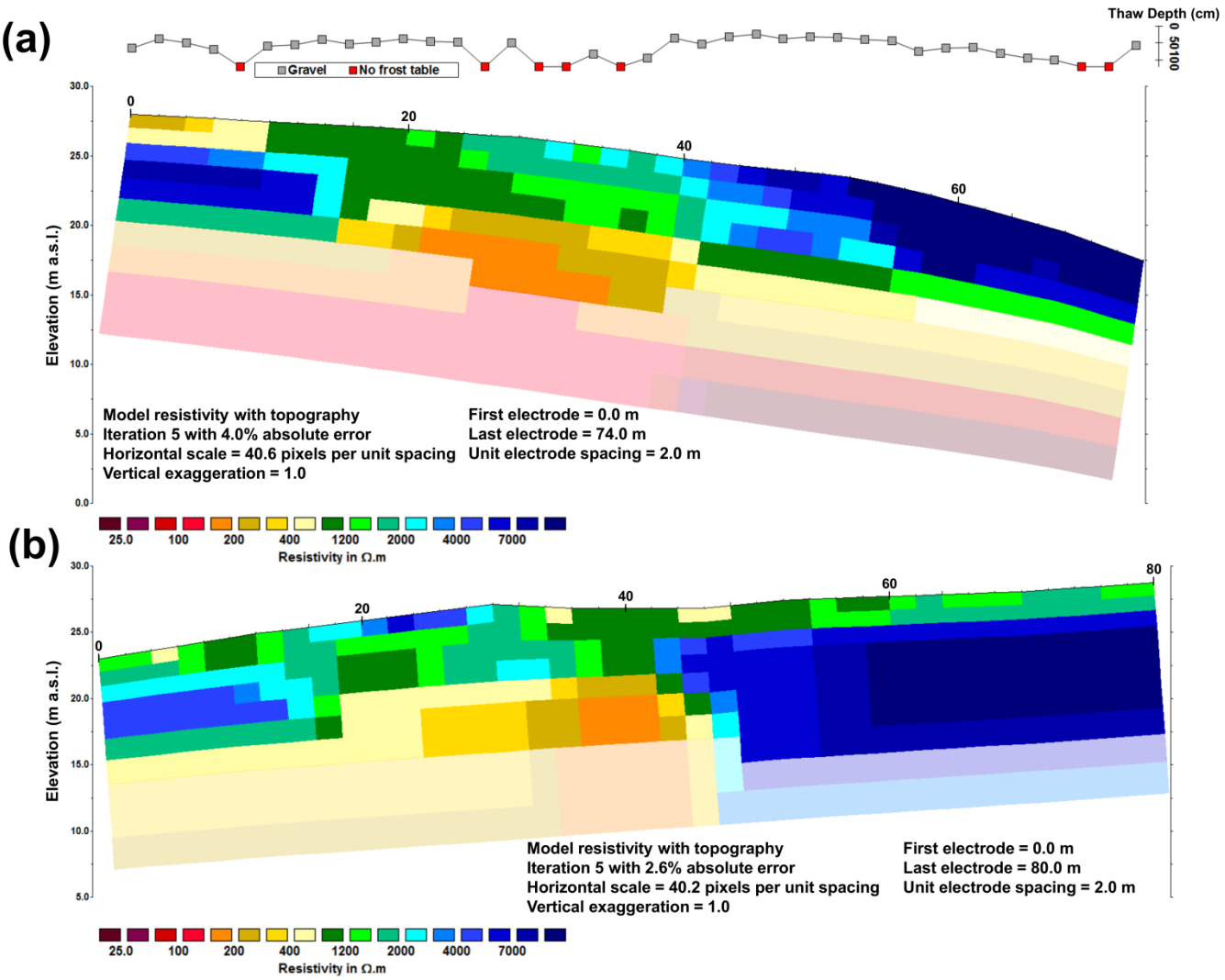

Figure 4-7: Field investigations of permafrost conditions at location E. (a) ERT profile results and inferred thaw depths from frost probing for survey 7; and (b) ERT profile results for survey 8. Note: probing was not possible due to clasts or gravel in parts of the profiles without an indication of frost table depth. Colour scales used in this figure differ from those used at the other Nain sites.

Location F (survey 9)

Location F (profile 9) was situated approximately 1.2 km southwest of location D at 95 m a.s.l. (Figure 4-2). The ERT profile proceeded upslope through the forest into the forest-tundra and then into open-tundra, terminating at ~110 m a.s.l. (Table 4-2). The ERT profile began on a path next to a gravel road and followed it across a relatively flat surface, entering the forest at 20 m along the transect. Nearly all the remaining profile was upslope with a mean slope of 14°. Forest cover of shorter Tamarack, White Spruce, Balsam Fir and Dwarf Birch was dominant between 22 m and 52 m and the forest cover opened with smaller trees that became sparser upslope between 54 m and 64 m. Between 66 m and 80 m the vegetation type was predominantly shrub tundra and barren with some grasses and organics in the near-surface. Bedrock was inferred to be near the surface farther upslope and surficial cover along this entire transect was inferred to be till with finer slopewash deposits in the thicker forest cover at the base of the slope. Resistivity values were almost all high (> 5000 Ω.m) in the upper 3 m of profile 9 with still higher values at greater depths (Figure 4-8). Values routinely exceeded 10^4 Ω.m throughout much of the profile below 3 m depth with the highest modelled resitivities (~10^6 Ω.m) observed between 38 and 80 m along the survey. Frost table probing along the profile provided ambiguous results due to coarse surficial materials and concealed near-surface bedrock, particularly on upslope sections (Figure 4-8). Two instantaneous temperature measurements (80 cm and 60 cm depths) were taken in a flat forested area 3 m and 9 m away from the survey line at approximately 28-31 m along the profile. At both points, the deepest measurements were positive (both ~0.77°C) and extrapolation of measured values did not indicate frozen ground within the upper 2 m. The above noted ambiguities and widespread bedrock mean that it was not possible to determine whether permafrost is present at this site.

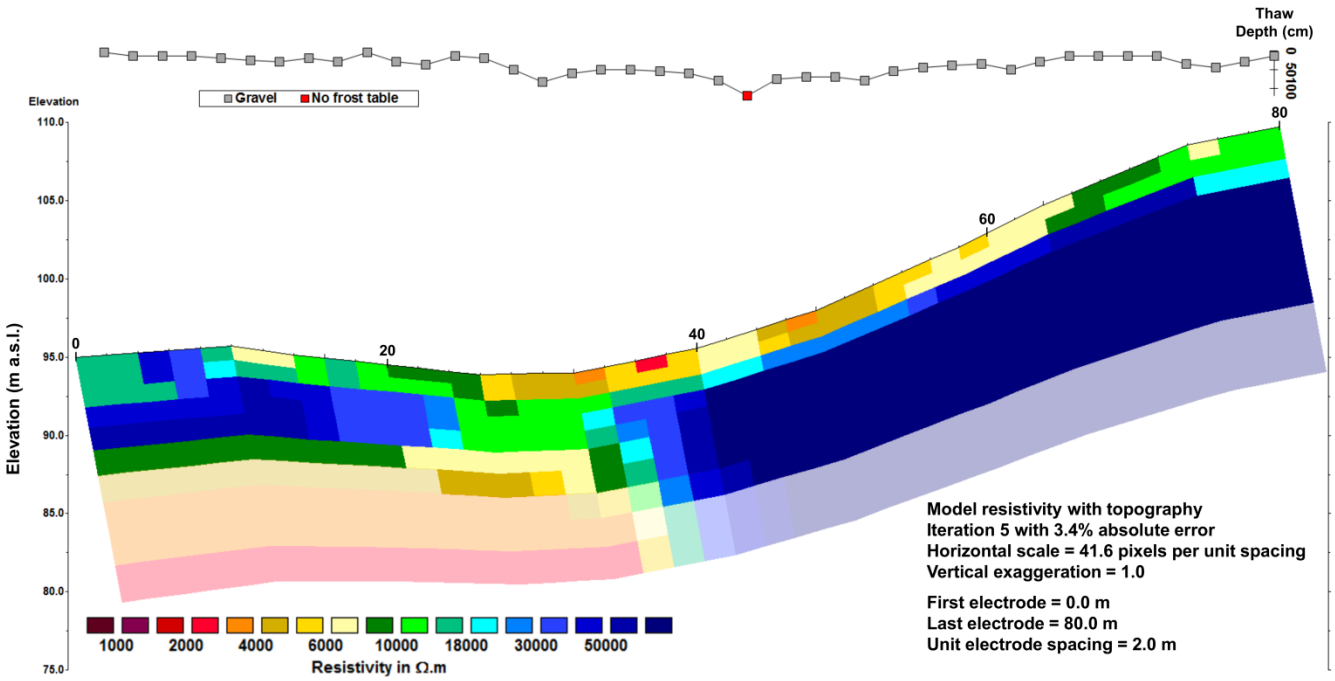

Figure 4-8: Field investigations of permafrost conditions at location F. (a) ERT profile results and inferred thaw depths from frost probing for survey 9. Note: probing was not possible due to clasts or gravel in parts of the profiles without an indication of frost table depth. Colour scales used in this figure differ from those used at the other Nain sites.

4.5 Discussion

4.5.1 Permafrost conditions in Nain

Interpretation of permafrost conditions in the areas around Nain was challenging due to several factors (Figure 4-9). First, permafrost was detected in both coarse (location D) and organic soils (location A) at undisturbed (location C) and disturbed locations (location B). Second, permafrost bodies may have been in different states of equilibrium, ranging from degraded (location B) to possibly stable (location C). Third, although ERT was useful for discriminating between frozen and unfrozen ground along most surveys, sources of external validation were required due to the challenging composition of the subsurface environment (e.g. location F). Fourth, permafrost was inferred to be present under a variety of land cover types (coastal tundra, forest, grassland) which included the first observations of permafrost in forested lowland terrain in Labrador. The 18 m thick permafrost detected beneath the future site of the Torngâsok Cultural Centre (location A) contrasts with other sections of the community where permafrost was completely absent or very thin (location E) implying that local factors have contributed to permafrost development at this site. Fine-grained marine sediments in the lower elevation sections of Nain may explain why permafrost was present in some sections of the community and not others, as is the case along the coast of Hudson's Bay (Beaulieu and Allard 2003).

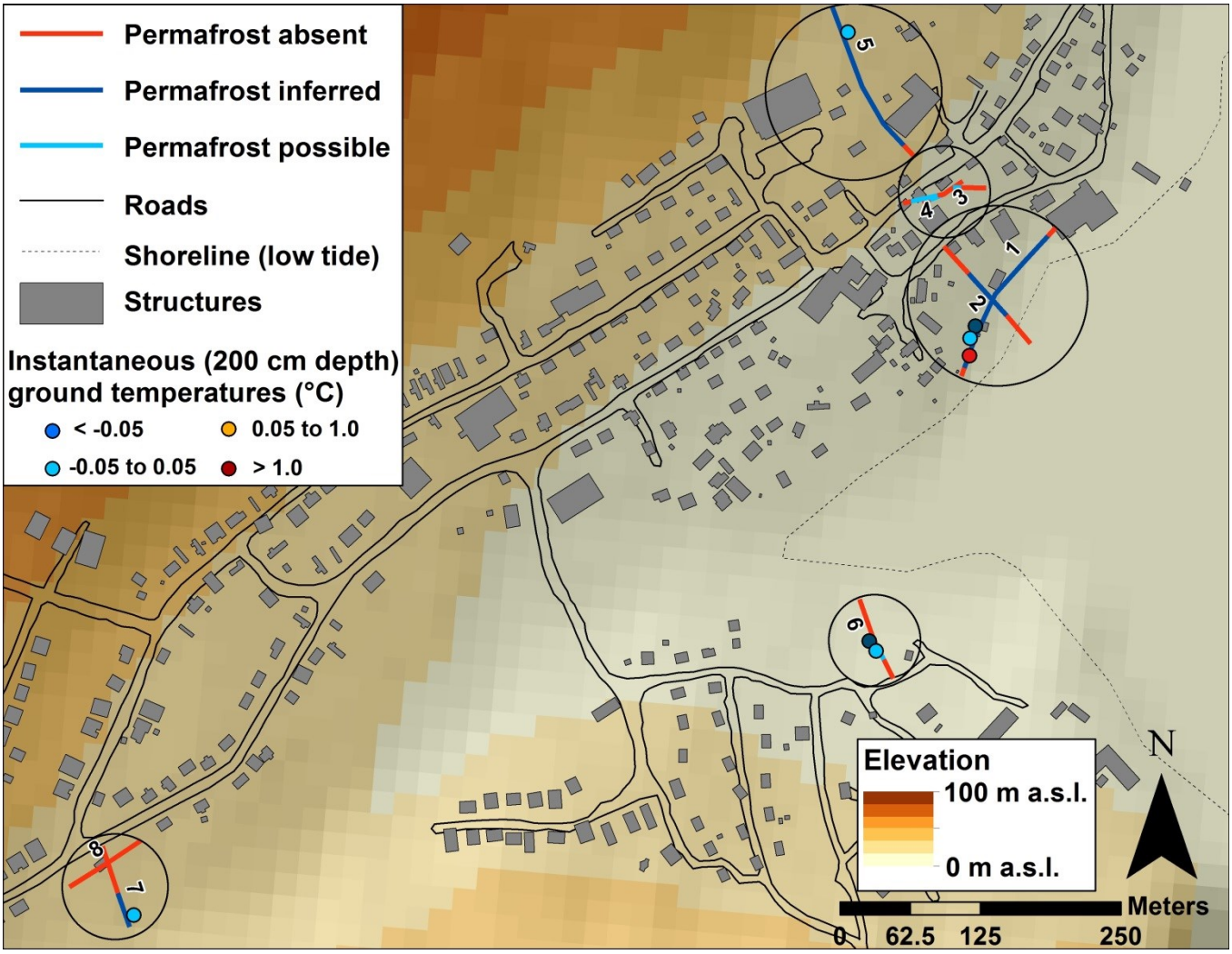

Figure 4-9: Inferred ground conditions from ERT surveys, frost probing and instantaneous ground temperature measurements at Nain. Surveys are classified with the interpreted permafrost conditions along each profile. Survey locations are overlain on a digital elevation model and labels correspond to the survey IDs which are also found in Table 4-2 and described in the text. Note: Black circles correspond to general locations described in the text. Arranged from north to south location circles correspond to locations C, B, A, D, and E.

The presence of fine-to-medium marine sediments in certain parts of Nain emphasizes the importance of detailed investigations of surficial materials and permafrost state prior to building construction, particularly given that ground subsidence has been noted within the community (location B). Fine-grained marine sediments can be particularly frost-susceptible and prone to ice lens formation (Bell et al. 2011; Fortier et al. 2011). Given that the geomorphology at location A appeared comparable to other sections of the community with marine sediments (e.g. location D), factors such as the history of human settlement and subsurface hydrology should be considered when evaluating the ongoing existence of this larger body of permafrost. The combined effects of several hundred years of human occupation and widespread surface disturbance suggest that formerly present permafrost bodies could have degraded, leaving only residual patches within the community itself. This interpretation is supported by modelling studies by Zhang et al. (2006) and Way and Lewkowicz (2016) which suggest that areas around Nain may have experienced widespread permafrost degradation in response to regional warming over the past century. Most contemporary foundation issues in community housing have been attributed to deep winter frost penetration in the coarse near-surface soils (Bell et al. 2011) but permafrost has potentially been of historical significance and thawing permafrost may have caused subsidence in older buildings within sections of the community where permafrost may no longer be detectable. Due to the variable ground thermal and hydrological conditions within the community, the establishment of a permafrost thermal monitoring program would be desirable for better understanding regional permafrost susceptibility to future climate change (e.g. Smith et al. 2005).

4.5.2 Challenges and limitations of detecting permafrost in coastal Labrador

Coastal Labrador is characterized by cool summers (Maxwell 1981; Way et al. 2017a) due to the cold Labrador Current, which may preserve seasonal frost long into the summer such as at location D. Consequently, discrimination between seasonal and perennially frozen ground in Nain was not always possible using techniques such as frost probing and instantaneous ground temperature measurements, particularly given the deep frost penetration (>200 cm) that can occur in coarse soils present in the till dominated sections of the community. ERT profiles and field data also indicated the presence of deep active layers and/or taliks (> 120 cm) at locations A and B which further complicate interpretations of geophysical data but highlight the utility of ERT.

The ERT results presented in this study required a variable resistivity boundary to delineate between frozen and unfrozen sediments due to differing surficial materials. This varied from 800 Ω.m at location A (marine and glaciomarine) to 1200 Ω.m at location C (colluvium) to 2000 Ω.m at location E

(glacial till) (Bell et al. 2011). At the first two locations, the selected resistivity boundaries are similar to those inferred for glacio-marine sediments in western Québec (Fortier et al. 2008) and slightly lower than those inferred for palsas in northern Sweden (>1700 Ω.m) (Sjoberg et al. 2015). However, lower resistivity boundaries (~176 Ω.m) have been used in an alpine meadow in the eastern Tibetan Plateau (You et al. 2013) and between 200-400 Ω.m in organic substrates in the southern Yukon (Lewkowicz et al. 2011) and the Yukon Flats, Alaska (Briggs et al. 2016). Near-surface bedrock along several ERT profiles and observed elsewhere in Nain also made the interpretation of resistivities a challenge. Generally, bedrock was linked to very high resistivities, but in sections of several transects (e.g. Figure 4-7), modelled resistivities believed to be caused by bedrock were virtually indistinguishable from those expected for warm or ice-poor permafrost. Therefore, the importance of local validation from field methods and boreholes for calibrating geophysical results is considered a necessity in heterogeneous surficial environments similar to Nain, NL.

4.6 Summary and conclusion

Investigation of permafrost conditions in Nain, NL revealed the presence of discontinuous permafrost at several locations at lower elevation in the community. Small and large patches of permafrost were found in both undisturbed and disturbed environments. These results are the first observations of permafrost thickness collected in coastal Labrador and demonstrate the utility of DC electrical resistivity for studying discontinuous permafrost in the region. The lack of surface features indicative of permafrost and the variable surficial materials represent challenges for interpreting conditions, but also demonstrate the utility of ERT as a permafrost detection technique in difficult environments. We emphasize the necessity of validating ERT results using either field methods such as frost probing, or information from boreholes. Without direct confirmation of permafrost presence or absence along an ERT transect, permafrost can only be inferred after calibration against sites with known subsurface characteristics. Future work in Nain should aim to identify the spatial extent of permafrost bodies and the primary drivers of permafrost persistence in this marginal environment.

Acknowledgements

We would like to thank the Nunatsiavut Government and community members in Nain, NL for their logistical support and for their valuable discussions which helped to facilitate this research. We would like to thank Jason Smith of EXP Engineering for providing useful discussions of permafrost conditions in the community of Nain, NL. We would also like to give a special thanks to Tom Sheldon, Christina

Goldhar and Carla Pamak for their help in facilitating the research in Nain. NL. Finally, we would like to thank our field assistant Alex Brooker for his contributions during the field season of 2014. R.G.W would like to acknowledge funding from the Natural Sciences and Engineering Research Council of Canada and the Association of Canadian Universities for Northern Studies. Fieldwork was funded by NSERC, the University of Ottawa, and a Northern Scientific Training Grant.

4.7 References

Allard, M., M. Lemay, C. Barrette, E. L'Hérault, D. Sarrazin, T. Bell, and G. Doré. 2012. Permafrost and climate change in Nunavik and Nunatsiavut: Importance for municipal and transportation infrastructures. In Nunavik and Nunatsiavut: From science to policy. An Integrated Regional Impact Study (IRIS) of climate change and modernization, 171–197.

Banfield, C. E., and J. D. Jacobs. 1998. Regional patterns of temperature and precipitation for Newfoundland and Labrador during the past century. The Canadian Geographer/Le Géographe canadien 42(4): 354–364.

Beaulieu, N., and M. Allard. 2003. The impact of climate change on an emerging coastline affected by discontinuous permafrost: Manitounuk Strait, northern Quebec. Canadian Journal of Earth Sciences 40(10): 1393–1404. doi: 10.1139/e03-056.

Bell, T., M. Putt, and T. Sheldon. 2011. Landscape hazard assessment in Nain, Phase 1: Inventory of surficial sediment types and infrastructure damage. Technical report. Nunatsiavut Government.

Briggs, M. A., S. Campbell, J. Nolan, M. A. Walvoord, D. Ntarlagiannis, F. D. Day-Lewis, and J. W. Lane. 2016. Surface Geophysical Methods for Characterising Frozen Ground in Transitional Permafrost Landscapes: Surface Geophysical Methods for Characterising Frozen Ground. Permafrost and Periglacial Processes. doi: 10.1002/ppp.1893.

Brown, R., M. Lemay, M. Allard, N. E. Barrand, C. Barrette, Y. Bégin, T. Bell, M. Bernier, S. Bleau, D. Chaumont, Y. Dibike, A. Frigon, P. Leblanc, D. Paquin, M. J. Sharp, and R. Way. 2012. Climate variability and change in the Canadian Eastern Subarctic IRIS region (Nunavik and Nunatsiavut). In Nunavik and Nunatsiavut: From science to policy. An Integrated Regional Impact Study (IRIS) of climate change and modernization, 57–93.

Brown, R. J. 1979. Permafrost distribution in the southern part of the discontinuous zone in Quebec and Labrador. Géographie physique et Quaternaire 33(3–4): 279–289.

Butler, D. H. 2011. Exploring soilscapes and places inside Labrador Inuit winter dwellings. Canadian Journal of Archaeology 35(1): 55–85.

Comiso, J. C., and D. K. Hall. 2014. Climate trends in the Arctic as observed from space: Climate trends in the Arctic as observed from space. Wiley Interdisciplinary Reviews: Climate Change 5(3): 389–409. doi: 10.1002/wcc.277.

Douglas, T. A., M. T. Jorgenson, D. R. N. Brown, S. W. Campbell, C. A. Hiemstra, S. P. Saari, K. Bjella, and A. K. Liljedahl. 2016. Degrading permafrost mapped with electrical resistivity tomography, airborne imagery and LiDAR, and seasonal thaw measurements. GEOPHYSICS 81(1): WA71-WA85. doi: 10.1190/geo2015-0149.1.

Fortier, R., M. Allard, S. Buteau, and F. Calmels. 2008. Internal structure and conditions of permafrost mounds at Umiujaq in Nunavik, Canada, inferred from field investigation and electrical resistivity tomography. Canadian Journal of Earth Sciences 45(3): 367–387. doi: 10.1139/E08-004.

Fortier, R., A.-M. LeBlanc, and W. Yu. 2011. Impacts of permafrost degradation on a road embankment at Umiujaq in Nunavik (Quebec), Canada. Canadian Geotechnical Journal 48(5): 720–740. doi: 10.1139/t10-101.

Hachem, S., M. Allard, and C. Duguay. 2009. Using the MODIS land surface temperature product for mapping permafrost: an application to northern Québec and Labrador, Canada. Permafrost and Periglacial Processes 20(4): 407–416. doi: 10.1002/ppp.672.

Hauck, C. 2013. New Concepts in Geophysical Surveying and Data Interpretation for Permafrost Terrain: Geophysical Surveying in Permafrost Terrain. Permafrost and Periglacial Processes 24(2): 131–137. doi: 10.1002/ppp.1774.

Hauck, C., D. Vonder Mühll, and H. Maurer. 2003. Using DC resistivity tomography to detect and characterize mountain permafrost. Geophysical prospecting 51(4): 273–284.

Heginbottom, J. A., M.-A. Dubreuil, and P. A. Harker. 1995. Canada – Permafrost. National Atlas of Canada, 5th Edition. Ottawa, Canada: Natural Resources Canada.

Hilbich, C., L. Marescot, C. Hauck, M. H. Loke, and R. Mäusbacher. 2009. Applicability of electrical resistivity tomography monitoring to coarse blocky and ice-rich permafrost landforms. Permafrost and Periglacial Processes 20(3): 269–284. doi: 10.1002/ppp.652.

Hong, E., R. Perkins, and S. Trainor. 2014. Thaw Settlement Hazard of Permafrost Related to Climate Warming in Alaska. ARCTIC 67(1): 93. doi: 10.14430/arctic4368.

James, M., A. G. Lewkowicz, S. L. Smith, and C. M. Miceli. 2013. Multi-decadal degradation and persistence of permafrost in the Alaska Highway corridor, northwest Canada. Environmental Research Letters 8(4): 045013. doi: 10.1088/1748-9326/8/4/045013.

Lewkowicz, A. G., and R. G. Way. 2014. Overview report for the Nunatsiavut Government on permafrost conditions in the Nain area. Technical report.

Lewkowicz, A. G., B. Etzelmüller, and S. L. Smith. 2011. Characteristics of discontinuous permafrost based on ground temperature measurements and electrical resistivity tomography, southern Yukon, Canada. Permafrost and Periglacial Processes 22(4): 320–342. doi: 10.1002/ppp.703.

Loke, M. H., and R. D. Barker. 1996. Rapid least-squares inversion of apparent resistivity pseudosections by a quasi-Newton method. Geophysical prospecting 44(1): 131–152.

Loke, M. H., I. Acworth, and T. Dahlin. 2003. A comparison of smooth and blocky inversion methods in 2D electrical imaging surveys. Exploration Geophysics 34(3): 182–187. doi: 10.1071/EG03182.

Maxwell, J. B. 1981. Climatic regions of the Canadian Arctic Islands. ARCTIC 34(3): 225–240.

Minsley, B. J., N. J. Pastick, B. K. Wylie, D. R. N. Brown, and M. Andy Kass. 2016. Evidence for nonuniform permafrost degradation after fire in boreal landscapes. Journal of Geophysical Research: Earth Surface 121(2): 320–335. doi: 10.1002/2015JF003781.

Nelson, F. E., O. A. Anisimov, and N. I. Shiklomanov. 2001. Subsidence risk from thawing permafrost. Nature 410(6831): 889–890.

Nicholson, F. H. 1979. Permafrost spatial and temporal variations near Schefferville, Nouveau-Québec. Géographie physique et Quaternaire 33(3–4): 265–277. doi: 10.7202/1000363ar.

Occhietti, S., M. Parent, P. Lajeunesse, F. Robert, and E. Govare. 2011. Late Pleistocene–Early Holocene decay of the Laurentide Ice Sheet in Québec-Labrador. Developments in Quaternary Science 11: 601–630. doi: 10.1016/B978-0-444-53447-7.00047-7.

Oldenborger, G. A., and A.-M. LeBlanc. 2015. Geophysical characterization of permafrost terrain at Iqaluit International Airport, Nunavut. Journal of Applied Geophysics 123: 36–49. doi: 10.1016/j.jappgeo.2015.09.016.

Roberts, B. A., N. P. P. Simon, and K. W. Deering. 2006. The forests and woodlands of Labrador, Canada: ecology, distribution and future management. Ecological Research 21(6): 868–880. doi: 10.1007/s11284-006-0051-7.

Sjöberg, Y., P. Marklund, R. Pettersson, and S. W. Lyon. 2015. Geophysical mapping of palsa peatland permafrost. The Cryosphere 9(2): 465–478. doi: 10.5194/tc-9-465-2015.

Smith, S. L., and M. M. Burgess. 2004. Sensitivity of permafrost to climate warming in Canada. Bulletin 579. Geological Survey of Canada.

Smith, S. L., and D. W. Riseborough. 2010. Modelling the thermal response of permafrost terrain to right-of-way disturbance and climate warming. Cold Regions Science and Technology 60(1): 92–103. doi: 10.1016/j.coldregions.2009.08.009.

Smith, S. L., M. M. Burgess, D. Riseborough, and F. Mark Nixon. 2005. Recent trends from Canadian permafrost thermal monitoring network sites. Permafrost and Periglacial Processes 16(1): 19–30. doi: 10.1002/ppp.511.

Stantec. 2012. Geotechnical Investigation, Torngasok Cultural Centre, Nain, NL. Geotechnical report 121615077. Stantec Consulting Ltd.

Voisey's Bay Nickel Corporation. 1997. Voisey's Bay Mine/Mill Project Environmental Impact Statement. Environmental Impact Statement. INCO Limited.

Way, R. G., and A. G. Lewkowicz. 2016. Modelling the spatial distribution of permafrost in Labrador–Ungava using the temperature at the top of permafrost. Canadian Journal of Earth Sciences 53(10): 1010–1028. doi: 10.1139/cjes-2016-0034.

Way, R. G., and A. E. Viau. 2015. Natural and forced air temperature variability in the Labrador region of Canada during the past century. Theoretical and Applied Climatology 121(3–4): 413–424. doi: 10.1007/s00704-014-1248-2.

Way, R. G., A. G. Lewkowicz, and P. P. Bonnaventure. 2017a. Development of moderate-resolution gridded monthly air temperature and degree-day maps for the Labrador-Ungava region of northern Canada. International Journal of Climatology 37(1): 493–508. doi: 10.1002/joc.4721.

Woo, M., A. G. Lewkowicz, and W. R. Rouse. 1992. Response of the Canadian permafrost environment to climatic change. Physical Geography 13(4): 287–317. doi: 10.1080/02723646.1992.10642459.

Woollett, J. 2010. Oakes Bay 1: A Preliminary Reconstruction of a Labrador Inuit Seal Hunting Economy in the Context of Climate Change. Geografisk Tidsskrift-Danish Journal of Geography 110(2): 245–259. doi: 10.1080/00167223.2010.10669510.

You, Y., Q. Yu, X. Pan, X. Wang, and L. Guo. 2013. Application of electrical resistivity tomography in investigating depth of permafrost base and permafrost structure in Tibetan Plateau. Cold Regions Science and Technology 87: 19–26. doi: 10.1016/j.coldregions.2012.11.004.

Zhang, Y., W. Chen, and D. W. Riseborough. 2006. Temporal and spatial changes of permafrost in Canada since the end of the Little Ice Age. Journal of Geophysical Research 111(D22). doi: 10.1029/2006JD007284.

Zhang, Y., W. Chen, and D. W. Riseborough. 2008. Transient projections of permafrost distribution in Canada during the 21st century under scenarios of climate change. Global and Planetary Change 60(3–4): 443–456. doi: 10.1016/j.gloplacha.2007.05.003.

CHAPTER 5: RELATIONS BETWEEN ENVIRONMENTAL SETTING AND TTOP PARAMETERS IN LABRADOR, NORTHEASTERN CANADA

Abstract

Field data from 83 monitoring stations across Labrador, 15 with permafrost, were used to analyze the interrelationships of key variables in the temperature at the top of permafrost model. Snow depth, not mean annual air temperature, was the strongest single determinant of mean temperatures at the ground surface and at the top of permafrost (TTOP), and its variability was in turn most related to land cover class. A critical late-winter snow depth of 70 cm or less was inferred to be sufficient to prevent the formation of permafrost at the monitoring sites which meant that permafrost was absent beneath forest but present in barren locations. Analyses showed no statistically significant relations between topographic indices and various station parameters challenging their utility for modelling in Labrador. Testing of several different land cover datasets for permafrost model parameterization gave errors in ground surface temperature ranging from ±0.9-2.1°C. These results highlight the importance of collecting local field data and emphasize the necessity of developing high quality land cover datasets for permafrost modelling at the regional to continental scale.

5.1 Introduction

Permafrost is the most challenging element of the cryosphere to represent spatially because its characteristics vary over local to regional domains and because it typically cannot be directly observed using remote sensing techniques (Gubler et al. 2011; Gubler et al. 2013a; Westermann et al. 2015b). The response of permafrost to climate change is also complicated by linkages and feedbacks with other ecosystem components that modify local sensitivity to external perturbations (Woo et al. 1992; Shur and Jorgenson 2007; Jorgenson et al. 2010). In order to spatially represent permafrost at larger scales, it is necessary to simplify landscape heterogeneity by linking ecosystem and geomorphic processes that influence ground temperatures to available environmental datasets (Riseborough et al. 2008; Bonnaventure et al. 2012; Lewkowicz et al. 2012; Gisnås et al. 2013; Westermann et al. 2015a; Nicolsky et al. 2016). These datasets may include a range of variables, from land cover class to surficial materials, which differ in their spatial and temporal resolution. Physically-based numerical models, often used to assess permafrost susceptibility to climate change, also rely on the availability and quality of these environmental datasets for model parameterization (Jafarov et al. 2012; Zhang 2013; Zhang et al. 2013; Zhang et al. 2014; Ou et al. 2016a; Ou et al. 2016b). The accuracy of spatial models therefore depends upon the fidelity of each dataset to local conditions.

The temperature at the top of permafrost (TTOP; Smith and Riseborough 1996) model is an analytical permafrost model that calculates mean ground temperature at the base of the active layer which is defined as the base of seasonal thawing for permafrost or the base of seasonal freezing for non-permafrost. Calculation of TTOP (see eq. (5-1)) requires input parameters to summarize differences in air and surface climate conditions and parameters which describe associations between surface and subsurface temperatures (Smith and Riseborough 1996; Smith and Riseborough 2002; Riseborough 2004).

$$TTOP = \frac{(rk * nT * TDDa) - (nF * FDDa)}{365} \quad (5\text{-}1)$$

$where$:

$TTOP = Temperature\ at\ the\ top\ of\ permafrost\ (°C)$

$$rk = \frac{Thawed\ ground\ thermal\ conductivity\ (Wm^{-1}K^{-1})}{Frozen\ ground\ thermal\ conductivity\ (Wm^{-1}K^{-1})}$$

$nT = Thawing\ n - factor$

$TDDa = Annual\ sum\ of\ daily\ air\ temperatures\ above\ 0°C$

$nF = Freezing\ n - factor$

$FDDa = Annual\ sum\ of\ daily\ air\ temperatures\ below\ 0°C$

Similar parameters have been used to force the GIPL 1.0 model in Alaska (Sazonova and Romanovsky 2003). Despite uncertainties associated with parameterizing soil moisture processes (Riseborough 2002) and applying equilibrium scenarios to transient conditions (Riseborough 2007), the model has been used for spatial prediction of permafrost at scales ranging from regional to continental in Europe (Juliussen and Humlum 2007; Gisnås et al. 2013; Gisnås et al. 2016a), North America (Henry and Smith 2001; Smith and Riseborough 2002; Wright et al. 2003; Bevington and Lewkowicz 2015; Way and Lewkowicz 2016) and Asia (Zhao et al. 2017). The TTOP model has also been used to calibrate basal temperature sub-routines for ice sheet modelling across North America since the Last Glacial Maximum (Tarasov and Peltier 2007).

In recent TTOP spatial modelling studies, the necessary TTOP parameters were assigned by extrapolating from local field studies (Wright et al. 2003; Gisnås et al. 2013; Gisnås et al. 2016b), by constraining model simulations to theoretical limits (Westermann et al. 2015a) or by using numerical model simulations (Way and Lewkowicz 2016). Due to the data-intensive input requirements for spatial modelling, regional-scale analyses of TTOP inputs using empirical field data are relatively rare. A recent analysis of field data in the southern Yukon and northern British Columbia by Bevington and Lewkowicz (2015) demonstrated that there was considerable uncertainty in estimating TTOP parameters using readily-available vegetation and surficial datasets. These conclusions need to be tested in regions where environmental conditions differ from those in western Canada.

In this study, we report on TTOP and other permafrost relevant parameters (Table 5-1) collected from more than 80 locations in Labrador (northeastern Canada). The data were collected across environmental settings that varied from Subarctic boreal forest to high Subarctic Tundra to coastal Arctic Cordilleran mountains, and represent the only contemporary empirical data on permafrost in Labrador. Unlike prior work undertaken in the region using an analytical model (Way and Lewkowicz 2016), this study examines relations between field data and station-specific local factors and evaluates uncertainties associated with TTOP modelling when employing gridded environmental datasets.

5.2 Study area

Labrador (area 294,000 km^2) contains the highest mountains in continental eastern Canada (Torngat Mountains National Park) and the southernmost limits of the Arctic in Canada (Maxwell 1981). The region encompasses a range of climatic zones with mean annual air temperatures varying from +1.5°C to -9°C and annual temperature amplitudes (July mean minus January mean) as low as 22°C in coastal areas and as high as 45°C in the interior (Way et al. 2017a). Approximately 60% of Labrador is forested

(Boreal and/or Subarctic) while nearly 30% consists of alpine tundra, high subarctic tundra or low Arctic tundra (Roberts et al. 2006). The remaining area is evenly divided between coastal barrens and wetlands (Roberts et al. 2006). Regional surficial materials are predominantly glacial tills, glaciomarine sediments (below the marine limit), and exposed or near-surface bedrock at all elevations (Occhietti et al. 2011). According to the Permafrost Map of Canada (Heginbottom et al. 1995), permafrost is continuous in the north and rare in the south. Spatial modelling of regional permafrost extent (Way and Lewkowicz 2016) suggests that permafrost covers approximately 15% of the land area with the lowest probabilities of occurrence in forested parts of south-central Labrador (< 0.1%) and the highest probabilities (> 90%) in the northeast coastal mountains (Figure 5-1).

Table 5-1: Measured and derived parameters at monitoring stations.

Parameter	Acronym	Units	Calculation method
Mean annual air temperature	MAAT	°C	(TDDa - FDDa) ÷ 365
Temperature amplitude	TA	°C	July air temperature - January air temperature
Air freezing degree days	FDDa	°C days	Annual sum of daily air temperatures below 0°C
Air thawing degree days	TDDa	°C days	Annual sum of daily air temperatures above 0°C
Surface freezing degree days	FDDs	°C days	Annual sum of daily surface temperatures below 0°C
Surface thawing degree days	TDDs	°C days	Annual sum of daily surface temperatures above 0°C
Freezing n-factor	nF	unitless	FDDs ÷ FDDa
Thawing n-factor	nT	unitless	TDDs ÷ TDDa
Nival offset	NVO	°C	(FDDa - FDDs) ÷ 365
Thawing season offset	TSO	°C	(TDDs - TDDa) ÷ 365
Annual ground surface temperature	GST	°C	(TDDs - FDDs) ÷ 365
Surface offset	SO	°C	GST - MAAT
Thermal offset	TO	°C	TTOP - GST
Estimated rk	rk	unitless	((TTOP x 365) + FDDs) ÷ TDDs
Temperature at the top of permafrost	TTOP	°C	Mean annual ground temperature at 50-125 cm
Snow depth days	SDD	cm days	Annual sum of daily mean snow depths
Mean winter snow depth (JFM)	WSD	cm	Mean of January, February & March daily snow depths
Late-winter snow depth	LWSD	cm	Maximum late-winter snow depth
Snow on ground days	SDS	days	Days with detectable snow on the ground
Critical freezing n-factor	nF_{crit}	unitless	(rk x TDDa x nT) / FDDa

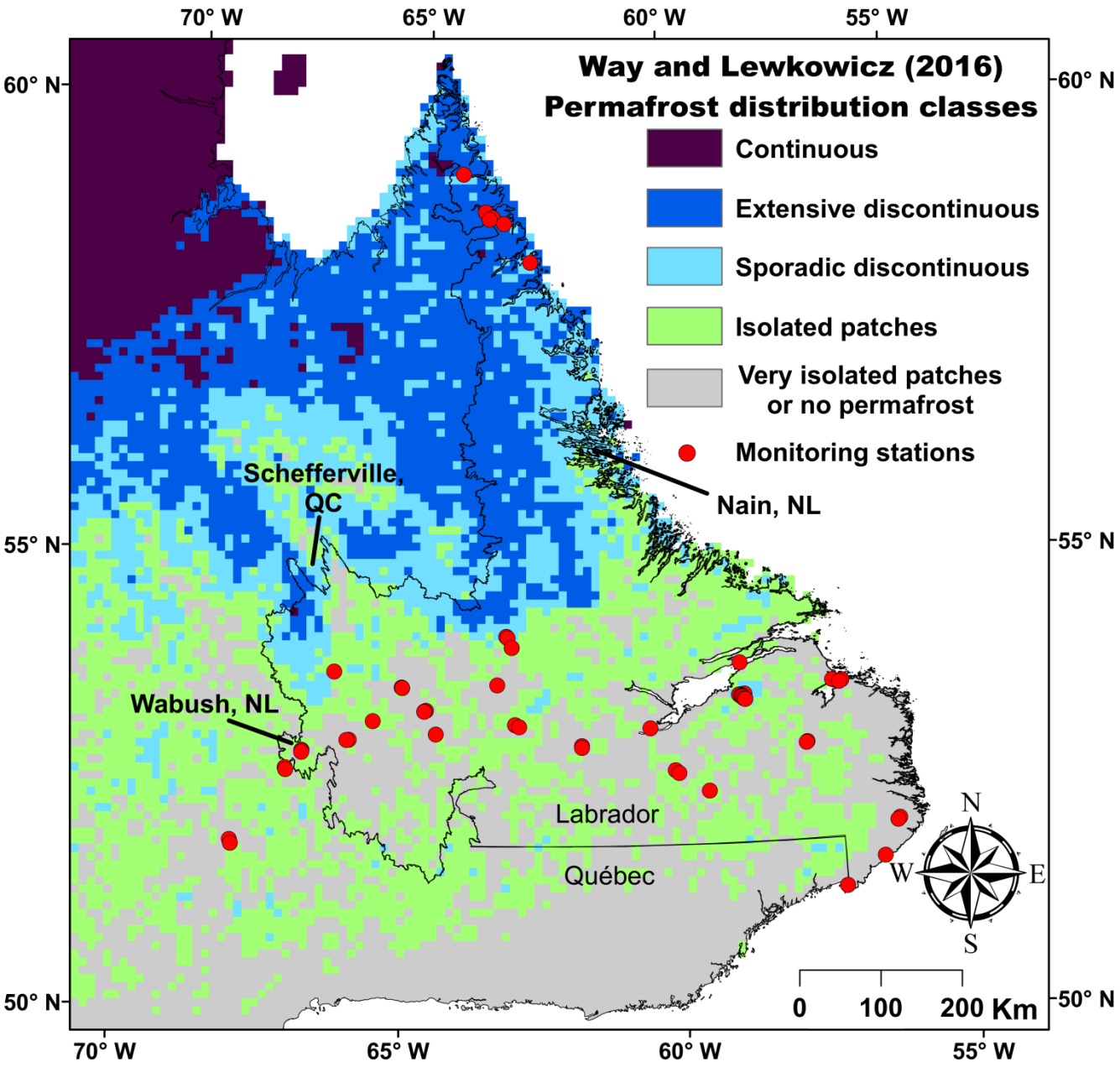

Figure 5-1: Spatial distribution of monitoring stations used in this study. Site locations are overlain on a 10 km resolution permafrost distribution map with the following classes: continuous (90-100%); extensive discontinuous (50-90%); sporadic discontinuous (10-50%); isolated patches (1-10%); very isolated patches or no permafrost (<1%) (Way and Lewkowicz, 2016).

5.3 Methods

5.3.1 Climate stations

Thirty-seven climate monitoring stations were established by the Labrador Permafrost Project between November 2012 and September 2015 with most of these stations still active in 2017 (Table B3). The monitoring stations record shielded air and ground surface temperatures, shallow ground temperatures (0.5-1.25 m depths) and snow depth using the ibutton method (Lewkowicz 2008). The aim was to sample all of the major physiographic, ecological and climatic zones in central and southern Labrador. Consequently, site elevations range from 5 m asl to 893 m asl (Figure 5-1).

Air and ground surface temperature data were also obtained from the Torngat Mountains National Park for six Parks Canada monitoring locations (2010-2016) and ground temperatures (1 m depth) were made available from one co-located borehole (2013-2015). Additional ground surface temperature data were obtained from the Labrador Highlands Research Group for 31 sites forming an elevational transect from boreal forest into high sub-Arctic tundra within the Mealy Mountains in southeastern Labrador (Jacobs et al. 2014; Trant et al. 2015) (Figure 5-1). Three climate stations were also positioned along this transect at 570, 600 and 995 m a.s.l. from 2001 to 2009 (Jacobs et al. 2014).

Combining the various data sources, sampled environments included forest (n=27), forest-tundra transitions (n=17), coastal palsa bogs (n=5), exposed rock (n=7), low-and-high shrubs (n=6) and alpine or coastal tundra (n=21) (Figure 5-2). Local surficial materials, where determinable, included glaciomarine (n=6), glaciolacustrine (n=2) and glaciofluvial (n=1) deposits, tills (n=21) and shallow bedrock (n=12). Values in Table B3 differ in their length of record but are calculated using only complete years and depend on the parameter being calculated and the record completeness at each site. The average record length for TTOP-relevant parameters is 19 months with a minimum of 11 months (estimated 12th month) and a maximum of 96 months.

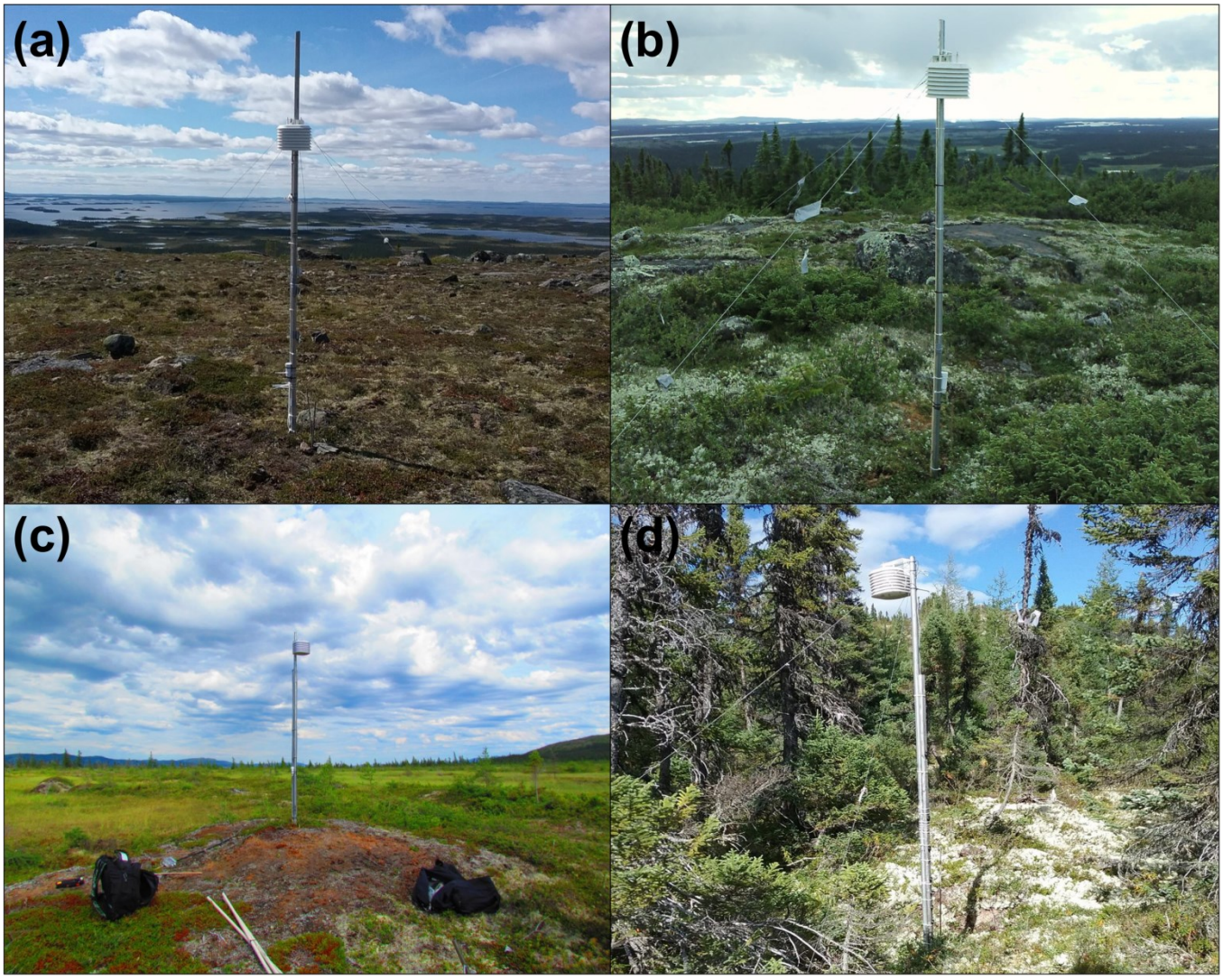

Figure 5-2: Range of monitored environments illustrated by examples of climate stations located in (a) tundra; (b) forest-tundra transition; (c) palsa bog; and (d) forest.

5.3.2 Air temperature

Air temperatures were measured using Onset Hobo Pro V2 (accuracy ±0.2°C) and Maxim Integrated high-resolution ibutton loggers (accuracy ±0.5°C) placed in radiation shields at 200 to 250 cm above the ground surface. The logging interval varied from 2 hours (Hobo Pro V2) to 3-4 hours (ibutton). Prior to processing, raw ibutton data were reconfigured and formatted using a custom R v3.3 script (Appendix A2). At selected sites (n=22), Hobo Pro V2s and high-resolution ibuttons were co-located for one year for instrument inter-comparison purposes. A regression-based calibration method was employed to correct systematic errors in ibutton measurements compared to Hobo Pro V2 data due to the low measurement limit of -40°C for ibutton loggers. Each monthly linear regression fit was statistically significant ($p < 0.01$) with $r^2 > 0.99$ and was used to homogenize ibutton-only air temperature sites with the Hobo Pro V2 data, and for gap-filling where sensor failures occurred. All air temperature data were aggregated from sub-daily to daily and monthly values, and summaries were generated for minimum/mean/maximum temperature, total thawing degree days (TDD) and total freezing degree days (FDD) using a custom R v3.3 script (Appendix A3). To enable comparisons with ground surface temperature (GST) monitoring sites in the Mealy Mountains, air temperatures were estimated for each GST logger location by adjusting local automatic climate station data for differences in elevation using monthly lapse rates measured in the region by Jacobs et al. (2014). This adjustment procedure was also used for calculating FDDs and TDDs.

5.3.3 Ground surface and shallow ground temperatures

Ground surface and shallow ground temperatures at University of Ottawa stations were measured using Onset Hobo Pro V2s and Maxim Integrated high or low resolution (±1°C) ibuttons with logging intervals which varied from 2 hours (Hobo Pro V2s) to 3-4 hours (ibuttons). At Parks Canada and Labrador Highlands Research Group stations, ground surface temperatures (GSTs) were measured with Onset Tidbit (±0.4°C) and Onset Pendant (±0.5°C) loggers (Jacobs et al. 2014). All GSTs (n=78) were measured at or just below the soil interface (2-3 cm depth) beneath near-surface vegetation cover, to ensure temperature differences with the air included the effects of bryophyte and lichen covers (e.g. Porada et al. 2016) and to avoid direct solar heating. Shallow ground temperatures (n=38) were measured at depths varying from 50 cm to 120 cm depending on the depth of probe penetration when establishing monitoring sites. The deepest thermistor was considered to be an approximation for the base of the annual freeze-thaw layer in non-permafrost environments and as the depth of TTOP where permafrost was present (e.g. Bevington and Lewkowicz 2015).

5.3.4 Snow depth

Snow depth was measured at 31 sites using vertically arranged low-resolution ibutton loggers (e.g. Lewkowicz 2008) installed at heights of 10, 20, 30, 40, 50, 60, 80, 100, 140 and 180 cm. Raw ibutton data was first reformatted (see Appendix A2) and then used to calculate daily temperature ranges at each height. Snow heights were determined using an empirically determined centred 11-day running r^2 between the temperature range at each measurement height and the temperature range at the uppermost ibutton (typically 180 cm). An empirical threshold r^2 of 0.8 was used to delineate between snow-covered and exposed ibutton heights. Site-specific minor manual adjustments to this threshold was required to remove outliers where the empirical threshold was too low or too high, potentially missing the presence of snow cover. Corrected daily snow depths were used to derive average winter (JFM) snow depth (WSD), late-winter snow depth (maximum between late-February to late-March) (LWSD), snow depth days (SDD) and days with measurable snow (SDS). Due to the vertical spacing of ibuttons, uncertainties in snow heights were greater at higher snow depths. These uncertainties were exacerbated by ibutton failures, particularly when they occurred at 100, 140 or 180 cm height, so it was not possible to calculate WSD and SDD for some sites (Table B3).

5.3.5 Gridded environmental datasets

Previous permafrost studies have used individual land cover products for spatial modelling (Gisnås et al. 2013; Bevington and Lewkowicz 2015; Westermann et al. 2015a; Way and Lewkowicz 2016) or have derived study-specific products from remote sensing data (Ou et al. 2016b; Ou et al. 2016a). However, there are several land cover products available for most high latitude regions based on differing processing methodologies, spatial or temporal resolutions and accuracies. We compiled a series of high resolution environmental datasets (land cover, surficial cover, climate and topography) for all of Labrador (Table 5-2) in order to assess their relative suitability for spatial modelling.

Some environmental datasets (CFS30m, TRC30m, SPOT20m, CRF1km) required pre-processing including mosaicking and/or averaging for overlapping areas, removal of background values and re-projecting prior to further analysis. All land cover datasets were reclassified into six types: rock, tundra, wetland, shrub, forest-tundra, and forest. Six topographic variables were also derived: topographic position index (TPI), topographic roughness index (TRI)(Riley 1999), landform classification (LFORM), heatload index (HLI) (McCune et al. 2002), slope (SLP) and slope position (SLPOS) (Table 5-2). These were calculated using ESRI ArcGIS 10 with the topography toolbox produced by Dilts (2016) using an aggregated 100 m digital elevation model prepared by Natural Resources Canada (CDED;

www.geogratis.ca). Surficial materials were characterized by interpolated coarse fragment percentage (CRF1km) surfaces generated by Soils1km for several near-surface layers (45 cm, 100 cm and 145 cm depths) (Hengl et al. 2014). All gridded datasets were compared to measured parameters at monitoring stations by sampling co-located grid cells in ESRI ArcGIS 10.

5.3.6 Correlation and land cover analysis

Pearson correlation analysis was performed between field-based parameters and gridded environmental datasets for continuous variables (e.g. TRC30m; HLI). Statistical significance was set at the 95% confidence interval ($p < 0.05$) after adjustment for multiple comparisons using the *psych* package in R v3.3.

Evaluation of land cover datasets was completed by comparing recorded GSTs from monitoring stations to modelled GSTs derived with eq. (5-2):

$$GST_{station\ N} = \frac{(nT_{land\ class} * TDDa_{observed}) - (nF_{land\ class} * FDDa_{observed})}{365} \qquad (5\text{-}2)$$

$where$:

$GST_{station\ N}\ is\ modelled\ ground\ surface\ temperature\ (°C) for\ monitoring\ station\ N$
$nT_{land\ class}\ is\ the\ median\ thawing\ n-factor\ of\ vegetation\ class\ at\ station\ N$
$TDDa_{observed}\ is\ Air\ thawing\ degree\ days\ observed\ for\ station\ N$
$nF_{land\ class}\ is\ the\ median\ freezing\ n-factor\ of\ vegetation\ class\ at\ station\ N$
$FDDa_{observed} = Air\ freezing\ degree\ days\ observed\ for\ station\ N$

Median nF and nT values were first derived for each land cover class from the field-based observations. Equation (5-2) was then used with the calculated FDDa and TDDa and the median n-factors which were stratified based on the land cover class observed in the field at each monitoring site. The deviations between the measured and modelled GSTs were due to replacing the site-specific n-factors with median values. The modelling was repeated, again using the measured FDDa and TDDa, but employing the median n-factors based on the gridded land cover class extracted for the monitoring site locations. Additional deviations between modelled and measured GSTs at each location were due to the misclassification of land cover types. Further sensitivity analyses were undertaken using either observed nF or observed nT values to isolate the magnitude of the error associated with each of these parameters.

Table 5-2: Data sources and summary information for gridded environmental datasets.

Data provider	Acronym	Resolution	Type	Reference
Canada Centre for Remote Sensing	CCRS250m	250 m	Land cover classification	Trishchenko et al. 2009
Canadian Forest Service	CFS30m	30 m	Land cover classification	Wulder et al. 2008
NL Nature Atlas	NCC1	30 m	Land cover classification	http://nlnatureatlas.ca/
Nature Conservancy of Canada	NCC2	30 m	Land cover classification	http://nlnatureatlas.ca/
Canada Centre for Remote Sensing	SPOT20m	20 m	Land cover classification	Olthof et al. 2015
SPOT20m aggregated to 100 m	SPOT100m	100 m	Land cover classification	Olthof et al. 2015
Global Land Cover Facility	TRC	30 m	Tree cover percentage	Sexton et al. 2013
Generated in ArcGIS 10	HLI	100 m	Heat load index	McCune and Keon 2002
Generated in ArcGIS 10	LFORM	100 m	Landform classification	Dilts 2016
Generated in ArcGIS 10	SLP	100 m	Slope	NA
Generated in ArcGIS 10	SLPOS	100 m	Slope position	Dilts 2016
Generated in ArcGIS 10	TPI	100 m	Topographic position index	Dilts 2016
Generated in ArcGIS 10	TRI	100 m	Topographic roughness index	Riley 1999
Soilgrids.org	CRF1km	1000 m	Coarse fragments (upper 1.5 m) percentage	Hengl et al. 2014
Natural Resources Canada	NRCSD	1000 m	Late-winter snow depth	NA

5.4 Results

5.4.1 Measured station parameters

The Labrador monitoring stations (n=83) (Table B3) had mean annual air temperatures ranging from -6.6°C to +0.6°C (median: -3.2°C), broadly decreasing from south to north and with increasing elevation, and air temperature amplitudes (TAs) from 21.0°C to 40.6°C (median: 32.3°C) which were related most strongly to distance from the coast. The median Winter Snow Depth (WSD) was 81 cm (n=27), but some sites had virtually no snow (WSD of 5 cm) while others had deep accumulations (maximum WSD: 136 cm). The range was still greater in the late winter when the maximum value reached 180 cm (n=34; median 100 cm).

The snow cover caused mean ground surface temperatures (n=80) to be higher than those in the air with a median GST of 2.1°C and a range from -3.2°C to 4.5°C (Figure 5-3). Surface offsets between air temperatures and ground surface temperatures (SO) (n=80) had a median value of 4.9°C with a minimum of 0.5°C and a maximum of 8.3°C (Figure 3). Freezing season offset related parameters comprising NVO and nF (n=80) had median values of 5.5°C and 0.13, respectively. In the thawing season, TSOs (n=77) ranged from -1.7°C to +1.4°C (median: -0.5°C) and nTs ranged between 0.59 and 1.33 (median: 0.86). Average ground temperatures close to or at the base of the freeze-thaw layer (TTOP) (n=38) ranged from -2.9°C to 4.3°C but were predominantly positive at the monitoring sites (median: 2.4°C). TOs (n=37) ranged from -2.7°C to +0.8°C (median: -0.3°C) and were used with FDDs and TDDs to calculate rk values (n=37) which ranged between 0.34 and 1.22 (median: 0.91).

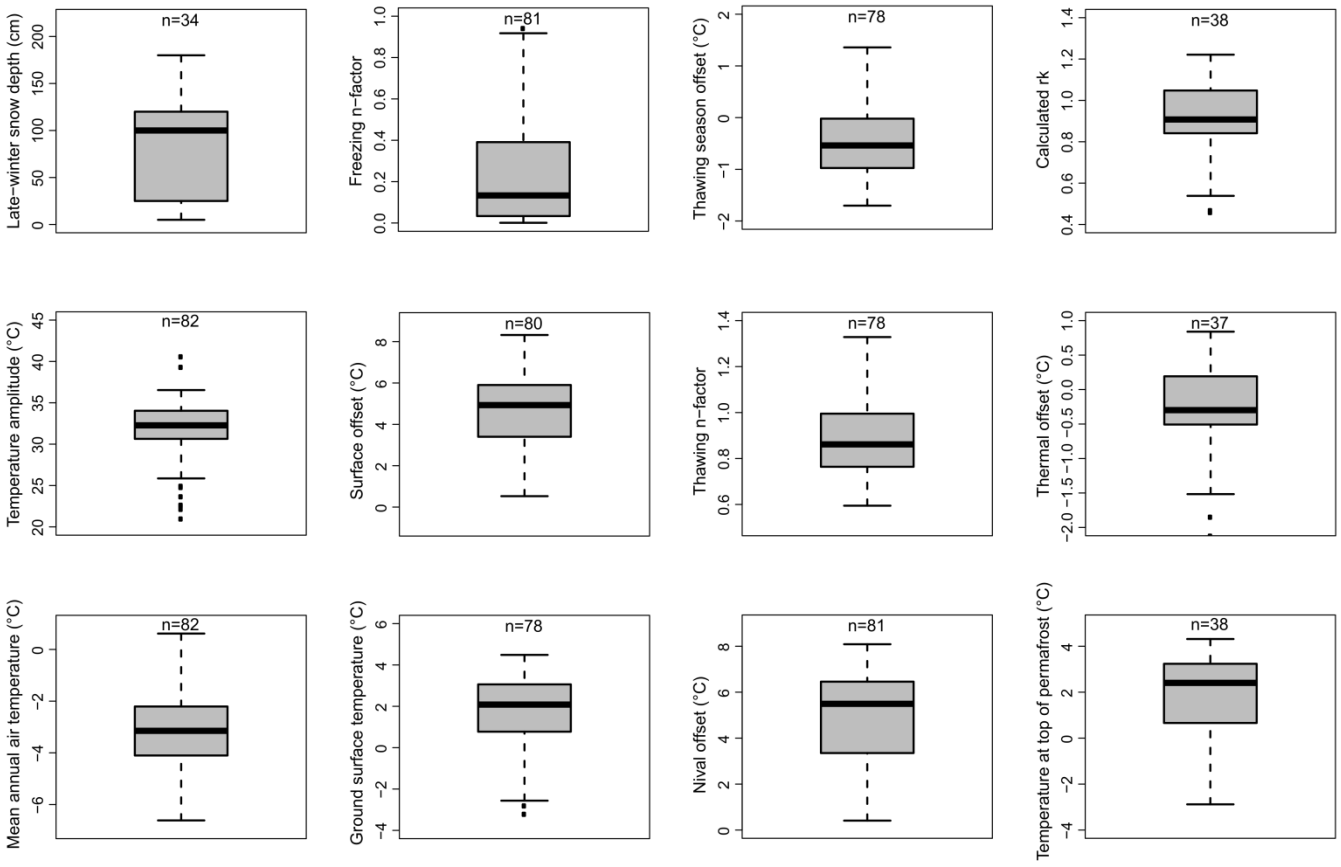

Figure 5-3: Summary of collected parameters across all monitoring stations used in this study. Note: Vertical axis values differ in units and scaling.

5.4.2 Environmental setting and measured parameters

GSTs and TTOPs showed clear differences in relation to land cover classes with the most vegetated class (forest) having the highest GSTs (median: 3.1°C) and TTOPs (median: 3.1°C), and no negative average temperatures recorded (Figure 5-4). In contrast, the least vegetated classes (rock and tundra) had much lower median GSTs of -1.9°C and 0.8°C, respectively, and values below zero were frequently recorded for both classes. No measurements were available for TTOP in the rock class but tundra sites had a median value of -1.6°C, similar to the median TTOP value of -1.4°C recorded in palsa bogs (Figure 5-4). TTOP values for forest-tundra and shrub sites were all greater than 0°C although values at some sites were close to this threshold.

WSD and LWSD also showed clear differences across the land cover classes (Figure 5-4). The greatest LWSDs were found in forest (median: 120 cm) and shrub (median: 160 cm) classes while the lowest median values were measured in palsa bogs (15 cm) and tundra (25 cm) (Figure 5-4). Similar patterns of snow redistribution were observed during snow surveys in the Mealy Mountains of eastern Labrador (Jacobs et al. 2014), in western Labrador/Québec (Granberg 1973; Granberg 1988) and in Gaspésie (Davesne et al. 2016). Freezing n-factor values were higher for palsa bog (median: 0.72; SD: 0.06) and rock classes (median: 0.77; SD: 0.13) whereas forest sites had the lowest nF values (median: 0.03) and less variability (SD: 0.03) than other classes (Figure 5-4). Tundra sites (n=21) showed the largest variability in measured nF values ranging from 0 to 0.88 (median: 0.31; SD: 0.26). Shrub (median: 0.07; SD: 0.17) and forest-tundra (median: 0.20; SD: 0.16) classes typically had low nF values with considerable variability.

Across land cover classes, variability in nT was less pronounced than in nF with greater overlap between class ranges of recorded values (Figure 5-4). Median nT values in forest environments (0.79) were the lowest with forest-tundra (0.84) and shrub (0.83) classes being the next lowest. The highest nT values were recorded in the rock class with a median of 1.17, indicating higher temperatures at the ground surface than in the air during the thaw season. Tundra site nTs (median: 0.98) were lower than those at rock sites but were higher than all other classes. nTs recorded in palsa bogs had a median value of 0.91 falling between forest-tundra and tundra observations. Within-class nT variability was greatest for tundra sites (SD: 0.16) and least for the palsa bogs (SD: 0.10). Overall, nT variability was fairly similar across the classes (SD: 0.02) whereas nF exhibited greater differences (SD: 0.08).

TOs showed minimal differences among forest-tundra, shrub and tundra classes with median values of 0.0°C, 0.1°C and -0.1°C, respectively. Forest sites showed slightly larger TOs (median: -0.4°C) while palsa bogs had very large TOs (median: -2.4°C) (Figure 5-4). Calculated rk values showed similar

across class variance to TOs with palsa bogs having the lowest median rk (0.46) and shrub having the highest (1.02). Forest-tundra and tundra both had calculated median rk values of 0.99 while forest had slightly lower rk values (median: 0.90).

5.4.3 Statistical associations

Statistically significant associations ($p < 0.05$) between the calculated parameters in Table 5-1 are shown in Table 5-3. Only the most relevant for TTOP model parameterization (e.g. nT, nF, rk, TO, SO, NVO, TSO) are described below.

Covariance between TTOP model inputs was greatest for those which were derivations of each other, such as rk and TO (r=0.99), and NVO and SO (r=0.95). Notably, nF and nT were more correlated (r=0.67) than NVO and TSO (r=-0.52). nT and TSO were nearly perfectly correlated (r=0.99) but nF and NVOs showed a slightly weaker association (r=-0.94). Amongst other parameters, TTOP and nF were strongly correlated (r=-0.92), as were TTOP and GST (r=0.92). Relevant climate parameters measured at each site showed several significant correlations with permafrost variables. For example, SO and TA were moderately correlated (r=0.54) as were SO and FDDa (r=0.48), and TDDa and GST (r=0.46). However, TTOP was not significantly correlated with MAAT or FDDa. Comparison between climate observations and nF showed no clear relation for FDDa, TDDa, MAAT and TA. In contrast, NVO was significantly correlated with TA (r=0.48) but not MAAT, FDDa or TDDa.

TTOP was highly correlated with LWSD (r=0.86), SDD (r=0.83) and WSD (r=0.86) but not SDS (Table 5-3). However, SO was correlated with all four collected parameters (LWSD, SDD, WSD, SDS) with coefficients ranging from 0.77 (LWSD) to 0.82 (SDS). The strongest relevant associations with snow variables were between nF and LWSD (r=-0.91), SDD (r=-0.90), WSD (r=-0.92) and SDS(r=-0.86). Relative to nF, slightly weaker associations were found between NVO and LWSD (r=0.84), SDD (r=-0.85) and WSD (r=0.87) but a slightly stronger correlation existed for SDS (r=0.89).

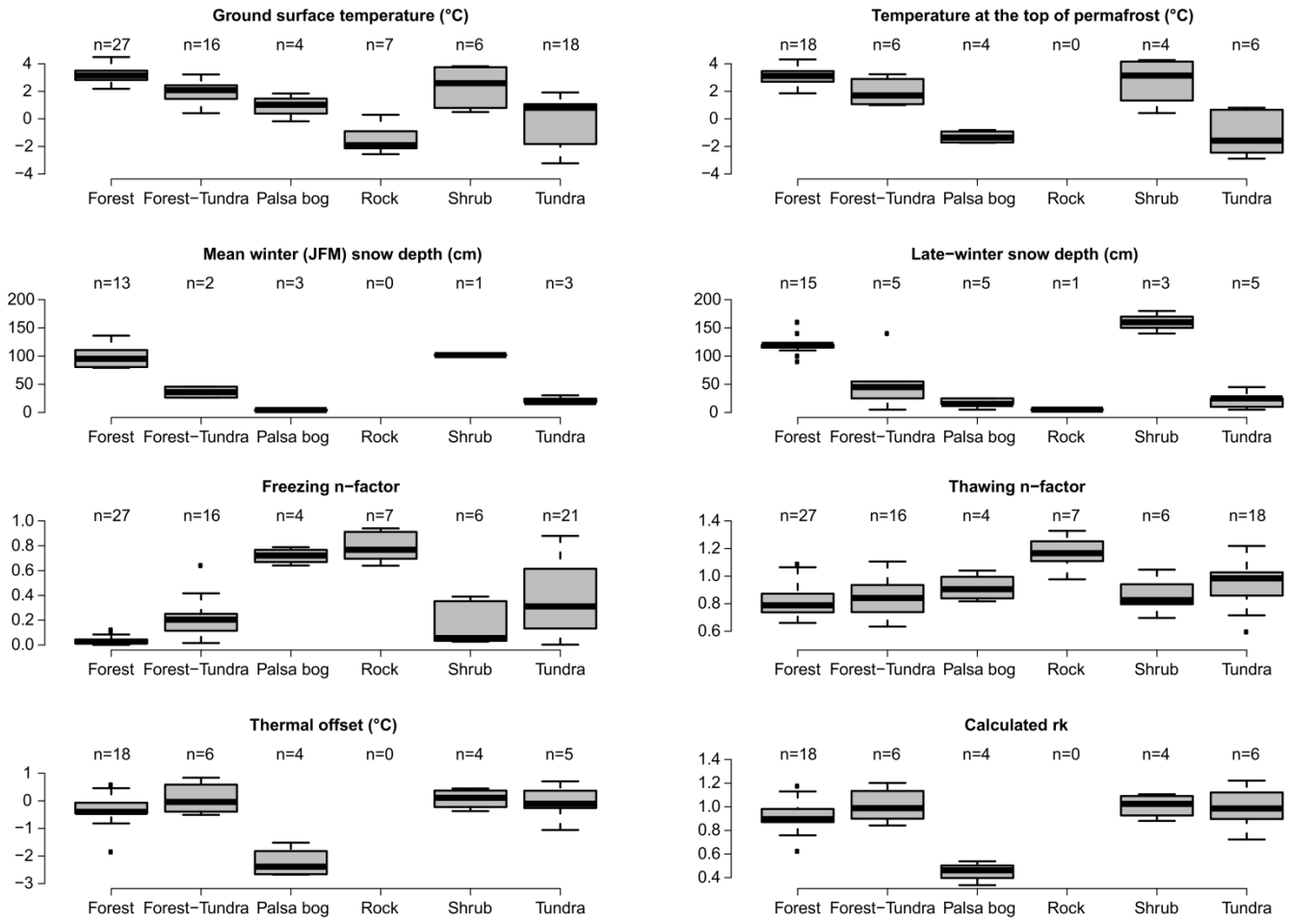

Figure 5-4: Summary of permafrost relevant parameters collected from monitoring stations used in this study stratified according to general land cover types (forest, forest-tundra, palsa bog, rock, shrub, tundra). Note: Vertical axis values differ in units and scaling.

Table 5-3: Pearson correlation coefficient (r) matrix between parameters shown in Table 5-1.

	TO	TTOP	nF	nT	rk	MAAT	TA	FDDa	FDDs	TDDa	TDDs	SO	GST	NVO	TSO	LWSD	SDD	WSD	SDS
TO	---																		
TTOP	---	---																	
nF	---	-0.92	---																
nT	---	---	0.67	---															
rk	0.99	---	---	---	---														
MAAT	---	---	---	---	---	---													
TA	---	---	---	---	---	-0.50	---												
FDDa	---	---	---	---	---	-0.81	0.80	---											
FDDs	---	-0.91	0.96	0.72	---	---	---	---	---										
TDDa	---	---	---	---	---	0.54	---	---	---	---									
TDDs	---	---	0.44	0.65	---	---	---	---	0.45	0.54	---								
SO	---	0.80	-0.84	---	---	-0.42	0.54	0.48	-0.72	---	---	---							
GST	---	0.92	-0.89	-0.54	---	---	---	---	-0.94	0.46	---	0.74	---						
NVO	---	0.83	-0.94	-0.53	---	---	0.48	---	-0.85	---	---	0.95	0.82	---					
TSO	---		0.67	0.99	---	---	---	---	0.72	---	0.63	---	-0.55	-0.52	---				
LWSD	---	0.86	-0.91	---	---	---	---	---	-0.85	---	---	0.77	0.80	0.84	---	---			
SDD	---	0.83	-0.90	---	---	---	---	---	-0.80	---	---	0.78	---	0.85	---	0.94	---		
WSD	---	0.86	-0.92	---	---	---	---	---	-0.83	---	---	0.81	0.75	0.87	---	0.96	0.98	---	
SDS	---	---	-0.86	---	---	---	0.80	---	---	---	---	0.82	---	0.89	---	0.82	0.88	0.86	---

Note: See Table 5-1 for explanation of acronyms. All correlations shown were statistically significant at $p < 0.05$ after adjustment for multiple comparisons.

5.4.4 Environmental variables and modelling

Few of the gridded environmental datasets produced statistically significant associations with the field station parameters (Table 5-4). For example, none of the topographic variables was significantly correlated ($p < 0.05$) with any station parameter. TRC30m showed the highest correlations with moderate associations found with GST (r=0.51), and strong associations with LWSD (r=0.65) and SDD (r=0.76). The only other notable statistically significant correlation was between CRF1km and TO (r=0.60) (Table 5-4).

Table 5-4: Pearson correlation coefficient (r) matrix between summary parameters in Table 5-1 and continuous gridded environmental datasets in Table 5-2 and those discussed in the text.

	NRCSD	SLP	SLPOS	TPI	TRI	TRC30m	LFORM	CRF1km	HLI
TO	---	---	---	---	---	---	---	0.60	---
TTOP	---	---	---	---	---	---	---	---	---
nF	---	---	---	---	---	---	---	---	---
nT	---	---	---	---	---	---	---	---	---
rk	---	---	---	---	---	---	---	---	---
MAAT	-0.57	---	---	---	---	---	---	-0.57	---
TA	---	---	---	---	---	---	---	---	---
FDDa	---	---	---	---	---	---	---	---	---
FDDs	---	---	---	---	---	---	---	---	---
TDDa	---	---	---	---	---	0.53	---	-0.43	---
TDDs	---	---	---	---	---	---	---	---	---
SO	---	---	---	---	---	---	---	---	---
GST	---	---	---	---	---	0.51	---	---	---
NVO	---	---	---	---	---	---	---	---	---
TSO	---	---	---	---	---	---	---	---	---
LWSD	---	---	---	---	---	0.65	---	---	---
SDD	---	---	---	---	---	0.76	---	---	---
WSD	---	---	---	---	---	---	---	---	---
SDS	---	---	---	---	---	---	---	---	---

Note: See Tables 5-1 and 5-2 for explanation of abbreviations and acronyms. All correlations shown were statistically significant at $p < 0.05$ after adjustment for multiple comparisons.

GST calculated with measured FDDa and TDDa and median n-factors for each land cover class observed at monitoring stations, exhibited a mean absolute difference of 0.75°C compared to measured GST, and a Pearson correlation coefficient of 0.79. The sensitivity of GST to misclassification in the six land cover datasets was calculated for nT and nF together and individually against the station observations and class median GSTs as described above (Table 5-5).

GSTs modelled using n-factors (nF & nT) assigned from CCRS250m, NCC2, SPOT20m and SPOT100m showed statistically significant correlations for station observations (r=0.44-0.51) and against class median scenarios (r=0.48-0.65). However, GSTs derived from CFS30m and NCC1 were not significantly correlated with observations for either comparison. The highest correlation between modelled GST scenarios and station observations was found using NCC2 (r=0.52) whereas against class medians the highest was SPOT100m (r=0.65). Mean absolute errors calculated for each GST model ranged from ±2.1°C (NCC1) to ±1.2°C (NCC2 / SPOT20m / SPOT100m) for comparisons against station observations, and ±1.8°C (NCC1) to ±0.9°C (NCC2 / SPOT20m / SPOT100m) against class medians (Table 5). NCC2 was consistently the best performing land cover classification whereas NCC1 was the worst across all model scenarios (Table 5-5). Model runs isolating only nT (nF) on average showed mean absolute errors of ±0.6°C (±1.8°C) against observations and ±0.9°C (±1.6°C) against class medians.

Table 5-5: Results of ground surface temperature modelling scenarios using various land cover datasets shown in Table 5-2 for n-factor parameterization.

Model scenario	Evaluation subset	CCRS250m	CFS30m	NCC1	NCC2	SPOT20m	SPOT100m
nF & nT MAD	Class medians	1.3	1.1	1.8	**0.9**	**0.9**	**0.9**
nF & nT MAD	Station observations	1.5	1.5	2.1	**1.2**	**1.2**	**1.2**
nT-only MAD	Class medians	**0.8**	**0.8**	1.3	**0.8**	0.9	0.9
nT-only MAD	Station observations	0.5	0.5	0.9	**0.4**	0.6	0.6
nF-only MAD	Class medians	1.6	1.4	2.8	**1.1**	1.4	1.4
nF-only MAD	Station observations	1.6	1.7	2.9	**1.3**	1.5	1.5

Note: Datasets with the best performance statistics for each scenario are bolded while the worst are underlined. MAD = Mean absolute difference (°C).

5.5 Discussion

5.5.1 Associations with land cover

Measured station parameters linked to permafrost modelling (e.g. nF, nT, GST, TTOP) varied according to land cover class, as has been found previously for subarctic and arctic environments (Juliussen and Humlum 2007; Jorgenson et al. 2010; Lewkowicz et al. 2012; Bevington and Lewkowicz 2015). Despite low MAATs, the only land cover classes that included negative TTOPs were rock, palsa bogs or tundra. A surprising result was the absence of statistically significant associations between MAAT and either GST or TTOP. This is likely a reflection of pervasive deep snow throughout Labrador and challenges the traditional usage of MAAT as a proxy for permafrost distribution in this region.

Observed nT variability was similar to observations in Alaska, the Northwest Territories, southern Yukon and southern Norway, with lower nT values recorded in forested zones and higher values in exposed rock and barren areas (Juliussen and Humlum 2007; Jorgenson et al. 2010; Lewkowicz et al. 2012; Gisnås et al. 2013; Bevington and Lewkowicz 2015; Morse et al. 2016). Accordingly, forest and rock nT values in Labrador were not statistically distinguishable from those in the Yukon (forest: $t = -0.92$, $p > 0.2$; rock: $t = -0.48$, $p > 0.2$) (Bevington and Lewkowicz 2015). These comparisons support previous inferences that nT values classed by vegetation cover are transferable between regions (e.g. Lewkowicz et al. 2012).

The distribution of measured values for nF in Labrador were lower in most classes compared to western Canada (Bevington and Lewkowicz 2015). This was due to thicker snow covers in the more heavily vegetated environments while less vegetated barren surfaces remained wind-scoured (Granberg 1994; e.g. Davesne et al. 2016). GST and TTOP values were all positive for forested sites but given the southerly distribution of the monitoring network, it cannot be concluded that permafrost does not exist anywhere in forested areas in Labrador. Moreover, permafrost has been inferred from electrical resistivity profiling at a forested site in Nain, NL (56.5°N) (Way and Lewkowicz 2015) and isolated patches of forest permafrost were encountered near Wabush (53°N) (Brown 1979) and Schefferville (55°N) (Granberg 1989) during the past 50 years.

The question of permafrost presence and vegetation cover was explored further by calculating critical nFs where TTOP = 0°C (nF_{crit}) (Smith and Riseborough 2002) for the monitoring sites. nF_{crit} varied from 0.27 to 0.71 with the lowest values typically found in the palsa bogs and forested sites. Critical late-winter snow depths ($LWSD_{crit}$) estimated using a 2nd degree polynomial fit between nF and LWSD ($r^2 = 0.83$; $p < 0.01$) ranged from 12 to 70 cm. Comparison between observed LWSD and $LWSD_{crit}$ show that none of the forested or shrub sites were close to having snow covers that were sufficiently shallow to permit permafrost to be present (Figure 5). In contrast, a number of forest-tundra sites were near or below

the critical snow threshold for permafrost formation, while most of the tundra sites and all of the palsa bog stations were below it. These results support previous conclusions from sites in western Labrador/Québec south of 55°N that permafrost is very rarely present in the forest or tundra where late-winter snow thicknesses exceed 75 cm (Nicholson 1979; Allard and Séguin 1987; Granberg 1988; Granberg 1989). They also contrast with the situation in northwest Canada and Alaska where permafrost is common in forested environments with less precipitation, albeit at higher latitudes (Jorgenson et al. 2010; Lewkowicz et al. 2011; Lewkowicz et al. 2012; Morse et al. 2016).

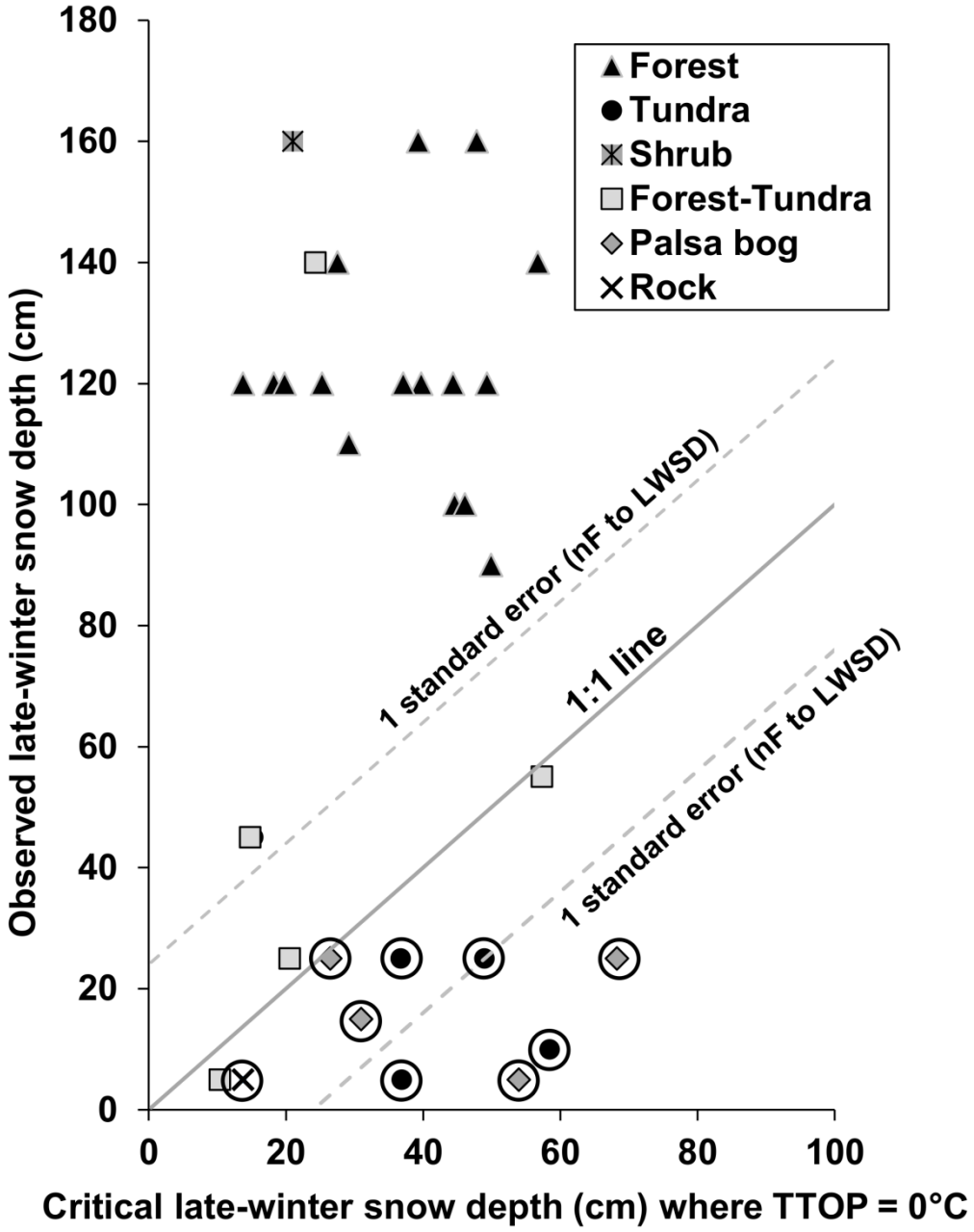

Figure 5-5: Comparison between late-winter snow depths recorded at monitoring stations and calculated critical late-winter snow depths required for permafrost occurrence (TTOP = 0°C) at each site. Areas above the 1:1 line are inferred to be absent of permafrost under equilibrium conditions whereas areas below are inferred to have permafrost. Critical late-winter snow depths were developed by first calculating critical freezing n-factors for each site using: nF_{crit} = (rk * TDDa * nT) / FDDa. Critical freezing n-factors were then converted to late-winter snow depths using the following polynomial equation (r^2 = 0.83; p-value < 0.01; standard error = ± 24 cm) derived from the monitoring station data: LWSD = (180.12*nF^2) – 306.43*nF) + 140.26. Note: Sites with permafrost observed are circled.

5.5.2 Snow and freezing n-factors

Riseborough (2004) showed on the basis of 1-D numerical simulations with the TONE program (Goodrich 1978; Goodrich 1982) that there was a stronger linkage between NVO and local (air) climate conditions (e.g. MAAT) than with nF. This interpretation is partially supported by the statistically significant correlation observed between TA and NVO whereas no significant correlation was found between any climate parameters and nF (Table 5-3). In contrast, the various snow depth parameters (except SDS) were more strongly related to nF than to NVO.

Although the linear associations between nF and snow depth parameters were moderate to strong, the association was best described by a 3rd degree polynomial (r=0.85) or log-normal relation (r=0.81). This statistical association is comparable to observational studies across the Northern Hemisphere which show a consistent curvilinear association between nF and LWSD (Ménard et al. 1998; Juliussen and Humlum 2007; Karunaratne et al. 2008; Morse et al. 2012; Gisnås et al. 2013; Davesne et al. 2016; Gisnås et al. 2016b; Morse et al. 2016) (Figure 5-6). However, given the considerable variability among these studies, it can be assumed that applying nF-snow depth associations from individual studies to broader regions could result in significant errors at TTOP. For example, the n-factor parameterization approach undertaken by Gisnås et al. (2016b), and used throughout Scandinavia, would overestimate nF in North American regions at late-winter snow depths between 50-200 cm (Figure 5-6). The impact of this on TTOP at the Labrador stations was assessed by using Labrador LWSD data with the logarithmic curve in Figure 5-6 to develop nF, and then determining corresponding TTOP using measured nT, FDD, TDD and rk values.

Comparison of modelled TTOP values produced in this way with observations reveal a moderate systematic temperature bias with a mean difference of -0.5°C and a mean absolute difference of ±1.1°C (Figure 5-7). For comparison, repeating this same calculation procedure using the numerical model-based nF parameterization approach of Way and Lewkowicz (2016) produces less biased results and smaller errors at TTOP (mean difference: 0°C / mean absolute difference: ±0.5°C) (Figure 5-7). These comparisons challenge the notion that statistical associations with nF from localized field data are transferable between regions while suggesting that nF calculation can be guided by numerical simulations and/or diverse compilations of field data.

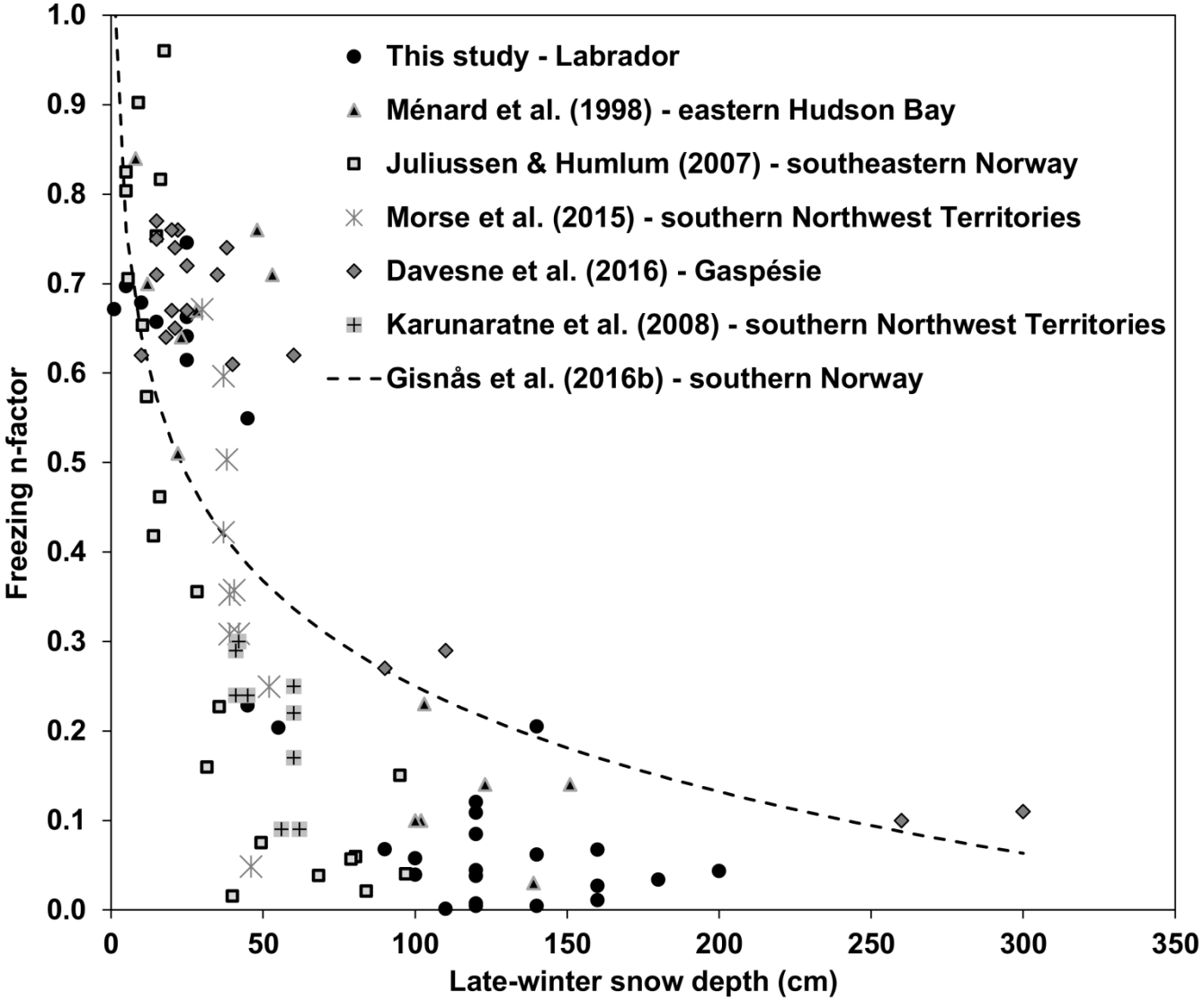

Figure 5-6: Comparison between late-winter snow depth and freezing n-factors for five different studies in high latitude Subarctic or low Arctic locations. A logarithmic fit (nF = (-0.17*ln(LWSD)) + 0.25) used by Gisnås et al. (2016b) for southern Norway is shown for comparison.

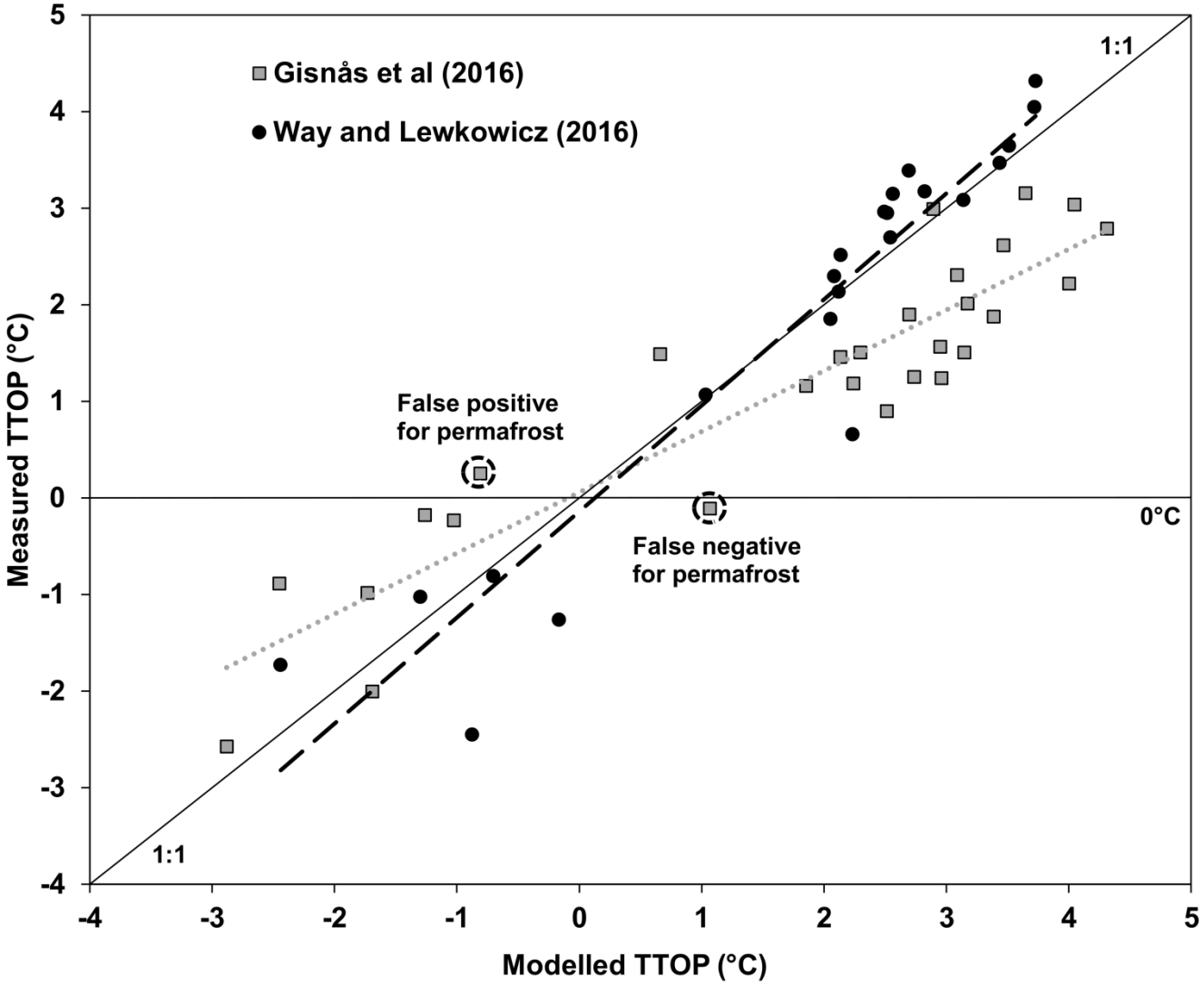

Figure 5-7: Modelled vs. measured temperatures at the top of permafrost for Labrador monitoring stations with freezing n-factors derived from the logarithmic fit with late-winter snow depth of Gisnås et al. (2016b) (see Figure 5-6) and using TONE simulations based on mean annual air temperature and average winter snow depths (Way and Lewkowicz 2016).

5.5.3 Environmental variables and prediction

The overall accuracy of TTOP modelling and the implications of land cover dataset selection has rarely been examined in detail for large samples. Our tests showed that using gridded land cover datasets resulted in average errors in modelled GST values of at least ±1°C due to the combined effects of using class median n-factors to model continuous parameters (> ±0.75°C) and the mischaracterization of land cover types in gridded datasets. The propagation of errors due to land cover types was mainly due to mischaracterization of nF which showed average errors twice as large as those due to nT (Table 5-5). Correlations between observed and modelled values across land cover datasets were generally low to moderate, with SPOT-based products (Olthof et al. 2015) consistently showing smaller biases. Surprisingly, the performance of the SPOT-based modelling did not appreciably decline with a change in resolution from 20 m to 100 m. The widely-used CFS30m product consistently produced high GST errors, suggesting that a different land cover dataset might have reduced errors at TTOP in Bevington and Lewkowicz (2015).

Several key points emerged from these analyses. First, increased spatial resolution of land cover datasets did not always result in a higher accuracy in representing GSTs. Second, statistical associations between various environmental and gridded datasets were relatively weak for most datasets and particularly for topographic indices. Third, simplified products such as tree cover percentage (TRC30m) produced comparable correlations to higher quality land cover classifications for some variables. However, while the TRC30m product did discriminate between forested and tundra classes at monitoring stations, it could not reliably do so between partially vegetated classes (Figure B3). Fourth, elucidating the influence of vegetation cover and surficial materials on the magnitude of TO (and calculated rk) remains a priority for future work. The moderate statistical correlations between coarse fragment percentage (CRF1km) (Hengl et al. 2014) and measured TO provides an indication of progress in representing surficial materials at finer spatial scales.

5.6 Conclusion

A number of conclusions can be reached based on this analysis of monitoring station data and gridded datasets in Labrador.

Observed differences in freezing and thawing season offset parameters were strongly linked to land cover types, albeit with considerable inter-site variability for less vegetated environments. Consequently, permafrost was absent at forested and heavily vegetated locations but was generally present at barren and rock sites. The absence of permafrost at forested sites, despite low mean annual air temperatures, was the

result of deep snow accumulation, with most locations having double the minimum depth of late-winter snow necessary to prevent permafrost formation. In contrast, late-winter snow depths at rock and tundra sites were typically shallow enough to permit permafrost presence, and shallow snow depths coupled with large thermal offsets allowed permafrost to exist in palsa bogs.

Comparison with other empirical field studies from discontinuous permafrost environments shows that the association between late-winter snow depth and observed freezing n-factors is consistently curvilinear. However, model tests suggest that the use of geographically-limited field datasets for characterizing these relations can result in average errors of at least ±1.1°C when applied to other regions.

Analysis of the suitability of gridded environmental datasets for parameterizing permafrost spatial modelling showed an average overall error of ±1.5°C with a range from ±0.9°C to ±2.1°C. These errors are similar in magnitude to those reported by Bevington and Lewkowicz (2015). Overall, these data suggest that careful analysis of the utility of land cover datasets is needed prior to their use for spatial modelling of ground temperatures and also that datasets of higher spatial resolution may not necessarily produce smaller modelling errors.

Acknowledgements

The authors are grateful to Dr. Darroch Whitaker of Parks Canada and Dr. John Jacobs of Memorial University of Newfoundland for generously providing monitoring station data that greatly helped to facilitate this study. We would also like to thank field assistants Alexander Brooker, Maxime Duguay and Caitlin Lapalme for their efforts in establishing and retrieving data at the University of Ottawa monitoring stations. The manuscript was improved through useful commentary and discussions with Dr. Luise Hermanutz, Dr. Philip Bonnaventure and Alexandre Bevington. The authors would like to thank community members of Cartwright for their help in identifying suitable sites for monitoring stations and for the logistical support provided by Patricia Way, Gary Bird, George Way and Brenda Way. RGW would like to acknowledge financial support from the Natural Sciences and Engineering Research Council of Canada, the W. Garfield Weston Foundation, the Royal Canadian Geographic Society, the University of Ottawa and the Northern Scientific Training Program. AGL acknowledges financial support from the Natural Sciences and Engineering Research Council of Canada and the University of Ottawa.

5.7 References

Allard, M., and M. K. Séguin. 1987. Le pergélisol au Québec nordique : bilan et perspectives. Géographie physique et Quaternaire 41(1): 141. doi: 10.7202/032671ar.

Bevington, A., and A. G. Lewkowicz. 2015. Assessment of a land cover driven TTOP model for mountain and lowland permafrost using field data, southern Yukon and northern British Columbia, Canada. In Proceedings of GéoQuebec: 68th Canadian Geotechnical Conference and 7th Canadian Permafrost Conference, 9. Québec City, Canada.

Bonnaventure, P. P., A. G. Lewkowicz, M. Kremer, and M. C. Sawada. 2012. A permafrost probability model for the southern Yukon and northern British Columbia, Canada. Permafrost and Periglacial Processes 23(1): 52–68. doi: 10.1002/ppp.1733.

Brown, R. J. 1979. Permafrost distribution in the southern part of the discontinuous zone in Quebec and Labrador. Géographie physique et Quaternaire 33(3–4): 279–289.

Davesne, G., D. Fortier, F. Dominé, and J. T. Gray. 2016. Wind driven snow conditions control the occurrence of contemporary marginal mountain permafrost in the Chic-Chocs Mountains, south-eastern Canada - a case study from Mont Jacques-Cartier. The Cryosphere Discussions: 1–31. doi: 10.5194/tc-2016-211.

Dilts, T. 2016. Topography Tools for ArcGIS 10.3 and earlier. http://www.arcgis.com/home/item.html?id=b13b3b40fa3c43d4a23a1a09c5fe96b9.

Gisnås, K., B. Etzelmüller, H. Farbrot, T. V. Schuler, and S. Westermann. 2013. CryoGRID 1.0: Permafrost distribution in Norway estimated by a spatial numerical model. Permafrost and Periglacial Processes 24(1): 2–19. doi: 10.1002/ppp.1765.

Gisnås, K., B. Etzelmüller, C. Lussana, J. Hjort, A. B. K. Sannel, K. Isaksen, S. Westermann, P. Kuhry, H. H. Christiansen, A. Frampton, and J. Åkerman. 2016a. Permafrost Map for Norway, Sweden and Finland: Permafrost map for Norway, Sweden and Finland. Permafrost and Periglacial Processes. doi: 10.1002/ppp.1922.

Gisnås, K., S. Westermann, T. V. Schuler, K. Melvold, and B. Etzelmüller. 2016b. Small-scale variation of snow in a regional permafrost model. The Cryosphere 10(3): 1201–1215. doi: 10.5194/tc-10-1201-2016.

Goodrich, L. E. 1978. Some results of a numerical study of ground thermal regimes. In Proceedings of the 3rd International Conference on Permafrost, 30–34. Edmonton, Canada: National Research Council of Canada.

Goodrich, L. E. 1982. The influence of snow cover on the ground thermal regime. Canadian Geotechnical Journal 19(4): 421–432. doi: 10.1139/t82-047.

Granberg, H. B. 1973. Indirect mapping of the snowcover for permafrost prediction at Schefferville, Québec. In Proceedings of the 2nd International Conference on Permafrost, 113–120. Washington, USA.

Granberg, H. B. 1988. On the spatial dynamics of snowcover - permafrost relationships at Schefferville. In Proceedings of the 5th International Conference on Permafrost, 159–164. Trondheim, Norway.

Granberg, H. B. 1989. Permafrost mapping at Schefferville, Québec. Physical Geography 10(3): 249–269.

Granberg, H. B. 1994. Mapping heat loss zones for permafrost prediction at the northern/alpine limit of the Boreal forest using high-resolution C-Band SAR. Remote sensing of environment 50(3): 280–286.

Gubler, S., J. Fiddes, M. Keller, and S. Gruber. 2011. Scale-dependent measurement and analysis of ground surface temperature variability in alpine terrain. The Cryosphere 5(2): 431–443. doi: 10.5194/tc-5-431-2011.

Gubler, S., S. Endrizzi, S. Gruber, and R. S. Purves. 2013. Sensitivities and uncertainties of modeled ground temperatures in mountain environments. Geoscientific Model Development 6(4): 1319–1336. doi: 10.5194/gmd-6-1319-2013.

Heginbottom, J. A., M.-A. Dubreuil, and P. A. Harker. 1995. Canada – Permafrost. National Atlas of Canada, 5th Edition. Ottawa, Canada: Natural Resources Canada.

Hengl, T., J. M. de Jesus, R. A. MacMillan, N. H. Batjes, G. B. M. Heuvelink, E. Ribeiro, A. Samuel-Rosa, B. Kempen, J. G. B. Leenaars, M. G. Walsh, and M. R. Gonzalez. 2014. SoilGrids1km — Global soil information based on automated mapping. Edited by Ben Bond-Lamberty. PLoS ONE 9(8): e105992. doi: 10.1371/journal.pone.0105992.

Henry, K., and M. Smith. 2001. A model-based map of ground temperatures for the permafrost regions of Canada. Permafrost and Periglacial Processes 12(4): 389–398. doi: 10.1002/ppp.399.

Jacobs, J. D., S. Chan, and E. Sutton. 2014. Climatology of the Forest-Tundra Ecotone at a Maritime Subarctic-Alpine Site, Mealy Mountains, Labrador. ARCTIC 67(1): 28–42. doi: 10.14430/arctic4358.

Jafarov, E. E., S. S. Marchenko, and V. E. Romanovsky. 2012. Numerical modeling of permafrost dynamics in Alaska using a high spatial resolution dataset. The Cryosphere 6(3): 613–624. doi: 10.5194/tc-6-613-2012.

Jorgenson, M. T., V. Romanovsky, J. Harden, Y. Shur, J. O'Donnell, E. A. G. Schuur, M. Kanevskiy, and S. Marchenko. 2010. Resilience and vulnerability of permafrost to climate change. Canadian Journal of Forest Research 40(7): 1219–1236. doi: 10.1139/X10-060.

Juliussen, H., and O. Humlum. 2007. Towards a TTOP ground temperature model for mountainous terrain in central-eastern Norway. Permafrost and Periglacial Processes 18(2): 161–184. doi: 10.1002/ppp.586.

Karunaratne, K. C., S. V. Kokelj, and C. R. Burn. 2008. Near-surface permafrost conditions near Yellowknife, Northwest Territories, Canada. In Proceedings of the 9th International Conference on Permafrost, 907–912. Fairbanks, Alaska, United States of America: Institute of Northern Engineering, University of Alaska-Fairbanks.

Lewkowicz, A. G. 2008. Evaluation of miniature temperature-loggers to monitor snowpack evolution at mountain permafrost sites, northwestern Canada. Permafrost and Periglacial Processes 19(3): 323–331. doi: 10.1002/ppp.625.

Lewkowicz, A. G., B. Etzelmüller, and S. L. Smith. 2011. Characteristics of discontinuous permafrost based on ground temperature measurements and electrical resistivity tomography, southern Yukon, Canada. Permafrost and Periglacial Processes 22(4): 320–342. doi: 10.1002/ppp.703.

Lewkowicz, A. G., P. P. Bonnaventure, S. L. Smith, and Z. Kuntz. 2012. Spatial and thermal characteristics of mountain permafrost, northwest Canada. Geografiska Annaler: Series A, Physical Geography 94(2): 195–213.

Maxwell, J. B. 1981. Climatic regions of the Canadian Arctic Islands. ARCTIC 34(3): 225–240.

McCune, B., D. Keon, and R. H. Marrs. 2002. Equations for potential annual direct incident radiation and heat load. Journal of vegetation science 13(4): 603–606.

Ménard, É., M. Allard, and Y. Michaud. 1998. Monitoring of ground surface temperatures in various biophysical micro-environments near Umiujaq, eastern Hudson Bay, Canada. In Proceedings of the 7th International Conference on Permafrost, 723–729. Yellowknife, Canada.

Morse, P. D., C. R. Burn, and S. V. Kokelj. 2012. Influence of snow on near-surface ground temperatures in upland and alluvial environments of the outer Mackenzie Delta, Northwest Territories. Canadian Journal of Earth Sciences 49(8): 895–913. doi: 10.1139/e2012-012.

Morse, P. D., S. A. Wolfe, S. V. Kokelj, and A. J. R. Gaanderse. 2016. The occurrence and thermal disequilibrium state of permafrost in forest ecotopes of the Great Slave Region, Northwest Territories, Canada. Permafrost and Periglacial Processes 27(2): 145–162. doi: 10.1002/ppp.1858.

Nicholson, F. H. 1979. Permafrost spatial and temporal variations near Schefferville, Nouveau-Québec. Géographie physique et Quaternaire 33(3–4): 265–277. doi: 10.7202/1000363ar.

Nicolsky, D. J., V. E. Romanovsky, santosh K. panda, S. Marchenko, and R. R. Muskett. 2016. Applicability of the ecosystem type approach to model permafrost dynamics across the Alaska North Slope. Journal of Geophysical Research: Earth Surface. doi: 10.1002/2016JF003852.

Occhietti, S., M. Parent, P. Lajeunesse, F. Robert, and E. Govare. 2011. Late Pleistocene–Early Holocene decay of the Laurentide Ice Sheet in Québec-Labrador. Developments in Quaternary Science 11: 601–630. doi: 10.1016/B978-0-444-53447-7.00047-7.

Olthof, I., R. Latifovic, and D. Pouliot. 2015. A medium resolution land cover map of Canada's forested regions from 2005-2010 SPOT 4/5 data. 4.

Ou, C., A. LaRocque, B. Leblon, Y. Zhang, K. Webster, and J. McLaughlin. 2016a. Modelling and mapping permafrost at high spatial resolution using Landsat and Radarsat-2 images in Northern Ontario, Canada: Part 2 – regional mapping. International Journal of Remote Sensing 37(12): 2751–2779. doi: 10.1080/01431161.2016.1151574.

Ou, C., B. Leblon, Y. Zhang, A. LaRocque, K. Webster, and J. McLaughlin. 2016b. Modelling and mapping permafrost at high spatial resolution using Landsat and Radarsat images in northern Ontario, Canada: Part 1 – model calibration. International Journal of Remote Sensing 37(12): 2727–2750. doi: 10.1080/01431161.2016.1157642.

Porada, P., A. Ekici, and C. Beer. 2016. Effects of bryophyte and lichen cover on permafrost soil temperature at large scale. The Cryosphere 10(5): 2291–2315. doi: 10.5194/tc-10-2291-2016.

Riley, S. J. 1999. Index that quantifies topographic heterogeneity. intermountain Journal of sciences 5(1–4): 23–27.

Riseborough, D. 2007. The effect of transient conditions on an equilibrium permafrost-climate model. Permafrost and Periglacial Processes 18(1): 21–32. doi: 10.1002/ppp.579.

Riseborough, D., N. Shiklomanov, B. Etzelmüller, S. Gruber, and S. Marchenko. 2008. Recent advances in permafrost modelling. Permafrost and Periglacial Processes 19(2): 137–156. doi: 10.1002/ppp.615.

Riseborough, D. W. 2002. The mean annual temperature at the top of permafrost, the TTOP model, and the effect of unfrozen water. Permafrost and Periglacial Processes 13(2): 137–143. doi: 10.1002/ppp.418.

Riseborough, D. W. 2004. Exploring the parameters of a simple model of the permafrost-climate relationship. PhD Thesis, Ottawa: Carleton University.

Roberts, B. A., N. P. P. Simon, and K. W. Deering. 2006. The forests and woodlands of Labrador, Canada: ecology, distribution and future management. Ecological Research 21(6): 868–880. doi: 10.1007/s11284-006-0051-7.

Sazonova, T. S., and V. E. Romanovsky. 2003. A model for regional-scale estimation of temporal and spatial variability of active layer thickness and mean annual ground temperatures. Permafrost and Periglacial Processes 14(2): 125–139. doi: 10.1002/ppp.449.

Shur, Y. L., and M. T. Jorgenson. 2007. Patterns of permafrost formation and degradation in relation to climate and ecosystems. Permafrost and Periglacial Processes 18(1): 7–19. doi: 10.1002/ppp.582.

Smith, M. W., and D. W. Riseborough. 1996. Permafrost monitoring and detection of climate change. Permafrost and Periglacial Processes 7(4): 301–309. doi: 10.1002/(SICI)1099-1530(199610)7:4<301::AID-PPP231>3.0.CO;2-R.

Smith, M. W., and D. W. Riseborough. 2002. Climate and the limits of permafrost: a zonal analysis. Permafrost and Periglacial Processes 13(1): 1–15. doi: 10.1002/ppp.410.

Tarasov, L., and W. R. Peltier. 2007. Coevolution of continental ice cover and permafrost extent over the last glacial-interglacial cycle in North America. Journal of Geophysical Research 112(F2). doi: 10.1029/2006JF000661.

Trant, A. J., K. Lewis, B. H. Cranston, J. A. Wheeler, R. G. Jameson, J. D. Jacobs, L. Hermanutz, and B. M. Starzomski. 2015. Complex changes in plant communities across a Subarctic alpine tree line in Labrador, Canada. ARCTIC 68(4): 500. doi: 10.14430/arctic4528.

Way, R. G., and A. G. Lewkowicz. 2015. Investigations of discontinuous permafrost in coastal Labrador with DC electrical resistivity tomography. In Proceedings of GéoQuebec: 68th Canadian Geotechnical Conference and 7th Canadian Permafrost Conference, 8. Québec City, Canada. doi: 10.13140/RG.2.1.1647.8803.

Way, R. G., and A. G. Lewkowicz. 2016. Modelling the spatial distribution of permafrost in Labrador–Ungava using the temperature at the top of permafrost. Canadian Journal of Earth Sciences 53(10): 1010–1028. doi: 10.1139/cjes-2016-0034.

Way, R. G., A. G. Lewkowicz, and P. P. Bonnaventure. 2017a. Development of moderate-resolution gridded monthly air temperature and degree-day maps for the Labrador-Ungava region of northern Canada. International Journal of Climatology 37(1): 493–508. doi: 10.1002/joc.4721.

Westermann, S., T. I. Østby, K. Gisnås, T. V. Schuler, and B. Etzelmüller. 2015a. A ground temperature map of the North Atlantic permafrost region based on remote sensing and reanalysis data. The Cryosphere 9(3): 1303–1319. doi: 10.5194/tc-9-1303-2015.

Westermann, S., C. R. Duguay, G. Grosse, and A. Kääb. 2015b. Remote sensing of permafrost and frozen ground. In Remote Sensing of the Cryosphere, ed. M. Tedesco, 307–344. John Wiley & Sons, Ltd.

Woo, M., A. G. Lewkowicz, and W. R. Rouse. 1992. Response of the Canadian permafrost environment to climatic change. Physical Geography 13(4): 287–317. doi: 10.1080/02723646.1992.10642459.

Wright, J. F., C. Duchesne, and M. M. Côté. 2003. Regional-scale permafrost mapping using the TTOP ground temperature model. In Proceedings of the 8th International Conference on Permafrost, 1241–1246. Zürich, Switzerland.

Zhang, Y. 2013. Spatio-temporal features of permafrost thaw projected from long-term high-resolution modeling for a region in the Hudson Bay Lowlands in Canada. Journal of Geophysical Research: Earth Surface 118(2): 542–552. doi: 10.1002/jgrf.20045.

Zhang, Y., X. Wang, R. Fraser, I. Olthof, W. Chen, D. Mclennan, S. Ponomarenko, and W. Wu. 2013. Modelling and mapping climate change impacts on permafrost at high spatial resolution for an Arctic region with complex terrain. The Cryosphere 7(4): 1121–1137. doi: 10.5194/tc-7-1121-2013.

Zhang, Y., I. Olthof, R. Fraser, and S. A. Wolfe. 2014. A new approach to mapping permafrost and change incorporating uncertainties in ground conditions and climate projections. The Cryosphere 8(6): 2177–2194. doi: 10.5194/tc-8-2177-2014.

Zhao, S.-P., Z.-T. Nan, Y.-B. Huang, and L. Zhao. 2017. The application and evaluation of simple permafrost distribution models on the Qinghai-Tibet Plateau. Permafrost and Periglacial Processes. doi: 10.1002/ppp.1939.

CHAPTER 6: MODELLING THE SPATIAL DISTRIBUTION OF PERMAFROST IN LABRADOR-UNGAVA USING THE TEMPERATURE AT THE TOP OF PERMAFROST

Abstract

Permafrost zonation in Labrador-Ungava ranges from very isolated patches through to continuous. Here we present a new estimate of the distribution of permafrost at high resolution (250 m x 250 m) using spatial numerical modelling supported by station data from 29 air and ground climate monitoring stations. Permafrost presence was estimated using a modified version of the temperature at the top of permafrost (TTOP) model. Mean ground surface temperatures were modelled using gridded air temperatures and a novel n-factor parameterization scheme that compensates for regional differences in continentality, snowfall and land cover and is transferable to other Subarctic environments. The thermal offset was modelled using land cover and surficial material datasets. Predicted TTOP temperatures for the average climate range regionally from -9°C (for high elevations in northern Québec) to +5°C (for southeastern Labrador-Québec). Modelling for specific temporal windows (1948-1962; 1982-1996; 2000-2014) suggests that permafrost area increased from the middle of the 20th Century to a potential peak extent (36% of the total land area) in the 1990s. Subsequent warming is predicted to have caused a decrease in permafrost extent of one-quarter (95 000 km^2) even if air temperatures rise no further, providing air and ground temperatures equilibrate. Zonal boundaries derived by upscaling the high resolution model are highly scale-dependent precluding direct comparison to the Permafrost Map of Canada that was generated without the use of GIS-based analyses.

6.1 Introduction

Rapid changes in permafrost conditions have been observed in the Québec portion of Labrador-Ungava in eastern Canada (Payette et al. 2004; Thibault and Payette 2009; Allard et al. 2012b) but there is limited information describing ground temperatures within Labrador itself. Air temperatures in Labrador have risen by more than 1°C over the past three decades (Way and Viau 2015) and satellite remote sensing indicates that regional ground surface temperatures have also increased (Hachem et al. 2009; Comiso and Hall 2014). The Permafrost Map of Canada (Heginbottom et al. 1995) shows the southernmost limit of discontinuous permafrost in eastern Labrador-Ungava lying close to the 50°N parallel. Changes in the distribution and thickness of permafrost in the region are probably underway but have not been quantified because little information has been collected since surveys in the 1960s (Brown 1975; Brown 1979), especially in the Labrador sector.

The paucity of recent field observations represents a major challenge for modelling present and future permafrost conditions in the region. Projected mineral and resource development and the construction of associated infrastructure require this information to avoid structural damage associated with future permafrost degradation (e.g. Smith and Riseborough 2010). The two alpine national parks in Labrador (Torngat Mountains established 2005, Mealy Mountains established 2016; Figure 6-1) are undergoing rapid environmental change (Fraser et al. 2011; Brown et al. 2012; McLennan et al. 2012; Way et al. 2014; Way et al. 2015) but there is little knowledge of permafrost dynamics inside their boundaries or how these changes may impact local ecosystems. Thawing permafrost has also had impacts in Nain (see Figure 6-1) where subsidence has caused damage to several buildings in the community (Way and Lewkowicz 2015).

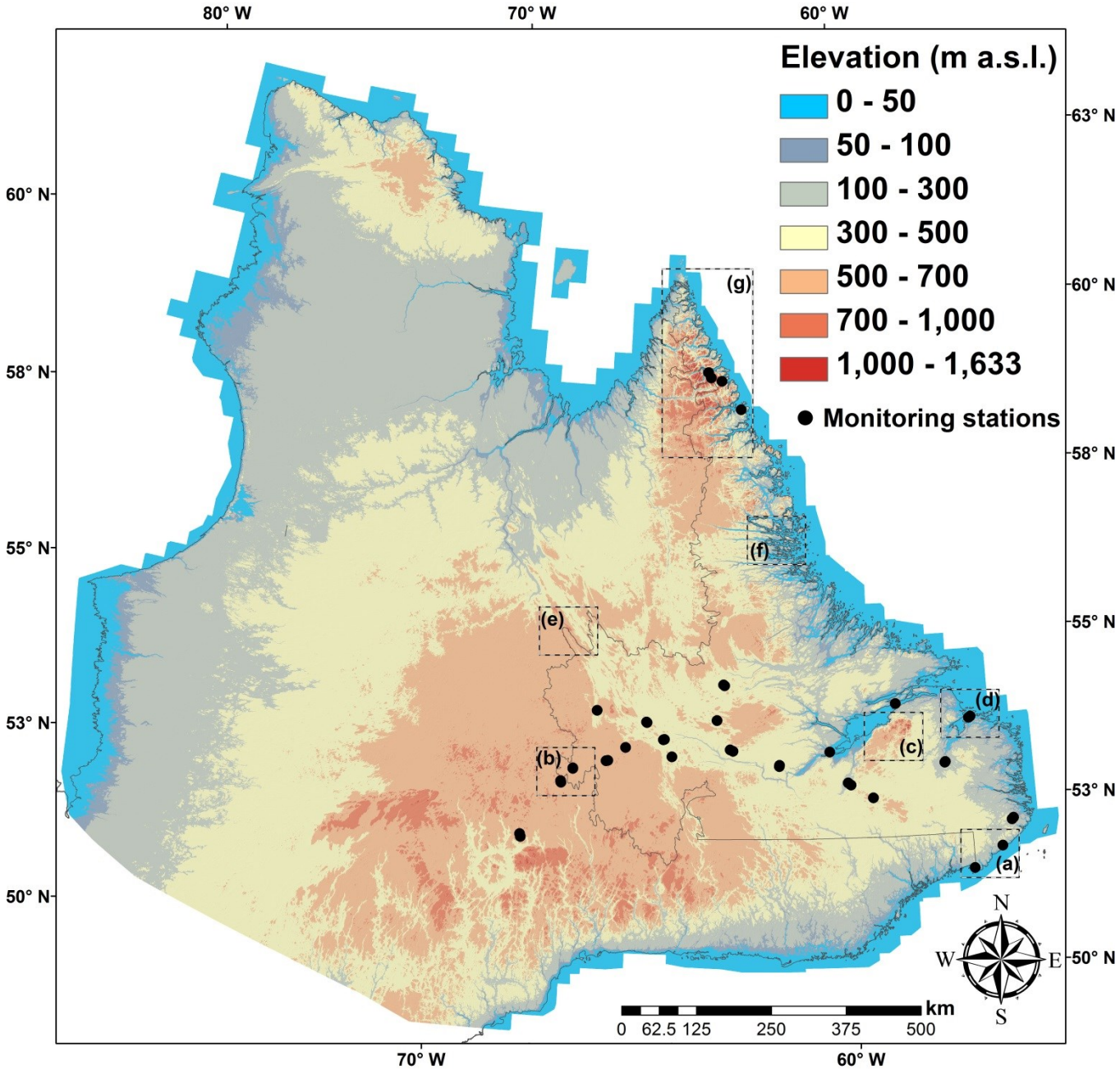

Figure 6-1: Digital elevation model from the National Topographic Database of the Labrador-Ungava region reclassified according to major elevation classes. Dotted boxes depict regions mentioned in the text: (a) Blanc Sablon, QC; (b) Labrador City, NL and Fermont, QC; (c) the Mealy Mountains; (d) Cartwright, NL; (e) Schefferville, QC; (f) Nain, NL and; (g) the Torngat Mountains. Black dots illustrate the locations of monitoring stations used in this study.

Several maps portraying permafrost conditions in Labrador-Ungava have been produced over the past several decades (e.g. Brown 1975; Brown 1979; Ives 1979; Allard and Séguin 1987; Heginbottom et al. 1995; Payette 2001; Allard et al. 2012b; Gruber 2012) (Figure 6-2). Most show broad zones and do not take into account the physiographic, topographic and vegetation contrasts in uplands and mountains. Extensive work in Schefferville (see Figure 6-1) in the 1960s and 1970s, however, demonstrated the importance of snow cover for permafrost distribution. Forested areas lacked permafrost while at higher elevation, thin snow covers due to wind scouring on the barren terrain engendered permafrost up to ~130 m thick (Nicholson 1979; Granberg 1989; Granberg 1994). Therefore, spatial modelling of permafrost distribution must include mapping snow depths in relation to land cover at the scale of individual terrain and land cover units. The Temperature at the Top of Permafrost (TTOP) model has been widely used for this purpose, including in southern Norway (Gisnås et al. 2013), and in Canada for the Mackenzie region of NWT (Wright et al. 2003) and for parts of the southern Yukon and northern British Columbia (Bevington and Lewkowicz 2015). Here we create and test a high resolution (250 m x 250 m grid cell) implementation of the TTOP model across Labrador-Ungava with the goal of providing a better estimate of the regional distribution of permafrost and a first-order assessment of the impact of recent climate change on permafrost extent.

6.2 Study area

The Labrador-Ungava region examined in this study extends from 55°W to 80°W and from 50°N to 63°N covering a land area of ~1,200,000 km^2 (Figure 6-1). Its physiography is characteristic of the Canadian Shield with numerous plateaus and mountain chains that reach the highest elevations in continental Canada east of the Rockies (Torngat Mountains, ~1600 m a.s.l.). The region encompasses vegetation biomes ranging from deciduous boreal forest in the south to Arctic tundra north of the tree-line at ~57°N (Elliott and Short 1979; Payette 2007; Luo et al. 2008). Labrador-Ungava includes the southernmost glaciers in the eastern Canadian Arctic (Brown et al. 2012; Way et al. 2014), the transition between continuous and discontinuous permafrost in eastern Canada (Brown 1979; Heginbottom et al. 1995; Hachem et al. 2009), and is the only region of the Arctic Cordillera south of 60°N.

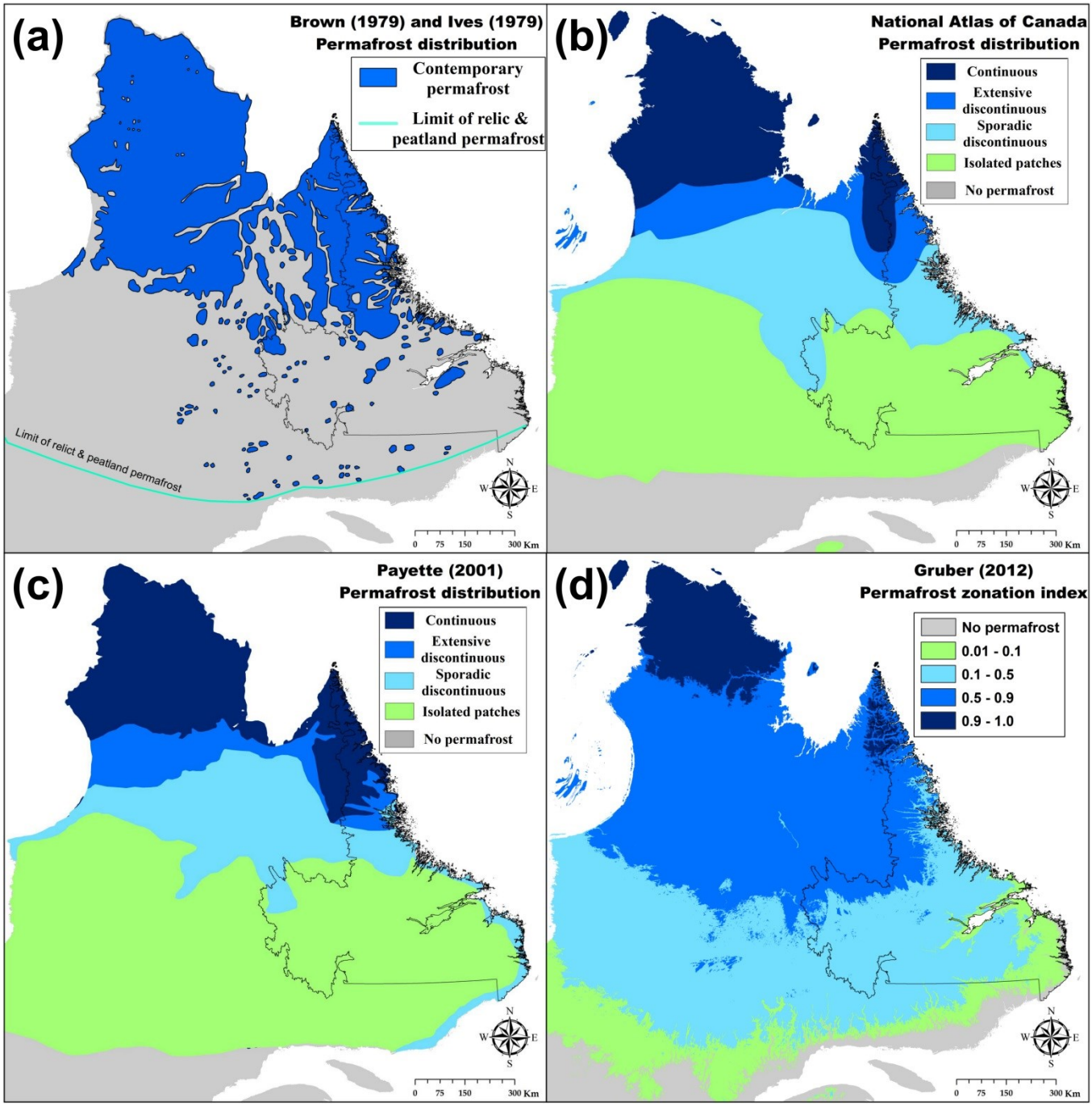

Figure 6-2: Maps of permafrost distribution in the Labrador-Ungava region redrawn from: (a) Brown (1979) and Ives (1979); (b) Heginbottom et al. (1995); (c) Payette (2001); and (d) Gruber (2012). Note: Brown (1979) outlined an additional area.

The position of the Arctic air masses and the seasonal sea ice cover in Hudson's Bay and Hudson Strait, result in deep penetration of cold air into the region during winter and spring. Seasonal sea ice cover along the Labrador coastline typically begins to form in December and does not dissipate until late May or early June (Banfield and Jacobs 1998). Consequently, surface air temperatures in Labrador-Ungava are colder than at the same latitudes in non-alpine portions of western Canada (Hijmans et al. 2005). Strong north-south and east-west temperature gradients are present, with mean annual air temperatures (MAATs) ranging from >1°C in southeastern Labrador to -12°C at high elevations in northern Québec (Way et al. 2017a). Regional MAAT increased by ~1.5°C from 1881 to 2011 with the greatest seasonal change in winter (+2.0°C) and the least in spring (+1.0°C) (Way and Viau 2015).

6.3 The TTOP model as implemented for Labrador-Ungava

6.3.1 Theory

The TTOP model (Smith and Riseborough 1996; Smith and Riseborough 2002; Riseborough 2004) employs minimal climatic and environmental inputs to estimate the equilibrium temperature at the top of permafrost at local to regional spatial scales. TTOP is used here to indicate average temperatures at the depth of the top of permafrost or the base of seasonal freezing if permafrost is absent (base of active layer). The TTOP model is parameterized using freezing and thawing degree days in the air, air-to-ground temperature transfer functions (n-factors) that account for a site's nival and surface offsets, and the ratio of freezing to thawing thermal conductivities to represent the thermal offset (Burn and Smith 1988; Smith and Riseborough 1996; Smith and Riseborough 2002; Karunaratne and Burn 2003; Bevington and Lewkowicz 2015).

The standard formulation of the TTOP model is:

EQ. 6-1

$$T_{Top} = \frac{(\frac{k_T}{k_F} n_T I_{TA} - n_F I_{FA})}{P}$$

$where$:

$T_{Top} = Temperature\ at\ the\ top\ of\ permafrost\ (^{\circ}\ C)$;

$k_T = Thermal\ conductivity\ of\ thawed\ ground\ (Wm^{-1}K^{-1})$;

$k_F = Thermal\ conductivity\ of\ frozen\ ground\ (Wm^{-1}K^{-1})$;

$n_T = Scaling\ factor\ between\ air\ and\ surface\ thawing\ index$;

$n_F = Scaling\ factor\ between\ air\ and\ surface\ freezing\ index$;

$I_{TA} = Cumulative\ air\ thawing\ degree\ days\ (^{\circ}\ Cd)$;

$I_{FA} = Cumulative\ air\ freezing\ degree\ days\ (^{\circ}\ Cd)$;

$P = Period\ (typically\ 365\ days)$.

EQ. 6-1 can be simplified by replacing the ratio of frozen to thawed thermal conductivity by the thermal offset, the temperature difference between the ground surface and the top of the permafrost table (Burn and Smith 1988):

EQ. 6-2

$$T_{Top} = \frac{(n_T I_{TA} - n_F I_{FA})}{P} + Toffset$$

$where$:

$Toffset = Thermal\ offset\ (^{\circ}\ C)$.

The TTOP model uses easily obtained data compared to transient models such as the northern ecosystem soil temperature model (Zhang 2003; Zhang et al. 2008a; Zhang et al. 2014) or the Geophysical Institute Permafrost Laboratory model (Jafarov et al. 2012; Jafarov et al. 2013), and it requires fewer inputs for modelling across large spatial domains (Riseborough et al. 2008). It assumes equilibrium conditions in relation to climate (Smith and Riseborough 2002) which could result in ecosystem-protected permafrost (e.g. Shur and Jorgenson 2007; Jorgenson et al. 2010; Morse et al. 2016) being modelled as unfrozen ground under a warming climate (Riseborough 2007). Unlike some areas of western Canada, where permafrost has persisted since the Last Glacial Maximum (Tarasov and Peltier 2007), non-equilibrium permafrost may not be a significant issue in southern Labrador-Ungava where permafrost probably formed during the Little Ice Age, or further north in the region where permafrost was in near-equilibrium with the climate during the second half of the 20th Century (see Ives 1979; Allard and Séguin 1987; Dionne and Richard 2006).

6.3.2 Input datasets

The model was built using the open source statistical analysis software R v3.0 and relies predominantly on the *raster* package for mathematical processing and masking inputs (see Appendix S1 for model implementation code). All datasets were transformed to a customized projection designed for eastern Labrador-Ungava based on the Universal Transverse Mercator projection. To examine the potential impact of climatic variation on equilibrium permafrost distribution, we generated model output for three climate scenarios corresponding to mean annual air temperatures for 1982-1996 (0.7°C below the long-term mean), 1948-1962 (0.1°C above the long-term mean), and 2000-2014 (0.9°C above the long-term mean) (e.g. Banfield and Jacobs 1998; Way and Viau 2015) (Figure 6-3).

6.3.2.1 Climate data

The air temperature indices required for EQ. 6-2 for the three periods were derived from a gridded monthly air temperature dataset available for nearly all of Labrador-Ungava north of 50°N (Way et al. 2017a). The dataset used infilled air temperature data to model monthly averages across the region at a spatial resolution of 250 m using a thin plate spline (Way and Bonnaventure 2015; Way et al. 2017a). Grids of annual freezing and thawing degree-days for the air were generated using an empirical-statistical relation with MAAT and temperature range with results indicating cumulative degree-day errors of less than 5% (Way et al. 2017a). To reduce errors, station data were averaged over each 15-year period prior to interpolating spatially rather than averaging months post-interpolation.

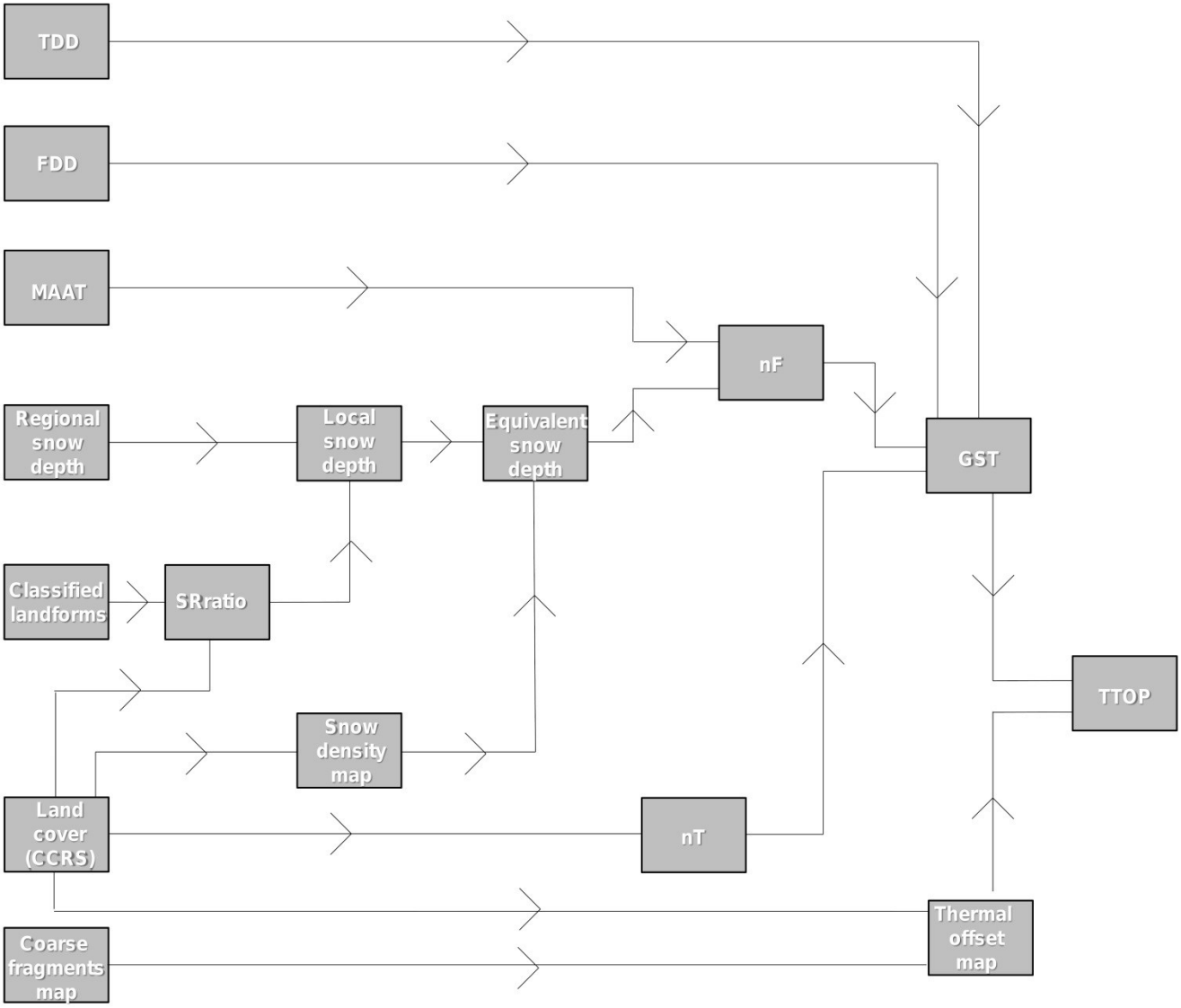

Figure 6-3: TTOP model implementation presented in this study. Note: TDD - Thawing degree-days; FDD - Freezing degree-days; MAAT - Mean annual air temperature (°C); nF - Freezing n-factor; GST - Ground surface temperature (°C); SRratio - Snow redistribution ratio; nT - Thawing n-factor; TTOP - Temperature at the top of permafrost (°C). For the surface-climate likelihood index the thermal offset was specified in a range from 0 to -2.0°C.

Regional snow depth data, needed to parameterize nF, (Figure 6-3) were obtained from the Canadian Meteorological Centre (CMC) using the approach outlined in Brown and Brasnett (2010). This dataset was originally developed by Brown et al. (2003) using snow depth data from climate stations across Canada and covers the period 1998-2014. Gridded mean winter (JFM) snow depth data over the full 1998-2014 snow analysis period were interpolated with ordinary kriging using the Geostatistical Analyst in ArcGIS 10 to match the resolution of the input climate and vegetation data (250 m) for all of Labrador-Ungava (Figure 6-4 d).

6.3.2.2 Land cover and surficial materials data

Land cover data, needed to parameterize n-factors and thermal offsets, (Figure 6-3) were obtained from Canada Centre for Remote Sensing (CCRS) at a 250 m resolution from the Canadian contribution to the North American Land Change Monitoring System. This dataset is derived from clear-sky MODIS satellite images collected at a 500 m resolution but the data are provided at a 250 m resolution through image fusion with several of MODIS' higher resolution bands (Luo et al. 2008; Trishchenko et al. 2009). Although the dataset includes 19 land cover classes, only 11 of them are present in Labrador-Ungava (Figure 6-5a). The CCRS data were selected instead of a ~20 m resolution product provided as part of the Earth Observation for Sustainable Development of Forests (EOSD) project (e.g., Wulder et al. 2008) because the latter does not cover a large section of northern Labrador and appears to have artificial land cover boundaries in the interior of Labrador-Ungava (Figure B4).

Digitally available regional compilations of surficial geology across Labrador were produced at too coarse a resolution (e.g. 1:2,500,000) to be useful for high resolution modelling. Consequently, we used information from the SoilGrids1km project that provides a variety of soil variables at various near-surface depths (Hengl et al. 2014). Soil properties and soil class maps produced by SoilsGrids1km use machine learning and geostatistical approaches based on training data from global soil profile datasets (Hengl et al. 2014). For the purposes of thermal offset parameterization, we generated a spatial grid that summarizes the coarse soils fraction in the upper 150 cm at a 250 m resolution to match that of the land cover data (Figure 6-5 b). It should be noted that the SoilsGrids1km dataset does not consider regional Quaternary geomorphology and therefore should be supplanted by surficial material information if this becomes available at high resolution in the future.

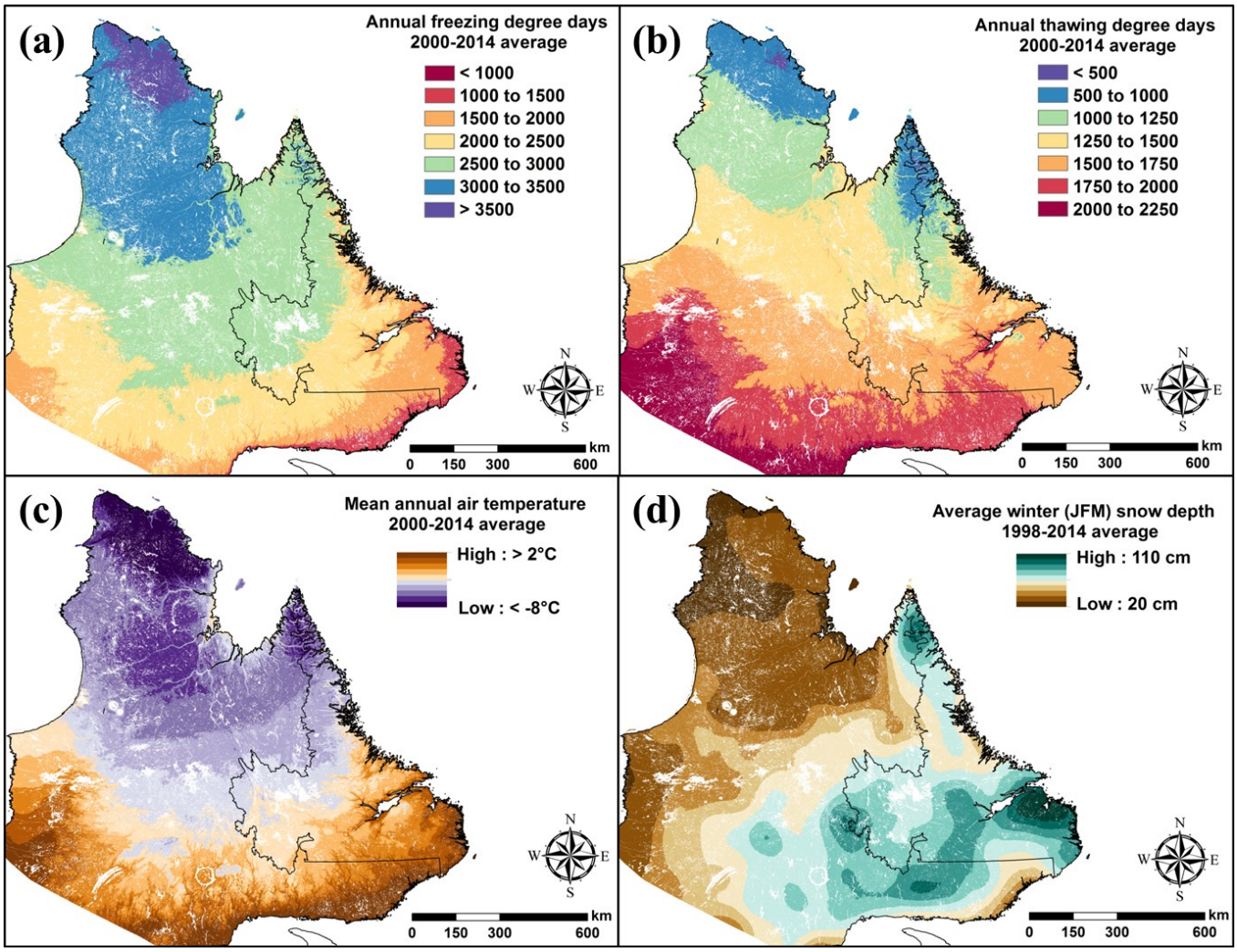

Figure 6-4: Climatological inputs used in TTOP modelling for the Labrador-Ungava region: (a) annual freezing degree-days; (b) annual thawing degree-days; (c) mean annual air temperature; and (d) average winter (JFM) snow depth. See text for the derivation of each grid.

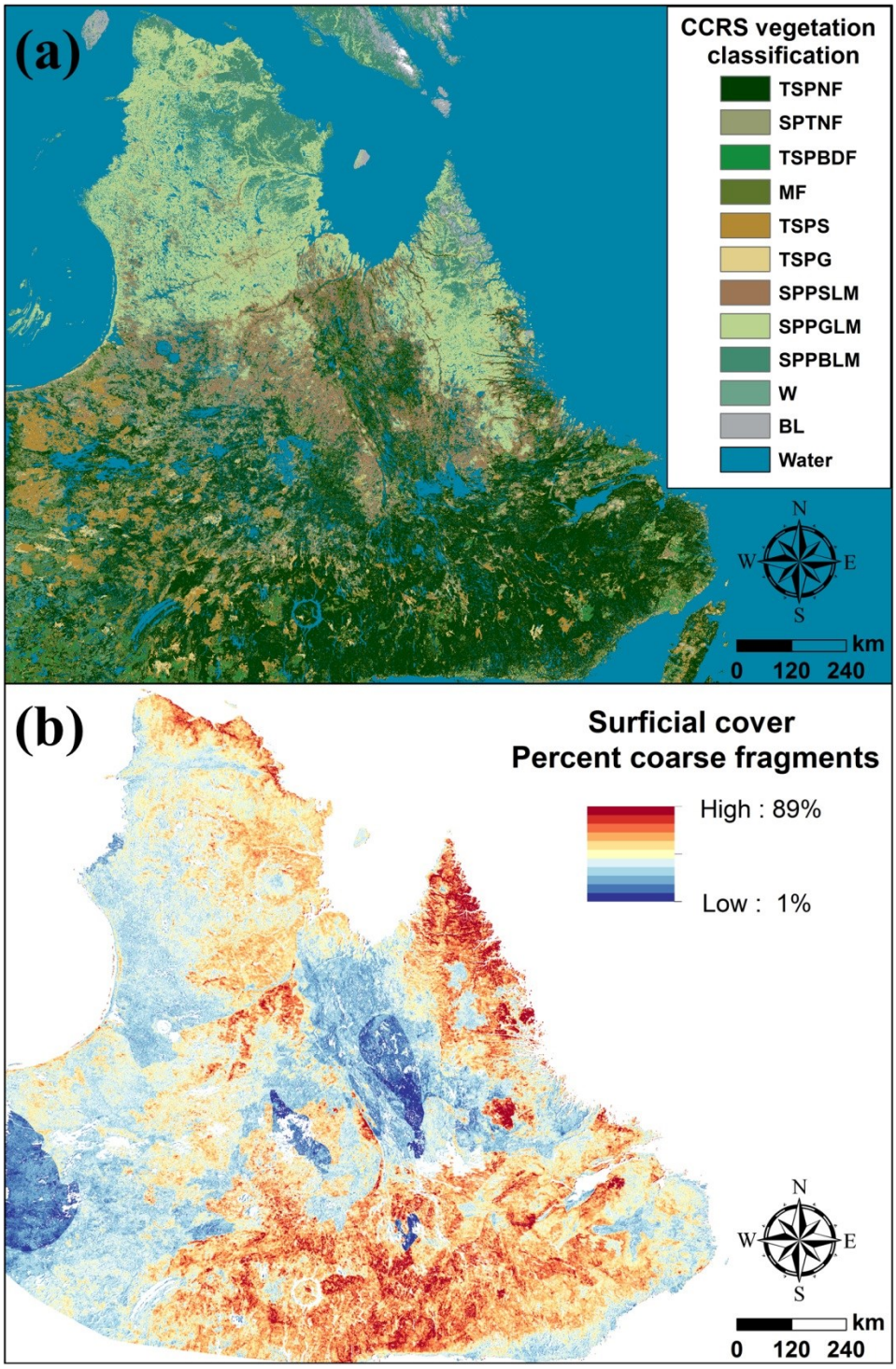

Figure 6-5: Land cover and surficial cover inputs used in TTOP modelling for Labrador-Ungava: (a) land cover from the North American Land Change Monitoring System (Luo et al. 2008, Trishchenko et al. 2009) and (b) coarse fragment percentage in the upper 150 cm (from Hengl et al. 2014). Land cover types consist of the following: Temperate or sub-polar needleleaf forest (TSPNF); Sub-polar taiga needleleaf forest (SPTNF); Temperature or sub-polar broadleaf deciduous forest (TSPBDF); Mixed forest (MF); Temperate or sub-polar shrubland (TSPS); Temperate or sub-polar grassland (TSPG); Sub-polar or polar shrubland-lichen-moss (SPPSLM); Sub-polar or polar grassland-lichen-moss (SPPGLM); Sub-polar or polar barren-lichen-moss (SPPBLM); Wetland (W); Barren Land (BL).

6.3.3 Model parameterization

The parameterization of freezing and thawing n-factors is the most challenging aspect of accurately characterizing ground surface conditions because they vary substantially over short distances and through time. Typically, n-factors are assigned to vegetation classes based on either field data (Ménard et al. 1998; Lewkowicz et al. 2012; Bevington and Lewkowicz 2015) or values found in the literature (Wright et al. 2003; Gisnås et al. 2013; Westermann et al. 2015a). Simulations of ground surface climate conditions using a range of n-factors can alleviate some of the concerns with selecting individual values if sufficient data are available to characterize sub-gridcell variability caused by heterogeneous terrain and its corresponding influences on snow cover, vegetation and soil wetness (Gubler et al. 2011; Gisnås et al. 2014; Bevington and Lewkowicz 2015; Hasler et al. 2015). In our model, nT was parameterized according to values measured at Labrador-Ungava monitoring stations (Table 6-1) and values derived from the literature, whereas nF was parameterized in several different ways described in *Section 6.3.3.2* (Figure 6-3).

6.3.3.1 nT

nT has been found to be fairly consistent for similar land cover classes in Alaska, southern Yukon and Norway in spite of regional differences in climate (Jorgenson et al. 2010; Lewkowicz et al. 2012; Gisnås et al. 2013; Bevington and Lewkowicz 2015). Measured nT values at monitoring sites in Labrador-Ungava are also comparable to those in the literature for similar land cover classes, varying from 0.66 for heavily shaded forested environments to 1.11 for exposed open-forest and barren environments (Table 6-1). nT was parameterized in the model using the recorded nT values for land covers at the monitoring stations. Values for land cover classes not sampled in the station dataset were estimated from the literature (Table 6-2).

Table 6-1: Summary parameters collected at Labrador Permafrost Project and Torngat Mountains National Park monitoring stations between 2010-2015 (series length varies according to station).

ID	Lat	Long	MAAT	nF	nT	Toff	mASD	eSD	Land cover type	SRratio	LFclass
AMET01	53.13	-66.13	-4.53	0.04	0.88		135.3	82.6	TSPNF	1.64	Plains
AMET02	53.13	-66.09	-4.81	0.06	0.78	-0.40	118.1	81.8	TSPNF	1.44	Mountain tops
AMET03	51.95	-68.14	-2.96	0.03	0.79		214.5	76.1	TSPS	2.82	Mountain tops
AMET05	52.79	-67.23	-4.31	0.01	1.05	-0.13	164.5	87.6	TSPNF	1.88	Plains
AMET06	52.77	-67.22	-5.27	0.66	0.87	0.86	14.6	92.2	SPPBLM	0.16	Mountain tops
AMET07	53.48	-64.69	-3.75	0.06	0.82	-0.40	105.3	72.6	TSPNF	1.45	U-shaped valleys
AMET08	53.48	-64.72	-4.03	0.23	0.74	-0.23	51.6	72.7	SPPSLM	0.71	Upper slopes
AMET09	54.31	-63.19	-4.33	0.04	0.88		129.6	72.7	SPTNF	1.78	Incised streams
AMET10	54.32	-63.21	-4.74	0.68	0.97	-0.72	12.9	72.5	SPPBLM	0.18	Mountain tops
AMET11	52.83	-60.10	-2.11	0.05	0.68	-0.97	117.0	77.7	TSPNF	1.50	Plains
AMET12	52.79	-60.03	-2.18	0.01	0.76	-0.59	167.6	77.0	TSPNF	2.18	Mountain tops
AMET13	53.71	-57.01				-2.47			W		Mountain tops
AMET15	52.59	-59.49	-2.48	0.04	0.73		125.9	73.4	SPTNF	1.72	Mountain tops
AMET16	53.87	-66.42	-4.43	0.06	1.11	-1.81	107.5	77.6	TSPNF	1.39	Plains
AMET21	52.16	-56.10	-0.82	0.03	0.77	-0.31	125.4	89.7	TSPNF	1.40	Incised streams
AMET22	52.14	-56.13	-1.70	0.18	0.92	-0.09	52.7	89.0	SPPSLM	0.59	Upper slopes
AMET23	53.06	-57.68	-2.05	0.07	0.87	-0.33	82.5	96.5	TSPNF	0.86	Plains
AMET25	53.32	-62.96	-3.54	0.14	0.92	0.64	51.0	75.5	SPTNF	0.68	Plains
AMET26	53.34	-63.03	-3.08	0.01	0.78	-0.44	166.0	74.7	TSPNF	2.22	Upper slopes
AMET27	53.23	-64.49	-2.82	0.04	0.83		130.7	73.6	MF	1.78	Plains
AMET29	53.11	-61.80	-5.09	0.11	0.75	-0.45	74.0	85.3	TSPNF	0.87	Mountain tops
AMET30	53.73	-65.16	-3.30	0.05	0.83		113.8	73.8	TSPS	1.54	Plains
AMET31	53.73	-65.14	-3.22	0.24	1.03		44.9	73.7	SPPSLM	0.61	Mountain tops
AMET32	52.98	-66.95	-5.31	0.02	0.66	0.14	153.5	91.9	TSPNF	1.67	U-shaped valleys
AMET33	52.99	-66.94	-5.46	0.61	0.76		17.1	91.7	SPPBLM	0.19	Mountain tops
TMNP1	58.45	-62.80	-3.95	0.71	1.20		10.7	71.1	SPPBLM	0.15	U-shaped valleys
TMNP2	58.94	-63.60	-4.25	0.10	0.98		119.8	90.0	SPPBLM	1.33	Incised streams
TMNP3	59.00	-63.75	-3.57	0.35	0.94		29.9	92.0	SPPSLM	0.33	Mountain tops
TMNP4	58.92	-63.67	-5.89	0.12	0.84		118.9	90.3	SPPBLM	1.32	Upper slopes
TMNP5	58.88	-63.36	-3.27	0.39	1.05		25.0	85.9	SPPSLM	0.29	U-shaped valleys

Notes: Lat - Latitude (°N); Long - Longitude (°E); MAAT - Mean annual air temperature (°C); nF - Freezing n-factor (ratio); nT - Thawing n-factor (ratio); Toff - Thermal offset (°C); mASD - Modelled winter average snow depth (cm); eSD - Gridcell estimated winter average snow depth from Brown and Brasnett (2010) (cm); Land cover type (see below); SRratio - Snow redistribution ratio; and LFclass - Landform classification (Dilts, 2015). Land cover types consist of the following: Temperate or sub-polar needleleaf forest (TSPNF); Sub-polar taiga needleleaf forest (SPTNF); Mixed forest (MF); Temperate or sub-polar shrubland (TSPS); Sub-polar or polar shrubland-lichen-moss (SPPSLM); Sub-polar or polar grassland-lichen-moss (SPPGLM); Sub-polar or polar barren-lichen-moss (SPPBLM); Wetland (W). SRratios were calculated by inverting the functional relation between nF, MAAT and average winter equivalent snow depth as described in *Section 6.3.2.2*.

Table 6-2: N-factors and snow redistribution ratios used for the reclassification of Canada Centre for Remote Sensing land cover data (from Luo et al. 2008) for the three main n-factor parameterizations used in this study.

Reclassification of CCRS	nT Labrador	nF Labrador	SRratio	Labrador data sources	nF west
Temperate or sub-polar needleleaf forest (TSPNF)	0.75	0.04	1.54	Field data from 12 sites	0.30
Sub-polar taiga needleleaf forest (SPTNF)	0.85	0.24	1.54	Field data from 3 sites	0.35
Temperate or sub-polar broadleaf deciduous forest (TSPBDF)	0.85	0.04	1.78	Same as TSPNF	0.25
Mixed forest (MF)	0.85	0.04	1.78	Field data from 1 site	0.30
Temperate or sub-polar shrubland (TSPS)	0.90	0.24	2.18	Field data from 2 sites	0.37
Temperate or sub-polar grassland (TSPG)	0.90	0.40	0.17	Same as SPPBLM	0.45
Sub-polar or polar shrubland-lichen-moss (SPPSLM)	0.90	0.30	0.51	Field data from 5 sites	0.37
Sub-polar or polar grassland-lichen-moss (SPPGLM)	0.90	0.40	0.17	Same as SPPBLM	0.45
Sub-polar or polar barren-lichen-moss (SPPBLM)	0.90	0.60	0.17	Field data from 6 sites	0.60
Wetland (W)	0.85	0.40	1.00	Estimated value	0.40
Barren land (BL)	1.00	0.70	0.17	Estimated value	0.82

Note: nF west values are based on measurements in western Canada (primarily in the Alaska, the Northwest Territories and the Yukon) by Karunaratne and Burn (2003), Wright et al. (2003), Jorgenson et al. (2010), Lewkowicz et al. (2012) and Bevington and Lewkowicz (2015).

6.3.3.2 nF

Published datasets from both North America and Scandinavian field sites (e.g. Lewkowicz et al. 2012; Gisnås et al. 2013; Bevington and Lewkowicz 2015) show that vegetation-induced snow characteristics can be taken into account using a land-cover based nF parameterization scheme. However, regional differences in snowfall and air temperature preclude the direct transfer of nF values from one environment to another. For example, nF values measured at forested sites in the southern Yukon and northern British Columbia (n=18) averaged 0.29 (Bevington and Lewkowicz 2015) whereas nF averaged 0.05 at similar sites in Labrador (n=16). Below we describe our preferred approach to nF parameterization which could be transferred from one region to another providing there is sufficient regional climate and snow depth data.

Regional and local snow distribution

Snow cover, and hence the nival offset, greatly affect the distribution of permafrost in central Labrador-Ungava (Nicholson 1979; Allard and Séguin 1987; Granberg 1994; Ménard et al. 1998), underlining the importance of accurate treatment of nF in the TTOP model. Our parameterization was

designed specifically to deal with the challenges of permafrost modelling across large areas with variable snow and vegetation conditions.

Coarse resolution regional average winter snow depth data (Brown et al. 2003; Brown and Brasnett 2010) for Labrador-Ungava (Figure 6-4d) was partitioned across landscapes at a high resolution (250 m) using a combination of vegetation and topographic indices. The influence of vegetation on snow depths was approximated by calculating snow redistribution ratios (SRratios) at field sites by comparing estimated site snow depths to the estimated regional depth (Table 6-1). These calculated SRratios were then distributed across Labrador-Ungava at a high resolution using the CCRS land cover product, with the exception of barren and tundra land covers for which topographic indices were used.

Very little snow accumulates on wind-exposed surfaces in mountainous terrain while thicker snowpacks develop in depressions. Consequently, a single SRratio based on land cover would underestimate local variability in ground surface temperatures (Gubler et al. 2011) and hence permafrost extent. This was evident in field data for the tundra and barren land cover classes (e.g. SPPBLM, SPPGLM, BL) with two clusters present, one having a mean SRratio of 0.17 (n=4) and the other a mean of 1.32 (n=2). To parameterize snow redistribution in these classes, we use a landform classification from Topography Tools (Dilts 2016) implemented in ArcGIS v10.3 with a digital elevation model to classify the region into ten landform types. Wind-exposed landform types (e.g. mountain tops, midslope ridges, hills in valleys) were assigned a snow redistribution ratio of 0.17, moderate slopes and flat areas (e.g. plains, open slopes, mesas, valley sides) were given a ratio of 1.0 and depressions and hollows (e.g. canyons, shallow valleys, upland drainages) were assigned a snow redistribution ratio of 1.83. These ratios were applied to the tundra and barren land cover class areas and the vegetation-specific snow redistribution ratios were applied elsewhere. The SRratios were then multiplied by the regional snow depth product to calculate average snow depths at high resolution across the study region (Table 6-2).

Converting snow depth to freezing n-factors

The snow depth maps were converted to nF values using a functional relation with mean annual air temperature (MAAT) developed by Smith and Riseborough (2002) and Riseborough (2004) based on numerical simulations with the TONE model (Goodrich 1978; Goodrich 1982). However, these simulations were performed at specific MAAT intervals therefore interpolation (thin plate spline, *fields* package in R v3.0) post-digitization was required to fill data gaps (Figure 6-6). Using this function, nF could then be spatially modelled across Labrador-Ungava from average winter snow depth and MAAT grids. Smith and Riseborough's (2002) model simulations were also conducted assuming an average

winter snow density of 250 kg m^{-3} which ignores differences in snow density between the major snow climate classes (e.g. alpine, tundra, taiga) that affect snow thermal conductivity (Sturm et al. 1995; Riseborough 2004; Sturm et al. 2010; Derksen et al. 2014). High resolution average winter snow depths were therefore normalized prior to nF derivation to have equivalent thermal properties to snow at a density of 250 kg m^{-3} using EQ. 6-3 (Riseborough 2004). Land cover data were first used to partition the landscape according to major snow classes (e.g. alpine, taiga, tundra) and were then normalized using thermal conductivity data summaries provided in Sturm et al. (2010). The use of a MAAT covariate by Smith and Riseborough (2002) was meant to serve as a proxy for active layer thickness and moisture content. However, numerical model simulations by Riseborough (2004) and analysis of field data by Throop et al (2012) suggest that the release of latent heat, mediated by substrate type, can alter the association between nF and snow depth.

EQ. 6-3

$$Zeq = Z_s \frac{k_{250}}{k_{den}}$$

$where$:

$Z_{eq} = equivalent\ snow\ depth\ (cm)$

$k_{250} = thermal\ conductivity\ of\ snow\ at\ density\ 250\ kg\ m^{-3} (0.21025\ Wm^{-1}K^{-1})$

$Z_s = observed\ snow\ depth\ (cm)$

$k_{den} = thermal\ conductivity\ of\ snow\ at\ observed\ density\ (Wm^{-1}K^{-1})$

Following the calculation of winter equivalent snow depth, the data were converted to nF using the statistical association produced with the thin plate spline fit (Figure 6-6). This approach is hereafter referred to as the snow redistribution nF.

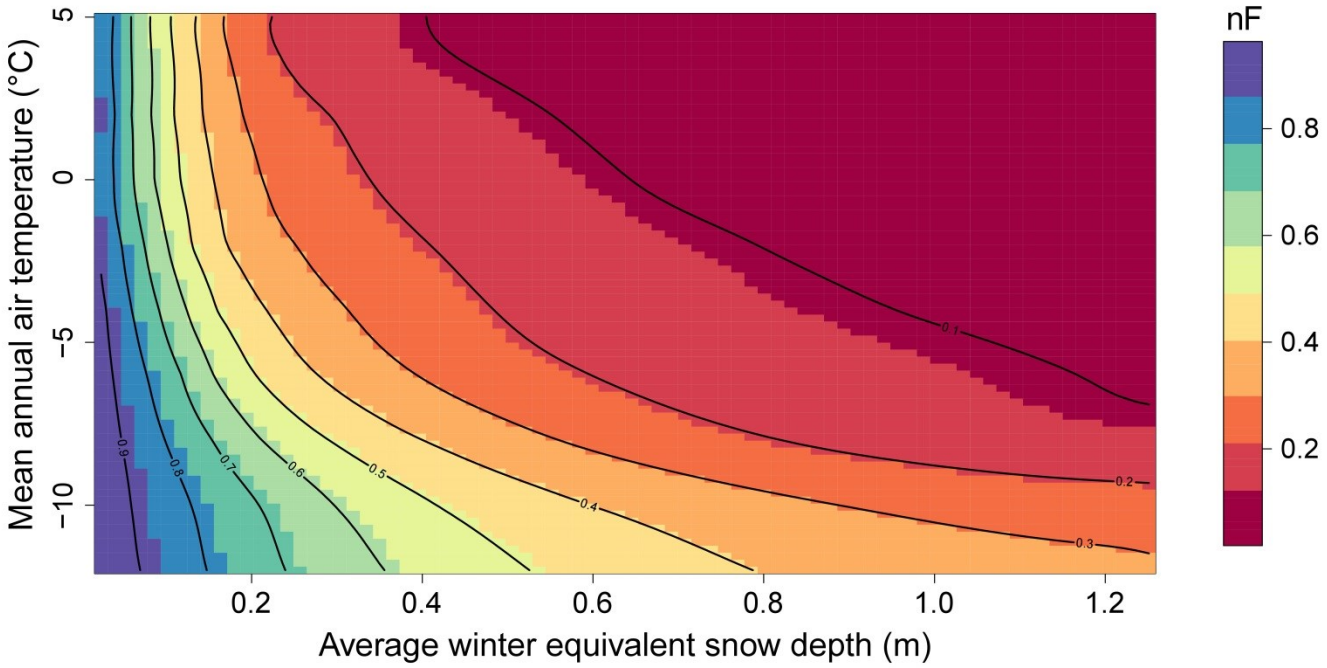

Figure 6-6: Thin plate spline statistical model fit between mean annual air temperature (°C), average winter equivalent snow depth (m) and freezing n-factors (unitless) derived from data Smith and Riseborough (2002). Lines were digitized from Figure 4 of Smith and Riseborough (2002) and shaded areas between were interpolated using a thin plate spline.

Other nF parameterizations

Three simpler approaches to nF parameterization were implemented for comparison with the approach described above. The purpose of these comparisons was to illustrate the uncertainties introduced into modelling through importing measured nF values from one region to another (e.g. Wright et al. 2003; Gisnås et al. 2013), or through the use of coarse snow cover datasets without considering local snow redistribution (e.g. Henry and Smith 2001; Smith and Riseborough 2002).

[1] Direct calculation of nF in conjunction with regional climate information (Way et al. 2017a) and snow depth data from the CMC (Brown et al. 2003; Brown and Brasnett 2010) that had been density adjusted to an equivalent snow depth following **EQ. 6-3** (hereafter the equivalent snow depth nF variant);

[2] Assignment of nF values to land cover classes based on detailed prior studies in similar Subarctic environments such as in Alaska, southern Norway and southern Yukon (Table 6-2) (hereafter the Alaska-Yukon nF variant);

[3] Assignment of nF values to land cover classes based on Labrador-Ungava monitoring stations and user-defined nF estimates (Table 6-2) (hereafter the Labrador-Ungava nF variant).

6.3.3.3 Thermal offset

Two different methods were used to parameterize the thermal offset. In the first, uniform scenarios of potential offsets from 0°C to -2.0°C at 0.1°C increments were used to produce a range of TTOP values. A climatologically-based permafrost likelihood index for each grid cell was then generated as the percentage of the 21 simulations in which TTOP was <0.00001°C (effectively ≤ 0°C). This index is based on surface climate conditions and assumes an equal likelihood for each thermal offset value.

The second approach generated site-specific thermal offsets using land cover and surficial materials grids as described in *Section 6.3.2.2*. Site-specific thermal offsets were estimated from data collected at Labrador-Ungava monitoring stations by differencing measured ground surface temperatures with co-located shallow ground temperatures located at the deepest attainable depths (~50 to ~125 cm depth) (Table 6-1). Estimated thermal offsets (shown in Table 6-3) were added to the modelled ground surface temperatures to provide TTOP values for the entire study region.

Table 6-3: Assumed thermal offsets based on combinations of surficial materials (Hengl et al., 2004) and land cover (Luo et al., 2008) classes.

Surficial materials	Land cover			
	Barren or rock	**Tundra**	**Forest**	**Wetland**
40-50% coarse fragments	0.00°C	-0.25°C	-0.50°C	-1.00°C
30-40% coarse fragments	-0.25°C	-0.50°C	-0.75°C	-1.25°C
20-30% coarse fragments	-0.50°C	-0.75°C	-1.00°C	-1.50°C
10-20% coarse fragments	-0.75°C	-1.00°C	-1.25°C	-1.75°C
0-10% coarse fragments	-1.00°C	-1.25°C	-1.50°C	-2.00°C

6.4 Results

6.4.1 Comparison of ground surface temperature (GST) models

Averaging all grid cells in Labrador-Ungava gave mean GST values between 0.8°C and 1.9°C depending on which of the four nF parameterization was used, with the warmest variant being the Labrador-Ungava parameterization and the coldest being the Alaska-Yukon nF variant (Table 6-4). The greatest range in GSTs was produced with the snow redistribution nF parameterization (-9.4°C to +5.6°C) while GST ranges for the other three variants were 3-4°C less, mainly because of higher minima (Table 6-4). The Alaska-Yukon nF variant differed substantially from the other three with its modal frequency in the 0°C and 2°C range compared to the others which exhibited modes between 2°C and 4°C (Figure 6-7). This difference is attributed to the way forested regions are treated and the Alaska-Yukon parameterization is considered to be unrealistically cold considering the absence of permafrost in most forested regions of Labrador-Ungava observed by us and others (Brown 1979; Granberg 1989). The snow redistribution nF parameterization scheme also differed appreciably from the other models in that it produced nearly double the number of grid cells with GSTs below -1.5°C and was the only nF variant with GSTs < -3°C across more than 5% of the region (Figure 6-8).

The various nF parameterizations produced GST results that are visually similar to the previously mapped extent of continuous permafrost (inferred for areas where nearly all GSTs ≤ 0°C) in the northern sections of both Québec and Labrador, and an absence of permafrost (inferred for areas where all GSTs ≥ 2°C) in the southern portions of Labrador-Ungava (Figure 6-7). In detail, however, the GST model results were sensitive to how nF was parameterized. For example, the southernmost extent of any GST ≤ 0°C, where permafrost is assumed to be extensive, differed among the nF model variants, particularly in north-central Labrador. Furthermore, there were major differences in the area with predicted GST values of 0-2°C where the size of the thermal offset determines the presence or absence of permafrost (Figures 6-7 and 6-8).

Table 6-4: Summary statistics for ground surface temperatures modelled for Labrador-Ungava with four different nF parameterizations.

GST nF parameterization	Min (°C)	Mean (°C)	Max (°C)	SD (°C)
Equivalent snow depth nF	-6.3	1.9	5.4	2.0
Labrador-Ungava nF	-7.2	1.8	5.2	2.1
Snow redistribution nF	-9.4	1.6	5.6	3.1
Alaska-Yukon nF	-8.5	0.8	4.2	1.7

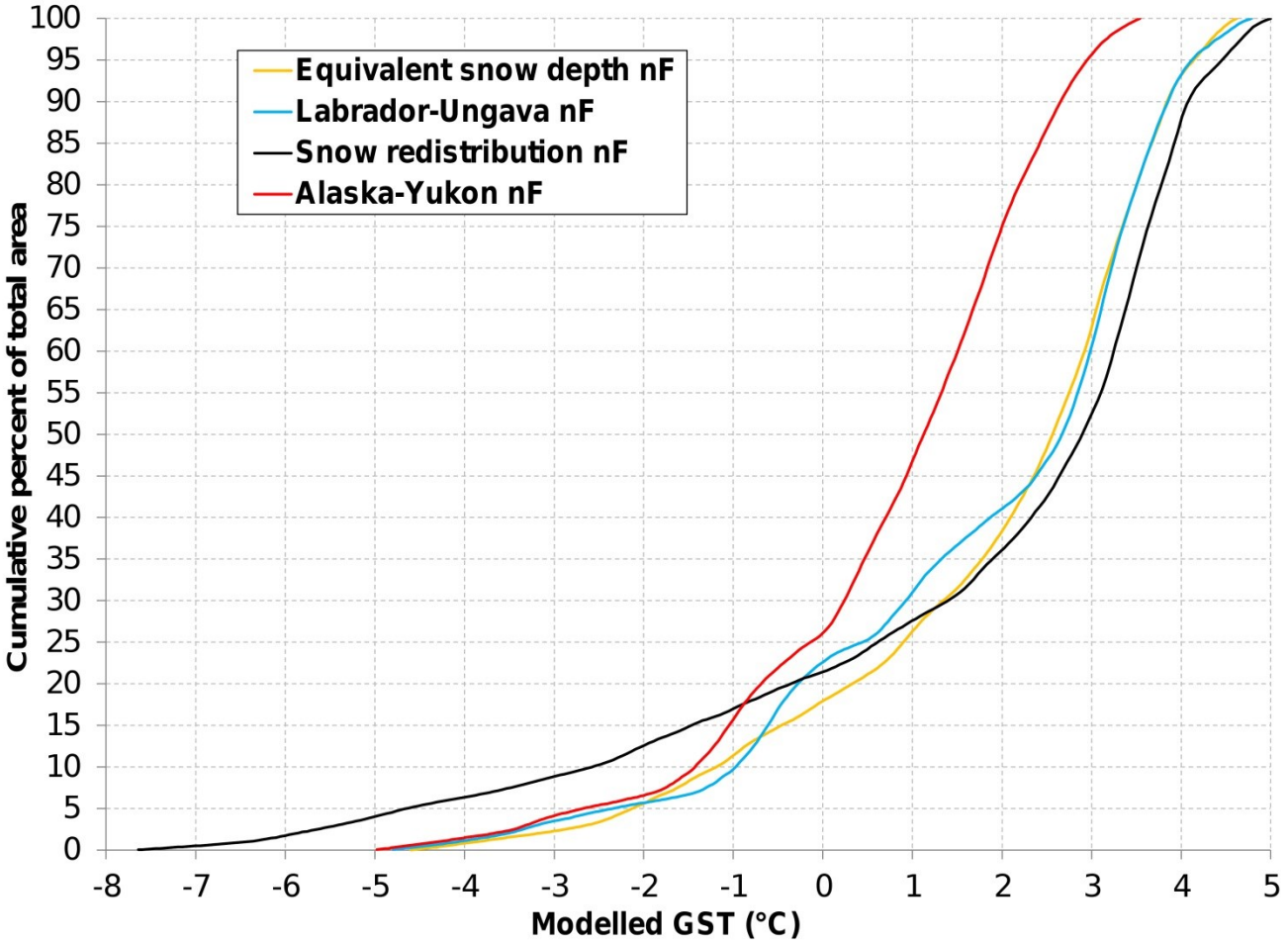

Figure 6-7: Cumulative frequency distribution of modelled GSTs across Labrador-Ungava according to the four nF parameterizations schemes used in this study.

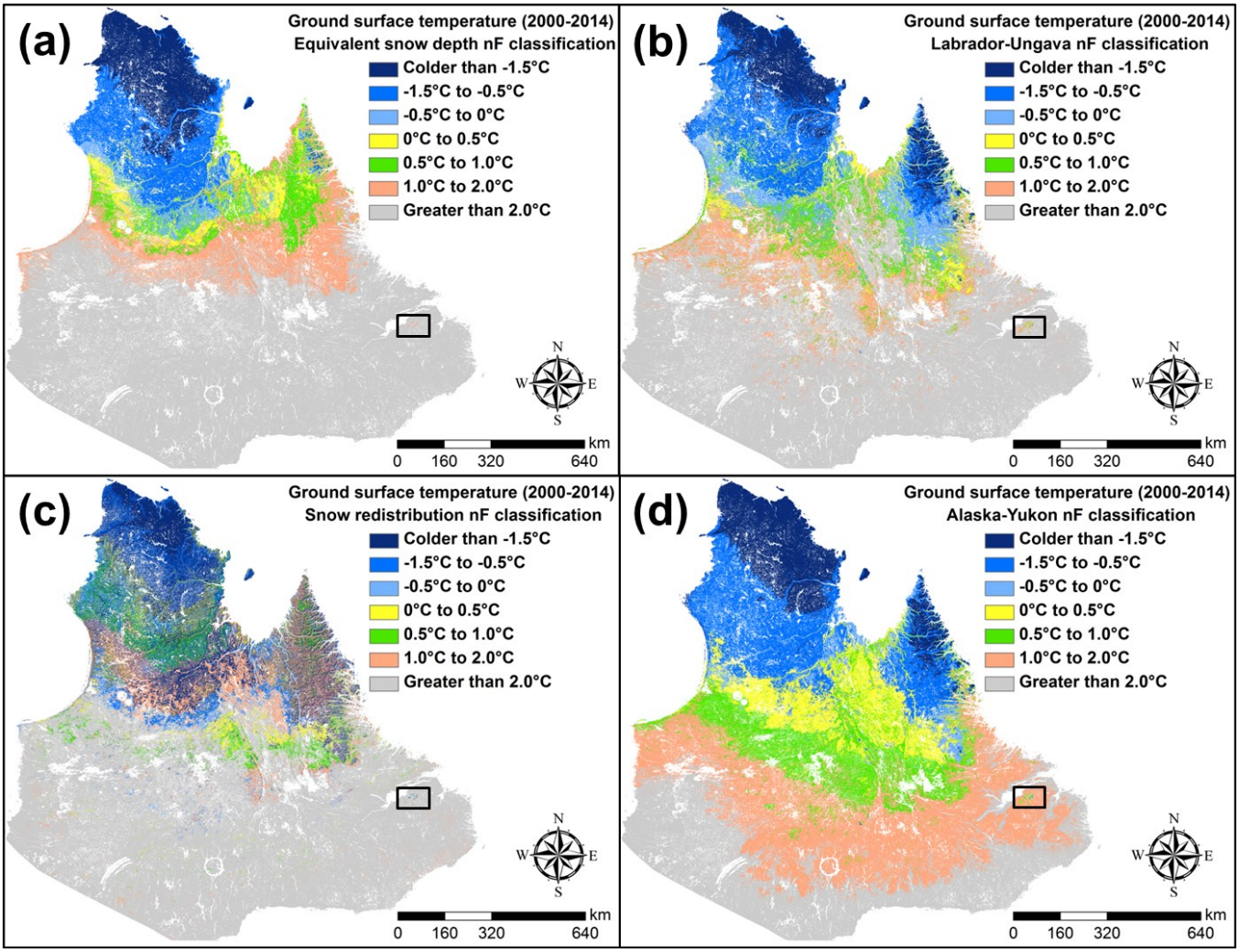

Figure 6-8: Modelled ground surface temperatures in Labrador-Ungava according to freezing n-factor parameterizations derived from the following four methods: (a) equivalent snow depth; (b) Labrador-Ungava data; (c) snow redistribution and equivalent snow depth; and (d) Alaska-Yukon data. The boxed area is enlarged in Figure 6-9.

The impact of the four different parameterizations of nF can be illustrated for a specific area, such as the Mealy Mountains in eastern Labrador (Figure 6-9). According to the equivalent snow depth parameterization (Figure 6-9a), ground surface temperatures in the Mealy Mountains would preclude the development of permafrost in most environments with the exception of the uppermost crests where it could exist if a large thermal offset were present. By contrast, all the other parameterizations predict permafrost to be present at upper elevations without a thermal offset (i.e. GST $\leq$ 0°C) with permafrost being possible at much lower elevations if large thermal offsets occur. Near-surface ground temperatures (70 cm & 100 cm depths) recorded at two sites at the forest-tundra interface during the early 2000s indicated the presence of permafrost with a temperature of -1.9°C on mountain crests at an elevation of 995 m a.s.l. (Mealy Mountains upper) and possible permafrost conditions at treeline near 600 m a.s.l. (~0°C) (Mealy Mountains base) (Jacobs et al. 2014). Likewise, GSTs measured for one year at 15 sites across a transect from the forest to the alpine tundra in the Mealy Mountains by Trant et al (2015) showed mean GSTs >3°C below treeline and GSTs <1.3°C above treeline. These data are in good agreement with the modelled GST values produced using both the Labrador-Ungava nF parameterization and the snow redistribution based parameterization. However, elsewhere in the southern interior of Labrador-Ungava, the snow redistribution parameterization appeared markedly superior at predicting GSTs with the potential for permafrost at sites where permafrost is known to exist according to our field data (e.g. Table 6-1). Given all the results, only the snow redistribution nF classification was retained for further analysis.

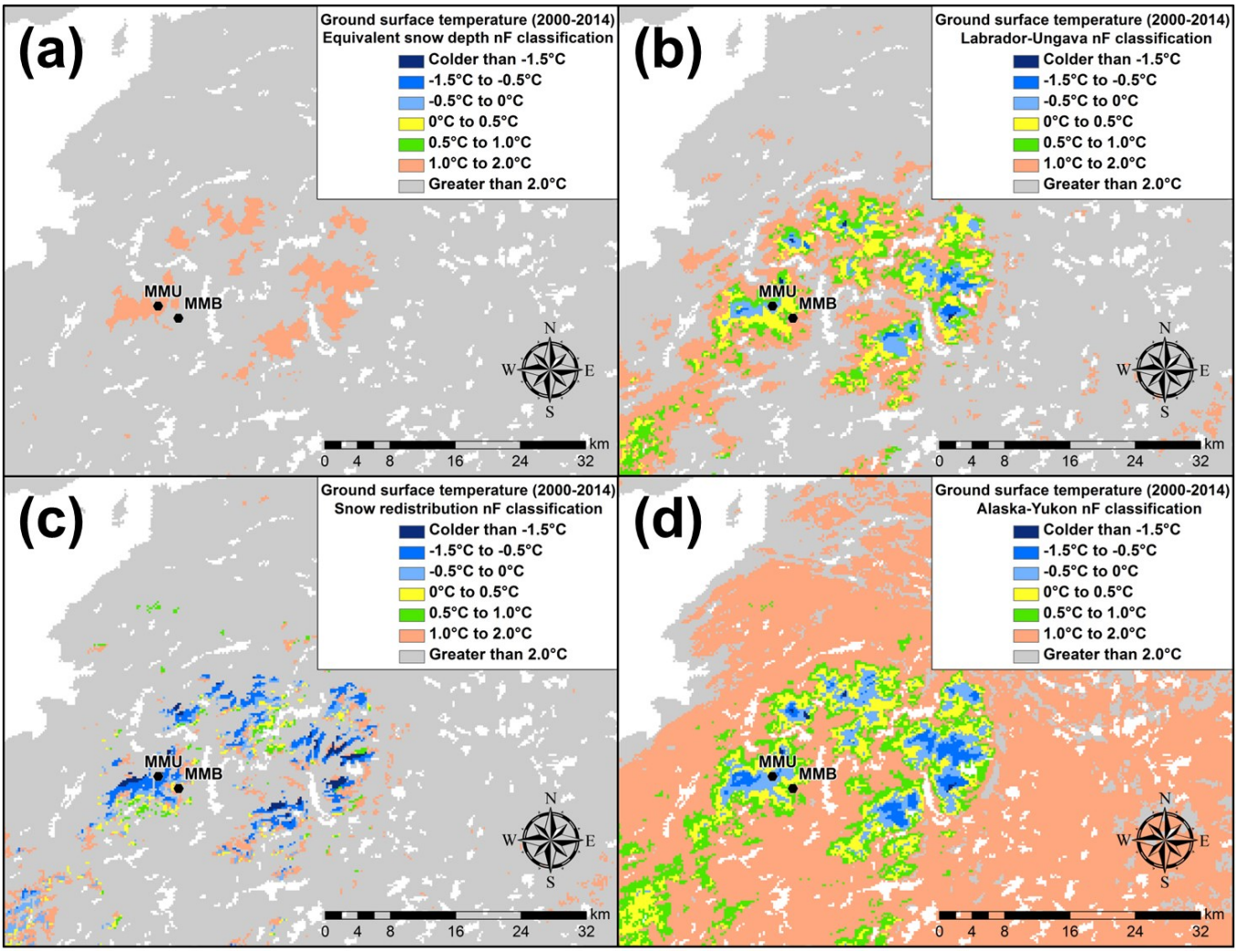

Figure 6-9: Modelled ground surface temperatures in the Mealy Mountains according to freezing n-factor parameterizations using four methods: (a) equivalent snow depth; (b) Labrador-Ungava data; (c) snow redistribution and equivalent snow depth; and (d) Alaska-Yukon data. Points depict the locations of ground temperature monitoring stations operated by Jacobs et al. (2014).

6.4.2 Temperatures at the top of permafrost

TTOP predictions were made using a scenario-based approach and also a direct thermal offset parameterization. Under a zero thermal offset scenario (in effect, minimum possible extent), permafrost is modelled to be present under most terrain types north of 56°N with only small patches in mountains farther south (Figure 6-10 a). With a uniform thermal offset of -1°C, mountain permafrost is abundant within Labrador and southern Québec and relatively common along the eastern coast of Hudson's Bay (Figure 6-10 b). A thermal offset of -2°C changes the regional distribution of permafrost substantially with the expansion of permafrost as far south as 50°N in the interior of the Labrador-Ungava and as far south as 51°N in coastal Labrador and eastern Quebec (Figure 6-10 c). Permafrost is more common in the southernmost portions of coastal Labrador than in the interior adjacent regions, a feature that is also identifiable in the surface-climate permafrost likelihood map (Figure 6-10 d). According to the latter, permafrost is likely to be widespread on the eastern coast of Hudson's Bay as far south as 54°N with modelled conditions indicating permafrost to be plausible as far south as ~52°N along the coastline where local factors such as the coastal climate and fine-grained surficial cover influence ground temperatures.

The application of a variable thermal offset based on land cover and surficial materials (Table 6-3) using an average of the output from the three climate periods provides our best estimate of TTOP across Labrador-Ungava (Figure 6-11 a). The gridcell mean TTOP value across Labrador-Ungava is 0.7°C (standard deviation of 2.8°C) and values range from -9.7°C to +5.2°C. Comparing these results to the GST values produced with the same model (Table 6-3) shows that the thermal offset averages -1.0°C on a regional basis. TTOP values change from >0°C to <-1.5°C over ~150 km in western Labrador, whereas in northern Québec the same transition occurs over approximately double that distance. Patches of TTOP values below 0°C are predicted along most of the coastline of Hudson's Bay and along the Labrador coastline with the southern interiors of Labrador and Québec having the majority of ground temperatures > 2°C. The southernmost patches of permafrost are in mountains in northeastern Québec, hundreds of km south of Labrador City. The northernmost areas of non-permafrost (excluding lakes) are present in the lowermost valleys of the Torngat Mountains (Figure 6-11 b). Although TTOP values are lower along portions of the east coast of Labrador, permafrost is rare at low elevations south of Nain (Figure 6-11 a). Isolated patches of permafrost, however, are modelled for mountainous regions of western Labrador and north-central Québec, mountainous terrain in central Labrador, and in the Mealy Mountains of eastern Labrador.

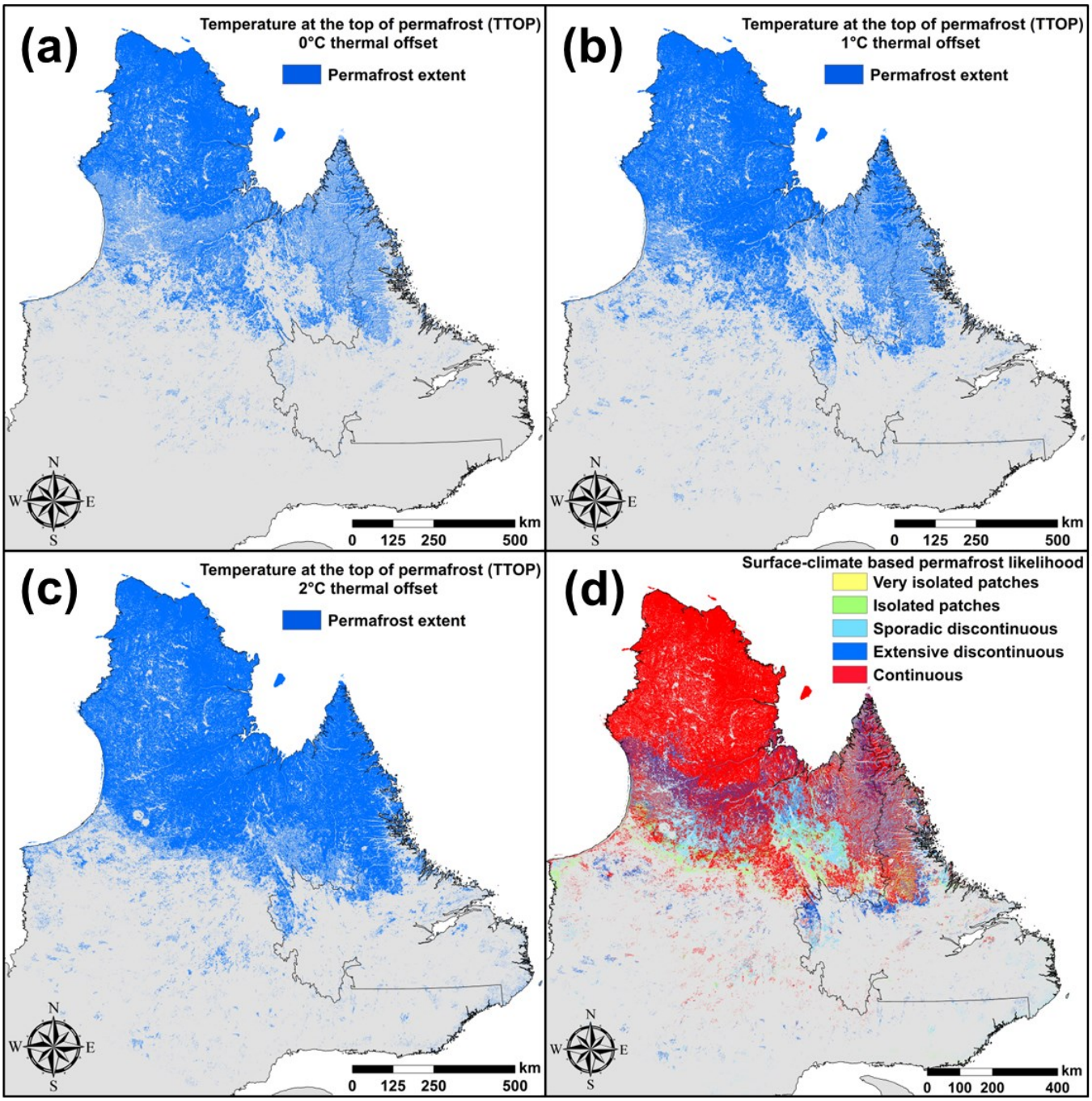

Figure 6-10: Modelled permafrost extent derived using the TTOP model assuming (a) no thermal offset; (b) 1°C thermal offset; (c) 2°C thermal offset; and (d) according to a surface-climate permafrost likelihood index. Note: The permafrost likelihood index is based on the percentage of 21 scenarios with a thermal offsets increasing from 0 to 2.0°C at 0.1°C increments having TTOP values ≤0°C. Lower boundaries of zones as follows: continuous - =>90% of scenarios with TTOP values ≤0°C; extensive discontinuous - =>50% of scenarios with TTOP values ≤0°C; sporadic discontinuous - =>10% of scenarios with TTOP values ≤0°C; isolated patches - =>1% of scenarios with TTOP values ≤0°C; very isolated patches => 0.1% with TTOP values ≤0°C.

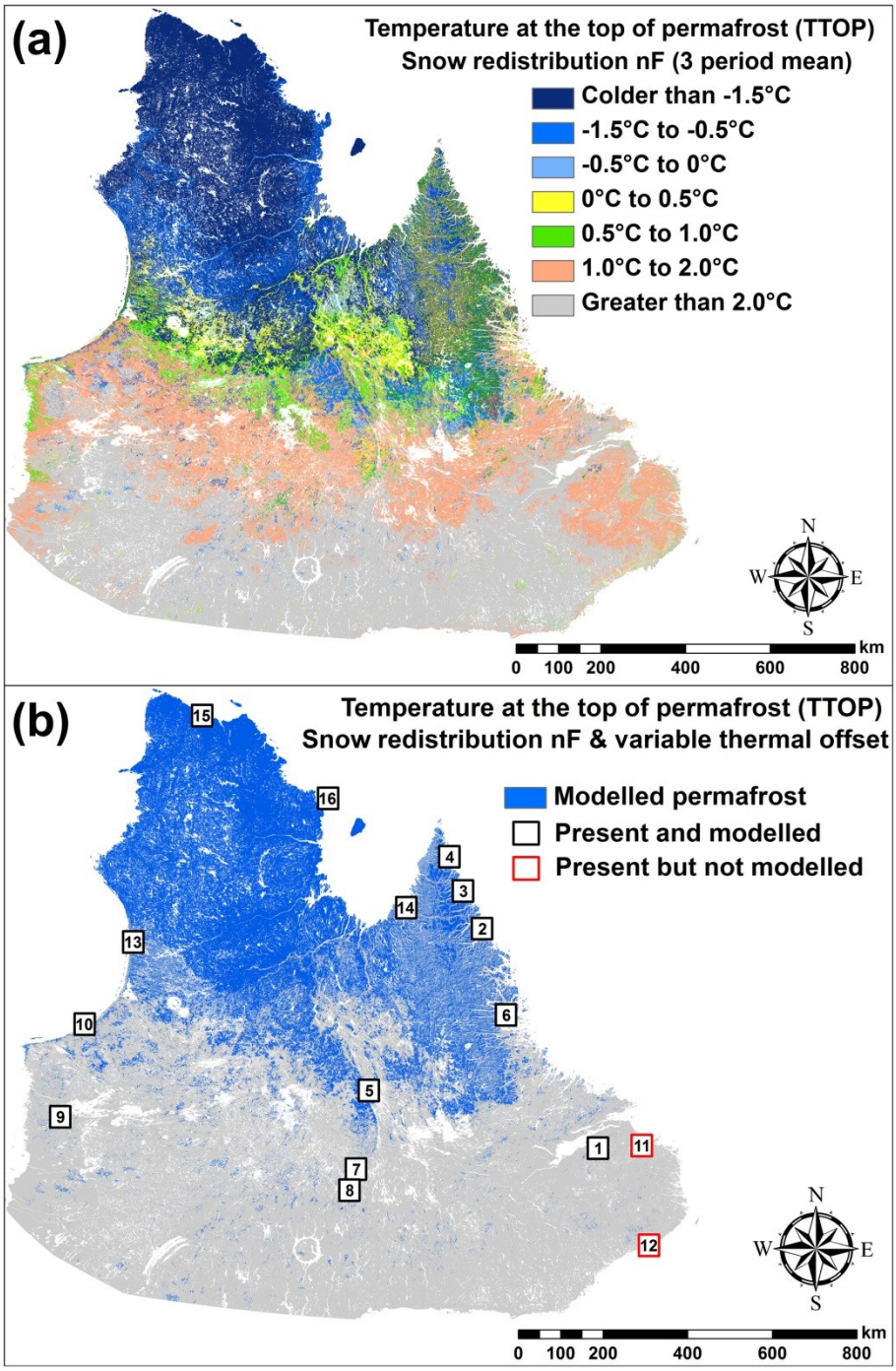

Figure 6-11: (a) Modelled temperatures at the top of permafrost derived using the snow redistribution freezing n-factor parameterization. (b) Modelled permafrost extent according to the temperature at the top of permafrost model overlain with squares depicting previously published permafrost observations. Permafrost observations referred to in the text are shown on map and are listed according to the following: (1) Mealy Mountains, NL; (2, 3, 4) Torngat Mountains, NL; (5) Schefferville, QC; (6) Nain, NL; (7) Labrador City, NL; (8) Fermont, QC; (9) La Grande, QC ; (10) Manitounuk Strait, QC; (11) Cartwright, NL; (12) Blanc Sablon, QC; (13) Umiujaq, QC - Ménard et al. (1998); (14) Kangiqsualujjuaq, QC - Allard et al. (1992); (15) Salluit, QC - Allard et al. (2012b); and (16) Quaqtaq, QC - Allard et al. (2012b).

The paucity of field and active borehole data throughout much of Labrador-Ungava precludes full validation of the TTOP model. However, evaluation of model accuracy was possible at 65 locations where shallow ground temperatures (50 cm to 125 cm) have been monitored at various intervals over the past decade (Table B3). Comparison between co-located model gridcells and observed ground temperatures (modelled for 2000-2014) provides an average mean absolute error of 1.6°C with a standard deviation of 1.16°C and a correlation (R) of 0.59 (p-value < 0.01) (Figure 6-12). Differences between modelled and measured shallow ground temperatures were normally distributed and almost 90% of modelled TTOP values are within 2.5°C of measured shallow ground temperatures. These error values reflect the combined effects of the coarse spatial resolution of the input vegetation data, the sub-gridcell heterogeneity of various factors (e.g. snow depth), the difference in climate periods evaluated, and the very short-term nature of some of the records (as short as one year).

6.4.3 Application of TTOP to differing climates

The potential evolution of temperatures at the top of permafrost was examined through the application of the snow redistribution nF model to the three climatically distinct time periods. Cumulative frequency curves of predicted TTOP show that, providing permafrost extent had time to reach equilibrium with the regional climate, its total area would have increased by about 15% (~56,500 km^2) between the first two periods to 428,000 km^2 (36% of the total land area) and then decreased by 22% (~95,000 km^2) between the mid-1990s and the present (Figure 6-13a). The time to arrive at equilibrium would be least in bedrock or coarse soils which require less latent heat to thaw and provide little buffering, and greatest in ice-rich fine-grained soils which require more latent heat to thaw.

Modelled permafrost aggradation between the first two periods was concentrated spatially in the coastal tundra terrain of southeastern Labrador-Ungava, the mountainous terrain south of Schefferville in central Labrador-Ungava, the northern interior of Labrador-Ungava west of the Torngat Mountains and in northwestern Québec (Figure 6-13 b). Modelled permafrost degradation for the most recent period is greater than prior aggradation in these areas and is also predicted for many of the mountainous areas through central and eastern Labrador-Ungava (Figure 6-13 b). Permafrost is hindcast as being relatively abundant along the coastline in southeastern Labrador during the 1982-1996 period but is effectively absent during the other two periods. This is also the case in the northern interior of Labrador-Ungava where large swaths of upland plateaus are modelled to have developed permafrost during 1982-1996 which subsequently would have begun to degrade. Despite its ongoing decline in extent, permafrost is modelled as persisting in isolated patches in southern Labrador-Ungava (Figure 6-13 b).

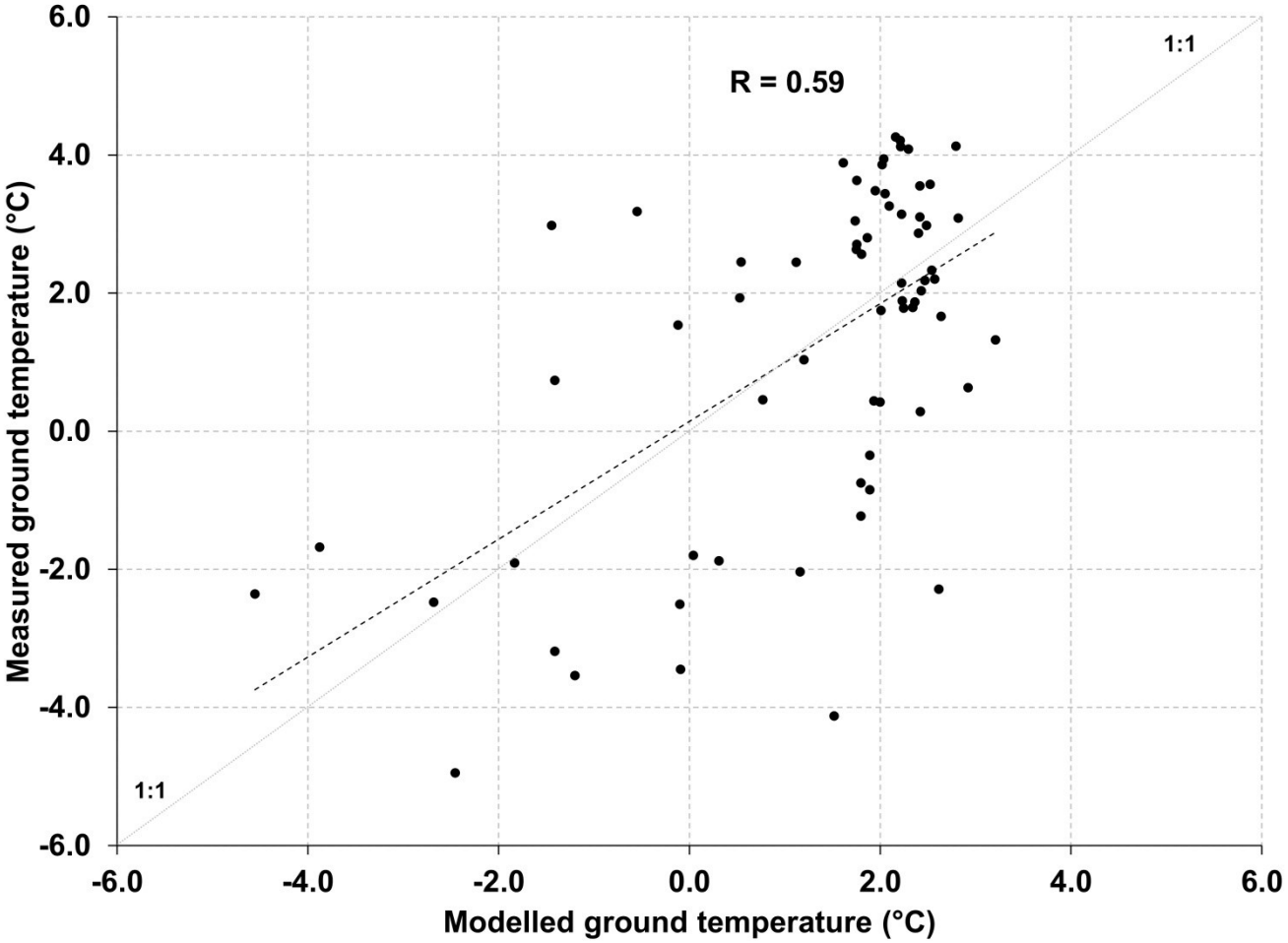

Figure 6-12: Evaluation of TTOP model output for 2000-2014 compared to co-located observations of ground temperature collected from field data presented in Table B4. Observations of shallow ground temperature were not temporally matched to the TTOP model output due to the short duration of most series.

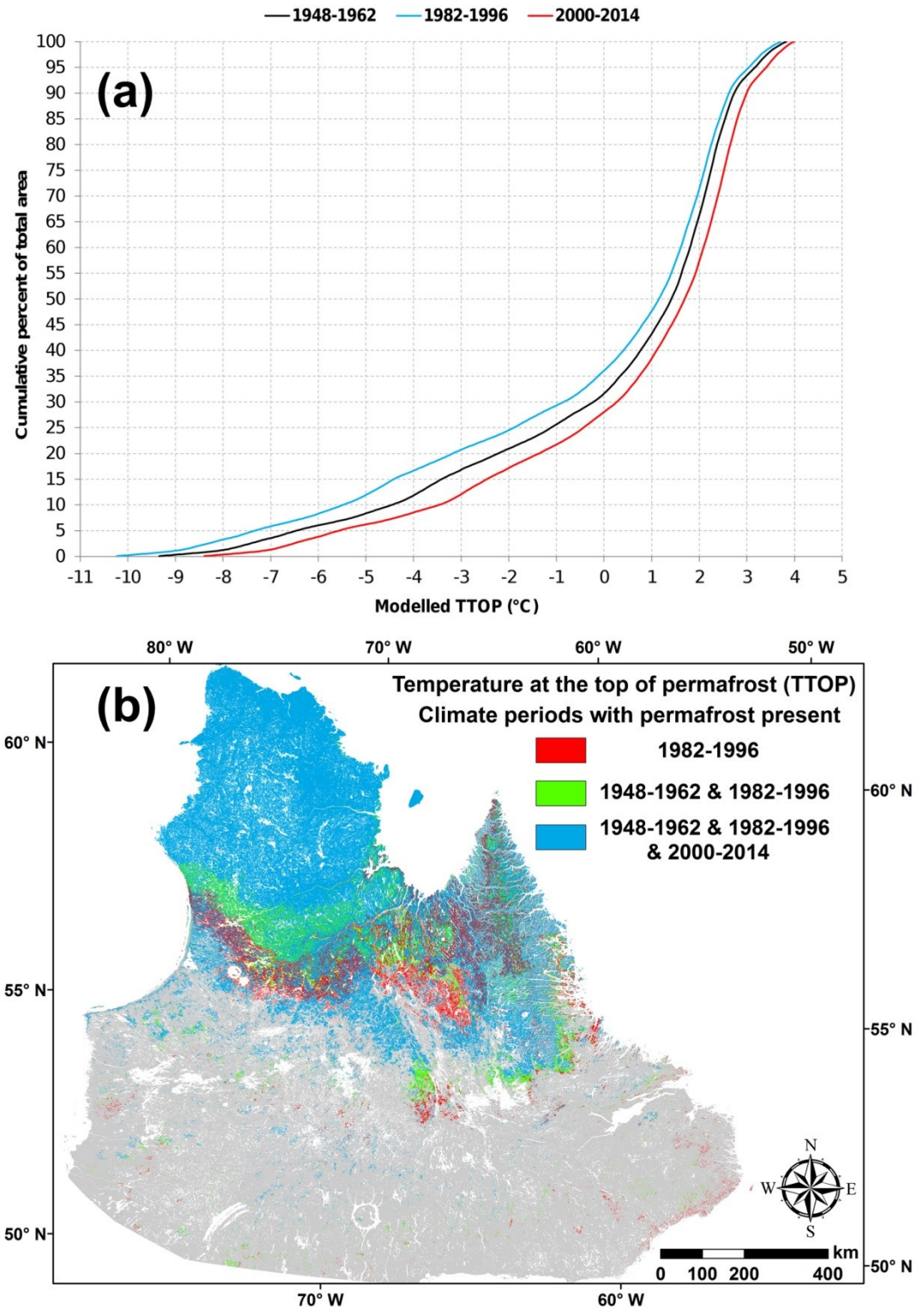

Figure 6-13: (a) Cumulative frequency curves of modelled TTOP values using the snow redistribution freezing n-factor for three different time periods. (b) Evolution of modelled permafrost extent according to simulations for the three time periods.

6.4.4 Scale effects on the TTOP results

The TTOP model results averaged for all three periods were used to generate permafrost distribution maps at differing spatial scales. A distribution index was produced within an area by summing the number of grid cells with TTOP ≤0°C, dividing by the maximum number of potential neighbours within the selected block and then multiplying by 100 to give a probability (%). Maps were generated for 1, 10, 25 and 50 km square blocks and were subsequently reclassified according to the standard permafrost zonation used in national scale maps (e.g. Heginbottom et al. 1995) (Figure 6-14). Due to the need to assign a lowermost limit of permafrost probability for inclusion in the isolated patches zone, a zone of very isolated patches was added with probabilities of between 0.1% and 1%.

Portrayal of permafrost boundaries in the Labrador-Ungava region is scale-dependent, with progressively less continuous permafrost evident with increasing block sizes. At the other end of the distribution, there is a progressive increase in terrain with isolated patches in southern Labrador due to grid cell aggregation so that Figure 6-14d resembles the Permafrost Map of Canada (Heginbottom et al. 1995; Figure 6-2b) much more than does Figure 6-14a. This scale dependency makes comparison with previous permafrost mapping efforts difficult, especially with those which were produced without using GIS techniques.

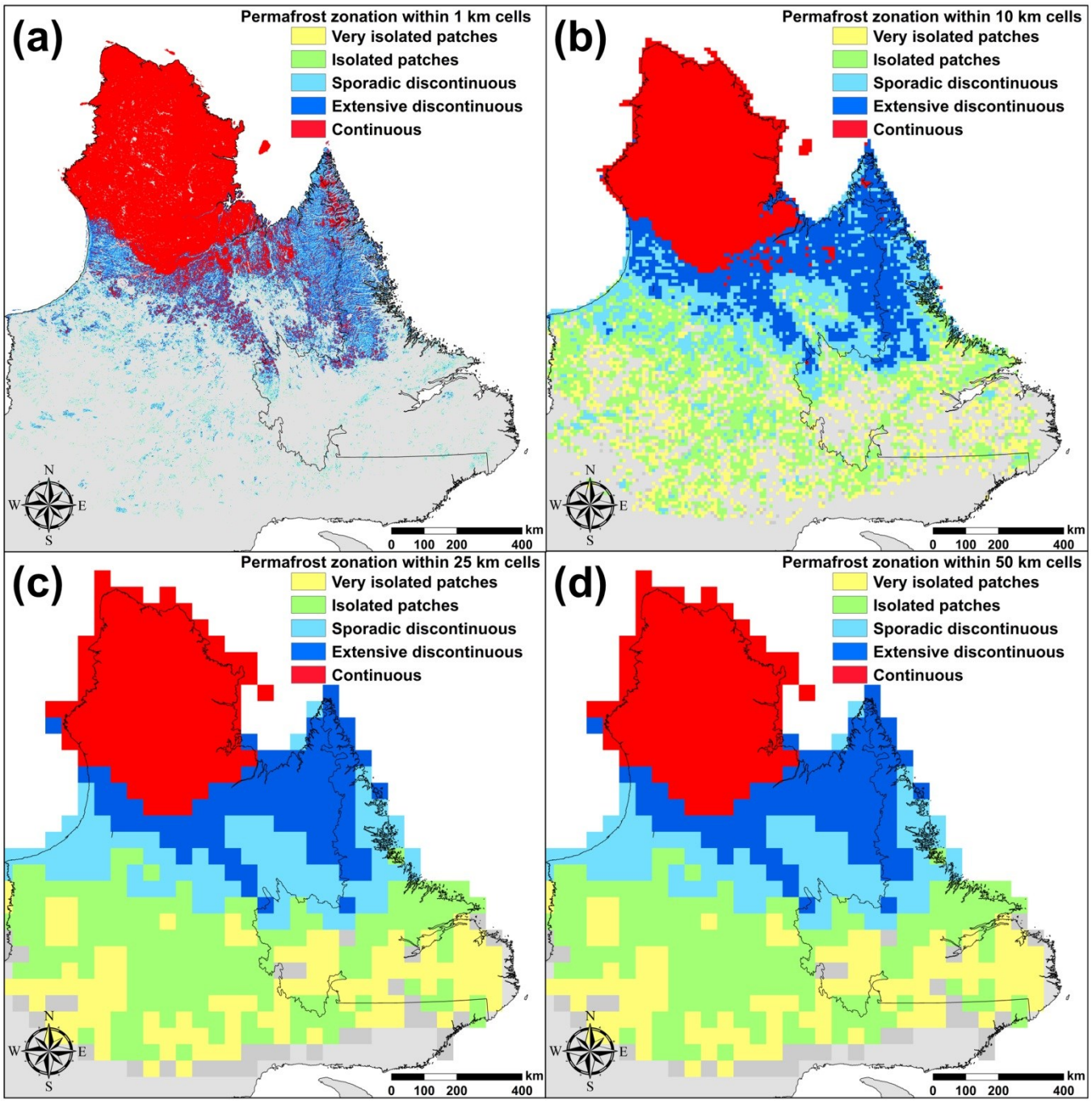

Figure 6-14: Permafrost distribution calculated from TTOP modelling for the three-period mean. Zones are calculated for the following four grid cell sizes: (a) 1 km by 1 km; (b) 10 km by 10 km; (c) 25 km by 25 km; and (d) 50 km by 50 km. Permafrost probabilities are reclassified according to standard permafrost limits (1-10%; 10-50%; 50-90%; 90-100%) with an additional class (very isolated patches) corresponding to 0.1-1% of the land surface area.

6.5 Discussion

The TTOP model results, when classified as permafrost presence or absence, agree with many published and unpublished field observations made within the region (Figure 6-11 b). The model correctly predicts the presence of permafrost above treeline in the Mealy Mountains of eastern Labrador where permafrost is likely widespread beneath the highest summits (Brown 1979; Jacobs et al. 2014) and at various elevations in the Torngat Mountains (Jordan 1980; Hendershot 1984). The model also correctly predicts the absence of permafrost in some low elevation coastal areas in the southern Torngat Mountains in agreement with observations of Parks Canada personnel (Table 6-1) and investigations of solifluction lobes (Evans and Rogerson 1988). It predicts large bodies of permafrost in the vicinity of Schefferville and an absence of permafrost farther north in agreement with the findings of detailed permafrost mapping undertaken in the region (Nicholson 1979; Granberg 1989). Permafrost is also projected to exist in exposed coastal regions near Nain in agreement with prior work in the area (Woollett 2010; Butler 2011; Way and Lewkowicz 2015). Mountaintop bodies of permafrost are modelled to be present near the adjacent communities of Fermont and Labrador City in agreement with observations by Brown (1979) and monitoring stations established as part of this study. On the eastern coast of Hudson's Bay, the TTOP model shows isolated patches of permafrost along the hypothesized southern margin of permafrost near La Grande indicated by Thibault and Payette (2009). Permafrost is also predicted for near-coastal zones of Manitounuk Strait 250 km to the north of the southern margin in agreement with observations by Beaulieu and Allard (2003). Permafrost bodies are predicted to occur in mountaintop regions in the interior of southern Québec close to the model geographic boundaries suggesting that isolated permafrost bodies might occur farther south at high elevations, as in fact they do in southern Québec in Charlevoix (Payette 1984; Zimmermann and Lavoie 2001) and Gaspé (Gray and Brown 1979) (Figure 6-11 b).

The model fails to predict permafrost where it is known to occur in palsa fields on marine terraces along the Labrador coastline between Blanc Sablon and Cartwright (Brown 1979; Dionne 1984; Roberts et al. 2006; Way and Lewkowicz 2015) (Figure 6-11 b). This discrepancy could be due to several factors. First, the spatial resolution of the vegetation classification dataset used is too coarse (250 m x 250 m) to properly capture the land cover in the small raised bogs which give rise to the palsas. Second, these locations are typically classified as temperate grasslands rather than wetlands within the land cover dataset, with corresponding effects on nF and thermal offset parameterizations. Third, the maximum thermal offset used in this study (-2°C; see Table 6-3) may be too small for palsas in the raised bogs. Fourth, localized influences on ground surface temperatures, such as coastal fog and local-scale inversions, are not represented in the input climate datasets. Finally, the palsas themselves may be out of equilibrium with the

recent climate and so cannot be accurately modelled with TTOP (Riseborough 2007). This problem is pervasive in the model results because permafrost is almost certainly in thermal disequilibrium at many sites (see Figure 6-13) and permafrost may have formed only during the Little Ice Age or earlier (e.g. Brown 1979; Ives 1979; Zhang et al. 2008a).

The TTOP model may also incorrectly predict the distribution of permafrost in some regions of mountainous terrain due to topography-induced snow accumulation. In the Torngat Mountains, for example, field data suggests that permafrost can be absent in topographic hollows, even at high elevations. The use of a landform classification index for parameterizing snow redistribution reduces some of these inaccuracies but more work is needed to properly describe permafrost in this mountainous terrain. It is also likely that factors other than snow depth and MAAT (as used in this study), such as soil moisture characteristics and substrate type influence nF (see Riseborough 2004; Throop et al. 2012), but spatial datasets to incorporate these factors are currently lacking.

Compared to previous permafrost maps (Figure 6-2), the TTOP model shows more permafrost in mountainous regions in southern Labrador and less permafrost overall in the Torngat Mountains. Hachem et al. (2008; 2009), for example, used MODIS land surface temperatures and a simple frost index classification to infer permafrost distribution across Labrador-Ungava at a 1 km spatial resolution. However, the derived map does not include snow and vegetation effects on GSTs, nor the thermal offset, and as shown above, these factors are critical for predicting permafrost at high resolution. It consequently underestimates the distribution of permafrost in southern Labrador-Ungava. The largest differences relative to our TTOP model predictions, however, are in north-central Labrador where we infer permafrost to be relatively widespread. More research is needed to better understand the utility of satellite-derived land surface temperatures for permafrost mapping applications.

Our model's gridcell size of 250 m x 250 m is smaller than most recent TTOP implementations in the North Atlantic Region (~1 km) (e.g. Gisnås et al. 2013; Westermann et al. 2015a) resulting in greater spatial detail. However, it is still too coarse to predict some of the small patches of permafrost present in the isolated patches and sporadic discontinuous zones. Furthermore, the model uses average inputs for each gridcell and therefore does not reflect sub-gridcell heterogeneity in n-factors and thermal offsets. Sub-gridcell variability in snow cover is considerable due to micro-topography and variability is also important at the regional scale due to macro terrain features such as mountains and plateaus. For example, Gisnas et al. (2014) showed that ground surface temperatures varied by as much as 6°C within a 0.5 km^2 area due to differences in snow depth (i.e. nF); similar observations for Labrador were made in Chapter 5.

The Labrador-Ungava TTOP model presented in this study has comparable errors (± 1.6°C) to a recent high resolution (1 km) TTOP model presented by Westermann et al. (2015a) but larger errors than those presented by Gisnås et al. (2013) (± 0.7°C). The lower measured accuracy of this work relative to Gisnås et al. (2013) likely reflects the regionally specific snow, surficial, and land cover data available for the latter study. Furthermore, unlike Gisnås et al. (2013), the modelled and observed shallow ground temperatures were not temporally matched prior to comparison which exaggerates model deviations.

We used two different approaches for calculating the impacts of thermal offsets on ground temperatures, with each having limitations. The scenario-based approach assigned thermal offsets from 0 to -2°C with each having an equal likelihood. However, the magnitude of a thermal offset is linked to surficial materials and land cover type so assigning an equal likelihood across a broad spatial domain is not optimal. The second approach assumed that surficial materials and land cover effects on thermal offsets are separate and quantifiable, but there is a paucity of field data examining the controlling mechanisms of thermal offsets and this is a major contributor to uncertainty in TTOP modelling (Bevington and Lewkowicz 2015; Westermann et al. 2015a). Furthermore, it would have been preferable to have adequate surficial geology data rather than using the near-surface coarse fragments percentage dataset. More detailed surficial cover mapping could be used as an input in future TTOP implementations if it were to become available.

6.6 Summary

We implemented a modified version of the TTOP model to predict the distribution of permafrost in the Labrador-Ungava region at high resolution. We developed a novel freezing n-factor parameterization scheme that is based on locally acquired field data and incorporates the spatially varying effects of regional climate and vegetation. The thermal offset was parameterized using land cover and surficial material characteristics rather than soil thermal conductivities. Given the limited input data available, it is likely the most complex model that can be run at present for the region.

Based on average conditions over the past half century, modelled permafrost extent is 377,000 km^2, representing 32% of the total land area. Continuous permafrost is modelled as being less extensive in northern Labrador than depicted on published maps. The southernmost limit of extensive discontinuous permafrost is modelled as being in Subarctic tundra terrain in the northern interior of Labrador and in coastal barrens along the eastern coast of Hudson's Bay. Permafrost in southern Labrador-Ungava is modelled as occurring only in isolated patches associated with mountains and coastal wetlands.

Modelling for three time periods hindcasts permafrost aggradation from the middle of the 20th Century to the mid-1990s during a phase of regional climatic cooling. Conversely, warming over the past 20 years is modelled to have caused permafrost degradation. If permafrost extent had time to fully equilibrate with the climate, these trends represent an increase in permafrost area of 56,500 km^2 (15%) followed by a decrease of 95,000 km^2 (22%). These results highlight the necessity of high-resolution permafrost mapping for informing policy-making in areas of future infrastructure development.

Acknowledgements

We thank all the organizations and individuals who have made climate and permafrost data available for Labrador-Ungava, especially Dr. John Jacobs of Memorial University of Newfoundland and Dr. Darroch Whitaker of Parks Canada for making weather station available for the Mealy Mountains, Kamestastin and the Torngat Mountains. A special thanks to all of the people in the communities of Goose Bay, Cartwright and Nain who helped to facilitate field work in various capacities. We also thank Steven Mosher for help with various programming and theoretical issues related to this project. We would like to thank our field assistants Alex Brooker, Caitlin Lapalme and Maxime Duguay for their assistance during field investigations in Labrador. We would also like to thank Olivier Bellehumeur-Génier, Dr. Philip Bonnaventure, Dr. Stefan Gruber, Dr. Sharon Smith and Dr. Yu Zhang for useful discussions which helped to inform this study. RGW acknowledges financial support from NSERC, the Association of Canadian Universities for Northern Studies, and the University of Ottawa. Funding for instrumentation and fieldwork was provided by the University of Ottawa, NSERC, and the Northern Scientific Training Program.

6.7 References

Allard, M., and M. K. Séguin. 1987. Le pergélisol au Québec nordique : bilan et perspectives. Géographie physique et Quaternaire 41(1): 141. doi: 10.7202/032671ar.

Allard, M., R. Fortier, and M. K. Seguin. 1992. The thermal regime of intertidal permafrost, George River estuary, Ungava Bay, Quebec. Canadian Journal of Earth Sciences 29(2): 249–259.

Allard, M., M. Lemay, C. Barrette, E. L'Hérault, D. Sarrazin, T. Bell, and G. Doré. 2012. Permafrost and climate change in Nunavik and Nunatsiavut: Importance for municipal and transportation infrastructures. In Nunavik and Nunatsiavut: From science to policy. An Integrated Regional Impact Study (IRIS) of climate change and modernization, 171–197.

Banfield, C. E., and J. D. Jacobs. 1998. Regional patterns of temperature and precipitation for Newfoundland and Labrador during the past century. The Canadian Geographer/Le Géographe canadien 42(4): 354–364.

Beaulieu, N., and M. Allard. 2003. The impact of climate change on an emerging coastline affected by discontinuous permafrost: Manitounuk Strait, northern Quebec. Canadian Journal of Earth Sciences 40(10): 1393–1404. doi: 10.1139/e03-056.

Bevington, A., and A. G. Lewkowicz. 2015. Assessment of a land cover driven TTOP model for mountain and lowland permafrost using field data, southern Yukon and northern British Columbia, Canada. In Proceedings of GéoQuebec: 68th Canadian Geotechnical Conference and 7th Canadian Permafrost Conference, 9. Québec City, Canada.

Brown, R., M. Lemay, M. Allard, N. E. Barrand, C. Barrette, Y. Bégin, T. Bell, M. Bernier, S. Bleau, D. Chaumont, Y. Dibike, A. Frigon, P. Leblanc, D. Paquin, M. J. Sharp, and R. Way. 2012. Climate variability and change in the Canadian Eastern Subarctic IRIS region (Nunavik and Nunatsiavut). In Nunavik and Nunatsiavut: From science to policy. An Integrated Regional Impact Study (IRIS) of climate change and modernization, 57–93.

Brown, R. D., and B. Brasnett. 2010. Canadian Meteorological Centre (CMC) Daily Snow Depth Analysis Data. National Snow and Ice Data Center: Environment Canada.

Brown, R. D., B. Brasnett, and D. Robinson. 2003. Gridded North American monthly snow depth and snow water equivalent for GCM evaluation. Atmosphere-Ocean 41(1): 1–14. doi: 10.3137/ao.410101.

Brown, R. J. 1979. Permafrost distribution in the southern part of the discontinuous zone in Quebec and Labrador. Géographie physique et Quaternaire 33(3–4): 279–289.

Brown, R. J. E. 1975. Permafrost Investigations in Quebec and Newfoundland (Labrador). Technical Paper 449. Ottawa, Ontario: National Research Council of Canada.

Burn, C. R., and C. A. S. Smith. 1988. Observations of the "thermal offset" in near-surface mean annual ground temperatures at several sites near Mayo, Yukon Territory, Canada. ARCTIC 41(2): 99–104. doi: 10.14430/arctic1700.

Butler, D. H. 2011. Exploring soilscapes and places inside labrador Inuit winter dwellings. Canadian Journal of Archaeology 35(1): 55–85.

Comiso, J. C., and D. K. Hall. 2014. Climate trends in the Arctic as observed from space: Climate trends in the Arctic as observed from space. Wiley Interdisciplinary Reviews: Climate Change 5(3): 389–409. doi: 10.1002/wcc.277.

Derksen, C., J. Lemmetyinen, P. Toose, A. Silis, J. Pulliainen, and M. Sturm. 2014. Physical properties of Arctic versus subarctic snow: Implications for high latitude passive microwave snow water equivalent retrievals. Journal of Geophysical Research: Atmospheres 119(12): 2013JD021264. doi: 10.1002/2013JD021264.

Dilts, T. 2016. Topography Tools for ArcGIS 10.3 and earlier. http://www.arcgis.com/home/item.html?id=b13b3b40fa3c43d4a23a1a09c5fe96b9.

Dionne, J.-C. 1984. Palses et limite méridionale du pergélisol dans l'hemisphere nord: le cas de Blanc-Sablon, Québec. Géographie physique et Quaternaire 38(2): 165–184. doi: 10.7202/032550ar.

Dionne, J.-C., and P. J. H. Richard. 2006. Origine, Age et taux d'accrétion verticale de la tourbiere palses de Blanc-Sablon, basse Cote-Nord, Golfe du Saint-Laurent, Québec. Géographie physique et Quaternaire 60(2): 199–205. doi: 10.7202/016829ar.

Elliott, D. L., and S. K. Short. 1979. The Northern Limit of Trees in Labrador: A Discussion. ARCTIC 32(3): 201–206. doi: 10.14430/arctic2620.

Evans, D. J., and R. J. Rogerson. 1988. A radiocarbon-dated gelifluction lobe in the Nachvak Fiord area, northern Labrador, Canada. Earth Surface Processes and Landforms 13(7): 657–662.

Fraser, R. H., I. Olthof, M. Carrière, A. Deschamps, and D. Pouliot. 2011. Detecting long-term changes to vegetation in northern Canada using the Landsat satellite image archive. Environmental Research Letters 6(4): 45502. doi: 10.1088/1748-9326/6/4/045502.

Gisnås, K., B. Etzelmüller, H. Farbrot, T. V. Schuler, and S. Westermann. 2013. CryoGRID 1.0: Permafrost distribution in Norway estimated by a spatial numerical model. Permafrost and Periglacial Processes 24(1): 2–19. doi: 10.1002/ppp.1765.

Gisnås, K., S. Westermann, T. V. Schuler, T. Litherland, K. Isaksen, J. Boike, and B. Etzelmüller. 2014. A statistical approach to represent small-scale variability of permafrost temperatures due to snow cover. The Cryosphere 8(6): 2063–2074. doi: 10.5194/tc-8-2063-2014.

Goodrich, L. E. 1978. Some results of a numerical study of ground thermal regimes. In Proceedings of the 3rd International Conference on Permafrost, 30–34. Edmonton, Canada: National Research Council of Canada.

Goodrich, L. E. 1982. The influence of snow cover on the ground thermal regime. Canadian Geotechnical Journal 19(4): 421–432. doi: 10.1139/t82-047.

Granberg, H. B. 1989. Permafrost mapping at Schefferville, Québec. Physical Geography 10(3): 249–269.

Granberg, H. B. 1994. Mapping heat loss zones for permafrost prediction at the northern/alpine limit of the Boreal forest using high-resolution C-Band SAR. Remote sensing of environment 50(3): 280–286.

Gray, J. T., and R. J. E. Brown. 1979. Permafrost presence and distribution in the Chic-Chocs Mountains, Gaspésie, Québec. Géographie physique et Quaternaire 33(3–4): 299. doi: 10.7202/1000366ar.

Gruber, S. 2012. Derivation and analysis of a high-resolution estimate of global permafrost zonation. The Cryosphere 6(1): 221–233. doi: 10.5194/tc-6-221-2012.

Gubler, S., J. Fiddes, M. Keller, and S. Gruber. 2011. Scale-dependent measurement and analysis of ground surface temperature variability in alpine terrain. The Cryosphere 5(2): 431–443. doi: 10.5194/tc-5-431-2011.

Hachem, S., M. Allard, and C. R. Duguay. 2008. A new permafrost map of Quebec-Labrador derived from near-surface temperature data of the Moderate Resolution Imaging Spectroradiometer (MODIS). In Proceedings of the 9th International Conference on Permafrost, 591–596. Fairbanks, United States of America.

Hachem, S., M. Allard, and C. Duguay. 2009. Using the MODIS land surface temperature product for mapping permafrost: an application to northern Québec and Labrador, Canada. Permafrost and Periglacial Processes 20(4): 407–416. doi: 10.1002/ppp.672.

Hasler, A., M. Geertsema, V. Foord, S. Gruber, and J. Noetzli. 2015. The influence of surface characteristics, topography and continentality on mountain permafrost in British Columbia. The Cryosphere 9(3): 1025–1038. doi: 10.5194/tc-9-1025-2015.

Heginbottom, J. A., M.-A. Dubreuil, and P. A. Harker. 1995. Canada – Permafrost. National Atlas of Canada, 5th Edition. Ottawa, Canada: Natural Resources Canada.

Hendershot, W. H. 1984. A Comparison of some Upland and Valley Soils in the Ungava-Labrador Peninsula. Géographie physique et Quaternaire 38(3): 243. doi: 10.7202/032566ar.

Hengl, T., J. M. de Jesus, R. A. MacMillan, N. H. Batjes, G. B. M. Heuvelink, E. Ribeiro, A. Samuel-Rosa, B. Kempen, J. G. B. Leenaars, M. G. Walsh, and M. R. Gonzalez. 2014. SoilGrids1km — Global soil information based on automated mapping. Edited by Ben Bond-Lamberty. PLoS ONE 9(8): e105992. doi: 10.1371/journal.pone.0105992.

Henry, K., and M. Smith. 2001. A model-based map of ground temperatures for the permafrost regions of Canada. Permafrost and Periglacial Processes 12(4): 389–398. doi: 10.1002/ppp.399.

Hijmans, R. J., S. E. Cameron, J. L. Parra, P. G. Jones, and A. Jarvis. 2005. Very high resolution interpolated climate surfaces for global land areas. International Journal of Climatology 25(15): 1965–1978. doi: 10.1002/joc.1276.

Ives, J. D. 1979. A proposed history of permafrost development in Labrador-Ungava. Géographie physique et Quaternaire 33(3–4): 233–244. doi: 10.7202/1000360ar.

Jacobs, J. D., S. Chan, and E. Sutton. 2014. Climatology of the Forest-Tundra Ecotone at a Maritime Subarctic-Alpine Site, Mealy Mountains, Labrador. ARCTIC 67(1): 28–42. doi: 10.14430/arctic4358.

Jafarov, E. E., S. S. Marchenko, and V. E. Romanovsky. 2012. Numerical modeling of permafrost dynamics in Alaska using a high spatial resolution dataset. The Cryosphere 6(3): 613–624. doi: 10.5194/tc-6-613-2012.

Jafarov, E. E., V. E. Romanovsky, H. Genet, A. D. McGuire, and S. S. Marchenko. 2013. The effects of fire on the thermal stability of permafrost in lowland and upland black spruce forests of interior Alaska in a changing climate. Environmental Research Letters 8(3): 35030. doi: 10.1088/1748-9326/8/3/035030.

Jordan, R. H. 1980. Preliminary Results from Archaeological Investigations on Avayalik Island, Extreme Northern Labrador. ARCTIC 33(3): 607–627. doi: 10.14430/arctic2586.

Jorgenson, M. T., V. Romanovsky, J. Harden, Y. Shur, J. O'Donnell, E. A. G. Schuur, M. Kanevskiy, and S. Marchenko. 2010. Resilience and vulnerability of permafrost to climate change. Canadian Journal of Forest Research 40(7): 1219–1236. doi: 10.1139/X10-060.

Karunaratne, K. C., and C. R. Burn. 2003. Freezing n-factors in discontinuous permafrost terrain, Takhini River, Yukon Territory, Canada. In Proceedings of the 8th International Conference on Permafrost, 519–524. Zürich, Switzerland: University of Zurich-Irchel.

Lewkowicz, A. G., P. P. Bonnaventure, S. L. Smith, and Z. Kuntz. 2012. Spatial and thermal characteristics of mountain permafrost, northwest Canada. Geografiska Annaler: Series A, Physical Geography 94(2): 195–213.

Luo, Y., A. P. Trishchenko, and K. V. Khlopenkov. 2008. Developing clear-sky, cloud and cloud shadow mask for producing clear-sky composites at 250-meter spatial resolution for the seven MODIS land bands over Canada and North America. Remote Sensing of Environment 112(12): 4167–4185. doi: 10.1016/j.rse.2008.06.010.

McLennan, D. S., T. Bell, D. Berteaux, W. Chen, L. Copland, R. Fraser, D. Gallant, G. Gauthier, D. Hik, C. J. Krebs, I. H. Myers-Smith, I. Olthof, D. Reid, W. Sladen, C. Tarnocai, W. F. Vincent, and Y. Zhang. 2012. Recent climate-related terrestrial biodiversity research in Canada's Arctic national parks: review, summary, and management implications. Biodiversity 13(3–4): 157–173. doi: 10.1080/14888386.2012.720818.

Ménard, É., M. Allard, and Y. Michaud. 1998. Monitoring of ground surface temperatures in various biophysical micro-environments near Umiujaq, eastern Hudson Bay, Canada. In Proceedings of the 7th International Conference on Permafrost, 723–729. Yellowknife, Canada.

Morse, P. D., S. A. Wolfe, S. V. Kokelj, and A. J. R. Gaanderse. 2016. The occurrence and thermal disequilibrium state of permafrost in forest ecotopes of the Great Slave Region, Northwest Territories, Canada. Permafrost and Periglacial Processes 27(2): 145–162. doi: 10.1002/ppp.1858.

Nicholson, F. H. 1979. Permafrost spatial and temporal variations near Schefferville, Nouveau-Québec. Géographie physique et Quaternaire 33(3–4): 265–277. doi: 10.7202/1000363ar.

Payette, S. 1984. Un îlot de Pergélisol sur les hauts sommets de Charlevoix, Québec. Géographie physique et Quaternaire 38(3): 305. doi: 10.7202/032570ar.

Payette, S. 2001. Les processus et les formes périglaciaires. In Écologie des tourbières du Québec-Labrador, 199–239. Québec City, Canada: Les Presses de l'Université Laval.

Payette, S. 2007. Contrasted Dynamics of Northern Labrador Tree Lines Caused by Climate Change and Migrational Lag. Ecology 88(3): 770–780. doi: 10.1890/06-0265.

Payette, S., A. Delwaide, M. Caccianiga, and M. Beauchemin. 2004. Accelerated thawing of subarctic peatland permafrost over the last 50 years. Geophysical Research Letters 31(18): L18208. doi: 10.1029/2004GL020358.

Riseborough, D. 2007. The effect of transient conditions on an equilibrium permafrost-climate model. Permafrost and Periglacial Processes 18(1): 21–32. doi: 10.1002/ppp.579.

Riseborough, D., N. Shiklomanov, B. Etzelmüller, S. Gruber, and S. Marchenko. 2008. Recent advances in permafrost modelling. Permafrost and Periglacial Processes 19(2): 137–156. doi: 10.1002/ppp.615.

Riseborough, D. W. 2004. Exploring the parameters of a simple model of the permafrost-climate relationship. PhD Thesis, Ottawa: Carleton University.

Roberts, B. A., N. P. P. Simon, and K. W. Deering. 2006. The forests and woodlands of Labrador, Canada: ecology, distribution and future management. Ecological Research 21(6): 868–880. doi: 10.1007/s11284-006-0051-7.

Shur, Y. L., and M. T. Jorgenson. 2007. Patterns of permafrost formation and degradation in relation to climate and ecosystems. Permafrost and Periglacial Processes 18(1): 7–19. doi: 10.1002/ppp.582.

Smith, M. W., and D. W. Riseborough. 1996. Permafrost monitoring and detection of climate change. Permafrost and Periglacial Processes 7(4): 301–309. doi: 10.1002/(SICI)1099-1530(199610)7:4<301::AID-PPP231>3.0.CO;2-R.

Smith, M. W., and D. W. Riseborough. 2002. Climate and the limits of permafrost: a zonal analysis. Permafrost and Periglacial Processes 13(1): 1–15. doi: 10.1002/ppp.410.

Smith, S. L., and D. W. Riseborough. 2010. Modelling the thermal response of permafrost terrain to right-of-way disturbance and climate warming. Cold Regions Science and Technology 60(1): 92–103. doi: 10.1016/j.coldregions.2009.08.009.

Sturm, M., J. Holmgren, and G. E. Liston. 1995. A Seasonal Snow Cover Classification System for Local to Global Applications. Journal of Climate 8(5): 1261–1283. doi: 10.1175/1520-0442(1995)008<1261:ASSCCS>2.0.CO;2.

Sturm, M., B. Taras, G. E. Liston, C. Derksen, T. Jonas, and J. Lea. 2010. Estimating Snow Water Equivalent Using Snow Depth Data and Climate Classes. Journal of Hydrometeorology 11(6): 1380–1394. doi: 10.1175/2010JHM1202.1.

Tarasov, L., and W. R. Peltier. 2007. Coevolution of continental ice cover and permafrost extent over the last glacial-interglacial cycle in North America. Journal of Geophysical Research 112(F2). doi: 10.1029/2006JF000661.

Thibault, S., and S. Payette. 2009. Recent permafrost degradation in bogs of the James Bay area, northern Quebec, Canada. Permafrost and Periglacial Processes 20(4): 383–389. doi: 10.1002/ppp.660.

Trant, A. J., K. Lewis, B. H. Cranston, J. A. Wheeler, R. G. Jameson, J. D. Jacobs, L. Hermanutz, and B. M. Starzomski. 2015. Complex changes in plant communities across a Subarctic alpine tree line in Labrador, Canada. ARCTIC 68(4): 500. doi: 10.14430/arctic4528.

Trishchenko, A. P., Y. Luo, K. V. Khlopenkov, W. M. Park, and S. Wang. 2009. Arctic circumpolar mosaic at 250 m spatial resolution for IPY by fusion of MODIS/TERRA land bands B1–B7. International Journal of Remote Sensing 30(6): 1635–1641. doi: 10.1080/01431160802348119.

Way, R. G., and P. P. Bonnaventure. 2015. Testing a reanalysis-based infilling method for areas with sparse discontinuous air temperature data in northeastern Canada: Reanalysis-based infilling in northeastern Canada. Atmospheric Science Letters 16(3): 398–407. doi: 10.1002/asl2.574.

Way, R. G., and A. G. Lewkowicz. 2015. Investigations of discontinuous permafrost in coastal Labrador with DC electrical resistivity tomography. In Proceedings of GéoQuebec: 68th Canadian Geotechnical Conference and 7th Canadian Permafrost Conference, 8. Québec City, Canada. doi: 10.13140/RG.2.1.1647.8803.

Way, R. G., and A. E. Viau. 2015. Natural and forced air temperature variability in the Labrador region of Canada during the past century. Theoretical and Applied Climatology 121(3–4): 413–424. doi: 10.1007/s00704-014-1248-2.

Way, R. G., T. Bell, and N. E. Barrand. 2014. An inventory and topographic analysis of glaciers in the Torngat Mountains, northern Labrador, Canada. Journal of Glaciology 60(223): 945–956. doi: 10.3189/2014JoG13J195.

Way, R. G., T. Bell, and N. E. Barrand. 2015. Glacier change from the early Little Ice Age to 2005 in the Torngat Mountains, northern Labrador, Canada. Geomorphology 246: 558–569. doi: 10.1016/j.geomorph.2015.07.006.

Way, R. G., A. G. Lewkowicz, and P. P. Bonnaventure. 2017a. Development of moderate-resolution gridded monthly air temperature and degree-day maps for the Labrador-Ungava region of northern Canada. International Journal of Climatology 37(1): 493–508. doi: 10.1002/joc.4721.

Westermann, S., T. I. Østby, K. Gisnås, T. V. Schuler, and B. Etzelmüller. 2015. A ground temperature map of the North Atlantic permafrost region based on remote sensing and reanalysis data. The Cryosphere 9(3): 1303–1319. doi: 10.5194/tc-9-1303-2015.

Woollett, J. 2010. Oakes Bay 1: A Preliminary Reconstruction of a Labrador Inuit Seal Hunting Economy in the Context of Climate Change. Geografisk Tidsskrift-Danish Journal of Geography 110(2): 245–259. doi: 10.1080/00167223.2010.10669510.

Wright, J. F., C. Duchesne, and M. M. Côté. 2003. Regional-scale permafrost mapping using the TTOP ground temperature model. In Proceedings of the 8th International Conference on Permafrost, 1241–1246. Zürich, Switzerland.

Wulder, M. A., J. C. White, M. Cranny, R. J. Hall, J. E. Luther, A. Beaudoin, D. G. Goodenough, and J. A. Dechka. 2008. Monitoring Canada's forests. Part 1: Completion of the EOSD land cover project. Canadian Journal of Remote Sensing 34(6): 549–562. doi: 10.5589/m08-066.

Zhang, Y. 2003. A process-based model for quantifying the impact of climate change on permafrost thermal regimes. Journal of Geophysical Research 108(D22). doi: 10.1029/2002JD003354.

Zhang, Y., W. Chen, and D. W. Riseborough. 2008. Disequilibrium response of permafrost thaw to climate warming in Canada over 1850–2100. Geophysical Research Letters 35(2). doi: 10.1029/2007GL032117.

Zhang, Y., I. Olthof, R. Fraser, and S. A. Wolfe. 2014. A new approach to mapping permafrost and change incorporating uncertainties in ground conditions and climate projections. The Cryosphere 8(6): 2177–2194. doi: 10.5194/tc-8-2177-2014.

Zimmermann, C., and C. Lavoie. 2001. A paleoecological analysis of a southern permafrost peatland, Charlevoix, Quebec. Canadian Journal of Earth Sciences 38(6): 909–919. doi: 10.1139/e00-110.

CHAPTER 7: CONCLUSIONS

7.1 Summary and conclusions

Prior to the initiation of this project, knowledge of permafrost in Labrador was substantially less than in other regions of Canada, particularly the Subarctic environments of western Québec, southern Yukon and southern Northwest Territories. For the last 30 years, permafrost in the interior of Labrador has been largely ignored with no recent research found in the peer reviewed literature. In coastal Labrador, systematic permafrost monitoring and mapping had never been undertaken despite evidence suggesting the presence of permafrost near several Labrador communities. This dissertation presents the results of extensive field investigations of permafrost conditions undertaken between 2013 and 2017 throughout much of Labrador. By combining detailed field observations with advanced numerical modelling techniques, this thesis has greatly increased knowledge of permafrost in Labrador and has produced results that have direct implications for understanding permafrost in Subarctic environments across Canada. An emphasis was placed on re-visiting permafrost sites identified from historical documentation and exploring regions that lacked historical documentation of permafrost presence or absence. Geophysics (DC electrical resistivity tomography), standard field methods and ground thermal monitoring were used to characterize permafrost bodies in coastal Labrador across a latitudinal gradient from the southern end of the isolated patches zone to the northern end of the sporadic discontinuous zone.

Overall, permafrost was found to be most widespread in areas with low vegetation cover near the coast, particularly where glacio-marine sediments are present. Permafrost was also found to be more abundant in southern coastal Labrador than would be expected from isotherms which show higher mean annual air temperatures than in the interior. This was interpreted as being due to a combination of coastal climate conditions, and well-drained peatlands with frost-susceptible marine and glacio-marine sediments below the marine limit (Chapter 3). The future of peatland permafrost features in southeastern Labrador was examined using the 1-dimensional northern ecosystem soil temperature model (NEST) (Zhang et al. 2003) with climate data spanning 1900 to 2100 according to representative concentration pathways 2.5, 4.5 and 8.5 (van Vuuren et al. 2011). These modelling results suggested that peatland permafrost aggraded at Blanc Sablon, QC and Cartwright, NL during the Little Ice Age and is projected to disappear from southeastern Labrador by 2070 under most climate scenarios. Field investigations conducted in the community of Nain, Nunatsiavut in northern Labrador identified contemporary permafrost bodies in a variety of disturbed and undisturbed environments at low elevation (Chapter 4). Notably, permafrost was found beneath a forested slope in the centre of the community contradicting the commonly held assumption that contemporary permafrost is not present in forested zones within Labrador.

The establishment of climate and permafrost monitoring stations throughout the southern half of Labrador was supplemented by Parks Canada monitoring stations in northern Labrador and from recent ecological research conducted in the Mealy Mountains of eastern Labrador (Jacobs et al. 2014; Trant et al. 2015). Climate information from the monitoring stations was also used in conjunction with the existing meteorological network and spatio-temporal infilling (Way and Bonnaventure 2015) to generate spatially and temporally consistent gridded climate datasets for 1948-2016 (Chapter 2). In total, data from 83 monitoring stations were used to examine linkages between climate, vegetation cover and permafrost characteristics across the region. Snow variability was the primary determinant of ground temperatures at the top of permafrost and its variability was linked to land cover type. A critical late-winter snow depth of 70 cm or less was inferred to be sufficient to prevent permafrost formation at monitoring sites but modelling results suggested that this threshold would vary spatially depending on the climatic elements (Chapter 5).

The above noted regional climate grids and information from monitoring stations facilitated spatial numerical modelling of ground temperatures across all of Labrador-Ungava, providing contemporary and historical estimates of the distribution and temperature of permafrost at fine spatial scales (250 m resolution) using the temperature at the top of permafrost model (TTOP) (Smith and Riseborough 1996; Smith and Riseborough 2002) (Chapter 6). The Labrador TTOP model showed the contemporary existence of zones of extensive discontinuous permafrost in high mountain regions within the southern half of Labrador while concurrently inferring unfrozen valley bottoms in northern sections of the region which have been mapped as continuous permafrost (e.g. Heginbottom et al. 1995). The historical TTOP model runs revealed a significant reduction in permafrost area at equilibrium across Labrador-Ungava between 1962-1980 and 2000-2014 (-39,000 km^2). The spatial distribution of equilibrium permafrost changes revealed a complex pattern that did not follow the traditionally assumed pathway for permafrost degradation (i.e. south-to-north). The modelled results further suggested the persistence of many isolated patches of permafrost in southern Labrador notwithstanding concurrent climate-driven permafrost degradation in the extensive and sporadic discontinuous zones of northern Labrador over the past 50 years. These modelling results suggest that future degradation of permafrost in Labrador will occur simultaneously in all major permafrost zones due to the influence of warming on the most thaw susceptible portions of the landscape.

7.2 Research objectives and key contributions

All five of the thesis objectives were met through the course of this dissertation and each is presented in Chapters 2-6. In achieving these objectives, this dissertation makes several key scientific contributions regarding permafrost in Labrador. These key contributions are described below:

1. Collation and summary of existing knowledge and observations of permafrost in Labrador;
2. Establishment of an open-source approach to generating gridded topoclimate products across large spatial domains, and the development of a methodology for testing the accuracy of the output products;
3. Creation of a systematic open-source approach for processing and infilling discontinuous climate data using gridded data from climate reanalysis datasets;
4. Systematic detection and characterization of permafrost conditions in a variety of previously unexamined locations within Labrador;
5. Detailed characterization of peatland permafrost features in southeastern Labrador including assessment of their susceptibility to future change;
6. Establishment of a network of climate and permafrost monitoring stations in lowland, upland and mountainous terrain in Labrador and northeastern Québec;
7. Identification of a critical late-winter snow depth of ~70 cm for preventing the formation of permafrost throughout the sporadic discontinuous and isolated patches zones in Labrador;
8. Development of a high resolution open-source TTOP modelling approach that is directly transferable to other Subarctic and Arctic environments;
9. Generation of maps predicting the spatial distribution of permafrost across all of Labrador and northern Québec at a high resolution (250 m) for historical and current climate scenarios using the TTOP model.

Several other relevant scientific contributions that can be drawn from this dissertation include the following:

1. Establishment of five boreholes along a latitudinal gradient in the permafrost terrain of coastal Labrador for long-term permafrost and ground temperature monitoring;
2. Generation of an empirical approach to creating FDD/TDD grids from monthly temperature grids;
3. Generation of an approach for isolating the vegetation and topographic effects on snow capture;

4. Testing the applicability of DC electrical resistivity tomography-based approaches for permafrost mapping in Labrador;
5. Development of low-cost, high precision techniques for determining permafrost absence/presence suitable for areas with deep active layers and/or coarse surficial materials;
6. Development of an open-source script for generating daily and monthly summaries from hourly/bi-hourly temperature recordings made by Onset Hobo loggers;
7. Consideration of snow density, depth and background climate conditions in parameterizing n-factors for spatial numerical modelling of permafrost;
8. Development of an open-source TTOP model that is computationally efficient and regionally-transferable;
9. Provision of code in the statistical software R for TTOP modelling used in this dissertation.

7.3 Research limitations

This dissertation represents a significant step towards characterizing the contemporary distribution of permafrost across Labrador, and understanding its linkages with the range of environmental settings observed throughout the region. However, several limitations remain and these will be discussed in detail within this section.

The most important limitation relates to the distribution of study sites. Due to the costs and logistical challenges of accessing remote regions in Labrador, it was not possible to sample the full range of environments across the region. Notably, the monitoring network established was distributed along accessible roads and trail routes. Data in this thesis were obtained from multiple sites within each of the ten ecoregions in Labrador (Roberts et al. 2006) with the notable exception of the low Arctic Tundra zone found in the northernmost section of the Torngat Mountains National Park. Furthermore, the mountainous northern interior of Labrador which includes the Harp Lake Complex and inland portions of Torngat Mountains National Park were not visited for field investigation (see Figure 1-4).

Many mountainous regions in southern Labrador were also too remote to be accessible so inferences had to be drawn from locations with similar environmental settings. At the local scale, site selection was dependent on site accessibility and distance. For example, monitoring stations established on hilltops were located on mountains with shorter, safer access routes than other potential study sites. These types of decisions may have introduced subtle biases into data collection and analysis even though considerable effort was made to acquire data from the less accessible locations that have been previously studied (including the Torngat Mountains National Park and the Mealy Mountains National Park Reserve).

The identification of representative monitoring locations also relies on a fundamental assumption of consistency in associations between variables affecting ground temperatures. However, this assumption could be invalid if undiscovered non-linear associations exist between variables. In support of the approach employed in this dissertation, we found consistent results across the various monitoring stations despite their distribution spanning continental, coastal and alpine ecozones (Chapter 5). Notably, snow depth was the primary determinant of ground surface temperatures, and correspondingly permafrost throughout Labrador. This finding is similar to inferences for the region as a whole made from field data in western Labrador and northern Québec (Allard and Séguin 1987; Granberg 1989).

In this dissertation, permafrost investigations were specifically targeted to support the application of the temperature at the top of permafrost (TTOP) model to Labrador. Field data collection attempted to use the best available permafrost detection techniques including DC electrical resistivity tomography (ERT) and standard field methods (frost probing, instantaneous ground temperature measurements). However, despite their widespread usage, detection of permafrost bodies with these techniques can be inexact and efficacy will depend on the substrate being examined (Lewkowicz et al. 2011; Hauck 2013; Oldenborger and LeBlanc 2015). For example, areas with coarser grained tills and near-surface bedrock were difficult to differentiate from warm permafrost with ERT because of their similar modelled resistivities (Chapter 4). To reduce uncertainties caused by imperfect field techniques, ground temperatures were recorded for 1 to 2 years at many locations using ibutton loggers placed at the deepest attainable depths. These ground temperatures were used to verify the presence and/or absence of permafrost according to the thermal definition. This technique was necessary for identifying permafrost at sites with near-surface bedrock and coarse surficial materials where active layers are thick or impenetrable. However, even this method is subject to error if climatic conditions during monitoring differ from long-term averages. The collection of permafrost/unfrozen ground cores at field sites would have been very useful to validate the geophysical investigations, and in the case of the palsa sites, could have assisted in model parameterization. Collection of shallow cores may have also permitted the calculation of active layer properties which could have helped calibrate inputs used in spatial modelling. Finally, cores taken at peatland sites would have helped to elucidate ice segregation processes and to date palsa formation as was done previously at Blanc Sablon, QC (Dionne and Richard 2006).

Permafrost modelling undertaken in support of this dissertation consisted of transient 1-dimensional modelling with the Northern Ecosystem Soil Temperature model (NEST) (Zhang et al. 2003) for coastal peatland permafrost and equilibrium spatial modelling across all of Labrador-Ungava using the temperature at the top of permafrost model (TTOP) (Smith and Riseborough 1996; Smith and Riseborough

2002). The transient modelling with NEST was conducted by Dr. Yu Zhang and was informed by field data and surficial observations collected for two coastal peatland permafrost sites as part of this dissertation. This analysis provided an estimate of permafrost thicknesses and temperatures for historical and future climate scenarios in southern areas of coastal Labrador. Although 1-dimensional modelling is a reasonable approach to predicting permafrost evolution, characterization of expected changes for localized features such as the palsas analyzed in this dissertation can be influenced by multiple potential degradational pathways. Under a warming scenario, 1-dimensional modelling may indicate greater palsa persistence than in a 2-dimensional modelling framework where lateral heat transfer can be considered (e.g. Smith and Riseborough 2010).

For spatial modelling, an equilibrium approach (TTOP) was used to analyze ground temperatures across the region. Unlike the 1-dimensional modelling with NEST, TTOP modelling does not consider factors affecting permafrost formation and degradation due to a disequilibrium from observed climate conditions (Riseborough 2007), particularly in finer surficial materials where excess ice is more common (Riseborough 2004; Riseborough 2007). The use of an equilibrium model therefore results in greater uncertainties in modelling permafrost distribution but the use of multiple (long) time periods for describing permafrost may reduce uncertainties at non-equilibrium permafrost locations (Chapter 6). The TTOP model presented in this dissertation was also run at a higher resolution (250 m) than in many recent studies, but remains significantly lower resolution than would be needed to characterize permafrost for effective infrastructure planning purposes (<30 m). Deciding on an appropriate spatial resolution was a particularly challenging problem because many of the input datasets (surficial materials, snow cover) were available only at coarser resolutions (Chapter 6). For higher resolution grids that are publicly available, it is worth considering whether they can increase the accuracy of predictions given the often-sparse input data networks. For the TTOP model used in this study, determination of the most appropriate performance metrics remains an open question because local-scale variability in snow cover and surficial material occurs over very small distances (<1 m) (Gubler et al. 2011; Gubler et al. 2013b; Gisnås et al. 2014). Given current satellite sensors, it is unlikely that either variable will be able to be predicted with high accuracy at a high resolution over large spatial domains in the near future (Chapter 5).

Representing snow cover is the greatest challenge in describing permafrost characteristics across larger spatial domains with TTOP or other modelling techniques (Gisnås et al. 2014; Gisnås et al. 2016b). The treatment of snow in the TTOP modelling in this dissertation was split into two components. The first was the redistribution of regional snow cover across the landscape and the second was the parameterization of the effect of snow cover on ground surface temperatures through freezing n-factors. The former was the

largest source of uncertainty in TTOP modelling because of the variation in how topography and vegetation cover redistribute regional-scale snowfall at the local-scale, particularly in mountainous environments (Gisnås et al. 2014; Gisnås et al. 2016b). By explicitly including topography and vegetation-induced snow redistribution in the Labrador Permafrost Project TTOP model, this dissertation took an important first step towards more accurate permafrost distribution characterization but more work is needed to refine this approach (Chapter 6). Improvements could be achieved with the development of region-specific gridded snow depth datasets that explicitly incorporate elevation-dependent snow accumulation at high resolution. The second major component of representing snow in TTOP was the determination of how snow affects the thermal properties of the ground through freezing n-factors (nF). In this dissertation, nF parameterization was guided by 1-dimensional model simulations performed by Riseborough (2004) which were digitized and interpolated (Chapter 6). This approach allowed for the effects of winter equivalent snow depth and mean annual air temperature to be combined when calculating nF and resulted in lower uncertainties than other commonly used nF parameterization methods per field data (Chapter 5). Further refinements to this process should include better calculation of the thermal equivalents for various snow depths using local snow density data (Derksen et al. 2014).

7.4 Future research directions

7.4.1 Regional studies

The focus of field investigations in this dissertation was primarily on permafrost towards the southern end of the discontinuous zone in Labrador. Future research endeavours should focus on understanding the current distribution of permafrost in northern Labrador and how it may respond to a warming climate. The recently launched Torngat Permafrost Project (est. 2016), a sub-component of the Labrador Permafrost Project, will serve as the primary research avenue for increasing our understanding of permafrost in Arctic Labrador. This project will focus on characterizing the regional distribution of permafrost within the Torngat Mountains National Park and will examine landscape susceptibility to change throughout the region.

A key question that has arisen is how rapid Arctic greening and shrubification in northern Labrador will impact regional permafrost in the future. Initial fieldwork in August 2016 provided the first empirical observations of permafrost in the Torngat Mountains National Park (TMNP) and when combined with co-located shrub sampling plots, will develop insights into the linkages between permafrost, land cover type and susceptibility to future change. Coastal areas south of TMNP in northern Labrador are expected to experience considerable change because organic soils are widespread below the marine limit. These

environments, found typically between Nain and the southern TMNP, include numerous peatland permafrost features which should be examined for historical change with aerial photography and satellite imagery (Figure 1-5). This area of northern Labrador is of interest because it coincides with the position of the Arctic treeline (Payette 2007). Furthermore, studies of permafrost across Labrador and northern Québec suggest that permafrost should not exist in forested environments and yet permafrost was encountered during field investigations of a forested slope at Nain (Chapter 4). Future model simulations should examine the variety of environments that would be suitable for permafrost under historical and contemporary scenarios in this region to better understand the evolution of permafrost in Labrador.

The newly established Mealy Mountains National Park Reserve (MMNPR) in eastern Labrador will provide a further opportunity to document the complex interactions permafrost and environmental setting while working in conjunction with Parks Canada and local Inuit and Innu to establish a regional monitoring system that is sustainable over longer timescales (e.g. decades). This region includes the boreal forest to coastal tundra transition at low elevations and subarctic taiga to high subarctic tundra transition at high elevations (Jacobs et al. 2014). Permafrost exists beneath wind-exposed slopes at high elevation (Jacobs et al. 2014) and in coastal peatlands adjacent to the Labrador Sea making a complicated distribution within MMNPR (Chapter 3). As a high snowfall (300+ cm) mountain range with 12 different terrestrial ecozones, MMNPR provides a unique opportunity to study permafrost interactions with snow variability across major vegetation transitions. Increasing our capacity to predict snow cover variability would require examining how snow depth and density is distributed across various ecotypes and correspondingly how this interacts with soil temperatures and shrub growth. MMNPR can be accessed by floatplane/helicopter in the summer but it is most readily accessed (like much of Labrador) via snowmobile in winter. To characterize permafrost in this region, it may be necessary to develop a means of setting up winter monitoring stations and/or collecting winter field data which can be used to inform high resolution spatial modelling. The inadequacy of existing snow depth datasets and the necessity for information on snow density suggest that the latter point would be also advantageous for informing permafrost research in other areas of Labrador. Although not reported directly in this dissertation, considerable effort has been placed on collecting winter data in Labrador using the basal temperature of snow method with several successful field seasons. As such, this technique could be employed reliably in MMNPR, perhaps in conjunction with satellite remote sensing and UAV data which may be needed to link between broader spatial patterns and local sources of variability (e.g. snow) that manifest at the sub-gridcell scale.

7.4.2 Modelling studies

This dissertation primarily demonstrated the efficacy and applicability of analytical permafrost modelling techniques, but many recent permafrost studies have used transient 1-dimensional models which have been employed over large spatial domains (Jafarov et al. 2012; Zhang 2013; Ou et al. 2016b; Ou et al. 2016a). Both techniques have advantages and disadvantages but progress should continue to be made in terms of improving their respective accuracies and applicability to permafrost-relevant solutions. More work is needed to ensure that primary climate data used as inputs for most permafrost spatial-modelling techniques is quality-controlled and temporally consistent to avoid further use of *ad hoc* approaches to representing climate at study sites (Chapter 2). Future studies should use techniques that have been developed and tested by those in the climate community to reduce duplication of efforts and to enhance dataset accuracy.

For the TTOP model used in this study and many others, future work should focus on incorporating the cumulative uncertainties into model outputs (e.g. Gubler et al. 2013b). Incorporation of cumulative uncertainties from data inputs into spatial numerical modelling remains a significant challenge that has not been addressed adequately to date. Recent studies have used a variety of simulations of relevant factors including rk and n-factors to estimate the uncertainties in ground temperature and permafrost distribution (Westermann et al. 2015a; Gisnås et al. 2016a). However, consideration should be given towards the use of a Bayesian framework that incorporates existing information on permafrost distribution in the form of informed priors that could optimize spatial modelling of permafrost (e.g. Matney 2014). This type of approach would allow for the cumulative uncertainties in input parameters to be included in the modelling framework without ignoring prior information on regional permafrost characteristics or its historical genesis.

A fundamental question arising from the use of TTOP modelling in this dissertation is what could be done to improve the modelling results? Several amendments to the TTOP modelling process are possible:

- The TTOP model in this dissertation should be run using updated climate data grids which incorporate more climate monitoring sites, including those established in this dissertation.
- Future TTOP modelling runs should include a new gridded snow depth dataset being generated by Natural Resources Canada (*Dr. Dan McKenney personal communication*) using techniques similar to those found in this dissertation for interpolating temperature in Chapter 2. This dataset has been suggested to be more accurate than the snow depth dataset used in TTOP modelling in this dissertation (*Ross Brown personal communication*).

- The TTOP model in this dissertation used the CCRS MODIS product (250 m resolution) (Trishchenko et al. 2009) for partitioning Labrador-Ungava into land cover classes because it is spatially and temporally consistent with no artificial boundaries. However, alternative land cover products should be considered. For example, in Chapter 5 a variety of land cover datasets were evaluated with several showing more accurate results at the Labrador monitoring stations than the CCRS MODIS product.
- The TTOP model in this dissertation would be improved by better parameterizing the distribution of thermal offsets. In this dissertation, a simplified scheme was used that assumed an equal influence of vegetation and surficial materials on the overall thermal offset with the latter estimated from an interpolated product (Hengl et al. 2014). It would be advantageous in the future to generate a Labrador-wide surficial materials map which includes detailed knowledge of the marine limit in coastal areas. This should allow rk to be directly parameterized in a more precise manner than using thermal offsets.
- To understand permafrost changes across the region, the amended TTOP model should be run for Little Ice Age and future climate scenarios. The Little Ice Age is particularly important for understanding the contemporary distribution of permafrost in the region as it has been shown that much of the peatland permafrost in northern Québec was formed during this period (Brown 1979; Payette et al. 2004; Dionne and Richard 2006). Running the TTOP model from Little Ice Age to present and then into the future would provide a means of evaluating which landscapes are most susceptible to future changes in regional climate.
- A different approach to generating permafrost probability maps should be developed to ensure that the range of environments within a gridcell is considered in the context of observed field data. A suggested option would be to convert output TTOP ground temperatures to permafrost probabilities directly using logistic regression against known observations of permafrost distribution. This method was used to produce a high precision map of permafrost distribution in western Labrador but this research goes beyond the scope of this dissertation.

Despite the various set of limitations and/or amendments discussed with respect to the Labrador TTOP model, the iteration presented in this dissertation is an important step towards refining the use of analytical models for characterizing permafrost environments. In the absence of evidence to the contrary, there is no reason to suggest that the model presented in this dissertation could not be employed elsewhere in Subarctic Canada with a relatively high degree of precision in representing ground temperature

variations across large spatial domains. By integrating field data, monitoring stations and spatial numerical modelling, this dissertation has shown that field and modelling data can be coupled effectively to produce a rapid understanding of understudied permafrost environments.

7.5 References

Allard, M., and M. K. Séguin. 1987. Le pergélisol au Québec nordique : bilan et perspectives. Géographie physique et Quaternaire 41(1): 141. doi: 10.7202/032671ar.

Brown, R. J. 1979. Permafrost distribution in the southern part of the discontinuous zone in Quebec and Labrador. Géographie physique et Quaternaire 33(3–4): 279–289.

Derksen, C., J. Lemmetyinen, P. Toose, A. Silis, J. Pulliainen, and M. Sturm. 2014. Physical properties of Arctic versus subarctic snow: Implications for high latitude passive microwave snow water equivalent retrievals. Journal of Geophysical Research: Atmospheres 119(12): 2013JD021264. doi: 10.1002/2013JD021264.

Dionne, J.-C., and P. J. H. Richard. 2006. Origine, Age et taux d'accrétion verticale de la tourbiere palses de Blanc-Sablon, basse Cote-Nord, Golfe du Saint-Laurent, Québec. Géographie physique et Quaternaire 60(2): 199–205. doi: 10.7202/016829ar.

Gisnås, K., S. Westermann, T. V. Schuler, T. Litherland, K. Isaksen, J. Boike, and B. Etzelmüller. 2014. A statistical approach to represent small-scale variability of permafrost temperatures due to snow cover. The Cryosphere 8(6): 2063–2074. doi: 10.5194/tc-8-2063-2014.

Gisnås, K., B. Etzelmüller, C. Lussana, J. Hjort, A. B. K. Sannel, K. Isaksen, S. Westermann, P. Kuhry, H. H. Christiansen, A. Frampton, and J. Åkerman. 2016a. Permafrost Map for Norway, Sweden and Finland: Permafrost map for Norway, Sweden and Finland. Permafrost and Periglacial Processes. doi: 10.1002/ppp.1922.

Gisnås, K., S. Westermann, T. V. Schuler, K. Melvold, and B. Etzelmüller. 2016b. Small-scale variation of snow in a regional permafrost model. The Cryosphere 10(3): 1201–1215. doi: 10.5194/tc-10-1201-2016.

Granberg, H. B. 1989. Permafrost mapping at Schefferville, Québec. Physical Geography 10(3): 249–269.

Gubler, S., J. Fiddes, M. Keller, and S. Gruber. 2011. Scale-dependent measurement and analysis of ground surface temperature variability in alpine terrain. The Cryosphere 5(2): 431–443. doi: 10.5194/tc-5-431-2011.

Gubler, S., S. Endrizzi, S. Gruber, and R. S. Purves. 2013. Sensitivities and uncertainties of modeled ground temperatures in mountain environments. Geoscientific Model Development 6(4): 1319–1336. doi: 10.5194/gmd-6-1319-2013.

Hauck, C. 2013. New Concepts in Geophysical Surveying and Data Interpretation for Permafrost Terrain: Geophysical Surveying in Permafrost Terrain. Permafrost and Periglacial Processes 24(2): 131–137. doi: 10.1002/ppp.1774.

Heginbottom, J. A., M.-A. Dubreuil, and P. A. Harker. 1995. Canada – Permafrost. National Atlas of Canada, 5th Edition. Ottawa, Canada: Natural Resources Canada.

Hengl, T., J. M. de Jesus, R. A. MacMillan, N. H. Batjes, G. B. M. Heuvelink, E. Ribeiro, A. Samuel-Rosa, B. Kempen, J. G. B. Leenaars, M. G. Walsh, and M. R. Gonzalez. 2014. SoilGrids1km — Global soil information based on automated mapping. Edited by Ben Bond-Lamberty. PLoS ONE 9(8): e105992. doi: 10.1371/journal.pone.0105992.

Jacobs, J. D., S. Chan, and E. Sutton. 2014. Climatology of the Forest-Tundra Ecotone at a Maritime Subarctic-Alpine Site, Mealy Mountains, Labrador. ARCTIC 67(1): 28–42. doi: 10.14430/arctic4358.

Jafarov, E. E., S. S. Marchenko, and V. E. Romanovsky. 2012. Numerical modeling of permafrost dynamics in Alaska using a high spatial resolution dataset. The Cryosphere 6(3): 613–624. doi: 10.5194/tc-6-613-2012.

Lewkowicz, A. G., B. Etzelmüller, and S. L. Smith. 2011. Characteristics of discontinuous permafrost based on ground temperature measurements and electrical resistivity tomography, southern Yukon, Canada. Permafrost and Periglacial Processes 22(4): 320–342. doi: 10.1002/ppp.703.

Matney, J. A. 2014. Bayesian hierarchical models for environmental datasets. MSc Thesis, East Lansing, Michigan, United States of America: Michigan State University.

Oldenborger, G. A., and A.-M. LeBlanc. 2015. Geophysical characterization of permafrost terrain at Iqaluit International Airport, Nunavut. Journal of Applied Geophysics 123: 36–49. doi: 10.1016/j.jappgeo.2015.09.016.

Ou, C., B. Leblon, Y. Zhang, A. LaRocque, K. Webster, and J. McLaughlin. 2016a. Modelling and mapping permafrost at high spatial resolution using Landsat and Radarsat images in northern Ontario, Canada: Part 1 – model calibration. International Journal of Remote Sensing 37(12): 2727–2750. doi: 10.1080/01431161.2016.1157642.

Ou, C., A. LaRocque, B. Leblon, Y. Zhang, K. Webster, and J. McLaughlin. 2016b. Modelling and mapping permafrost at high spatial resolution using Landsat and Radarsat-2 images in Northern Ontario, Canada: Part 2 – regional mapping. International Journal of Remote Sensing 37(12): 2751–2779. doi: 10.1080/01431161.2016.1151574.

Payette, S. 2007. Contrasted Dynamics of Northern Labrador Tree Lines Caused by Climate Change and Migrational Lag. Ecology 88(3): 770–780. doi: 10.1890/06-0265.

Payette, S., A. Delwaide, M. Caccianiga, and M. Beauchemin. 2004. Accelerated thawing of subarctic peatland permafrost over the last 50 years. Geophysical Research Letters 31(18): L18208. doi: 10.1029/2004GL020358.

Riseborough, D. 2007. The effect of transient conditions on an equilibrium permafrost-climate model. Permafrost and Periglacial Processes 18(1): 21–32. doi: 10.1002/ppp.579.

Riseborough, D. W. 2004. Exploring the parameters of a simple model of the permafrost-climate relationship. PhD Thesis, Ottawa: Carleton University.

Roberts, B. A., N. P. P. Simon, and K. W. Deering. 2006. The forests and woodlands of Labrador, Canada: ecology, distribution and future management. Ecological Research 21(6): 868–880. doi: 10.1007/s11284-006-0051-7.

Smith, M. W., and D. W. Riseborough. 1996. Permafrost monitoring and detection of climate change. Permafrost and Periglacial Processes 7(4): 301–309. doi: 10.1002/(SICI)1099-1530(199610)7:4<301::AID-PPP231>3.0.CO;2-R.

Smith, M. W., and D. W. Riseborough. 2002. Climate and the limits of permafrost: a zonal analysis. Permafrost and Periglacial Processes 13(1): 1–15. doi: 10.1002/ppp.410.

Smith, S. L., and D. W. Riseborough. 2010. Modelling the thermal response of permafrost terrain to right-of-way disturbance and climate warming. Cold Regions Science and Technology 60(1): 92–103. doi: 10.1016/j.coldregions.2009.08.009.

Trant, A. J., K. Lewis, B. H. Cranston, J. A. Wheeler, R. G. Jameson, J. D. Jacobs, L. Hermanutz, and B. M. Starzomski. 2015. Complex changes in plant communities across a Subarctic alpine tree line in Labrador, Canada. ARCTIC 68(4): 500. doi: 10.14430/arctic4528.

Trishchenko, A. P., Y. Luo, K. V. Khlopenkov, W. M. Park, and S. Wang. 2009. Arctic circumpolar mosaic at 250 m spatial resolution for IPY by fusion of MODIS/TERRA land bands B1–B7. International Journal of Remote Sensing 30(6): 1635–1641. doi: 10.1080/01431160802348119.

van Vuuren, D. P., J. Edmonds, M. Kainuma, K. Riahi, A. Thomson, K. Hibbard, G. C. Hurtt, T. Kram, V. Krey, J.-F. Lamarque, T. Masui, M. Meinshausen, N. Nakicenovic, S. J. Smith, and S. K. Rose. 2011. The representative concentration pathways: an overview. Climatic Change 109(1–2): 5–31. doi: 10.1007/s10584-011-0148-z.

Way, R. G., and P. P. Bonnaventure. 2015. Testing a reanalysis-based infilling method for areas with sparse discontinuous air temperature data in northeastern Canada: Reanalysis-based infilling in northeastern Canada. Atmospheric Science Letters 16(3): 398–407. doi: 10.1002/asl2.574.

Westermann, S., T. I. Østby, K. Gisnås, T. V. Schuler, and B. Etzelmüller. 2015. A ground temperature map of the North Atlantic permafrost region based on remote sensing and reanalysis data. The Cryosphere 9(3): 1303–1319. doi: 10.5194/tc-9-1303-2015.

Zhang, Y. 2013. Spatio-temporal features of permafrost thaw projected from long-term high-resolution modeling for a region in the Hudson Bay Lowlands in Canada. Journal of Geophysical Research: Earth Surface 118(2): 542–552. doi: 10.1002/jgrf.20045.

Zhang, Y., W. Chen, and J. Cihlar. 2003. A process-based model for quantifying the impact of climate change on permafrost thermal regimes. Journal of Geophysical Research 108(D22). doi: 10.1029/2002JD003354.

7.6 Thesis bibliography

Aalto, J., P. Pirinen, J. Heikkinen, and A. Venäläinen. 2013. Spatial interpolation of monthly climate data for Finland: comparing the performance of kriging and generalized additive models. Theoretical and Applied Climatology 112(1–2): 99–111. doi: 10.1007/s00704-012-0716-9.

Allard, M., and L. Rousseau. 1999. The internal structure of a palsa and peat plateau in the Riviere Boniface region, Québec: Inferences on the formation of ice segregation mounds. Géographie physique et Quaternaire 53(3): 373–387.

Allard, M., and M. K. Séguin. 1987. Le pergélisol au Québec nordique : bilan et perspectives. Géographie physique et Quaternaire 41(1): 141. doi: 10.7202/032671ar.

Allard, M., R. Fortier, and M. K. Seguin. 1992. The thermal regime of intertidal permafrost, George River estuary, Ungava Bay, Quebec. Canadian Journal of Earth Sciences 29(2): 249–259.

Allard, M., M. Lemay, C. Barrette, E. L'Hérault, D. Sarrazin, T. Bell, and G. Doré. 2012a. Permafrost and climate change in Nunavik and Nunatsiavut: Importance for municipal and transportation infrastructures. In Nunavik and Nunatsiavut: From science to policy. An Integrated Regional Impact Study (IRIS) of climate change and modernization, 171–197.

Allard, M., M. Lemay, C. Barrette, E. L'Hérault, D. Sarrazin, T. Bell, and G. Doré. 2012b. Permafrost and climate change in Nunavik and Nunatsiavut: Importance for municipal and transportation infrastructures. In Nunavik and Nunatsiavut: From science to policy. An Integrated Regional Impact Study (IRIS) of climate change and modernization, 171–197.

Allard, M., D. Sarrazin, and E. L'Hérault. 2014. Borehole monitoring temperatures in northeastern Canada v. 1.2 (1988-2014). Scientific data. Nordicana D8. Centre D'Étude Nordiques.

Allen, J. C. 1976. A modified sine wave method for calculating degree days. Environmental Entomology 5(3): 388–396.

An, W., and M. Allard. 1995. A mathematical approach to modelling palsa formation: Insights on processes and growth conditions. Cold Regions Science and Technology 23(3): 231–244.

Anderson, R. K., G. H. Miller, J. P. Briner, N. A. Lifton, and S. B. DeVogel. 2008. A millennial perspective on Arctic warming from 14C in quartz and plants emerging from beneath ice caps. Geophysical Research Letters 35: 01502.

Andrews, J. T. 1961. Permafrost in southern Labrador-Ungava. Canadian Geographer 5(3): 34–35.

Atkinson, D. E., and K. Gajewski. 2002. High-Resolution Estimation of Summer Surface Air Temperature in the Canadian Arctic Archipelago. Journal of Climate 15(24): 3601–3614. doi: 10.1175/1520-0442(2002)015<3601:HREOSS>2.0.CO;2.

Aznar, J.-C., E. Gloaguen, D. Tapsoba, S. Hachem, D. Caya, and Y. Bégin. 2013. Interpolation of monthly mean temperatures using cokriging in spherical coordinates. International Journal of Climatology 33(3): 758–769. doi: 10.1002/joc.3468.

Banfield, C. E., and J. D. Jacobs. 1998. Regional patterns of temperature and precipitation for Newfoundland and Labrador during the past century. The Canadian Geographer/Le Géographe canadien 42(4): 354–364.

Barrand, N. E., R. G. Way, T. Bell, and M. J. Sharp. 2017. Recent changes in area and thickness of Torngat Mountain glaciers (northern Labrador, Canada). The Cryosphere 11(1): 157–168. doi: 10.5194/tc-11-157-2017.

Beaulieu, N., and M. Allard. 2003. The impact of climate change on an emerging coastline affected by discontinuous permafrost: Manitounuk Strait, northern Quebec. Canadian Journal of Earth Sciences 40(10): 1393–1404. doi: 10.1139/e03-056.

Belcher, D. J. 1949. The use of aerial photographs for pre-determining ground conditions in the Arctic and sub-Arctic regions of North America. Unpublished research report. Arctic Institute of North America.

Bell, T., M. Putt, and T. Sheldon. 2011. Landscape hazard assessment in Nain, Phase 1: Inventory of surficial sediment types and infrastructure damage. Technical report. Nunatsiavut Government.

Bevington, A., and A. G. Lewkowicz. 2015. Assessment of a land cover driven TTOP model for mountain and lowland permafrost using field data, southern Yukon and northern British Columbia, Canada. In Proceedings of GéoQuebec: 68th Canadian Geotechnical Conference and 7th Canadian Permafrost Conference, 9. Québec City, Canada.

Bonifacio, C., T. E. Barchyn, C. H. Hugenholtz, and S. W. Kienzle. 2015. CCDST: A free Canadian climate data scraping tool. Computers & Geosciences 75: 13–16. doi: 10.1016/j.cageo.2014.10.010.

Bonnaventure, P. P., and A. G. Lewkowicz. 2011. Modelling climate change effects on the spatial distribution of mountain permafrost at three sites in northwest Canada. Climatic Change 105(1–2): 293–312. doi: 10.1007/s10584-010-9818-5.

Bonnaventure, P. P., and A. G. Lewkowicz. 2013. Impacts of mean annual air temperature change on a regional permafrost probability model for the southern Yukon and northern British Columbia, Canada. The Cryosphere 7(3): 935–946. doi: 10.5194/tc-7-935-2013.

Bonnaventure, P. P., A. G. Lewkowicz, M. Kremer, and M. C. Sawada. 2012. A permafrost probability model for the southern Yukon and northern British Columbia, Canada. Permafrost and Periglacial Processes 23(1): 52–68. doi: 10.1002/ppp.1733.

Borge, A. F., S. Westermann, I. Solheim, and B. Etzelmüller. 2017. Strong degradation of palsas and peat plateaus in northern Norway during the last 60 years. The Cryosphere 11(1): 1–16. doi: 10.5194/tc-11-1-2017.

Briggs, M. A., S. Campbell, J. Nolan, M. A. Walvoord, D. Ntarlagiannis, F. D. Day-Lewis, and J. W. Lane. 2016. Surface Geophysical Methods for Characterising Frozen Ground in Transitional Permafrost Landscapes: Surface Geophysical Methods for Characterising Frozen Ground. Permafrost and Periglacial Processes. doi: 10.1002/ppp.1893.

Brown, R., M. Lemay, M. Allard, N. E. Barrand, C. Barrette, Y. Bégin, T. Bell, M. Bernier, S. Bleau, D. Chaumont, Y. Dibike, A. Frigon, P. Leblanc, D. Paquin, M. J. Sharp, and R. Way. 2012. Climate variability and change in the Canadian Eastern Subarctic IRIS region (Nunavik and Nunatsiavut). In Nunavik and Nunatsiavut: From science to policy. An Integrated Regional Impact Study (IRIS) of climate change and modernization, 57–93.

Brown, R. D., and B. Brasnett. 2010. Canadian Meteorological Centre (CMC) Daily Snow Depth Analysis Data. National Snow and Ice Data Center: Environment Canada.

Brown, R. D., B. Brasnett, and D. Robinson. 2003. Gridded North American monthly snow depth and snow water equivalent for GCM evaluation. Atmosphere-Ocean 41(1): 1–14. doi: 10.3137/ao.410101.

Brown, R. J. 1979. Permafrost distribution in the southern part of the discontinuous zone in Quebec and Labrador. Géographie physique et Quaternaire 33(3–4): 279–289.

Brown, R. J. E. 1960. The distribution of permafrost and its relation to air temperature in Canada and the USSR. Arctic: 163–177.

Brown, R. J. E. 1967. Permafrost investigations in British Columbia and Yukon Territory. 253. Division of Building Research. National Research Council of Canada.

Brown, R. J. E. 1975. Permafrost Investigations in Quebec and Newfoundland (Labrador). Technical Paper 449. Ottawa, Ontario: National Research Council of Canada.

Burn, C. R., and C. A. S. Smith. 1988. Observations of the “thermal offset” in near-surface mean annual ground temperatures at several sites near Mayo, Yukon Territory, Canada. ARCTIC 41(2): 99–104. doi: 10.14430/arctic1700.

Buteau, S., R. Fortier, G. Delisle, and M. Allard. 2004. Numerical simulation of the impacts of climate warming on a permafrost mound. Permafrost and Periglacial Processes 15(1): 41–57. doi: 10.1002/ppp.474.

Butler, D. H. 2011. Exploring soilscapes and places inside Labrador Inuit winter dwellings. Canadian Journal of Archaeology 35(1): 55–85.

Cawley, G. C., K. Cowtan, R. G. Way, P. Jacobs, and A. Jokimäki. 2015. On a minimal model for estimating climate sensitivity. Ecological Modelling 297: 20–25. doi: 10.1016/j.ecolmodel.2014.10.018.

CEN. 2013. Environmental data from Boniface river region in Nunavik, Quebec, Canada, v. 1.1 (1988-2013). Scientific data 7. Nordicana D. Centre D'Étude Nordiques.

CEN. 2014. Environmental data from the Blanc-Sablon station, Quebec, Canada, v. 1.0 (1990-2012). Scientific data 5. Nordicana D. Centre D'Étude Nordiques.

Chan, S. 2010. Regional and Local Climatology of a Subarctic Alpine Treeline, Mealy Mountains, Labrador. MSc Thesis, St. John's, Newfoundland and Labrador: Memorial University of Newfoundland.

Clark, C. D., J. K. Knight, and J. T. Gray. 2000. Geomorphological reconstruction of the Labrador sector of the Laurentide Ice Sheet. Quarternary Science Reviews 19(13): 1343–1366.

Comiso, J. C., and D. K. Hall. 2014. Climate trends in the Arctic as observed from space: Climate trends in the Arctic as observed from space. Wiley Interdisciplinary Reviews: Climate Change 5(3): 389–409. doi: 10.1002/wcc.277.

Cook, J., D. Nuccitelli, S. A. Green, M. Richardson, B. Winkler, R. Painting, R. Way, P. Jacobs, and A. Skuce. 2013. Quantifying the consensus on anthropogenic global warming in the scientific literature. Environmental Research Letters 8(2): 024024. doi: 10.1088/1748-9326/8/2/024024.

Cooper, M. D. A., C. Estop-Aragonés, J. P. Fisher, A. Thierry, M. H. Garnett, D. J. Charman, J. B. Murton, G. K. Phoenix, R. Treharne, S. V. Kokelj, S. A. Wolfe, A. G. Lewkowicz, M. Williams, and I. P. Hartley. 2017. Limited contribution of permafrost carbon to methane release from thawing peatlands. Nature Climate Change 7(7): 507–511. doi: 10.1038/nclimate3328.

Cowtan, K., and R. G. Way. 2014. Coverage bias in the HadCRUT4 temperature series and its impact on recent temperature trends: Coverage Bias in the HadCRUT4 Temperature Series. Quarterly Journal of the Royal Meteorological Society 140(683): 1935–1944. doi: 10.1002/qj.2297.

Daly, C. 2006. Guidelines for assessing the suitability of spatial climate data sets. International Journal of Climatology 26(6): 707–721. doi: 10.1002/joc.1322.

Daly, C., M. Halbleib, J. I. Smith, W. P. Gibson, M. K. Doggett, G. H. Taylor, J. Curtis, and P. P. Pasteris. 2008. Physiographically sensitive mapping of climatological temperature and precipitation across the conterminous United States. International Journal of Climatology 28(15): 2031–2064. doi: 10.1002/joc.1688.

D'Arrigo, R., R. Wilson, and G. Jacoby. 2006. On the long-term context for late twentieth century warming. Journal of Geophysical Research 111(D3). doi: 10.1029/2005JD006352.

Davesne, G., D. Fortier, F. Dominé, and J. T. Gray. 2016. Wind driven snow conditions control the occurrence of contemporary marginal mountain permafrost in the Chic-Chocs Mountains, south-eastern Canada - a case study from Mont Jacques-Cartier. The Cryosphere Discussions: 1–31. doi: 10.5194/tc-2016-211.

Derksen, C., S. L. Smith, M. Sharp, L. Brown, S. Howell, L. Copland, D. R. Mueller, Y. Gauthier, C. G. Fletcher, A. Tivy, M. Bernier, J. Bourgeois, R. Brown, C. R. Burn, C. Duguay, P. Kushner, A. Langlois, A. G. Lewkowicz, A. Royer, and A. Walker. 2012. Variability and change in the Canadian cryosphere. Climatic Change 115(1): 59–88. doi: 10.1007/s10584-012-0470-0.

Derksen, C., J. Lemmetyinen, P. Toose, A. Silis, J. Pulliainen, and M. Sturm. 2014. Physical properties of Arctic versus subarctic snow: Implications for high latitude passive microwave snow water

equivalent retrievals. Journal of Geophysical Research: Atmospheres 119(12): 2013JD021264. doi: 10.1002/2013JD021264.

Dilts, T. 2016. Topography Tools for ArcGIS 10.3 and earlier. Http://Www.arcgis.com/Home/item.html?id=b13b3b40fa3c43d4a23a1a09c5fe96b9.

Dionne, J.-C. 1983. Réseaux reliques de polygones de tourbe, moyenne et basse Côte-Nord du Saint-Laurent, Québec. Géographie physique et Quaternaire 37(2): 127. doi: 10.7202/032510ar.

Dionne, J.-C. 1984. Palses et limite méridionale du pergélisol dans l'hemisphere nord: le cas de Blanc-Sablon, Québec. Géographie physique et Quaternaire 38(2): 165–184. doi: 10.7202/032550ar.

Dionne, J.-C., and V. Gérardin. 1988. Observations sur les buttes organiques de la Cote-Nord du golfe du Saint-Laurent, Québec. Géographie physique et Quaternaire 42(3): 289–301. doi: 10.7202/032737ar.

Dionne, J.-C., and P. J. H. Richard. 2006. Origine, Age et taux d'accrétion verticale de la tourbiere palses de Blanc-Sablon, basse Cote-Nord, Golfe du Saint-Laurent, Québec. Géographie physique et Quaternaire 60(2): 199–205. doi: 10.7202/016829ar.

Doré, G., F. Niu, and H. Brooks. 2016. Adaptation methods for transportation infrastructure built on degrading permafrost. Permafrost and Periglacial Processes 27(4): 352–364. doi: 10.1002/ppp.1919.

Douglas, T. A., M. T. Jorgenson, D. R. N. Brown, S. W. Campbell, C. A. Hiemstra, S. P. Saari, K. Bjella, and A. K. Liljedahl. 2016. Degrading permafrost mapped with electrical resistivity tomography, airborne imagery and LiDAR, and seasonal thaw measurements. GEOPHYSICS 81(1): WA71-WA85. doi: 10.1190/geo2015-0149.1.

Dyke, A. S. 2004. An outline of North American deglaciation with emphasis on central and northern Canada. Developments in Quaternary Science 2(B): 373–424.

Elias, S. A. 1982. Paleoenvironmental Interpretation of Holocene Insect Fossils from Northeastern Labrador, Canada. Arctic and Alpine Research 14(4): 311. doi: 10.2307/1550794.

Elliott, D. L., and S. K. Short. 1979. The Northern Limit of Trees in Labrador: A Discussion. ARCTIC 32(3): 201–206. doi: 10.14430/arctic2620.

Evangelista, P. H., S. Kumar, T. J. Stohlgren, and N. E. Young. 2011. Assessing forest vulnerability and the potential distribution of pine beetles under current and future climate scenarios in the Interior West of the US. Forest Ecology and Management 262(3): 307–316. doi: 10.1016/j.foreco.2011.03.036.

Evans, D. J., and R. J. Rogerson. 1988. A radiocarbon-dated gelifluction lobe in the Nachvak Fiord area, northern Labrador, Canada. Earth Surface Processes and Landforms 13(7): 657–662.

Fiddes, J., S. Endrizzi, and S. Gruber. 2015. Large-area land surface simulations in heterogeneous terrain driven by global data sets: application to mountain permafrost. The Cryosphere 9(1): 411–426. doi: 10.5194/tc-9-411-2015.

Finnis, J. 2013. Projected impacts of climate change for the province of Newfoundland and Labrador. Technical report. St. John's, Newfoundland and Labrador: Office of Climate Change, Energy Efficiency and Emissions Trading, Provincial Government of Newfoundland and Labrador.

Fortier, R., M. Allard, S. Buteau, and F. Calmels. 2008. Internal structure and conditions of permafrost mounds at Umiujaq in Nunavik, Canada, inferred from field investigation and electrical resistivity tomography. Canadian Journal of Earth Sciences 45(3): 367–387. doi: 10.1139/E08-004.

Fortier, R., A.-M. LeBlanc, and W. Yu. 2011. Impacts of permafrost degradation on a road embankment at Umiujaq in Nunavik (Quebec), Canada. Canadian Geotechnical Journal 48(5): 720–740. doi: 10.1139/t10-101.

Fortin, M.-C., and K. Gajewski. 2012. Potential problems with the use of gridded climate data in regional quantitative paleoenvironmental studies from data-poor regions. Journal of Paleolimnology 48(3): 641–650. doi: 10.1007/s10933-012-9639-9.

Foster, D. R., and P. H. Glaser. 1986. The raised bogs of south-eastern Labrador, Canada: classification, distribution, vegetation and recent dynamics. Journal of Ecology 74(1): 47–71.
Foster, D. R., H. E. Wright, M. Thelaus, and G. A. King. 1988. Bog development and landform dynamics in central Sweden and south-eastern Labrador, Canada. Journal of Ecology 76(4): 1164–1185.
Fraser, R. H., I. Olthof, M. Carrière, A. Deschamps, and D. Pouliot. 2011. Detecting long-term changes to vegetation in northern Canada using the Landsat satellite image archive. Environmental Research Letters 6(4): 045502. doi: 10.1088/1748-9326/6/4/045502.
Fulton, R. J. 1995. Surficial Materials of Canada. Geological Survey of Canada Map. Natural Resources Canada.
Gajewski, K. 2015. Quantitative reconstruction of Holocene temperatures across the Canadian Arctic and Greenland. Global and Planetary Change 128: 14–23. doi: 10.1016/j.gloplacha.2015.02.003.
Gennaretti, F., D. Arseneault, A. Nicault, L. Perreault, and Y. Begin. 2014. Volcano-induced regime shifts in millennial tree-ring chronologies from northeastern North America. Proceedings of the National Academy of Sciences 111(28): 10077–10082. doi: 10.1073/pnas.1324220111.
Gisnås, K., B. Etzelmüller, H. Farbrot, T. V. Schuler, and S. Westermann. 2013. CryoGRID 1.0: Permafrost distribution in Norway estimated by a spatial numerical model. Permafrost and Periglacial Processes 24(1): 2–19. doi: 10.1002/ppp.1765.
Gisnås, K., S. Westermann, T. V. Schuler, T. Litherland, K. Isaksen, J. Boike, and B. Etzelmüller. 2014. A statistical approach to represent small-scale variability of permafrost temperatures due to snow cover. The Cryosphere 8(6): 2063–2074. doi: 10.5194/tc-8-2063-2014.
Gisnås, K., B. Etzelmüller, C. Lussana, J. Hjort, A. B. K. Sannel, K. Isaksen, S. Westermann, P. Kuhry, H. H. Christiansen, A. Frampton, and J. Åkerman. 2016a. Permafrost Map for Norway, Sweden and Finland: Permafrost map for Norway, Sweden and Finland. Permafrost and Periglacial Processes. doi: 10.1002/ppp.1922.
Gisnås, K., S. Westermann, T. V. Schuler, K. Melvold, and B. Etzelmüller. 2016b. Small-scale variation of snow in a regional permafrost model. The Cryosphere 10(3): 1201–1215. doi: 10.5194/tc-10-1201-2016.
Glaser, P. H. 1992. Raised Bogs in Eastern North America--Regional Controls for Species Richness and Floristic Assemblages. The Journal of Ecology 80(3): 535. doi: 10.2307/2260697.
Goodrich, L. E. 1978. Some results of a numerical study of ground thermal regimes. In Proceedings of the 3rd International Conference on Permafrost, 30–34. Edmonton, Canada: National Research Council of Canada.
Goodrich, L. E. 1982. The influence of snow cover on the ground thermal regime. Canadian Geotechnical Journal 19(4): 421–432. doi: 10.1139/t82-047.
Granberg, H. B. 1973. Indirect mapping of the snowcover for permafrost prediction at Schefferville, Québec. In Proceedings of the 2nd International Conference on Permafrost, 113–120. Washington, USA.
Granberg, H. B. 1988. On the spatial dynamics of snowcover - permafrost relationships at Schefferville. In Proceedings of the 5th International Conference on Permafrost, 159–164. Trondheim, Norway.
Granberg, H. B. 1989. Permafrost mapping at Schefferville, Québec. Physical Geography 10(3): 249–269.
Granberg, H. B. 1994. Mapping heat loss zones for permafrost prediction at the northern/alpine limit of the Boreal forest using high-resolution C-Band SAR. Remote sensing of environment 50(3): 280–286.
Gray, J. T., and R. J. E. Brown. 1979. Permafrost presence and distribution in the Chic-Chocs Mountains, Gaspésie, Québec. Géographie physique et Quaternaire 33(3–4): 299. doi: 10.7202/1000366ar.
Gruber, S. 2012. Derivation and analysis of a high-resolution estimate of global permafrost zonation. The Cryosphere 6(1): 221–233. doi: 10.5194/tc-6-221-2012.

Gubler, S., J. Fiddes, M. Keller, and S. Gruber. 2011. Scale-dependent measurement and analysis of ground surface temperature variability in alpine terrain. The Cryosphere 5(2): 431–443. doi: 10.5194/tc-5-431-2011.

Gubler, S., S. Endrizzi, S. Gruber, and R. S. Purves. 2013a. Sensitivities and uncertainties of modeled ground temperatures in mountain environments. Geoscientific Model Development 6(4): 1319–1336. doi: 10.5194/gmd-6-1319-2013.

Gubler, S., S. Endrizzi, S. Gruber, and R. S. Purves. 2013b. Sensitivities and uncertainties of modeled ground temperatures in mountain environments. Geoscientific Model Development 6(4): 1319–1336. doi: 10.5194/gmd-6-1319-2013.

Gurney, S. D. 2001. Aspects of the genesis, geomorphology and terminology of palsas: perennial cryogenic mounds. Progress in Physical Geography 25(2): 249–260.

Hachem, S., M. Allard, and C. R. Duguay. 2008. A new permafrost map of Quebec-Labrador derived from near-surface temperature data of the Moderate Resolution Imaging Spectroradiometer (MODIS). In Proceedings of the 9th International Conference on Permafrost, 591–596. Fairbanks, United States of America.

Hachem, S., M. Allard, and C. Duguay. 2009. Using the MODIS land surface temperature product for mapping permafrost: an application to northern Québec and Labrador, Canada. Permafrost and Periglacial Processes 20(4): 407–416. doi: 10.1002/ppp.672.

Harris, I., P. D. Jones, T. J. Osborn, and D. H. Lister. 2014. Updated high-resolution grids of monthly climatic observations–the CRU TS3. 10 Dataset. International Journal of Climatology 34(3): 623–642.

Hasler, A., M. Geertsema, V. Foord, S. Gruber, and J. Noetzli. 2015. The influence of surface characteristics, topography and continentality on mountain permafrost in British Columbia. The Cryosphere 9(3): 1025–1038. doi: 10.5194/tc-9-1025-2015.

Hauck, C. 2013. New Concepts in Geophysical Surveying and Data Interpretation for Permafrost Terrain: Geophysical Surveying in Permafrost Terrain. Permafrost and Periglacial Processes 24(2): 131–137. doi: 10.1002/ppp.1774.

Hauck, C., D. Vonder Mühll, and H. Maurer. 2003. Using DC resistivity tomography to detect and characterize mountain permafrost. Geophysical prospecting 51(4): 273–284.

Heginbottom, J. A., M.-A. Dubreuil, and P. A. Harker. 1995. Canada – Permafrost. National Atlas of Canada, 5th Edition. Ottawa, Canada: Natural Resources Canada.

Helm, V., A. Humbert, and H. Miller. 2014. Elevation and elevation change of Greenland and Antarctica derived from CryoSat-2. The Cryosphere 8(4): 1539–1559. doi: 10.5194/tc-8-1539-2014.

Hendershot, W. H. 1984. A Comparison of some Upland and Valley Soils in the Ungava-Labrador Peninsula. Géographie physique et Quaternaire 38(3): 243. doi: 10.7202/032566ar.

Hendershot, W. H. 1985. Comparison of Canadian and American classification systems for some arctic soils of the Ungava-Labrador Peninsula. Canadian journal of soil science 65(2): 283–291.

Hengl, T., J. M. de Jesus, R. A. MacMillan, N. H. Batjes, G. B. M. Heuvelink, E. Ribeiro, A. Samuel-Rosa, B. Kempen, J. G. B. Leenaars, M. G. Walsh, and M. R. Gonzalez. 2014. SoilGrids1km — Global soil information based on automated mapping. Edited by Ben Bond-Lamberty. PLoS ONE 9(8): e105992. doi: 10.1371/journal.pone.0105992.

Henningsmoen, K. E. 1977. Pollen-analytical investigations in the L'Anse aux Meadows area, Newfoundland. In The Discovery of a Norse Settlement in America, 289–340. Oslo: Universitetsforlaget.

Henry, K., and M. Smith. 2001. A model-based map of ground temperatures for the permafrost regions of Canada. Permafrost and Periglacial Processes 12(4): 389–398. doi: 10.1002/ppp.399.

Hijmans, R. J., S. E. Cameron, J. L. Parra, P. G. Jones, and A. Jarvis. 2005. Very high resolution interpolated climate surfaces for global land areas. International Journal of Climatology 25(15): 1965–1978. doi: 10.1002/joc.1276.

Hijmans, R. J., J. van Etten, J. Cheng, M. Mattiuzzi, M. Sumner, J. A. Greenberg, O. P. Lamigueiro, A. Bevan, E. B. Racine, A. Shortridge, and M. R. J. Hijmans. 2015. raster (version 2.5-2). Geographic Data Analysis and Modeling.

Hilbich, C., L. Marescot, C. Hauck, M. H. Loke, and R. Mäusbacher. 2009. Applicability of electrical resistivity tomography monitoring to coarse blocky and ice-rich permafrost landforms. Permafrost and Periglacial Processes 20(3): 269–284. doi: 10.1002/ppp.652.

Hong, E., R. Perkins, and S. Trainor. 2014. Thaw Settlement Hazard of Permafrost Related to Climate Warming in Alaska. ARCTIC 67(1): 93. doi: 10.14430/arctic4368.

Hopkinson, R. F., D. W. McKenney, E. J. Milewska, M. F. Hutchinson, P. Papadopol, and L. A. Vincent. 2011. Impact of Aligning Climatological Day on Gridding Daily Maximum–Minimum Temperature and Precipitation over Canada. Journal of Applied Meteorology and Climatology 50(8): 1654–1665. doi: 10.1175/2011JAMC2684.1.

Hopkinson, R. F., M. F. Hutchinson, D. W. McKenney, E. J. Milewska, and P. Papadopol. 2012a. Optimizing Input Data for Gridding Climate Normals for Canada. Journal of Applied Meteorology and Climatology 51(8): 1508–1518. doi: 10.1175/JAMC-D-12-018.1.

Hopkinson, R. F., M. F. Hutchinson, D. W. McKenney, E. J. Milewska, and P. Papadopol. 2012b. Optimizing input data for gridding climate normals for Canada. Journal of Applied Meteorology and Climatology 51(8): 1508–1518. doi: 10.1175/JAMC-D-12-018.1.

Hu, J., and Z. Jiang. 2010. Predicting the potential distribution of the endangered Przewalski's gazelle: Potential distribution of Przewalski's gazelle. Journal of Zoology 282(1): 54–63. doi: 10.1111/j.1469-7998.2010.00715.x.

Hustich, I. 1939. Notes on the coniferous forest and tree limit on the east coast of Newfoundland-Labrador. Acta Geographica 7(1): 5–77.

Hutchinson, M. F., D. W. McKenney, K. Lawrence, J. H. Pedlar, R. F. Hopkinson, E. Milewska, and P. Papadopol. 2009. Development and testing of Canada-wide interpolated spatial models of daily minimum-maximum temperature and precipitation for 1961–2003. Journal of Applied Meteorology and Climatology 48(4): 725–741. doi: 10.1175/2008JAMC1979.1.

Ives, J. D. 1960. Permafrost in central Labrador-Ungava. Journal of Glaciology 3(28): 789–790.

Ives, J. D. 1979. A proposed history of permafrost development in Labrador-Ungava. Géographie physique et Quaternaire 33(3–4): 233–244. doi: 10.7202/1000360ar.

Jacobs, J. D., A. R. Maarouf, and E. A. Perkins. 1996. The recent record of climate on the range of the George River Caribou Herd, Northern Québec and Labrador, Canada. Rangifer 16(4): 193–200.

Jacobs, J. D., S. Chan, and E. Sutton. 2014. Climatology of the Forest-Tundra Ecotone at a Maritime Subarctic-Alpine Site, Mealy Mountains, Labrador. ARCTIC 67(1): 28–42. doi: 10.14430/arctic4358.

Jafarov, E. E., S. S. Marchenko, and V. E. Romanovsky. 2012. Numerical modeling of permafrost dynamics in Alaska using a high spatial resolution dataset. The Cryosphere 6(3): 613–624. doi: 10.5194/tc-6-613-2012.

Jafarov, E. E., V. E. Romanovsky, H. Genet, A. D. McGuire, and S. S. Marchenko. 2013. The effects of fire on the thermal stability of permafrost in lowland and upland black spruce forests of interior Alaska in a changing climate. Environmental Research Letters 8(3): 035030. doi: 10.1088/1748-9326/8/3/035030.

James, M., A. G. Lewkowicz, S. L. Smith, and C. M. Miceli. 2013. Multi-decadal degradation and persistence of permafrost in the Alaska Highway corridor, northwest Canada. Environmental Research Letters 8(4): 045013. doi: 10.1088/1748-9326/8/4/045013.

Jameson, R. G., A. J. Trant, and L. Hermanutz. 2015. Insects can limit seed productivity at the treeline. Canadian Journal of Forest Research 45(3): 286–296. doi: 10.1139/cjfr-2014-0385.

Jordan, R. H. 1980. Preliminary Results from Archaeological Investigations on Avayalik Island, Extreme Northern Labrador. ARCTIC 33(3): 607–627. doi: 10.14430/arctic2586.

Jorgenson, M. T., V. Romanovsky, J. Harden, Y. Shur, J. O'Donnell, E. A. G. Schuur, M. Kanevskiy, and S. Marchenko. 2010. Resilience and vulnerability of permafrost to climate change. Canadian Journal of Forest Research 40(7): 1219–1236. doi: 10.1139/X10-060.

Ju, J., and J. G. Masek. 2016. The vegetation greenness trend in Canada and US Alaska from 1984–2012 Landsat data. Remote Sensing of Environment 176: 1–16. doi: 10.1016/j.rse.2016.01.001.

Juliussen, H., and O. Humlum. 2007. Towards a TTOP ground temperature model for mountainous terrain in central-eastern Norway. Permafrost and Periglacial Processes 18(2): 161–184. doi: 10.1002/ppp.586.

Karunaratne, K. C., and C. R. Burn. 2003. Freezing n-factors in discontinuous permafrost terrain, Takhini River, Yukon Territory, Canada. In Proceedings of the 8th International Conference on Permafrost, 519–524. Zürich, Switzerland: University of Zurich-Irchel.

Karunaratne, K. C., S. V. Kokelj, and C. R. Burn. 2008. Near-surface permafrost conditions near Yellowknife, Northwest Territories, Canada. In Proceedings of the 9th International Conference on Permafrost, 907–912. Fairbanks, Alaska, United States of America: Institute of Northern Engineering, University of Alaska-Fairbanks.

Kasprzak, M. 2015. High-resolution electrical resistivity tomography applied to patterned ground, Wedel Jarlsberg Land, south-west Spitsbergen. Polar Research 34(0). doi: 10.3402/polar.v34.25678.

Kilibarda, M., T. Hengl, G. B. M. Heuvelink, B. Gräler, E. Pebesma, M. Perčec Tadić, and B. Bajat. 2014. Spatio-temporal interpolation of daily temperatures for global land areas at 1 km resolution. Journal of Geophysical Research: Atmospheres 119(5): 2294–2313. doi: 10.1002/2013JD020803.

Kilibarda, M., M. P. Tadić, T. Hengl, J. Luković, and B. Bajat. 2015. Global geographic and feature space coverage of temperature data in the context of spatio-temporal interpolation. Spatial Statistics 14: 22–38. doi: 10.1016/j.spasta.2015.04.005.

Kriticos, D. J., B. L. Webber, A. Leriche, N. Ota, I. Macadam, J. Bathols, and J. K. Scott. 2012. CliMond: global high-resolution historical and future scenario climate surfaces for bioclimatic modelling. Methods in Ecology and Evolution 3(1): 53–64. doi: 10.1111/j.2041-210X.2011.00134.x.

Laberge, M.-J., and S. Payette. 1995. Long-Term Monitoring of Permafrost Change in a Palsa Peatland in Northern Quebec, Canada: 1983-1993. Arctic and Alpine Research 27(2): 167. doi: 10.2307/1551898.

Ladd, M., R. G. Way, and A. E. Viau. 2015. The impact of using different modern climate data sets in pollen-based paleoclimate reconstructions of North America. Quaternary Science Reviews 112: 78–85. doi: 10.1016/j.quascirev.2015.01.020.

Lamb, H. F. 1985. Palynological Evidence for Postglacial Change in the Position of Tree Limit in Labrador. Ecological Monographs 55(2): 241–258. doi: 10.2307/1942559.

Lane, A., and A. Jarvis. 2007. Changes in climate will modify the geography of crop suitability: agricultural biodiversity can help with adaptation. SAT ejournal 4(1): 1–12.

Laprise, D., and S. Payette. 1988. Évolution récente d'une tourbière à palses (Québec subarctique): analyse cartographique et dendrochronologique. Canadian Journal of Botany 66(11): 2217–2227.

Leverington, D. 1995. A field survey of late-summer depths to frozen ground at two study areas near mayo, Yukon Territory, Canada. Permafrost and Periglacial Processes 6(4): 373–379.

Lewkowicz, A. G. 2008. Evaluation of miniature temperature-loggers to monitor snowpack evolution at mountain permafrost sites, northwestern Canada. Permafrost and Periglacial Processes 19(3): 323–331. doi: 10.1002/ppp.625.

Lewkowicz, A. G., and M. Ednie. 2004. Probability mapping of mountain permafrost using the BTS method, Wolf Creek, Yukon Territory, Canada. Permafrost and Periglacial Processes 15(1): 67–80. doi: 10.1002/ppp.480.

Lewkowicz, A. G., and R. G. Way. 2014. Overview report for the Nunatsiavut Government on permafrost conditions in the Nain area. Technical report.

Lewkowicz, A. G., B. Etzelmüller, and S. L. Smith. 2011. Characteristics of discontinuous permafrost based on ground temperature measurements and electrical resistivity tomography, southern Yukon, Canada. Permafrost and Periglacial Processes 22(4): 320–342. doi: 10.1002/ppp.703.

Lewkowicz, A. G., P. P. Bonnaventure, S. L. Smith, and Z. Kuntz. 2012. Spatial and thermal characteristics of mountain permafrost, northwest Canada. Geografiska Annaler: Series A, Physical Geography 94(2): 195–213.

Lewkowicz, A. G., O. Bellehumeur-Génier, C. M. Miceli, and S. L. Smith. 2016. Change in discontinuous permafrost in the Alaska Highway corridor examined by repeated electrical resistivity tomography and ground temperature monitoring, northwest Canada. In Proceedings of the 10th International Conference on Permafrost. Potsdam, Germany.

Loke, M. H., and R. D. Barker. 1996. Rapid least-squares inversion of apparent resistivity pseudosections by a quasi-Newton method. Geophysical prospecting 44(1): 131–152.

Loke, M. H., I. Acworth, and T. Dahlin. 2003. A comparison of smooth and blocky inversion methods in 2D electrical imaging surveys. Exploration Geophysics 34(3): 182–187. doi: 10.1071/EG03182.

Luo, Y., A. P. Trishchenko, and K. V. Khlopenkov. 2008. Developing clear-sky, cloud and cloud shadow mask for producing clear-sky composites at 250-meter spatial resolution for the seven MODIS land bands over Canada and North America. Remote Sensing of Environment 112(12): 4167–4185. doi: 10.1016/j.rse.2008.06.010.

Mackay, R. J. 1977. Probing for the bottom of the active layer. 77–1A. Geological Survey of Canada.

Mackay, R. J. 1995. Active layer changes (1968 to 1993) following the forest-tundra fire near Inuvik, N.W.T., Canada. Arctic and Alpine Research 27(4): 323–336.

Marquette, G. C., J. T. Gray, J. C. Gosse, F. Courchesne, L. Stockli, G. Macpherson, and R. Finkel. 2004. Felsenmeer persistence under non-erosive ice in the Torngat and Kaumajet mountains, Quebec and Labrador, as determined by soil weathering and cosmogenic nuclide exposure dating. Canadian Journal of Earth Sciences 41(1): 19–38. doi: 10.1139/e03-072.

Matney, J. A. 2014. Bayesian hierarchical models for environmental datasets. MSc Thesis, East Lansing, Michigan, United States of America: Michigan State University.

Maxwell, J. B. 1981. Climatic regions of the Canadian Arctic Islands. ARCTIC 34(3): 225–240.

McCune, B., D. Keon, and R. H. Marrs. 2002. Equations for potential annual direct incident radiation and heat load. Journal of vegetation science 13(4): 603–606.

McKenney, D. W., M. F. Hutchinson, P. Papadopol, K. Lawrence, J. Pedlar, K. Campbell, E. Milewska, R. F. Hopkinson, D. Price, and T. Owen. 2011. Customized spatial climate models for North America. Bulletin of the American Meteorological Society 92(12): 1611–1622.

McLennan, D. S., T. Bell, D. Berteaux, W. Chen, L. Copland, R. Fraser, D. Gallant, G. Gauthier, D. Hik, C. J. Krebs, I. H. Myers-Smith, I. Olthof, D. Reid, W. Sladen, C. Tarnocai, W. F. Vincent, and Y. Zhang. 2012. Recent climate-related terrestrial biodiversity research in Canada's Arctic national parks: review, summary, and management implications. Biodiversity 13(3–4): 157–173. doi: 10.1080/14888386.2012.720818.

Ménard, É., M. Allard, and Y. Michaud. 1998. Monitoring of ground surface temperatures in various biophysical micro-environments near Umiujaq, eastern Hudson Bay, Canada. In Proceedings of the 7th International Conference on Permafrost, 723–729. Yellowknife, Canada.

Metz, M., D. Rocchini, and M. Neteler. 2014. Surface temperatures at the continental scale: tracking changes with remote sensing at unprecedented detail. Remote Sensing 6(5): 3822–3840. doi: 10.3390/rs6053822.

Milewska, E. J., R. F. Hopkinson, and A. Niitsoo. 2005. Evaluation of geo-referenced grids of 1961–1990 Canadian temperature and precipitation normals. Atmosphere-Ocean 43(1): 49–75.

Minsley, B. J., N. J. Pastick, B. K. Wylie, D. R. N. Brown, and M. Andy Kass. 2016. Evidence for nonuniform permafrost degradation after fire in boreal landscapes. Journal of Geophysical Research: Earth Surface 121(2): 320–335. doi: 10.1002/2015JF003781.

Moran, P. A. P. 1950. Notes on Continuous Stochastic Phenomena. Biometrika 37(1/2): 17–23. doi: 10.2307/2332142.

Morse, P. D., C. R. Burn, and S. V. Kokelj. 2012. Influence of snow on near-surface ground temperatures in upland and alluvial environments of the outer Mackenzie Delta, Northwest Territories. Canadian Journal of Earth Sciences 49(8): 895–913. doi: 10.1139/e2012-012.

Morse, P. D., S. A. Wolfe, S. V. Kokelj, and A. J. R. Gaanderse. 2016. The occurrence and thermal disequilibrium state of permafrost in forest ecotopes of the Great Slave Region, Northwest Territories, Canada. Permafrost and Periglacial Processes 27(2): 145–162. doi: 10.1002/ppp.1858.

Naulier, M., M. M. Savard, C. Bégin, F. Gennaretti, D. Arseneault, J. Marion, A. Nicault, and Y. Bégin. 2015. A millennial summer temperature reconstruction for northeastern Canada using oxygen isotopes in subfossil trees. Climate of the Past 11(9): 1153–1164. doi: 10.5194/cp-11-1153-2015.

Nelson, F. E., O. A. Anisimov, and N. I. Shiklomanov. 2001. Subsidence risk from thawing permafrost. Nature 410(6831): 889–890.

Nicholson, F. H. 1979. Permafrost spatial and temporal variations near Schefferville, Nouveau-Québec. Géographie physique et Quaternaire 33(3–4): 265–277. doi: 10.7202/1000363ar.

Nicolsky, D. J., V. E. Romanovsky, santosh K. panda, S. Marchenko, and R. R. Muskett. 2016. Applicability of the ecosystem type approach to model permafrost dynamics across the Alaska North Slope. Journal of Geophysical Research: Earth Surface. doi: 10.1002/2016JF003852.

Nychka, D., R. Furrer, J. Paige, and S. Sain. 2015. fields (version 8.3-6). Tools for Spatial Data.

Occhietti, S., M. Parent, P. Lajeunesse, F. Robert, and E. Govare. 2011. Late Pleistocene–Early Holocene decay of the Laurentide Ice Sheet in Québec-Labrador. Developments in Quaternary Science 11: 601–630. doi: 10.1016/B978-0-444-53447-7.00047-7.

Oldenborger, G. A., and A.-M. LeBlanc. 2015. Geophysical characterization of permafrost terrain at Iqaluit International Airport, Nunavut. Journal of Applied Geophysics 123: 36–49. doi: 10.1016/j.jappgeo.2015.09.016.

Olthof, I., R. Latifovic, and D. Pouliot. 2015. A medium resolution land cover map of Canada's forested regions from 2005-2010 SPOT 4/5 data. 4. doi: 10.4095/295751.

Ou, C., B. Leblon, Y. Zhang, A. LaRocque, K. Webster, and J. McLaughlin. 2016a. Modelling and mapping permafrost at high spatial resolution using Landsat and Radarsat images in northern Ontario, Canada: Part 1 – model calibration. International Journal of Remote Sensing 37(12): 2727–2750. doi: 10.1080/01431161.2016.1157642.

Ou, C., A. LaRocque, B. Leblon, Y. Zhang, K. Webster, and J. McLaughlin. 2016b. Modelling and mapping permafrost at high spatial resolution using Landsat and Radarsat-2 images in Northern Ontario, Canada: Part 2 – regional mapping. International Journal of Remote Sensing 37(12): 2751–2779. doi: 10.1080/01431161.2016.1151574.

Oyler, J. W., A. P. Ballantyne, K. Jencso, M. Sweet, and S. W. Running. 2015. Creating a topoclimatic daily air temperature dataset for the conterminous United States using homogenized station data and remotely sensed land skin temperature. International Journal of Climatology 35(9): 2258–2279.

Parmentier, B., B. J. McGill, A. M. Wilson, J. Regetz, W. Jetz, R. Guralnick, M.-N. Tuanmu, and M. Schildhauer. 2015. Using multi-timescale methods and satellite-derived land surface temperature for the interpolation of daily maximum air temperature in Oregon. International Journal of Climatology 35(13): 3862–3878. doi: 10.1002/joc.4251.

Pastick, N. J., M. T. Jorgenson, B. K. Wylie, S. J. Nield, K. D. Johnson, and A. O. Finley. 2015. Distribution of near-surface permafrost in Alaska: Estimates of present and future conditions. Remote Sensing of Environment 168: 301–315. doi: 10.1016/j.rse.2015.07.019.

Paul, F., C. Huggel, and A. Kääb. 2004. Combining satellite multispectral image data and a digital elevation model for mapping debris-covered glaciers. Remote Sensing of Environment 89(4): 510–518. doi: 10.1016/j.rse.2003.11.007.

Payette, S. 1984. Un îlot de Pergélisol sur les hauts sommets de Charlevoix, Québec. Géographie physique et Quaternaire 38(3): 305. doi: 10.7202/032570ar.

Payette, S. 1993. The range limit of boreal tree species in Québec-Labrador: an ecological and palaeoecological interpretation. Review of Palaeobotany and Palynology 79(1): 7–30.

Payette, S. 2001. Les processus et les formes périglaciaires. In Écologie des tourbières du Québec-Labrador, 199–239. Québec City, Canada: Les Presses de l'Université Laval.

Payette, S. 2007. Contrasted Dynamics of Northern Labrador Tree Lines Caused by Climate Change and Migrational Lag. Ecology 88(3): 770–780. doi: 10.1890/06-0265.

Payette, S., A. Delwaide, M. Caccianiga, and M. Beauchemin. 2004. Accelerated thawing of subarctic peatland permafrost over the last 50 years. Geophysical Research Letters 31(18): L18208. doi: 10.1029/2004GL020358.

Porada, P., A. Ekici, and C. Beer. 2016. Effects of bryophyte and lichen cover on permafrost soil temperature at large scale. The Cryosphere 10(5): 2291–2315. doi: 10.5194/tc-10-2291-2016.

Price, D. T., D. W. McKenney, I. A. Nalder, M. F. Hutchinson, and J. L. Kesteven. 2000. A comparison of two statistical methods for spatial interpolation of Canadian monthly mean climate data. Agricultural and Forest meteorology 101(2): 81–94.

Pryer, R. W. 1963. Mine railroads in Labrador-Ungava. In Proceedings of the 1st International Conference on Permafrost, 503–508. 1287. Washington, USA: National Academy of Sciences and National Research Council Publication.

Rapaić, M., R. Brown, M. Markovic, and D. Chaumont. 2015. An evaluation of temperature and precipitation surface-based and reanalysis datasets for the Canadian Arctic, 1950–2010. Atmosphere-Ocean 53(3): 283–303. doi: 10.1080/07055900.2015.1045825.

Riley, S. J. 1999. Index that quantifies topographic heterogeneity. intermountain Journal of sciences 5(1–4): 23–27.

Riseborough, D. 2007. The effect of transient conditions on an equilibrium permafrost-climate model. Permafrost and Periglacial Processes 18(1): 21–32. doi: 10.1002/ppp.579.

Riseborough, D., N. Shiklomanov, B. Etzelmüller, S. Gruber, and S. Marchenko. 2008. Recent advances in permafrost modelling. Permafrost and Periglacial Processes 19(2): 137–156. doi: 10.1002/ppp.615.

Riseborough, D. W. 2002. The mean annual temperature at the top of permafrost, the TTOP model, and the effect of unfrozen water. Permafrost and Periglacial Processes 13(2): 137–143. doi: 10.1002/ppp.418.

Riseborough, D. W. 2004. Exploring the parameters of a simple model of the permafrost-climate relationship. PhD Thesis, Ottawa: Carleton University.

Riseborough, D. W., S. Wolfe, and C. Duchesne. 2012. Simplified climate statistics for permafrost modeling: Yellowknife case study. In Proceedings of the 10th International Conference on Permafrost, 335–340. Salekhard, Russia.

Roberts, B. A., N. P. P. Simon, and K. W. Deering. 2006. The forests and woodlands of Labrador, Canada: ecology, distribution and future management. Ecological Research 21(6): 868–880. doi: 10.1007/s11284-006-0051-7.

Rohde, R., R. A. Muller, R. Jacobsen, E. Muller, and C. Wickham. 2013a. A new estimate of the average earth surface land temperature spanning 1753 to 2011. Geoinformatics & Geostatistics: An Overview 01(01). doi: 10.4172/2327-4581.1000101.

Rohde, R., R. Muller, R. Jacobsen, S. Perlmutter, and S. Mosher. 2013b. Berkeley Earth temperature averaging process. Geoinformatics & Geostatistics: An Overview 01(02). doi: 10.4172/2327-4581.1000103.

Romanovsky, V. E., S. L. Smith, and H. H. Christiansen. 2010. Permafrost thermal state in the polar Northern Hemisphere during the international polar year 2007-2009: a synthesis. Permafrost and Periglacial Processes 21(2): 106–116. doi: 10.1002/ppp.689.

Sarrazin, D., and M. Allard. 2014. Environmental data from the Kangiqsualujjuaq region in Nunavik, Quebec, Canada, v. 1.1 (1988-2013). Scientific data 14. Nordicana D. Centre D'Étude Nordiques.

Sazonova, T. S., and V. E. Romanovsky. 2003. A model for regional-scale estimation of temporal and spatial variability of active layer thickness and mean annual ground temperatures. Permafrost and Periglacial Processes 14(2): 125–139. doi: 10.1002/ppp.449.

Schuur, E. A. G., A. D. McGuire, C. Schädel, G. Grosse, J. W. Harden, D. J. Hayes, G. Hugelius, C. D. Koven, P. Kuhry, D. M. Lawrence, S. M. Natali, D. Olefeldt, V. E. Romanovsky, K. Schaefer, M. R. Turetsky, C. C. Treat, and J. E. Vonk. 2015. Climate change and the permafrost carbon feedback. Nature 520(7546): 171–179. doi: 10.1038/nature14338.

Seppälä, M. 1982. An experimental study of the formation of palsas. In Proc. 4th Can. Permafrost Conf, 36–42.

Seppälä, M. 2011. Synthesis of studies of palsa formation underlining the importance of local environmental and physical characteristics. Quaternary Research 75(2): 366–370. doi: 10.1016/j.yqres.2010.09.007.

Serreze, M. C., and R. G. Barry. 2011. Processes and impacts of Arctic amplification: A research synthesis. Global and Planetary Change 77(1–2): 85–96. doi: 10.1016/j.gloplacha.2011.03.004.

Serreze, M. C., B. Raup, C. Braun, D. R. Hardy, and R. S. Bradley. 2017. Rapid wastage of the Hazen Plateau ice caps, northeastern Ellesmere Island, Nunavut, Canada. The Cryosphere 11(1): 169–177. doi: 10.5194/tc-11-169-2017.

Shur, Y., K. M. Hinkel, and F. E. Nelson. 2005. The transient layer: implications for geocryology and climate-change science. Permafrost and Periglacial Processes 16(1): 5–17. doi: 10.1002/ppp.518.

Shur, Y. L., and M. T. Jorgenson. 2007. Patterns of permafrost formation and degradation in relation to climate and ecosystems. Permafrost and Periglacial Processes 18(1): 7–19. doi: 10.1002/ppp.582.

Simms, É., and H. Ward. 2013. Multisensor NDVI-Based Monitoring of the Tundra-Taiga Interface (Mealy Mountains, Labrador, Canada). Remote Sensing 5(3): 1066–1090. doi: 10.3390/rs5031066.

Singh, V. P., P. Singh, and U. K. Haritashya, ed. 2011. Encyclopedia of Snow, Ice and Glaciers. Encyclopedia of Earth Sciences Series. Dordrecht: Springer Netherlands. doi: 10.1007/978-90-481-2642-2.

Sjöberg, Y., P. Marklund, R. Pettersson, and S. W. Lyon. 2015. Geophysical mapping of palsa peatland permafrost. The Cryosphere 9(2): 465–478. doi: 10.5194/tc-9-465-2015.

Slater, A. G., and D. M. Lawrence. 2013. Diagnosing Present and Future Permafrost from Climate Models. Journal of Climate 26(15): 5608–5623. doi: 10.1175/JCLI-D-12-00341.1.

Smith, M. W., and D. W. Riseborough. 1996. Permafrost monitoring and detection of climate change. Permafrost and Periglacial Processes 7(4): 301–309. doi: 10.1002/(SICI)1099-1530(199610)7:4<301::AID-PPP231>3.0.CO;2-R.

Smith, M. W., and D. W. Riseborough. 2002. Climate and the limits of permafrost: a zonal analysis. Permafrost and Periglacial Processes 13(1): 1–15. doi: 10.1002/ppp.410.

Smith, S. L., and P. P. Bonnaventure. 2017. Quantifying Surface Temperature Inversions and Their Impact on the Ground Thermal Regime at a High Arctic Site. Arctic, Antarctic, and Alpine Research 49(1): 173–185. doi: 10.1657/AAAR0016-039.

Smith, S. L., and M. M. Burgess. 2004. Sensitivity of permafrost to climate warming in Canada. Bulletin 579. Geological Survey of Canada.

Smith, S. L., and D. W. Riseborough. 2010. Modelling the thermal response of permafrost terrain to right-of-way disturbance and climate warming. Cold Regions Science and Technology 60(1): 92–103. doi: 10.1016/j.coldregions.2009.08.009.

Smith, S. L., M. M. Burgess, D. Riseborough, and F. Mark Nixon. 2005. Recent trends from Canadian permafrost thermal monitoring network sites. Permafrost and Periglacial Processes 16(1): 19–30. doi: 10.1002/ppp.511.

Smith, S. L., V. E. Romanovsky, A. G. Lewkowicz, C. R. Burn, M. Allard, G. D. Clow, K. Yoshikawa, and J. Throop. 2010. Thermal state of permafrost in North America: a contribution to the international polar year. Permafrost and Periglacial Processes 21(2): 117–135. doi: 10.1002/ppp.690.

Staiger, J. K. W., J. C. Gosse, J. V. Johnson, J. Fastook, J. T. Gray, D. F. Stockli, L. Stockli, and R. Finkel. 2005. Quaternary relief generation by polythermal glacier ice. Earth Surface Processes and Landforms 30(9): 1145–1159. doi: 10.1002/esp.1267.

Stantec. 2012. Geotechnical Investigation, Torngasok Cultural Centre, Nain, NL. Geotechnical report 121615077. Stantec Consulting Ltd.

Sturm, M., J. Holmgren, and G. E. Liston. 1995. A Seasonal Snow Cover Classification System for Local to Global Applications. Journal of Climate 8(5): 1261–1283. doi: 10.1175/1520-0442(1995)008<1261:ASSCCS>2.0.CO;2.

Sturm, M., B. Taras, G. E. Liston, C. Derksen, T. Jonas, and J. Lea. 2010. Estimating Snow Water Equivalent Using Snow Depth Data and Climate Classes. Journal of Hydrometeorology 11(6): 1380–1394. doi: 10.1175/2010JHM1202.1.

Suo, L., O. Helge Otterå, M. Bentsen, Y. Gao, and O. M. Johannessen. 2013. External forcing of the early 20th century Arctic warming. Tellus A 65(0). doi: 10.3402/tellusa.v65i0.20578.

Tarasov, L., and W. R. Peltier. 2007. Coevolution of continental ice cover and permafrost extent over the last glacial-interglacial cycle in North America. Journal of Geophysical Research 112(F2). doi: 10.1029/2006JF000661.

Tarnocai, C. 2006. The effect of climate change on carbon in Canadian peatlands. Global and Planetary Change 53(4): 222–232. doi: 10.1016/j.gloplacha.2006.03.012.

Tarnocai, C. 2009. The impact of climate change on Canadian peatlands. Canadian Water Resources Journal 34(4): 453–466.

Thibault, S., and S. Payette. 2009. Recent permafrost degradation in bogs of the James Bay area, northern Quebec, Canada. Permafrost and Periglacial Processes 20(4): 383–389. doi: 10.1002/ppp.660.

Throop, J., A. G. Lewkowicz, S. L. Smith, and C. R. Burn. 2012. Climate and ground temperature relations at sites across the continuous and discontinuous permafrost zones, northern Canada. Canadian Journal of Earth Sciences 49(8): 865–876. doi: 10.1139/e11-075.

Trant, A. J., and L. Hermanutz. 2014. Advancing towards novel tree lines? A multispecies approach to recent tree line dynamics in subarctic alpine Labrador, northern Canada. Edited by Ole Vetaas. Journal of Biogeography 41(6): 1115–1125. doi: 10.1111/jbi.12287.

Trant, A. J., R. G. Jameson, and L. Hermanutz. 2011. Persistence at the tree line: old trees as opportunists. Arctic: 367–370.

Trant, A. J., J. D. Jacobs, and T. Sable. 2012. Teaching and learning about climate change with Innu Environmental Guardians. Polar Geography 35(3–4): 229–244. doi: 10.1080/1088937X.2012.682229.

Trant, A. J., K. Lewis, B. H. Cranston, J. A. Wheeler, R. G. Jameson, J. D. Jacobs, L. Hermanutz, and B. M. Starzomski. 2015. Complex changes in plant communities across a Subarctic alpine tree line in Labrador, Canada. ARCTIC 68(4): 500. doi: 10.14430/arctic4528.

Tremblay, S., N. Bhiry, M. Lavoie, and A. de Vernal. 2014. Long-term dynamics of a palsa in the sporadic permafrost zone of northwestern Quebec (Canada). Canadian Journal of Earth Sciences 51(5): 500–509. doi: 10.1139/cjes-2013-0123.

Trishchenko, A. P., Y. Luo, K. V. Khlopenkov, W. M. Park, and S. Wang. 2009. Arctic circumpolar mosaic at 250 m spatial resolution for IPY by fusion of MODIS/TERRA land bands B1–B7. International Journal of Remote Sensing 30(6): 1635–1641. doi: 10.1080/01431160802348119.

Van Everdingen, R. 2005a. Palsa. Multi-language glossary of permafrost and related ground-ice terms. Boulder, Colorado, USA: National Snow and Ice Data Center.

Van Everdingen, R. 2005b. Pereletok. Multi-language glossary of permafrost and related ground-ice terms. Boulder, Colorado, USA: National Snow and Ice Data Center.

Van Everdingen, R. 2005c. Permafrost. Multi-language glossary of permafrost and related ground-ice terms. Boulder, Colorado, USA: National Snow and Ice Data Center.

Viau, A. E., and K. Gajewski. 2009. Reconstructing Millennial-Scale, Regional Paleoclimates of Boreal Canada during the Holocene. Journal of Climate 22(2): 316–330. doi: 10.1175/2008JCLI2342.1.

Vincent, L. A., X. L. Wang, E. J. Milewska, H. Wan, F. Yang, and V. Swail. 2012. A second generation of homogenized Canadian monthly surface air temperature for climate trend analysis. Journal of Geophysical Research: Atmospheres 117(D18): n/a-n/a. doi: 10.1029/2012JD017859.

Voisey's Bay Nickel Corporation. 1997. Voisey's Bay Mine/Mill Project Environmental Impact Statement. Environmental Impact Statement. INCO Limited.

Vorren, K.-D. 2017. The first permafrost cycle in Færdesmyra, eastern Finnmark, Norway? Norsk Geografisk Tidsskrift - Norwegian Journal of Geography: 1–8. doi: 10.1080/00291951.2017.1316309.

van Vuuren, D. P., J. Edmonds, M. Kainuma, K. Riahi, A. Thomson, K. Hibbard, G. C. Hurtt, T. Kram, V. Krey, J.-F. Lamarque, T. Masui, M. Meinshausen, N. Nakicenovic, S. J. Smith, and S. K. Rose. 2011. The representative concentration pathways: an overview. Climatic Change 109(1–2): 5–31. doi: 10.1007/s10584-011-0148-z.

Wang, T., A. Hamann, D. L. Spittlehouse, and T. Q. Murdock. 2012. ClimateWNA - High-Resolution Spatial Climate Data for Western North America. Journal of Applied Meteorology and Climatology 51(1): 16–29. doi: 10.1175/JAMC-D-11-043.1.

Way, R. G. 2015. Multidecadal Recession of Grinnell and Terra Nivea Ice Caps, Baffin Island, Canada. ARCTIC 68(1): 45. doi: 10.14430/arctic4461.

Way, R. G., and P. P. Bonnaventure. 2015. Testing a reanalysis-based infilling method for areas with sparse discontinuous air temperature data in northeastern Canada: Reanalysis-based infilling in northeastern Canada. Atmospheric Science Letters 16(3): 398–407. doi: 10.1002/asl2.574.

Way, R. G., and A. G. Lewkowicz. in revision. Relations between environmental setting and TTOP parameters in Labrador, northeast Canada. Permafrost and Periglacial Processes.

Way, R. G., and A. G. Lewkowicz. 2014. Modelling the distribution of permafrost in the Labrador region of northeastern Canada. In 4th European Conference on Permafrost. Evora, Portugal.

Way, R. G., and A. G. Lewkowicz. 2015. Investigations of discontinuous permafrost in coastal Labrador with DC electrical resistivity tomography. In Proceedings of GéoQuebec: 68th Canadian Geotechnical Conference and 7th Canadian Permafrost Conference, 8. Québec City, Canada. doi: 10.13140/RG.2.1.1647.8803.

Way, R. G., and A. G. Lewkowicz. 2016. Modelling the spatial distribution of permafrost in Labrador–Ungava using the temperature at the top of permafrost. Canadian Journal of Earth Sciences 53(10): 1010–1028. doi: 10.1139/cjes-2016-0034.

Way, R. G., and A. E. Viau. 2015. Natural and forced air temperature variability in the Labrador region of Canada during the past century. Theoretical and Applied Climatology 121(3–4): 413–424. doi: 10.1007/s00704-014-1248-2.

Way, R. G., T. Bell, and N. E. Barrand. 2014. An inventory and topographic analysis of glaciers in the Torngat Mountains, northern Labrador, Canada. Journal of Glaciology 60(223): 945–956. doi: 10.3189/2014JoG13J195.

Way, R. G., T. Bell, and N. E. Barrand. 2015. Glacier change from the early Little Ice Age to 2005 in the Torngat Mountains, northern Labrador, Canada. Geomorphology 246: 558–569. doi: 10.1016/j.geomorph.2015.07.006.

Way, R. G., A. G. Lewkowicz, and P. P. Bonnaventure. 2017a. Development of moderate-resolution gridded monthly air temperature and degree-day maps for the Labrador-Ungava region of northern Canada. International Journal of Climatology 37(1): 493–508. doi: 10.1002/joc.4721.

Way, R. G., F. Oliva, and A. E. Viau. 2017b. Underestimated warming of northern Canada in the Berkeley Earth temperature product. International Journal of Climatology 37(4): 1746–1757. doi: 10.1002/joc.4808.

Wenner, C. G. 1947. Pollen diagrams from Labrador. Geographiska Annaler 29(3–4): 137–373.

Westermann, S., T. V. Schuler, K. Gisnås, and B. Etzelmüller. 2013. Transient thermal modeling of permafrost conditions in Southern Norway. The Cryosphere 7(2): 719–739. doi: 10.5194/tc-7-719-2013.

Westermann, S., T. I. Østby, K. Gisnås, T. V. Schuler, and B. Etzelmüller. 2015a. A ground temperature map of the North Atlantic permafrost region based on remote sensing and reanalysis data. The Cryosphere 9(3): 1303–1319. doi: 10.5194/tc-9-1303-2015.

Westermann, S., C. R. Duguay, G. Grosse, and A. Kääb. 2015b. Remote sensing of permafrost and frozen ground. In Remote Sensing of the Cryosphere, ed. M. Tedesco, 307–344. John Wiley & Sons, Ltd.

Wolfe, S. A., C. W. Stevens, A. J. Gaanderse, and G. A. Oldenborger. 2014. Lithalsa distribution, morphology and landscape associations in the Great Slave Lowland, Northwest Territories, Canada. Geomorphology 204: 302–313. doi: 10.1016/j.geomorph.2013.08.014.

Woo, M., A. G. Lewkowicz, and W. R. Rouse. 1992. Response of the Canadian permafrost environment to climatic change. Physical Geography 13(4): 287–317. doi: 10.1080/02723646.1992.10642459.

Woollett, J. 2010. Oakes Bay 1: A Preliminary Reconstruction of a Labrador Inuit Seal Hunting Economy in the Context of Climate Change. Geografisk Tidsskrift-Danish Journal of Geography 110(2): 245–259. doi: 10.1080/00167223.2010.10669510.

Wright, J. F., C. Duchesne, and M. M. Côté. 2003. Regional-scale permafrost mapping using the TTOP ground temperature model. In Proceedings of the 8th International Conference on Permafrost, 1241–1246. Zürich, Switzerland.

Wulder, M. A., J. C. White, M. Cranny, R. J. Hall, J. E. Luther, A. Beaudoin, D. G. Goodenough, and J. A. Dechka. 2008. Monitoring Canada's forests. Part 1: Completion of the EOSD land cover project. Canadian Journal of Remote Sensing 34(6): 549–562. doi: 10.5589/m08-066.

You, Y., Q. Yu, X. Pan, X. Wang, and L. Guo. 2013. Application of electrical resistivity tomography in investigating depth of permafrost base and permafrost structure in Tibetan Plateau. Cold Regions Science and Technology 87: 19–26. doi: 10.1016/j.coldregions.2012.11.004.

Zeileis, A., G. Grothendieck, J. A. Ryan, F. Andrews, and A. Zeileis. 2015. zoo (version 1.7-12). S3 Infrastructure for Regular and Irregular Time Series.

Zhang, Y. 2003. A process-based model for quantifying the impact of climate change on permafrost thermal regimes. Journal of Geophysical Research 108(D22). doi: 10.1029/2002JD003354.

Zhang, Y. 2013. Spatio-temporal features of permafrost thaw projected from long-term high-resolution modeling for a region in the Hudson Bay Lowlands in Canada. Journal of Geophysical Research: Earth Surface 118(2): 542–552. doi: 10.1002/jgrf.20045.

Zhang, Y., W. Chen, and J. Cihlar. 2003. A process-based model for quantifying the impact of climate change on permafrost thermal regimes. Journal of Geophysical Research 108(D22). doi: 10.1029/2002JD003354.

Zhang, Y., W. Chen, and D. W. Riseborough. 2006. Temporal and spatial changes of permafrost in Canada since the end of the Little Ice Age. Journal of Geophysical Research 111(D22). doi: 10.1029/2006JD007284.

Zhang, Y., W. Chen, and D. W. Riseborough. 2008a. Disequilibrium response of permafrost thaw to climate warming in Canada over 1850–2100. Geophysical Research Letters 35(2). doi: 10.1029/2007GL032117.

Zhang, Y., W. Chen, and D. W. Riseborough. 2008b. Transient projections of permafrost distribution in Canada during the 21st century under scenarios of climate change. Global and Planetary Change 60(3–4): 443–456. doi: 10.1016/j.gloplacha.2007.05.003.

Zhang, Y., J. Li, X. Wang, W. Chen, W. Sladen, L. Dyke, L. Dredge, J. Poitevin, D. McLennan, H. Stewart, S. Kowalchuk, W. Wu, G. P. Kershaw, R. K. Brook, and C. R. Burn. 2012. Modelling and mapping permafrost at high spatial resolution in Wapusk National Park, Hudson Bay Lowlands. Canadian Journal of Earth Sciences 49(8): 925–937. doi: 10.1139/e2012-031.

Zhang, Y., X. Wang, R. Fraser, I. Olthof, W. Chen, D. Mclennan, S. Ponomarenko, and W. Wu. 2013. Modelling and mapping climate change impacts on permafrost at high spatial resolution for an Arctic region with complex terrain. The Cryosphere 7(4): 1121–1137. doi: 10.5194/tc-7-1121-2013.

Zhang, Y., I. Olthof, R. Fraser, and S. A. Wolfe. 2014. A new approach to mapping permafrost and change incorporating uncertainties in ground conditions and climate projections. The Cryosphere 8(6): 2177–2194. doi: 10.5194/tc-8-2177-2014.

Zhao, S.-P., Z.-T. Nan, Y.-B. Huang, and L. Zhao. 2017. The application and evaluation of simple permafrost distribution models on the Qinghai-Tibet Plateau. Permafrost and Periglacial Processes. doi: 10.1002/ppp.1939.

Zimmermann, C., and C. Lavoie. 2001. A paleoecological analysis of a southern permafrost peatland, Charlevoix, Quebec. Canadian Journal of Earth Sciences 38(6): 909–919. doi: 10.1139/e00-110.

Zoltai, S. C. 1972. Palsas and peat plateaus in central Manitoba and Saskatchewan. Canadian Journal of Forest Research 2(3): 291–302.

Zoltai, S. C., and C. Tarnocai. 1975. Perennially frozen peatlands in the western Arctic and Subarctic of Canada. Canadian Journal of Earth Sciences 12(1): 28–43.

APPENDICES

APPENDIX A – PROGRAMMING CODE

Appendix A1: R v3.3 code for leave-one-out cross validation using the thin plate spline implementation used Chapter 2.

```
### Set Working Directory ###
setwd("…")
### Load required packages ###
library(fields)
library(raster)
library(spatial.tools)
### Use all computer resources ###
sfQuickInit()
### Load X-Data (Independent variables) (x,y,elev) ###
xdata <- file.choose()
x <- read.csv(xdata, TRUE, ",")
### Load Y-Data (Dependent variable) (air temperature; time = columns) ###
ydata <- file.choose()
ydata <- read.csv(ydata, TRUE, ",")

### Leave-one out cross validation ###
### Build data frames to load values into ###
RMSE2 <- NULL
MAE2 <- NULL
stats2 <- NULL

### Outer loop for replication ###
for (i in 1:(ncol(ydata))){
y <- ydata[,i]

### Set to length of the stations ###
pe_tps <- 1:97

### Inner loop for cross validation ###
for (i in seq(along = pe_tps)) {
tpsi <- Tps(x[-i, ], y[-i])
pri <- predict(tpsi, x[i, , drop = FALSE])
pe_tps[i] <- y[i] - pri
}
stats <- pe_tps
RMSE <- round(sqrt(mean(pe_tps^2)), 2)
MAE <- mean(abs(pe_tps))
stats2 <- cbind(stats2,stats)
RMSE2 <- cbind(RMSE2,RMSE)
MAE2 <- cbind(MAE2,MAE)
}
### Output files ###
write.csv(stats2,"stats2.csv")
write.csv(RMSE2, "RMSE2v2.csv")
write.csv(MAE2, "MAE2v2.csv")
sfQuickStop()
```

Appendix A2: R v3.3 code for pre-processing Maxim Integrated Ibutton loggers.

```
### Way, R.G. (2017). Tools for processing Maxim Integrated Ibutton logger temperature data. DOI:

### This function was used in support of the following manuscript ###
### Way, R.G. and Lewkowicz, A.G. (Under revision). Relations between environmental ###
### setting and TTOP parameters in Labrador, northeast Canada. ###
### Permafrost and Periglacial Processes. ###

### This function was developed by Robert G. Way ###
### with a great deal of help from Steven Mosher ###
### from the Berkeley Earth Surface Temperature project ###
### who streamlined and simplified some challenging sections. ###
### An earlier version of some code for processing ibuttons ###
### was developed by Dr. Luke Owen Frishkoff ###
### at the University of Toronto. ###

### This function is meant to be used to pre-process Maxim Integrated Ibutton output ###
### to a format that can be readily used for permafrost applications ###
### There are many issues which can arise during pre-processing including ###
### changing date formats and header lines ###

### The input file should be a .csv corresponding to the output from Maxim Integrated Ibuttons ###

### Set the appropriate working drive for the input files ###
### Should only include the files (.csv) that you are using as inputs ###
setwd("SELECT_WORKING_DRIVE")

### Gather list of names of files in working folder ###
fileNames<- list.files()

### Use the below function if ibuttons produce date formats with month, day, year ###
### Else see the alternative function (read.ibutton.dmy) ###

read.ibutton.mdy <- function(file,skiplines){
### Running functions ###
library(chron)
library(zoo)
library(stringr)

### Gather list of names of files in working folder ###
Header <- readLines(file, n=skiplines-1)
DATA   <- read.csv(file, header=TRUE, skip=skiplines,stringsAsFactors=FALSE)
#   Trim leading and trailing space
DATA$Date.Time <-str_trim(DATA$Date.Time)
#   Find the space (separates  date and hour)
#   Grab the first  8 or 11 characters  depending on where the space is
#   trim the result
DT  <-str_trim(str_sub(DATA$Date.Time,1,str_locate(DATA$Date.Time," ")[,2]))
#   Look at the front of the string  ^  if you see a 0, replace with space
DT  <-str_replace(DT,pattern="^0","")
#   Look for 4 digit  years  ( 2014, 2015).. strip out the 20, replace with /1
DT  <-str_replace(DT,pattern="/201","/1")
#   Format the date
DT2  <-as.Date(DT,format="%m/%d/%y")
#   find the space and take everything after the space
TIME  <-str_trim(str_sub(DATA$Date.Time,str_locate(DATA$Date.Time," ")[,2]))
#   get the  HOUR   but  sometime the hour  is  4:
#   strip out the ":" &  make it numeric
HOUR  <-as.numeric(str_replace((str_sub(TIME,1,2)),":",""))
#   find the lines with  PM and AM
PM   <- grepl("PM",TIME)
AM   <- grepl("AM",TIME)
#   find noon and midnight
H    <- HOUR ==12
HOUR[!H & PM]<-HOUR[!H & PM]+12
HOUR[H  & AM]<-HOUR[H & AM]+12
#   adjust to 24-hour clock
HOUR[HOUR==0]<-24
#   Strip out months from date
Month <- strftime(DT2, "%m")
#   Strip out year from date
Year <- strftime(DT2, "%Y")
```

```
#   Strip out day from date
Day <- strftime(DT2, "%d")
#   Convert HOUR to hour
Hour <- HOUR
#   Create a data frame with dates, times, temps
data3 <- data.frame(Year, Month, Day, Hour, DATA$Value)
#   Rename the value field to something temp related
names(data3)[names(data3)=="DATA.Value"] <- "T"
#   Generate output
return(data3)
}

### Use the below function if ibuttons produce date formats with day, month, year ###
### Else see the alternative function (read.ibutton.mdy) ###

read.ibutton.dmy <- function(file,skiplines){
### Running functions ###
library(chron)
library(zoo)
library(stringr)

### Gather list of names of files in working folder ###
Header <- readLines(file, n=skiplines-1)
DATA   <- read.csv(file, header=TRUE, skip=skiplines,stringsAsFactors=FALSE)
#   Trim leading and trailing space
DATA$Date.Time <-str_trim(DATA$Date.Time)
#   Find the space (separates  date and hour)
#   Grab the first  8 or 11 characters  depending on where the space is
#   trim the result
DT  <-str_trim(str_sub(DATA$Date.Time,1,str_locate(DATA$Date.Time," ")[,2]))
#   Look at the front of the string  ^  if you see a 0, replace with space
DT  <-str_replace(DT,pattern="^0","")
#   Look for 4 digit  years  ( 2014, 2015).. strip out the 20, replace with /1
DT  <-str_replace(DT,pattern="/201","/1")
#   Format the date
DT2  <-as.Date(DT,format="%d/%m/%y")
#   find the space and take everything after the space
TIME  <-str_trim(str_sub(DATA$Date.Time,str_locate(DATA$Date.Time," ")[,2]))
#   get the  HOUR   but  sometime the hour  is  4:
#   strip out the ":" &  make it numeric
HOUR  <-as.numeric(str_replace((str_sub(TIME,1,2)),":",""))
#   find the lines with  PM and AM
PM   <- grepl("PM",TIME)
AM   <- grepl("AM",TIME)
#   find noon and midnight
H     <- HOUR ==12
HOUR[!H & PM]<-HOUR[!H & PM]+12
HOUR[H  & AM]<-HOUR[H & AM]+12
#   adjust to 24-hour clock
HOUR[HOUR==0]<-24
#   Strip out months from date
Month <- strftime(DT2, "%m")
#   Strip out year from date
Year <- strftime(DT2, "%Y")
#   Strip out day from date
Day <- strftime(DT2, "%d")
#   Convert HOUR to hour
Hour <- HOUR
#   Create a data frame with dates, times, temps
data3 <- data.frame(Year, Month, Day, Hour, DATA$Value)
#   Rename the value field to something temp related
names(data3)[names(data3)=="DATA.Value"] <- "T"
#   Generate output
return(data3)
}


### Running function in a loop ###
### This will take the input ibuttons and ###
### export to a format that can be read by ###
### hour2day2month.r function found in Appendix 2 ###

for (fileName in fileNames) {
```

```
### Select your working drive ###
setwd("SELECT_WORKING_DRIVE")
### Change the skiplines depending on what type of ibutton ###
### If Hi-res then it is 19, if low-res it is 14) ###
### Change function selected depending on Ibutton output format ###
### Choose read.ibutton.mdy if using a mdy date format and ###
### read.ibutton.dmy if using a dmy date format. ###
  z <- read.ibutton.mdy(fileName, skiplines=19)
### Make sure to pick your output file location or will overwrite ###
                setwd("SELECT_OUTPUT_LOCATION")
                fname <- basename(fileName)
                print(fileName)
                write.csv(z,fname)
                }
```

Appendix A3: R v3.3 code for generating daily and monthly summaries from sub-daily data.

```
### Way, R.G. (2017). Generating sub-daily to daily to monthly temperature summaries for permafrost applications. DOI: 10.13140/RG.2.2.19192.44808

### This function was used in support of the following manuscript ###
### Way, R.G. and Lewkowicz, A.G. (Under revision). Relations between environmental ###
### setting and TTOP parameters in Labrador, northeast Canada. ###
### Permafrost and Periglacial Processes. ###

### This function was developed by Robert G. Way ###
### Department of Geography, Environment and Geomatics ###
### It will take subdaily resolution temperature data ###
### and convert to daily and monthly summaries for ###
### daily minimum maximum and mean, accumulated freezing degree days ###
### and accumulated thawing degree days ###

### The input file should be a .csv with the date format of year, month, day ###
### each in separate columns and a column for temperature named T ###
### This can be easily adapted for other input formats ###

### Set the appropriate working drive for the input files ###
### Should only include the files (.csv) that you are using as inputs ###
setwd("SELECT_WORKING_DRIVE")

### Load the zoo package in R ###
library(zoo)

### Gather list of names of files in working folder ###
fileNames<- list.files()

### Function requires having parrallel folders corresponding to Hourly, Daily and Monthly
### Set the working drive before running to Hourly folder
### The function will automatically move back one folder and enter into the Daily/Monthly folder

hour2day2month <- function(file){
library(zoo)
  # read old data:
z <- read.csv(file, header = TRUE, sep = ",")

fname <- basename(file)

hourly <- with(z,
   zoo(T, as.Date(paste(Year, Month, Day, Hour, sep = "-")))
)

### Create function which calculates daily min, max, mean and count ###
stat <- function(x) c(min = min(x, na.rm=TRUE), max = max(x, na.rm=TRUE), mean = mean(x, na.rm=TRUE), count = sum(!is.na(x)))

### Aggregate hourly to daily using the function above ###
zz <- aggregate(hourly, as.Date, FUN= stat)

### Set the appropriate working drive for the output daily files ###
setwd("..")
setwd("Daily")

### Write out the file with the daily summaries ###
write.zoo(zz, sep=",", fname)

### Create function which calculates monthly min, max, mean, count, FDD and TDD ###
stat2 <- function(x) c(min = min(x, na.rm=TRUE), max = max(x, na.rm=TRUE), mean = mean(x, na.rm=TRUE), count = sum(!is.na(x)),
TDD = abs(sum(x[x>0], na.rm=TRUE)), FDD = abs(sum(x[x<0], na.rm=TRUE)))

### Aggregate daily data to monthly using the function above ###
zzz <- aggregate(zz$mean, as.yearmon, FUN= stat2)

### Set the appropriate working drive for the output monthly files ###
setwd("..")
setwd("Monthly")

### Write out the file with the monthly summaries ###
write.zoo(zzz, sep=",", fname)

setwd("..")
```

```
setwd("Hourly")
}

###################
### Begin Loop  ###
###################

### Calculation will use make object into 'zoo' format (e.g. time) ###
### Will use same name as input ###
### Make sure you have backup copy of files in case of overwrite ###
for (fileName in fileNames) {
setwd("SELECT_WORKING_DRIVE")
                j <- hour2day2month(fileName)
                print(fileName)
}
```

Appendix A4: R v3.3 code for the Labrador-Ungava region TTOP implementation

```
### TTOP modelling code developed by R.G. Way for Way and Lewkowicz (2016)

#Way, R.G. & Lewkowicz, A.G. 2016. Modelling the spatial distribution of permafrost in Labrador–Ungava using the temperature at the top of #permafrost. 
Canadian Journal of Earth Sciences 53 : 1010–1028. DOI: 10.1139/cjes-2016-0034

### Reference (currently) is below:
### Way, R.G. (2016). R Code for TTOP modelling in the Labrador-Ungava region of northeastern Canada. ###
### DOI: 10.13140/RG.2.1.4558.5686 ###

############################
### Set Working Directory ###
############################

setwd("...")

############################
### Load required packages ###
############################

library(fields)
library(raster)
library(spatial.tools)
library(gdalUtils)
library(mapplots)
library(rgdal)
library(gstat)
library(RColorBrewer)

################################
### Use all computer resources ###
################################

################################
### Use all computer resources ###
################################

sfQuickInit()

rasterOptions(overwrite=TRUE, progress="text")

### Necessary Files ###
### Ensure that files cover *exactly* the same extent ###
### This can be done in R but it takes a really long time ###
### Advise you do it in GIS software and maintain clipping extent ###
### Ensure projection is the same as well ###

### Landcover [vegetation] dataset
# CCRS_msk <- raster("CCRS_v4.tif")

### Thawing degree days grid ###
### Other time periods labelled similarly (e.g. TDD_msk4862) ###
# TDD_msk0014 <- raster("TDD_msk0014.tif")

### Freezing degree days grid ###
### Other time periods labelled similarly (e.g. FDD_msk4862) ###
# FDD_msk0014 <- raster("FDD_msk0014.tif")

### Regional snow depth grid ###
# WavgSD <- raster("SD_Lab_JFM_v2.tif")

### Mean annual air temperature grid ###
### Other time periods labelled similarly (e.g. MAAT1; MAAT2) ###
# MAAT3 <- raster("MAAT3.tif")

### Landform classification grid ###
# Lform <- raster("Lform_2_5_250m.tif")

### Thermal offset grid ###
# VTOFF <- raster("Var_T_Offsets.tif")

##############################################################################################
```

```
### Begin ###
#############################################################################################

### Load EOSD data ###
CCRS_msk <- raster("CCRS.tif")

### Load TDD ###
TDD_msk0014 <- raster("TDD_0014.tif")

### Load FDD ###
FDD_msk0014 <- raster("FDD_0014.tif")

##########################
### Processing nT data ###
##########################

### Create matrix for classification ###
nTclass <- matrix(c(0,1,0.75,
1,2,0.85,
2,3,NA,
3,4,NA,
4,5,0.85,
5,6,0.85,
6,7,NA,
7,8,0.9,
8,9,NA,
9,10,0.9,
10,11,0.9,
11,12,0.9,
12,13,0.9,
13,14,0.85,
14,15,NA,
15,16,1.0,
16,17,NA,
17,18,NA,
18,19,NA,
19,255,NA), nrow=20, ncol=3, byrow=TRUE)

### Reclassify EOSD values to nT values ###
nT <- reclassify(CCRS_msk, nTclass, filename="nT_1.tif", overwrite=TRUE)

##########################
### Processing nF data ###
##########################

### Expert Assessment

### Create matrix for classification ###
nFclass1 <- matrix(c(0,1,0.04,
1,2,0.24,
2,3,NA,
3,4,NA,
4,5,0.04,
5,6,0.04,
6,7,NA,
7,8,0.24,
8,9,NA,
9,10,0.40,
10,11,0.30,
11,12,0.40,
12,13,0.60,
13,14,0.40,
14,15,NA,
15,16,0.70,
16,17,NA,
17,18,NA,
18,19,NA,
19,255,NA), nrow=20, ncol=3, byrow=TRUE)

### Reclassify EOSD values to nT values ###
nF1 <- reclassify(CCRS_msk, nFclass1, filename="nF_1.tif", overwrite=TRUE)

##########################
```

```
### Processing nF data ###
##########################

### Yukon Values ###

### Create matrix for classification ###
nFclass2 <- matrix(c(0,1,0.30,
1,2,0.35,
2,3,NA,
3,4,NA,
4,5,0.25,
5,6,0.30,
6,7,NA,
7,8,0.37,
8,9,NA,
9,10,0.45,
10,11,0.37,
11,12,0.45,
12,13,0.60,
13,14,0.40,
14,15,NA,
15,16,0.82,
16,17,NA,
17,18,NA,
18,19,NA,
19,255,NA), nrow=20, ncol=3, byrow=TRUE)

### Reclassify EOSD values to nT values ###
nF2 <- reclassify(CCRS_msk, nFclass2, filename="nF_2.tif", overwrite=TRUE)

##########################
### Processing nF data ###
##########################

### Regional snow depth-based nFs (with/without density adjustments) ###

### Create matrix for classification of snow densities ###
snowDen <- matrix(c(0,1,1.298,
1,2,1.298,
2,3,NA,
3,4,NA,
4,5,1.298,
5,6,1.298,
6,7,NA,
7,8,1.298,
8,9,NA,
9,10,0.819,
10,11,0.819,
11,12,0.819,
12,13,0.819,
13,14,0.819,
14,15,NA,
15,16,0.746,
16,17,NA,
17,18,NA,
18,19,NA,
19,255,NA), nrow=20, ncol=3, byrow=TRUE)

### Reclassify EOSD values to density values ###
snowDen <- reclassify(CCRS_msk, snowDen, filename="snowDen.tif", overwrite=TRUE)

### Input regional snow depth product ###
WavgSD <- raster("SD_CMC_9814.tif")

### Calculate equivalent snow depth
eSD <- (WavgSD*snowDen)

### Output equivalent snow depth raster ###
writeRaster(eSD, "eq_snow_depth.tif", overwrite=TRUE)

### Thin plate spline fitting of Riseborough data ###
### Data was manually digitized from Smith and Riseborough (2002) ###
### Email R.G. Way for access ###
```

```
### Input mean annual air temperature product ###
### 2000-2014 ###
MAAT3 <- raster("MAT0014.tif")

### Read input csv ###
a <- read.csv("Riseborough_Digitize3.csv", TRUE, ",")
a2 <-  data.frame(a$ASC_cm, a$MAAT)
y <- a$NF

### Create thin plate spline fit object ###
TPSfit <- Tps(a2[,1:2], y)

### Plot fit to ensure it looks okay ###
surface(TPSfit, levels=c(0.1, 0.2,0.3,0.4,0.5,0.6,0.7,0.8,0.9), xlab="Average winter equivalent snow depth (m)",
ylab="Mean annual air temperature (°C)", zlab="Freezing n-factor",extrap=TRUE,
labcex=0.75, cex.lab=1.25,
col=brewer.pal(10,"Spectral"))

### Calculate snow depth-based nF ###
### Create stack of x-variables for predicting ###
stk3 <- stack(WavgSD, MAAT3)

### Calculate nF based on snow depth and MAAT ###
nF3 <- predict(stk3, TPSfit)

### Output snow depth nF raster ###
writeRaster(nF3, "nF3_TPS.tif", overwright=TRUE)

### Calculate equivalent snow depth-based nF ###
### Create stack of x-variables for predicting ###
stk5 <- stack(eSD, MAAT3)

### Calculate nF based on snow depth and MAAT ###
nF5 <- predict(stk5, TPSfit)

### Output snow depth nF raster ###
writeRaster(nF5, "nF5_TPS.tif", overwright=TRUE)

#######################################
### Snow redistribution adjusted nF ###
#######################################

#### Create matrix for classification ###
SRratio <- matrix(c(0,1,1.54,
1,2,1.54,
2,3,NA,
3,4,NA,
4,5,1.78,
5,6,1.78,
6,7,NA,
7,8,2.18,
8,9,NA,
9,10,0.17,
10,11,0.51,
11,12,0.17,
12,13,0.17,
13,14,1,
14,15,NA,
15,16,0.17,
16,17,NA,
17,18,NA,
18,19,NA,
19,255,NA), nrow=20, ncol=3, byrow=TRUE)

### Calculate SR ratioing raster ###
SRratio <- reclassify(CCRS_msk, SRratio, filename="SR_ratio.tif", overwrite=TRUE)

#############################################################################################################
### Landform classification ###
#### Create matrix for classification ###
Mask_Tundra <- matrix(c(0,1,NA,
1,2,NA,
```

```
2,3,NA,
3,4,NA,
4,5,NA,
5,6,NA,
6,7,NA,
7,8,NA,
8,9,NA,
9,10,1,
10,11,NA,
11,12,1,
12,13,1,
13,14,NA,
14,15,NA,
15,16,1,
16,17,NA,
17,18,NA,
18,19,NA,
19,255,NA), nrow=20, ncol=3, byrow=TRUE)

### Calculate Tundra mask raster ###
Tundra_Mask <- reclassify(CCRS_msk, Mask_Tundra, filename="Tundra_Mask.tif", overwrite=TRUE)

### Bring in TPI ###
# TPI <- raster("TPI_250mv3.tif")
### Create TPI mask ###
# TPI_mask <- Tundra_Mask*TPI
# TPIreclass <- matrix(c(-95,-0.00009,1.32,
# 0,202,0.17), nrow=2, ncol=3, byrow=TRUE)

### Input Landform classification ###
Lform <- raster("Lform_2_5_250m.tif")

### Mask to only Tundra ###
Lform_mask <- Tundra_Mask*Lform

### Create redistribution reclassification matrix for tundra ###
Lform_reclass <- matrix(c(0,1,1.83,
1,2,1.83,
2,3,1.83,
3,4,1.0,
4,5,1.0,
5,6,1.0,
6,7,1.0,
7,8,0.17,
8,9,0.17,
9,10,0.17), nrow=10, ncol=3, byrow=TRUE)

### Reclassify tundra terrain for snow reclassification ###
SRtundraLform <- reclassify(Lform_mask, Lform_reclass, filename="SRtundraLform.tif", overwrite=TRUE)

### Combine two datasets ###
SRratio2 <- cover(SRtundraLform, SRratio, filename="SRratioLform.tif")

##############################################################################################

### Input mean annual air temperature products ###
### 1948-1962 ###
MAAT1 <- raster("MAT4862.tif")

### 1982-1996 ###
MAAT2 <- raster("MAT8296.tif")

### 2000-2014 ###
MAAT3 <- raster("MAT0014.tif")

### Mean regional snow depth ###
SR_SD <- WavgSD*SRratio2

### Calculate SR equivalent snow depth ###
SR_ESD <- SR_SD*snowDen

### Calculate SR equivalent snow depth-based nF ###
### Create stacks of x-variables for predicting ###
```

```
### 1948-1962 ###
stk6 <- stack(SR_ESD, MAAT1)
### 1982-1996 ###
stk7 <- stack(SR_ESD, MAAT2)
### 2000-2014 ###
stk8 <- stack(SR_ESD, MAAT3)

### Calculate SR nF based on snow depth and MAAT ###
nF43n1 <- predict(stk6, TPSfit)
nF43n2 <- predict(stk7, TPSfit)
nF43n3 <- predict(stk8, TPSfit)

Con=function(condition, trueValue, falseValue){
   return(condition * trueValue + (!condition)*falseValue)
   }

nF43n1new <- Con(nF43n1 < 0, 0, nF43n1)
writeRaster(nF43n1new, "nF43_4862TPS.tif", overwrite=TRUE)

nF43n2new <- Con(nF43n2 < 0, 0, nF43n2)
writeRaster(nF43n2new, "nF43_8296TPS.tif", overwrite=TRUE)

nF43n3new <- Con(nF43n3 < 0, 0, nF43n3)
writeRaster(nF43n3new, "nF43_0014TPS.tif", overwrite=TRUE)

SR_SD2 <- WavgSD*SRratio
SR_ESD2 <- SR_SD2*snowDen
stk9 <- stack(SR_ESD2, MAAT3)
nF6 <- predict(stk9, TPSfit)
writeRaster(nF6, "nF6_TPS.tif", overwright=TRUE)

#####################################
### Running GST model variations ###
#####################################

GST <- function(a,b,c,d,e){
((a*b)-(c*d))/e
}

TTOP <- function(a,b,c,d,e,f){
(((a*b)-(c*d))/e)-f
}

### Calculation Period ###
period <- 365

GST_0014_1 <- GST(TDD_msk0014, nT, FDD_msk0014, nF1, period)
writeRaster(GST_0014_1, "GST_0014_1.tif", overwrite=TRUE)

GST_0014_2 <- GST(TDD_msk0014,nT,FDD_msk0014,nF2,period)
writeRaster(GST_0014_2, "GST_0014_2.tif", overwrite=TRUE)

GST_0014_3 <- GST(TDD_msk0014,nT,FDD_msk0014,nF3,period)
writeRaster(GST_0014_3, "GST_0014_3.tif", overwrite=TRUE)

GST_0014_5 <- GST(TDD_msk0014,nT,FDD_msk0014,nF5,period)
writeRaster(GST_0014_5, "GST_0014_5.tif", overwrite=TRUE)

GST_0014_43 <- GST(TDD_msk0014,nT,FDD_msk0014,nF43n3new,period)
writeRaster(GST_0014_43, "GST_0014_43.tif", overwrite=TRUE)

GST_0014_6 <- GST(TDD_msk0014,nT,FDD_msk0014,nF6,period)
writeRaster(GST_0014_6, "GST_0014_6.tif", overwrite=TRUE)

### 1948 to 1962 ###

TDD_msk4862 <- raster("TDD_msk4862.tif")
FDD_msk4862 <- raster("FDD_msk4862.tif")

period <- 365

GST4862 <- GST(TDD_msk4862,nT,FDD_msk4862,nF43n1new,period)
writeRaster(GST4862, "GST_4862_43.tif", overwrite=TRUE)
```

```
### 1982 to 1996 ###

TDD_msk8296 <- raster("TDD_msk8296.tif")
FDD_msk8296 <- raster("FDD_msk8296.tif")

period <- 365

GST8296 <- GST(TDD_msk8296,nT,FDD_msk8296,nF43n2new,period)
writeRaster(GST8296, "GST_8296_43.tif", overwrite=TRUE)

### Run TTOP Models for time periods ###
### Input variable thermal offsets ###
VTOFF <- raster("Var_Toffsets.tif")

### Run TTOP models ###
TTOP_0014_1 <- GST_0014_1 - VTOFF
writeRaster(TTOP_0014_1, "TTOP_0014_1.tif", overwrite=TRUE)

TTOP_0014_2 <- GST_0014_2 - VTOFF
writeRaster(TTOP_0014_2, "TTOP_0014_2.tif", overwrite=TRUE)

TTOP_0014_3 <- GST_0014_3 - VTOFF
writeRaster(TTOP_0014_3, "GST_0014_3.tif", overwrite=TRUE)

TTOP_0014_5 <- GST_0014_5 - VTOFF
writeRaster(TTOP_0014_5, "TTOP_0014_5.tif", overwrite=TRUE)

TTOP_0014_6 <- GST_0014_6 - VTOFF
writeRaster(TTOP_0014_6, "TTOP_0014_6.tif", overwrite=TRUE)

TTOP_0014_43 <- GST_0014_43 - VTOFF
writeRaster(TTOP_0014_43, "TTOP_0014_43.tif", overwrite=TRUE)

TTOP_4862_43 <- GST4862 - VTOFF
writeRaster(TTOP_4862_43, "TTOP_4862_43.tif", overwrite=TRUE)

TTOP_8296_43 <- GST8296 - VTOFF
writeRaster(TTOP_8296_43, "TTOP_8296_43.tif", overwrite=TRUE)

GST_3avg_43 <- (GST4862 + GST8296 + GST_0014_43) / 3
writeRaster(GST_3avg_43, "GST_3avg_43.tif", overwrite=TRUE)

TTOP_3avg_43 <- (TTOP_0014_43 + TTOP_4862_43 + TTOP_8296_43) / 3
writeRaster(TTOP_3avg_43, "TTOP_3avg_43.tif", overwrite=TRUE)

### End using all computer resources ###
sfQuickStop()
```

APPENDIX B – SUPPLEMENTAL FIGURES AND TABLES

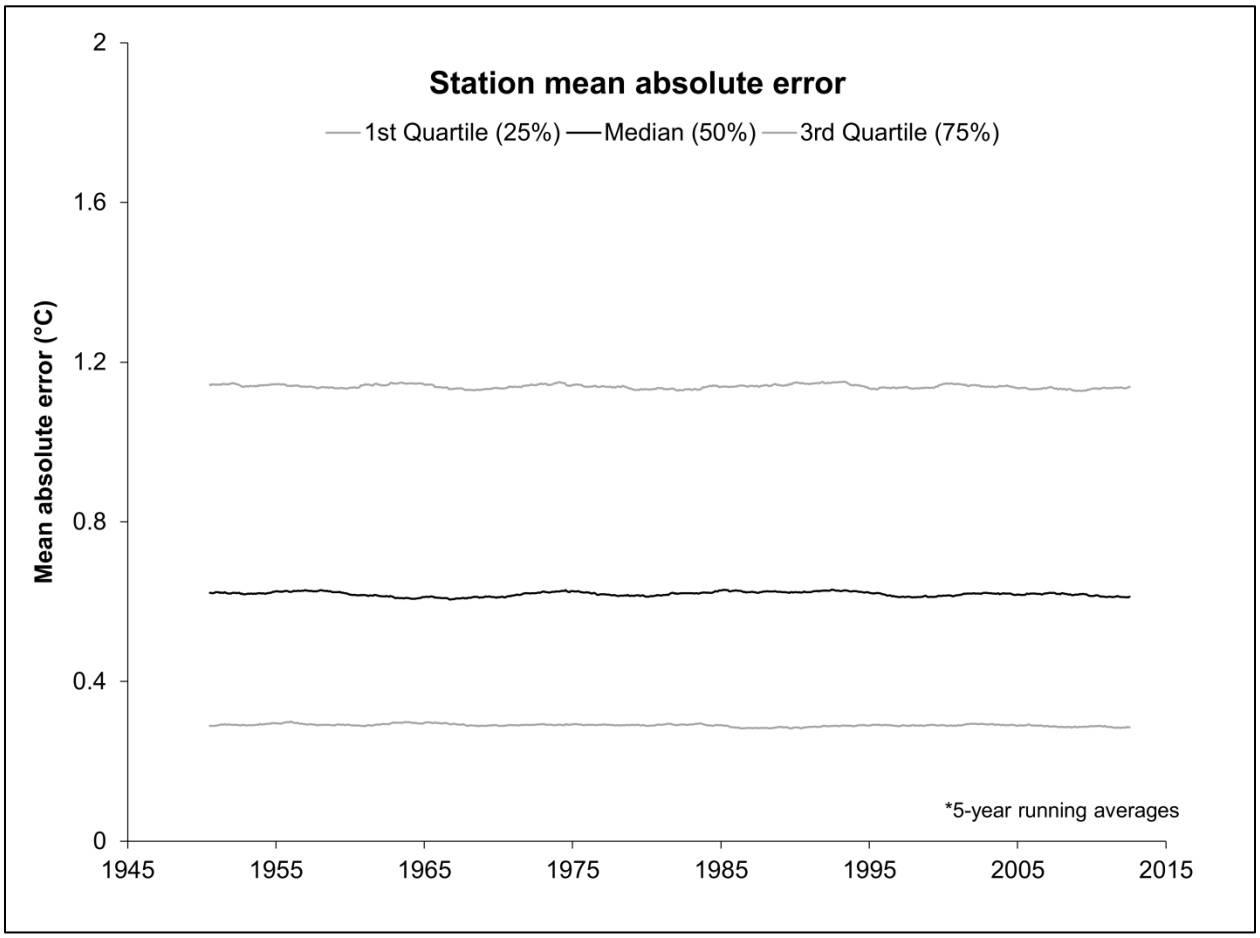

Figure B1: Temporal variability of mean absolute errors from the leave-one-out cross validation error analysis presented Chapter 2.

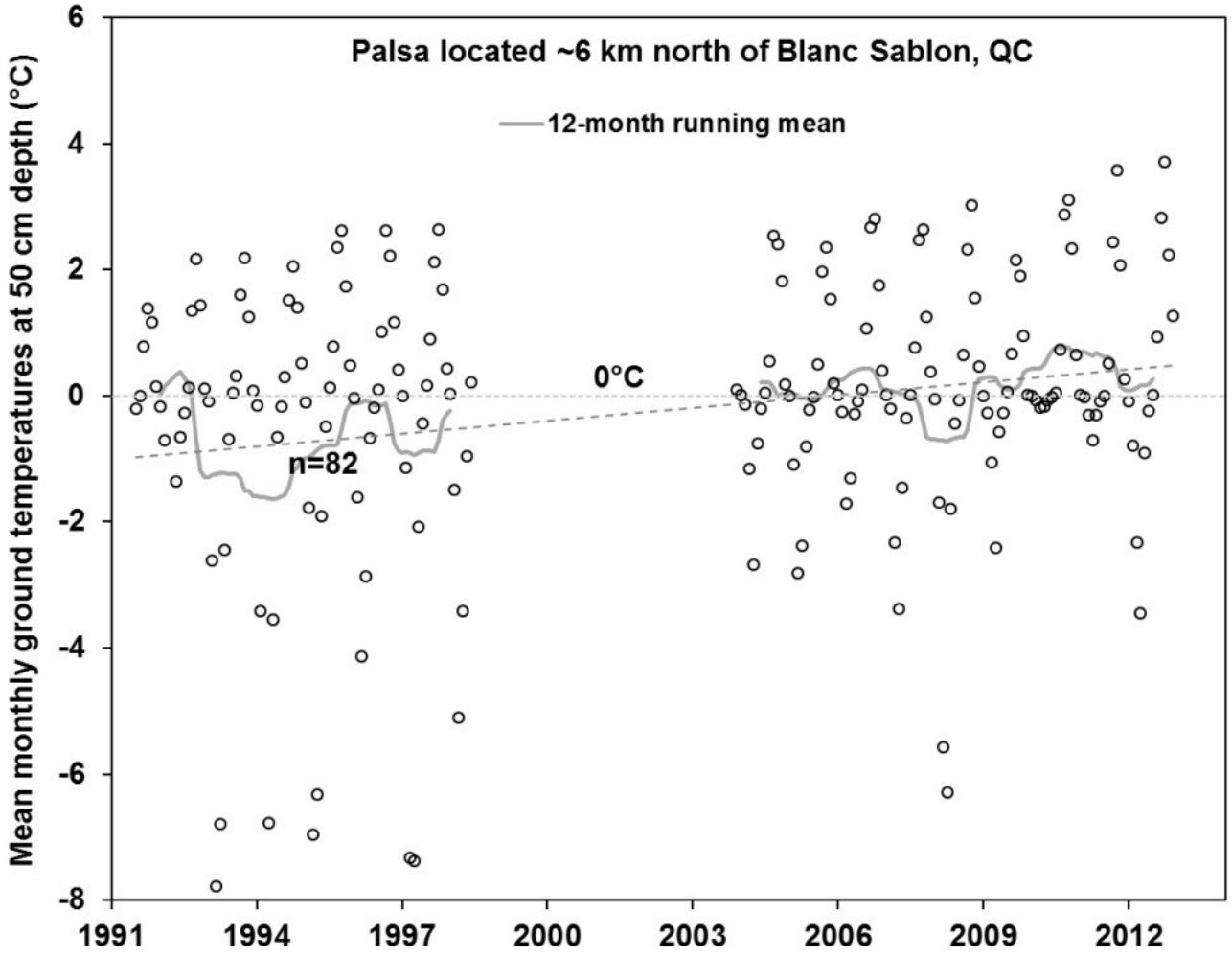

Figure B2: Fifty cm depth ground temperatures observed between 1991-2012 in a palsa field north of Blanc Sablon, QC by Allard et al. (2014).

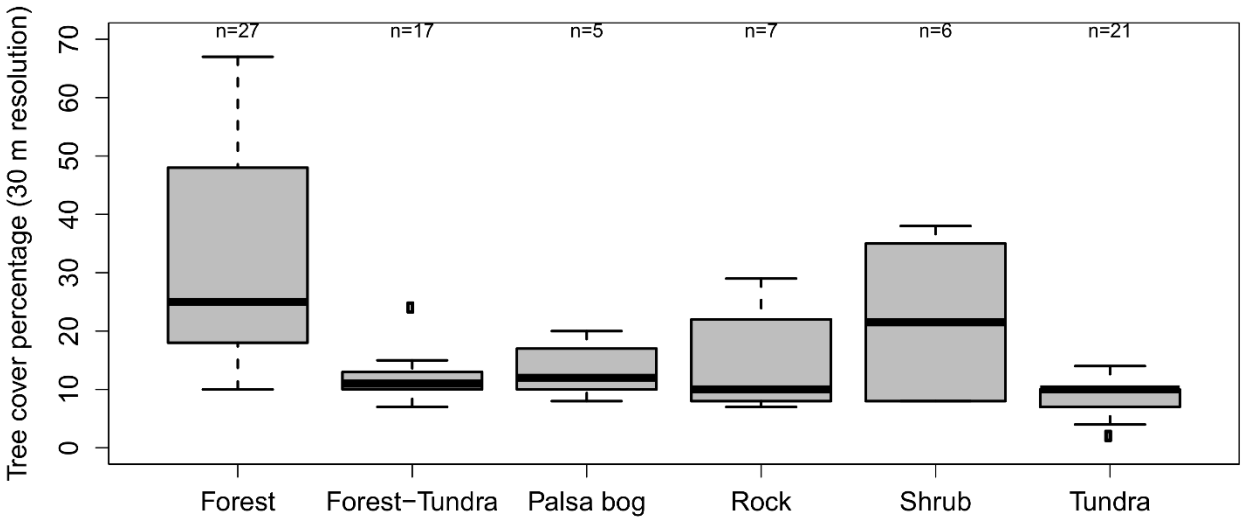

Figure B3: Tree cover percentage dataset (TRC30m) sampled across land cover types at monitoring stations used in Chapter 5.

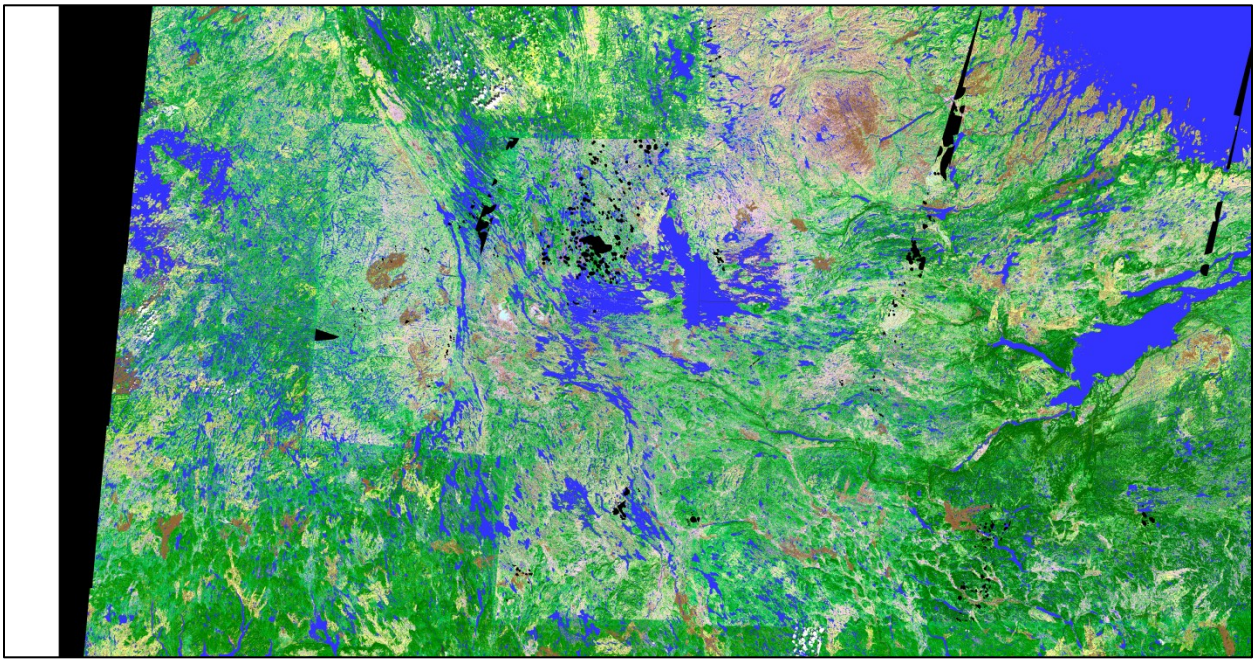

Figure B4: High resolution (~20 m) Earth Observation for Sustainable Development of Forests (EOSD) land cover data for western Labrador. Image illustrates the presence of land cover discontinuities across vegetation classes and the presence of missing data within the Labrador-Ungava region.

Table B1: Characteristics of input climate stations used in Chapter 2 for spatial modelling of air temperature and degree-days across the Labrador-Ungava region.

Acronym	Station	Data Source	LAT	LONG	Elevation	Months
AKA	Akulivik A	Berkeley Earth	60.81700	-78.15000	16	175
BAS	Basecamp Torngat	Parks Canada	58.451	-62.797	5	47
BCA	Baie Comeau A	Berkeley Earth	49.13300	-68.20000	37.5	559
BJB	Baie Johan Beetz	Berkeley Earth	50.28000	-62.80000	8	378
BTH	Battle Harbour	Berkeley Earth	52.25000	-55.60000	12	1365
BEI	Belle Isle	Berkeley Earth	51.88300	-55.38300	130.05	1181
BLS	Blanc Sablon	Berkeley Earth	51.43280	-57.19380	22.28	538
BSP	Blanc Sablon Palsa	Centre D'Études Nordiques	51.49993	-57.15352	60	254
BON	Bonnard	Berkeley Earth	50.73000	-71.03396	501.5	577
BOR	Border	Berkeley Earth	55.33300	-63.21700	482.5	391
CAH	Cape Harrison	Berkeley Earth	54.76600	-58.45000	10.05	218
CHA	Cape Hopes Advance	Berkeley Earth	61.08300	-69.55000	73	404
CKA	Cape Kakkiviak	Berkeley Earth	59.98382	-64.16768	551	140
CKI	Cape Kiglapait	Berkeley Earth	57.13424	-61.47796	834	135
CAW	Cartwright	Berkeley Earth	53.70000	-57.03385	8.22	949
CHI	Chibougamau-Chapais	Berkeley Earth	49.79200	-74.47500	394.5	1210
CHU	Churchill Falls	Berkeley Earth	53.55625	-64.09667	437.45	521
CHP	Chute des Passes	Berkeley Earth	49.86500	-71.21000	398.28	246
CIR	Cirque Valley	Parks Canada	58.943	-63.602	487.68	36
CPW	Cape Whittle	Environment Canada	50.1541	-60.0534	7	251
ERA	Eastmain River A	Berkeley Earth	52.23300	-75.51700	7.5	353
FOG	Fort George	Berkeley Earth	53.83080	-79.01000	8.05	482
FOM	Fort Mackenzie	Berkeley Earth	56.88000	-69.05250	75.95	149
GAA	Gagnon A	Berkeley Earth	51.95000	-68.13300	570.5	234
GEE	Gethsemanie	Berkeley Earth	50.22000	-60.67000	8	178
GSB	Goose Bay	Berkeley Earth	53.31700	-60.41700	46.45	866
HAH	Harrington Harbour	Berkeley Earth	50.53000	-59.50000	7.95	741
HSP	Havre St Pierre A	Berkeley Earth	50.28300	-63.60000	38	326
HOE	Hopedale	Berkeley Earth	55.45025	-60.22500	11.2	822
IHL	Indian House Lake	Berkeley Earth	56.23300	-64.73300	308.27	224
INA	Inukjuak A	Berkeley Earth	58.45810	-78.10410	15.5	1096
IVI	Ivitak Cove	Parks Canada	59.00100	-63.74600	32.79	48
IVK	Ivujivik	Berkeley Earth	62.41700	-77.91700	38	274
JOL	Joutel	Berkeley Earth	49.47000	-78.30000	290	253
KAM	Kamestastin	Dr. John Jacobs	55.93591	-63.15376	341	44
KAN	Kangidluasuk	Global Summary of the Day	58.45100	-62.79700	10	36
KAA	Kangiksualujjuaq A	Berkeley Earth	58.71700	-65.98300	60	99
KA1	Kangiqsualujjuaq 1	Centre D'Études Nordiques	58.69442	-65.93853	10	85
KA2	Kangiqsualujjuaq 2	Centre D'Études Nordiques	58.70843	-65.99503	110	209
KA3	Kangiqsualujjuaq 3	Centre D'Études Nordiques	58.71666	-65.96666	103	97
KNA	Kangiqsujuaq A	Berkeley Earth	61.58300	-71.91650	151	132

KKA	Kangirsuk A	Berkeley Earth	60.01700	-70.00000	123	214
KEP	Kepimits	Hydro Québec	52.65300	-64.83800	503	117
KUQ	Kuujjuaq	Berkeley Earth	58.10000	-68.41700	37.73	871
KJA	Kuujjuarapik A	Berkeley Earth	55.28320	-77.75670	17	1051
LB1	Lac Bush 1	Centre D'Études Nordiques	57.95569	-75.91058	179	213
LG3	La Grande 3	Berkeley Earth	53.56700	-76.20000	233	290
LG4	La Grande 4	Berkeley Earth	53.75233	-73.67092	306.5	336
LGR	La Grande Riviere	Berkeley Earth	53.62090	-77.70110	193	451
LGA	La Grande Airport	Environment Canada	53	-73.383	283	72
LTE	La Tabatiere	Berkeley Earth	50.83000	-58.97000	8	139
LAB	Lac Benoit	Berkeley Earth	51.53293	-71.11410	549	205
LAE	Lac Eon	Berkeley Earth	51.86722	-63.28356	577	645
LIM	Little Macatina	Berkeley Earth	52.23300	-61.31700	321	34
MAK	Makkovik1	Berkeley Earth	55.08300	-59.18300	71	179
MAN	Manicouagan	Berkeley Earth	50.65000	-68.83300	406	120
MNE	Manouane Est	Environment Canada	50.65301	-70.53265	497	213
MC03	MC03	Parks Canada	58.92100	-63.66500	599.08	48
MEC	Mecatina	Berkeley Earth	51.83300	-62.88300	524	98
MLU	Mealy Mountains Upper	Dr. John Jacobs	53.6295	-58.87317	995	95
MLL	Mealy Mountains Lower	Dr. John Jacobs	53.61067	-58.81717	570	56
MLB	Mealy Mountains Base	Dr. John Jacobs	53.615	-58.83667	600	50
MEN	Menihek Rapids	Berkeley Earth	54.47000	-66.62000	489	90
MET	Metchin River	Hydro Québec	53.43900	-63.25900	348	117
MIC	Michikimats	Hydro Québec	54.56400	-64.11900	522	105
MIS	Mistassini Post	Berkeley Earth	50.40000	-73.90000	381.73	782
NAN	Nain	Berkeley Earth	56.55346	-61.68167	9.72	958
NAT	Natashquan A	Berkeley Earth	50.18333	-61.80670	7.5	1190
NEM	Nemiscau A	Berkeley Earth	51.70000	-76.11700	244	320
PAN	Pangnirtung	Berkeley Earth	53.20000	-70.90000	537	53
PNP	Parc National Des Pingua	Berkeley Earth	61.30000	-73.66700	503	70
PDD	Passe Dangereuse Dam	Berkeley Earth	49.88000	-71.27000	457	233
PYR	Payne River	Global Summary of the Day	60.100000	-71.066000	164	52
PTE	Pentecote	Global Summary of the Day	49.73	-67.17	15	165
POM	Poste Montagnais	Berkeley Earth	51.88000	-65.73000	610	260
PUQ	Puvirnituq	Berkeley Earth	60.05000	-77.28300	23	203
RAM	Ramah	Parks Canada	58.87500	-63.35500	54.48	48
REB	Red Bay	Berkeley Earth	51.73000	-56.43000	18.3	67
RB1	Riviere Boniface 1	Centre D'Études Nordiques	57.72818	-76.08452	139	209
RB2	Riviere Boniface 2	Centre D'Études Nordiques	57.72686	-76.08697	130	98
RB3	Riviere Boniface 3	Centre D'Études Nordiques	57.73167	-76.07750	130	257
RB4	Riviere Boniface 4	Centre D'Études Nordiques	57.73131	-76.07858	130	74
RAF	Rivere aux Feuilles	Berkeley Earth	57.90460	-72.97090	171	89
RAR	Rivere aux Rats	Berkeley Earth	49.42000	-72.20000	186	119
RSA	Rivere St Augustin	Berkeley Earth	51.22000	-58.63000	8	234
RAT	Riviere au Tonnere	Berkeley Earth	50.28000	-64.78000	15	514

SGA	Saglek A	Berkeley Earth	58.47492	-62.65000	50	80
SLT	Salliut	Environment Canada	62.175	-75.667	229	195
SCH	Schefferville	Berkeley Earth	54.80000	-66.80458	520	783
SEP	Sept Iles	Berkeley Earth	50.21850	-66.25750	53.77	831
TAA	Tasiujaq A	Berkeley Earth	58.66700	-69.95000	31	131
TAB	Tete A La Baleine	Berkeley Earth	50.70000	-59.32000	9	341
TUB	Tukialik Bay	Berkeley Earth	54.72000	-58.35146	683	106
TWF	Twin Falls	Environment Canada	53.5	-64.52	483.1	73
UMI	Umiujaq	Berkeley Earth	56.53300	-76.51700	71	181
WAL	Wabush Lake	Berkeley Earth	52.93029	-66.87040	549.5	628
WAA	Waskaganish A	Berkeley Earth	51.48300	-78.75000	23	129
WSM	West St Modest	Berkeley Earth	51.60000	-56.70000	12	135

Note: Data sources can be found below:
(1) Berkeley Earth - http://berkeleyearth.org/data/
(2) Centre D'Études Nordiques - http://www.cen.ulaval.ca/nordicanad/
(3) Environment Canada - http://climate.weather.gc.ca/
(4) Global Summary of the Day - https://data.noaa.gov/dataset/global-surface-summary-of-the-day-gsod
(5) Dr. John Jacobs – Department of Geography, Memorial University of Newfoundland

Table B2: General information and observed characteristics of palsas surveyed with ERT for this study. Excess ice fractions were calculated per **EQ 3-1**.

Palsa ID	Thaw depth (cm)	Maximum mound height (m)	Inferred PF depth (m)	PF thickness (m)	ERT ID	Excess ice fraction
P1	60	0.92	3.4	2.8	1	0.33
P2	57	1.22	4.5	3.93	1	0.31
P3	60	1.38	6.5	5.9	1 & 2	0.23
P4	62	0.44	4.3	3.68	1	0.12
P5	58	0.42	2.5	1.92	3	0.22
P6	60	0.43	3.3	2.7	3	0.16
P7	54	1.09	4.5	3.96	3	0.28
P8	41	0.46	1.2	0.79	3	0.58
P9	61	0.46	3.4	2.79	4	0.16
P10	65	0.82	2.3	1.65	4	0.50
P11	63	0.67	5.2	4.57	4	0.15
P12	47	0.63	2.33	1.86	5	0.34
P13	49	0.39	2.73	2.24	5	0.17
P14	45	1.3	5.8	5.35	5	0.29
P15	39	0.28	3.04	2.65	5	0.11
P16	46	0.25	2.94	2.48	5	0.10
P17	51	0.52	5.12	4.61	5	0.11
P18	44	0.81	4.31	3.87	6	0.21
P19	37	0.59	3.49	3.12	7	0.19
P20	40	0.82	5.03	4.63	7	0.18
P21	40	0.95	5.6	5.2	7	0.18
P22	37	0.65	5.36	4.99	7	0.13
P23	40	0.65	5.23	4.83	8	0.13
P24	42	0.313	2.77	2.35	9	0.13
P25	46	0.613	4.12	3.66	9	0.17
P26	41	0.47	4.07	3.66	10	0.13
P27	40	0.285	3.31	2.91	11	0.10

Table B3: Summary statistics for monitoring stations used in Chapter 5.

ID	Lat	Long	Elev	Site owner	MAAT	TA	GST	TTOP	nF	nT	Toff	LWSD	Class
AMET01	53.127	-66.131	579	University of Ottawa	-4.1	36.1	3.5	3.4	0.04	0.89	-0.07	120	Forest
AMET02	53.133	-66.089	750	University of Ottawa	-4.2	34.7	2.6	2.2	0.06	0.81	-0.37	140	Forest
AMET03	51.954	-68.139	578	University of Ottawa	-2.1	34.0	3.7	4.0	0.03	0.80	0.30	160	Tall shrub
AMET04	51.913	-68.115	776	University of Ottawa	-2.6	33.1	3.6	3.2	0.01	0.80	-0.45	160	Forest
AMET05	52.789	-67.231	691	University of Ottawa	-3.8	35.2	4.5	4.3	0.00	1.06	-0.17	140	Forest
AMET06	52.766	-67.219	880	University of Ottawa	-5.4	34.2	-2.8	-2.5	0.66	0.89	0.37	25	Barren
AMET07	53.483	-64.690	502	University of Ottawa	-3.4	35.2	3.1	2.7	0.06	0.82	-0.41	100	Forest
AMET08	53.476	-64.719	658	University of Ottawa	-3.7	35.1	1.6	1.1	0.20	0.75	-0.51	55	Forest-Tundra
AMET09	54.306	-63.189	476	University of Ottawa	-4.0	34.9	3.4	3.0	0.04	0.88	-0.40	100	Forest
AMET10	54.318	-63.215	593	University of Ottawa	-4.5	34.3	-1.8	-2.9	0.68	0.99	-1.06	10	Barren
AMET11	52.825	-60.101	265	University of Ottawa	-1.7	33.4	3.0	2.1	0.07	0.70	-0.82	160	Forest
AMET12	52.792	-60.032	467	University of Ottawa	-1.9	32.4	3.5	2.9	0.00	0.79	-0.57	120	Forest
AMET13	53.710	-57.007	11	University of Ottawa	-0.1	25.9	0.9	-1.7	0.64	0.86	-2.67	25	Wetland
AMET14	53.726	-56.963	158	University of Ottawa	-1.1	23.6	0.8	0.7	0.55	0.90	-0.10	45	Barren
AMET15	52.587	-59.491	568	University of Ottawa	-2.5	33.1	2.8		0.04	0.90			Forest
AMET16	53.874	-66.420	501	University of Ottawa	-3.5	36.5	4.4	2.5	0.07	1.09	-1.85	90	Forest
AMET17	53.296	-60.538	271	University of Ottawa	-1.2	28.5	3.1	3.6	0.04	0.77	0.58	120	Forest
AMET18	53.985	-58.836	12	University of Ottawa								15	Wetland
AMET19	51.457	-57.118	115	University of Ottawa	0.5	22.1	1.1	-1.0	0.79	0.95	-2.13	15	Wetland
AMET20	51.759	-56.414	77	University of Ottawa	0.6	21.0	1.8	-0.8	0.75	1.04	-2.65	25	Wetland
AMET21	52.161	-56.098	217	University of Ottawa	-0.4	24.9	2.9	2.7	0.04	0.76	-0.24	120	Forest
AMET22	52.138	-56.135	333	University of Ottawa	-1.3	24.8	2.4	2.3	0.23	0.95	-0.10	45	Forest-Tundra
AMET23	53.064	-57.680	190	University of Ottawa	-1.5	30.2	3.5	3.1	0.08	0.91	-0.40	120	Forest
AMET24	53.074	-57.665	302	University of Ottawa	-0.7	27.0							Forest-Tundra
AMET25	53.322	-62.961	382	University of Ottawa	-3.2	35.8	3.3	3.5	0.11	0.92	0.21	120	Forest
AMET26	53.344	-63.035	518	University of Ottawa	-3.2	31.3	3.4	3.1	0.01	0.78	-0.30	120	Forest
AMET27	53.226	-64.492	484	University of Ottawa	-2.9	39.3	3.7	3.9	0.04	0.82	0.19		Forest
AMET28	53.092	-61.804	390	University of Ottawa	-2.0	30.9	3.7	3.2	0.01	0.86	-0.44		Forest
AMET29	53.110	-61.802	526	University of Ottawa	-2.8	33.3	2.3	1.9	0.12	0.74	-0.40	120	Forest
AMET30	53.733	-65.155	479	University of Ottawa	-3.3	40.6	3.8	4.3	0.05	0.84	0.45		Shrub
AMET31	53.727	-65.144	569	University of Ottawa	-3.1	33.0	2.9	2.9	0.21	0.93	0.02	140	Forest-Tundra
AMET32	52.985	-66.948	770	University of Ottawa	-4.5	34.6	2.6	2.1	0.02	0.74	-0.51		Forest
AMET33	52.993	-66.945	886	University of Ottawa	-4.7	34.4	-2.0	-1.3	0.61	0.86	0.71	25	Barren
AMET34	53.348	-65.665	650	University of Ottawa	-2.9	31.8	2.4	3.2	0.25	1.00	0.84		Forest-Tundra
AMET35	53.782	-63.372	504	University of Ottawa	-3.2	35.6	3.5	4.0	0.00	0.79	0.46	110	Forest
AMET36	54.196	-63.109	578	University of Ottawa	-2.9	31.7	2.6		0.03	0.70		180	Tall shrub
AMET37	53.736	-57.133	9	University of Ottawa	-0.9	22.6	-0.2	-1.7	0.70	0.82	-1.52	5	Wetland
IB048	51.458	-57.122	143	University of Ottawa	0.5	22.5	1.1	0.8	0.39	0.59	-0.26		Barren
TMNP1	58.451	-62.797	30	Parks Canada	-3.5	29.6	-0.6		0.64	1.22			Barren
TMNP2	58.943	-63.602	488	Parks Canada	-4.2	31.0	1.8		0.10	0.98			Wetland
TMNP3	59.001	-63.746	152	Parks Canada	-3.5	29.7	0.5	0.4	0.35	0.94	-0.08		Low shrubs

TMNP4	58.921	-63.665	599	Parks Canada	-5.8	33.5	1.1		0.12	0.84			Blockfield
TMNP5	58.875	-63.355	54	Parks Canada	-3.2	29.4	0.8		0.39	1.05			Low shrubs
TMNP6	59.412	-64.239	52	Parks Canada	-4.5	29.1	-3.2		0.88	1.18			Barren
Cairn2	53.343	-63.035	540	University of Ottawa	-3.2	34.0	0.3		0.64	1.17			Rock
Cairn3	53.477	-64.718	655	University of Ottawa	-4.3	35.1	-1.0		0.72	1.23			Rock
Cairn4	53.473	-64.720	666	University of Ottawa	-4.3	35.1	-2.2		0.91	1.33			Rock
Cairn6	52.970	-66.948	840	University of Ottawa	-5.3	34.4	-1.9		0.67	1.13		5	Rock
Cairn9	53.727	-65.144	571	University of Ottawa	-2.3	36.0	-0.8		0.77	0.98			Rock
Cairn10	54.318	-63.214	590	University of Ottawa	-4.2	34.3	-2.6		0.92	1.28			Rock
Cairn11	54.196	-63.110	584	University of Ottawa	-2.9	31.7	-2.1		0.94	1.08			Rock
OC1	53.609	-58.815	658	Jacobs et al (2014)	-3.4	31.0	2.4		0.03	0.73			Forest
OC2	53.609	-58.815	670	Jacobs et al (2014)	-3.4	31.0	2.2		0.03	0.67			Forest
CC1	53.610	-58.818	567	Jacobs et al (2014)	-2.8	31.4	2.4		0.02	0.66			Forest
CC2	53.610	-58.818	575	Jacobs et al (2014)	-2.9	31.4	2.4		0.03	0.68			Forest
K2	53.612	-58.819	557	Jacobs et al (2014)	-2.7	31.5	0.8		0.25	0.64			Forest-Tundra
DB1	53.616	-58.836	621	Jacobs et al (2014)	-3.1	31.2	2.8		0.09	0.94			Forest-Tundra
DB2	53.616	-58.837	636	Jacobs et al (2014)	-3.2	31.1	1.6		0.20	0.80			Forest-Tundra
WM2	53.623	-58.850	747	Jacobs et al (2014)	-3.9	30.6			0.13				Tundra
H1	53.640	-58.776	767	Jacobs et al (2014)	-4.0	30.6	1.1		0.24	0.89			Tundra
UPCTLS	53.630	-58.873	975	Jacobs et al (2014)	-6.6	29.6			0.16				Tundra
UPCTLN	53.630	-58.873	975	Jacobs et al (2014)	-6.6	29.6			0.00				Tundra
A1	53.630	-58.873	990	Jacobs et al (2014)	-5.4	29.6	1.9		0.10	1.08			Tundra
F1A	53.588	-58.794	520	Jacobs et al (2014)	-1.8	32.9	3.3		0.00	0.79			Forest
F1B	53.588	-58.794	520	Jacobs et al (2014)	-1.8	32.9	2.8		0.00	0.68			Forest
F2A	53.578	-58.763	522	Jacobs et al (2014)	-1.9	32.9	3.1		0.01	0.77			Forest
F2B	53.579	-58.763	524	Jacobs et al (2014)	-1.9	32.9	3.1		0.02	0.76			Forest
FT1A	53.616	-58.827	600	Jacobs et al (2014)	-2.2	32.5	2.2		0.18	0.82			Forest-Tundra
FT1B	53.617	-58.827	607	Jacobs et al (2014)	-2.3	32.5	3.2		0.03	0.86			Forest-Tundra
FT2B	53.617	-58.840	667	Jacobs et al (2014)	-2.6	32.2	2.0		0.14	0.76			Forest-Tundra
FT4A	53.608	-58.816	592	Jacobs et al (2014)	-2.2	32.6	2.4		0.02	0.63			Forest-Tundra
FT4B	53.608	-58.816	592	Jacobs et al (2014)	-2.2	32.6	2.4		0.02	0.64			Forest-Tundra
FT3A	53.612	-58.838	623	Jacobs et al (2014)	-2.4	32.4	1.4		0.24	0.73			Forest-Tundra
FT3B	53.612	-58.838	623	Jacobs et al (2014)	-2.4	32.4	1.4		0.34	0.90			Forest-Tundra
T1A	53.631	-58.855	796	Jacobs et al (2014)	-3.2	31.6	1.8		0.13	0.76			Tundra
T1B	53.631	-58.855	796	Jacobs et al (2014)	-3.2	31.6	1.0		0.22	0.72			Tundra
SC1	53.629	-58.873	990	Jacobs et al (2014)	-4.2	30.7	1.0		0.28	1.00			Tundra
SC2	53.629	-58.873	990	Jacobs et al (2014)	-4.2	30.7	0.7		0.33	1.01			Tundra
SO1	53.629	-58.873	990	Jacobs et al (2014)	-4.2	30.7	0.8		0.31	1.01			Tundra
SO2	53.629	-58.873	990	Jacobs et al (2014)	-4.2	30.7	0.7		0.35	1.03			Tundra
LC10cm	53.611	-58.816	565	Jacobs et al (2014)	-1.2	32.7	1.5	1.1	0.42	0.86	-0.39	25	Forest-Tundra
Base10cm	53.614	-58.837	600	Jacobs et al (2014)	-2.2	32.5	0.4	1.0	0.64	1.11	0.59	5	Forest-Tundra
Upper1m	53.630	-58.873	995	Jacobs et al (2014)	-4.2	28.8	-1.9	-1.9	0.76	1.10	0.00	5	Tundra

Table B4: Ground temperature data collected at Labrador Permafrost Project and Centre D'Études Nordiques (Allard et al. 2014) monitoring stations.

Station Name	Lat	Long	Modelled TTOP	Observed TTOP
AMET02	53.13289	-66.08898	1.97	2.15
AMET05	52.78897	-67.23068	2.04	4.12
AMET06	52.76550	-67.21879	-2.09	-3.19
AMET07	53.48348	-64.69016	1.47	2.70
AMET08	53.47635	-64.71851	1.66	0.44
AMET10	54.31758	-63.21454	1.18	-4.13
AMET11	52.82540	-60.10069	2.16	2.03
AMET12	52.79199	-60.03203	2.11	2.87
AMET14	53.72567	-56.96340	1.73	0.42
AMET16	53.87442	-66.41994	1.54	2.56
AMET21	52.16106	-56.09765	1.59	2.80
AMET22	52.13848	-56.13468	0.49	2.44
AMET23	53.06401	-57.67964	2.52	3.09
AMET24	53.07393	-57.66487	2.61	0.63
AMET25	53.32167	-62.96143	2.21	3.58
AMET26	53.34353	-63.03482	1.46	3.05
AMET29	53.11037	-61.80171	2.00	1.89
AMET32	52.98475	-66.94768	1.82	1.75
TMNP3	59.00100	-63.74600	0.23	0.45
TMNP4	58.92100	-63.66500	0.72	1.03
TMNP5	58.87500	-63.35500	-2.32	0.73
Site09	53.59131	-60.80119	2.11	2.18
Site32	53.69383	-57.01027	2.08	1.79
Site43	52.58654	-59.49076	1.55	3.63
Site53	53.34344	-63.03482	1.46	2.63
Site70	54.24228	-63.07343	2.12	3.26
Site74	54.19726	-63.11063	1.56	-1.23
Site76	54.19654	-63.10953	1.56	-0.85
Site79	53.77720	-63.39331	1.72	3.44
035ibutton	53.11033	-61.80175	2.00	1.78
CPBIbutton_Long	53.69194	-57.01815	2.33	2.33
Site39	53.72576	-56.96357	1.73	1.87
Lobstick Lower	53.73297	-65.15544	1.93	4.21
Site92	53.56032	-64.51027	1.76	3.94
Site94	53.13299	-66.08869	1.97	3.14
Site105	53.53081	-64.76850	2.47	3.10
Site108	53.34230	-65.68967	2.12	3.55
Site110	52.97258	-66.94809	2.35	2.20
Site112	52.96910	-66.94620	-1.84	3.18
IB006	51.63514	-56.71669	2.86	1.32

IB012	53.67329	-60.89992	2.39	1.66
IB014	53.29796	-62.67206	2.47	4.13
IB015	53.41544	-63.39329	1.31	3.88
IB016	53.52972	-64.52640	1.62	3.48
IB017	53.78087	-63.37918	1.72	3.86
IB018	53.53142	-64.76952	1.46	4.26
IB019	53.43250	-65.20194	1.99	4.08
IB020	53.33800	-65.65192	2.12	2.98
IB022	52.76538	-67.22078	1.55	-2.04
IB023	52.76466	-67.21975	-2.09	1.53
IB025	52.76465	-67.21440	2.41	-2.29
IB026	54.19726	-63.11063	1.56	-0.75
IB027	54.19654	-63.10953	1.56	-0.35
Akulivik	60.81738	-78.15498	-2.68	-2.48
Umiujaq	58.70000	-76.52165	-1.44	2.98
Tasiujaq1	58.66993	-69.95223	-3.88	-1.68
Tasiujaq2	58.70000	-69.91666	-4.00	-2.51
Kangiqsualujjuaq1	58.69442	-65.93853	0.04	-1.80
Puvirnituq	60.05670	-77.28697	-4.55	-2.36
Quaqtaq	61.04407	-69.61398	-0.09	-3.45
Salluit1	62.18003	-75.66897	-2.45	-4.95
Salluit2	62.19210	-75.63592	-1.20	-3.54
Lac Bush	57.95569	-75.91058	0.31	-1.88
Boniface Forest	57.72818	-76.08452	0.53	1.93
Boniface Tundra	57.73131	-76.07858	0.54	2.45

Note: Ground temperatures were collected using a variety of methods and are of variable lengths and cover differing periods (all post-2000).

Data citation:

Allard, M., Sarrazin, D., L'Hérault, E. 2014. Borehole and near-surface ground temperatures in northeastern Canada, v. 1.3 (1988-2014). Nordicana D8, doi: 10.5885/45291SL-34F28A9491014AFD.